TKK Dissertations 118
Espoo 2008

THERMAL MODELING AND EVALUATION OF HARMONIC EFFECTS ON A DRY-TYPE AIR-CORE REACTOR

Doctoral Dissertation

Kari Nurminen

Helsinki University of Technology
Faculty of Electronics, Communications and Automation
Department of Electrical Engineering

TKK Dissertations 118
Espoo 2008

THERMAL MODELING AND EVALUATION OF HARMONIC EFFECTS ON A DRY-TYPE AIR-CORE REACTOR

Doctoral Dissertation

Kari Nurminen

Dissertation for the degree of Doctor of Science in Technology to be presented with due permission of the Faculty of Electronics, Communications and Automation for public examination and debate in Auditorium S4 at Helsinki University of Technology (Espoo, Finland) on the 16th of May, 2008, at 12 noon.

Helsinki University of Technology
Faculty of Electronics, Communications and Automation
Department of Electrical Engineering

Teknillinen korkeakoulu
Elektroniikan, tietoliikenteen ja automaation tiedekunta
Sähkötekniikan laitos

Distribution:
Helsinki University of Technology
Faculty of Electronics, Communications and Automation
Department of Electrical Engineering
P.O. Box 3000
FI - 02015 TKK
FINLAND
URL: http://powersystems.tkk.fi/
Tel. +358-9-4511
E-mail: kari.nurminen@tkk.fi

ISBN 978-951-22-9343-8
ISBN 978-951-22-9344-5 (PDF)
ISSN 1795-2239
ISSN 1795-4584 (PDF)
URL: http://lib.tkk.fi/Diss/2008/isbn9789512293445/

TKK-DISS-2460

Picaset Oy
Helsinki 2008

ABSTRACT OF DOCTORAL DISSERTATION	HELSINKI UNIVERSITY OF TECHNOLOGY P.O. BOX 1000, FI-02015 TKK http://www.tkk.fi

Author Kari Nurminen

Name of the dissertation
Thermal modeling and evaluation of harmonic effects on a dry-type air-core reactor

Manuscript submitted 08.01.2008	Manuscript revised 20.03.2008
Date of the defense 16.05.2008	
x Monograph	Article dissertation (summary + original articles)

Faculty	Faculty of Electronics, Communications and Automation
Department	Department of Electrical Engineering
Field of research	Power Systems
Opponent(s)	Professor Steffen Großmann TU Dresden, Germany
Supervisor	Professor Matti Lehtonen

For the design engineers of reactors as well as for the most economical use of that equipment, the temperatures of different parts of reactors should be precisely known so that the thermal losses can be optimized and minimized. Through conventional surface testing methods the exact locations of hot spots inside reactor coils can only be estimated by means of empirical mathematical calculations. Therefore, the ability to directly measure the temperatures inside the coils between the conductors would lead to better design of the reactors, and at the same time would show the exact locations of hottest-spot areas and temperatures. In the IEC and IEEE standards, the test methods for determining temperatures and hot spots are mainly described as surface-temperature measuring methods, since modern dry-type air-core reactors usually employ fully encapsulated windings. Therefore, direct access to the winding is not possible for the measurement of hot spot temperatures during a heat-run test. However, it is possible to measure winding surface temperatures with some degree of accuracy. Such winding surface temperature measurements are essentially a measurement of winding hot spot due to the fact that the winding encapsulation medium is thin compared to the winding conductor cross section.
Since energy costs are on the increase, losses are becoming a more significant component of the total operating cost. Further, the correct current distribution between the coils causes even temperatures in each coil and helps to optimize the manufacturing and losses of the whole reactor. For this reason, the research work behind this thesis was started and a test reactor manufactured. During the manufacturing process, several fiber optic wires (instead of fiber optic probes, as mentioned in the IEEE standards) were installed in the middle and at the surface of several cylinder windings, for temperature monitoring purposes. Through these optic wires, it became possible to measure the dynamic temperature changes in several cylinders of the reactor, because the temperatures depend on the location and time. The dynamic temperature behavior could be determined in the middle of the windings for the whole length, from bottom to top. At the same time, with other optic wires, the surface temperatures could also be measured from bottom to top. For comparison, some surface temperatures as well as cooling air temperatures in the air ducts were also measured by means of thermocouples and infrared cameras. In this dissertation, the modeling methods for calculating the temperature distribution and hot-spot temperatures in large multi cylinder air-core reactors are studied and a new method is proposed for thermal loss optimization.

Keywords hot-spot-temperatures, optical wire measurement

ISBN (printed) 978-951-22-9343-8	ISSN (printed) 1795-2239
ISBN (pdf) 978-951-22-9344-5	ISSN (pdf) 1795-4584
Language English	Number of pages 219 p.

Publisher Helsinki University of Technology / Faculty of Electronics, Communications and Automation

Print distribution Department of Electrical Engineering

x The dissertation can be read at http://lib.tkk.fi/Diss/2008/isbn9789512293445

VÄITÖSKIRJAN TIIVISTELMÄ	TEKNILLINEN KORKEAKOULU PL 1000, 02015 TKK http://www.tkk.fi
Tekijä Kari Nurminen	
Väitöskirjan nimi Ilmasydämisen kuristinkelan lämpenemän mallintaminen sekä harmonisten yliaaltojen vaikutusten arviointi	
Käsikirjoituksen päivämäärä 08.01.2008	Korjatun käsikirjoituksen päivämäärä 20.03.2008
Väitöstilaisuuden ajankohta 16.05.2008	
x Monografia	☐ Yhdistelmäväitöskirja (yhteenveto + erillisartikkelit)
Tiedekunta Elektroniikan, tietoliikenteen ja automaation tiedekunta Laitos Sähkötekniikan laitos Tutkimusala Sähköjärjestelmät Vastaväittäjä(t) Professori Steffen Großmann TU Dresden, Saksa Työn valvoja Professori Matti Lehtonen	

Reaktorin (kuristikela) suunnittelulle sekä mahdollisimman taloudelliselle käytölle kelan lämpötilat sen eri kohdissa on tunnettava tarkalleen häviöiden optimoimiseksi ja minimoimiseksi. Perinteisellä reaktorin pinnan lämpötilamittauksella reaktorin sylinterien korkein lämpötilapiste (ns.hot-spot piste) ja -paikka voidaan vain arvioida ja laskea empiirisesti saatujen tulosten perusteella. Tämän vuoksi keino, jolla lämpötilat voidaan määritellä reaktorin sylinterien sisällä käämilankojen välissä, johtaa parempiin tuloksiin reaktorien suunnittelussa ja samalla ilmoittaa tarkalleen suurimman lämpötila-alueen ja -arvon. IEC- ja IEEE-normeissa on esitetty reaktorien pintalämpötilojen- sekä hot-spot pisteiden lämpötilojen mittaukseen pintalalämpötila-mittausmenetelmiä, koska nykyaikaisilla kuivatyyppisillä ilmasydämisillä reaktoreilla sylinterien käämilangat ovat eristettyjä sekä umpeen valettuja, ja siten täysin suljettuja ulkopuolelta. Tämän vuoksi käämin sisäisen lämpötilan ja siten myös hot-spot pisteen mittaus ei ole mahdollista lämpenemäkokeen aikana. Joissakin tapauksissa jos reaktorin sylinterien käämien eristys on hyvin ohut verrattuna käämin johtimen poikkipintaan, voidaan käämin lankojen pinta- ja hot-spot lämpötilat määritellä mittaamalla ja arvioimalla muutamien asteiden tarkkuudella. Energiahintojen jatkuva nousu aiheuttaa sen, että häviöiden osuus ja merkitys kasvaa kokonaiskustannuksissa. Tämän vuoksi oikea virranjako reaktorin sylinterien välillä johtaa yhtenäisempään lämpenemään ja siten auttaa optimoimaan reaktorin valmistusta ja sen häviöitä. Edellä mainitun seikan vuoksi valmistettiin koekela, johon asennettiin sen valmistusvaiheessa useita optisia kuituja (IEEE-normissa mainitun optisen anturin asemesta) sekä sylinterien pinnoille että niiden sisään lämpötilan mittausta varten. Optisilla kuiduilla on voitu mitata eri sylintereissä tapahtuvia käytönaikaisia lämpötilamuutoksia, jotka ovat riippuvaisia sekä ajasta että paikasta. Tällä mittausmenetelmällä on pystytty mittaamaan lämpötilan muutokset sylinterien käämien keskellä koko sylinterin pituudelta alhaalta ylös sekä samanaikaisesti niiden pintalämpötilat samoissa paikoissa. Mittaustulosten vertailun vuoksi joidenkin sylinterien pintalämpötilat sekä jäähdytysilman lämpötilat mitattiin käyttäen anturina lämpöpareja ja lisäksi infrapuna-kameran avulla..Tässä työssä on tutkittu lämpötilan jakautumista ja sen mallintamista suuressa monisylinterisessä ilmasydämisessä kuristinkelassa sekä kehitetty uusi menetelmä lämpöhäviöiden optimoimiseksi.

Asiasanat	”hot-spot”- lämpötilat, kuitumittaus	
ISBN (painettu)	978-951-22-9343-8	ISSN (painettu) 1795-2239
ISBN (pdf)	978-951-22-9344-5	ISSN (pdf) 1795-4584
Kieli Eng.		Sivumäärä 219 s.
Julkaisija Teknillinen korkeakoulu / Elektroniikan, tietoliikenteen ja automaation tiedekunta		
Painetun väitöskirjan jakelu Sähkötekniikan laitos		
x Luettavissa verkossa osoitteessa http://lib.tkk.fi/Diss/2008/isbn9789512293445		

Abstract

In electricity transmission and distribution systems, the controlling of reactive power in the network, limiting of short circuit currents as well as the minimizing and filtering of harmonic frequencies from the system involves the use of reactors. The widespread use of static rectification equipment in industrial loads on small and medium power transformers and reactors has resulted in a dramatic increase in the harmonic content of the load current for this equipment. It is quite common for the harmonic factor of the current to exceed 0.05 per unit, which is the limit specified for "usual service conditions" in IEEE Std C57.12.00-1993 and IEEE Std C57.12.01-1998. It is also well known that higher harmonic content in the current causes higher eddy current loss in winding conductors and the structural parts linked by the leakage flux field and, consequently, higher operating temperatures. Precise determination of the extra eddy current loss produced by harmonic currents is a complex subject that is highly dependent on the design and construction of the transformer or reactor, and may involve sophisticated computer analysis.

In the IEC and IEEE standards, the test methods for determining temperatures and hot spots are mainly described as surface-temperature measuring methods since modern dry-type air-core reactors usually employ fully encapsulated windings. Therefore, direct access to the winding is not possible for the measurement of hot spot temperatures during the heat-run test. However, it is possible to measure winding surface temperatures with some degree of accuracy. Such winding surface temperature measurements are essentially a measurement of winding hot spot because the winding encapsulation medium is thin compared to the winding conductor cross section.

For the design engineers of reactors as well as for the most economical use of that equipment, the temperatures in different parts of reactors should be known exactly so the thermal losses can be optimized and minimized. With conventional surface testing methods, the exact locations of hot spots inside reactor coils can only be estimated by means of empirical mathematical calculations. Therefore, the ability to test the temperatures directly inside and between the coil turns should lead to better design of reactors, and at the same time would show the test engineers the exact locations of hottest-spot areas and temperatures.

The total inductance and current density of the reactor are one of the major figures required for calculating the reactor dimensions and number of cylinders. Not only this but also other things must be considered, namely the hot-spot temperatures caused by the thermal losses (which can be different between the cylinders because of the out-of-step warming-up of the reactor cylinders caused by the different current distribution between the coils) and the eddy-current losses. The eddy-current losses which are frequency dependent and are caused by the electrical and magnetic fields as well as stray losses caused by the magnetic flux in other metallic parts of the reactor and in the reactor support structure. The two eddy-current effects, the skin and proximity effects occur simultaneously in a conductor that carries an alternating current and is positioned in an external alternating field. This is exactly the situation that exists for the conductors in the layers of any winding. The essence of the combination of these effects is that the current in each conductor produces a skin effect in itself and a proximity effect in other conductors that are close to it. The circulating eddy currents due to skin and proximity effects cause the power losses in windings to increase dramatically with frequency.

Since the energy costs increase, losses become a more significant component of the total operating cost. Further, the correct current distribution between the coils causes the temperatures in each coil to be similar and helps to optimize the manufacturing and losses of the whole reactor. For this reason the research work has been started with a group of reactor users and with the Finnish reactor manufacturer Nokian Capacitors Oy (NC), who has manufactured a test reactor. During the manufacturing process, several wire optic wires (instead of wire optic probes, as mentioned in IEEE standards) were installed in the middle and at the surface of several cylinder windings. Through those optic wires, it becomes possible to measure the dynamic temperature changes in several cylinders of the reactor, because the temperatures are dependent on the location and time. This enables the dynamic temperature behaviors in the middle of the windings to be determined over the whole length, from bottom to top, and with other optic wires, the corresponding surface temperatures. For comparative measuring reasons some surface temperatures as well as cooling air temperatures in the air ducts where also measured by means of thermocouples and infrared cameras.

In this dissertation, the modeling methods for calculating the temperature distribution and hot-spot temperatures in large multi cylinder air-core reactors were studied and a new method was proposed for thermal loss optimization.

Preface

The research work related to this thesis was carried out within years 2005 - 2007 in the research group “Power Systems” of the Department of Electrical Engineering (EE) of the Faculty of Electronics, Communications and Automation, and has been financed by the National Technology Agency of Finland (TEKES) as well as by Nokian Capacitors Oy (NC), who manufactured the test reactor, by Fingrid Oy (FG) and by Helsingin Energia Oy (HE).

The Optical-Wire temperature measurements have been carried out in the Laboratory of High Voltage Engineering with the DTS-measuring instrument that was borrowed from Fortum Service Oy, Helsinki.

The executive group for this project was formed up from the following experts in the field:

Matti Lehtonen (EE/chairman), Matti Lahtinen (FG), Markku Hyvärinen (HE)
Yrjö Enqvist (NC), Jussi Pöntys (NC), Jari Kotiniitty (NC/secretary)

The head of the Department of Electrical Engineering (EE) Professor Matti Lehtonen supervised the research work.

First, I want to give my greatest gratitude to Professor Matti Lehtonen, who motivated and gave me many practical advices to my work. Further, I would like to express my sincere thanks to the members of the executive group for their good co-operation.

I wish to express my best thanks to the pre-examiners Professor Jaan Järvik and Dr. Kai Juslin for their objective comments and corrections to the manuscript.

I would like to thank all my colleagues at the Department of Electrical Engineering that have been involved in the organization and preparation of this work. Especially I am grateful to Professor Tapani Jokinen, who guided me in some thermal calculations as well as to Dr. Pirjo Heine and to Dr. John Millar for their help during my writing this thesis.

Further, I would like to thank Jorma Suonpää, Harri Stenius and Markku Helanen from Nokian Capacitors Oy for their participation in this project. I also thank Hannu Kokkola from High Voltage laboratory and Asko Mitrunen from Fortum Service Oy for the technical support and help of preparation and completion of the temperature measurements.

Last, but not least, I would like to thank my daughter Laura and my little wife Meeri for their great support and patience throughout on my way in obtaining this goal.

Espoo, April 2008

Kari Nurminen

Contents

8 Appendixes

List of symbols and abbreviations

A = cross-sectional area
a = radius/cm (= D/2)
b = air pressure
b = length/cm
B = magnetic flux density
c_p = specific heat
C = total thermal capacitance
C_{coil} = thermal capacitance of coil
C_m = mutual-capacitance
C_s = self-capacitance

D = mean diameter of one cylinder
d = diameter of conductor
D = electric flux density
D = mean diameter of one cylinder
DTS = Distributed Temperature Sensing
E = electric field intensity
f = frequency
FEM = finite element method
H = height
h = height
H = magnetic field intensity
h = number of harmonic
i_s = mean current density
I = current
j = imaginary factor
Ja = current density
J_{coil} = current of one coil
J_s = surface current density
Jsφ = surface current density
K = Nagaoga-factor
k = relations factor
k = thermal conductivity
L = inductance
L = length

$L_s = L_{nn}$ = self-inductance

m = weight of cylinder

M_{nm} = mutual-inductance

N = number of turns of one cylinder (sum of each layer)

N = number of winding turns

n = number of turns of one cylinder (sum of each layer)

N_u = Nusselt number

NC = Nokian Capacitors

OW = optical wire

P_{ec} = eddy current losses

P_h = electrical losses of one coil

P_r = Prandl number

P_{th} = thermal total losses

P_w = thermal AC-losses

Q = heat flow

q = heat flux density

Q_{al} = thermal losses of coil (P_w)

Q_{coil} = thermal energy (heat) stored in the coil

Q_{out} = thermal energy (heat) leaving out from the coil (convection and radiation)

r = radius

R = radius

R_s = total resistance

R_{ac} = electrical AC-resistance

R_{dc} = electrical DC-resistance

R_e = Reynolds number

R_{th} = thermal resistance

r_{wire} = radius of conductor

s = circle

T = temperature

t = time

TC = thermocouples

U = voltage

[U] = uniform matrix vector

V = volume

[V] = voltage matrix vector

x = the level of surface counted from bottom of cylinder

Z = impedance

α_k = heat transfer coefficient

λ_{res} = resultant heat transfer coefficient

γ = density
δ = skin depth
Θ = temperature
Θa = inside temperature of cylinder
Θ_{amb} = ambient temperature in level x
Θb = outside surface temperature of cylinder
Θ_{coil} = over temperature of one coil
Θ_{wall} = temperature at cylinder wall in level x
μ_o = permeability of vacuum ($4\pi 10^{-7}$ Vs/Am)
ρ = specific electrical resistance
σ = electric conductivity
τ = time constants
$\omega = 2\pi f$ = angular speed
ε = emissivity
σ = Stefan-Boltzmann constant ($5.7*10^{-8}$ W/m^{2}K^4)

1 Introduction

1.1 Background

In electricity transmission and distribution systems the controlling of reactive power in the network, limiting of short circuit currents as well as the minimizing and filtering of harmonic frequencies from the system requires the use of reactors. There are many types of reactor, but the most used today is the air-cooled dry-type reactor, which is also the reactor type used for this researcher work.

The widespread use of static rectification equipment in industrial loads on small and medium power transformers and reactors has resulted in a dramatic increase in the harmonic content of the load current for this equipment. It is quite common for the harmonic factor of the current to exceed 0.05 per unit, which is the limit specified for "usual service conditions" in IEEE Std C57.12.00-1993 and IEEE Std C57.12.01-1998. It is also well known that higher harmonic content in the current causes higher eddy current losses in winding conductors and structural parts linked by the leakage flux field and, consequently, higher operating temperatures. Precise determination of the extra eddy current losses produced by harmonic currents is a complex subject that is highly dependent on the design and construction of the transformer or reactor and may involve sophisticated computer analysis (IEEE Std C57.110-1998).

In the IEC and IEEE standards (e.g. IEEE Std C57.16-1996) the test methods for determining temperatures and hot-spots are mainly described as surface-temperature measuring methods since modern dry-type air-core reactors usually employ fully encapsulated windings. Therefore, direct access to the winding is not possible for the measurement of hot spot temperatures during the heat-run test. However, it is possible to measure winding surface temperatures with some degree of accuracy. Such winding surface temperature measurements are essentially a measurement of winding hot spot because the winding encapsulation medium is thin compared to the winding conductor cross section.

For the design engineers of reactors as well as for most economical use of that equipment, the temperatures of different parts of the reactors should be known and so the thermal losses can be optimized and minimized. Through the conventional surface testing methods the exact locations of hot spots inside reactor coils can only be estimated by means of empirical mathematical calculations. Therefore the ability to test the temperatures directly inside and between the coil turns could lead to better results when designing the reactors, and at the same time would show the test engineers the exact locations of hottest-spot areas and temperatures.

Winding hot spots can be measured using thermometers, thermocouples, or wire-optic probes. In all cases, the method for fixing the temperature-measuring device to the surface of the winding is extremely critical. Hottest-spot location and, hence, measurement point location, is typically in the last turns of the upper winding. Exact location, and, hence, the temperature measuring device placement decision, can best be determined by the manufacturer because to his detailed knowledge of the product.

In this research work, the winding temperatures between the conductors have been measured in real-time during heat-run tests.

Table 1.1: Temperature limits
(IEEE Std C57.21-1990)

Limits of Temperature Rise for Continuously Rated Shunt Reactors

Type of Shunt Reactor	Insulation Temperature Class	Average Winding Temp. Rise by Resistance (deg. C)	Hottest-Spot Winding Temp. Rise (deg. C)
Oil-immersed	---	65	80
Dry-Type	105	55	65
	130	80	90
	155	100	115
	180	125	140
	220	150	180

For example, according to IEEE standards shunt reactors shall be designed so that the hottest-spot conductor temperature rise above the ambient temperature, when operated at 105% of rated voltage, will not exceed the values given in the table 1.1.

According to IEC 289 sub clause 17.9.1, the temperature rise after a temperature test shall be calculated as follows:

$$\Delta\Theta_N = \Delta\Theta_t \, [I_N/I_t]^{\,q} \qquad (1.1)$$

Where

$\Delta\Theta_N$ = temperature rise at rated current
I_N = rated continuous current
I_t = test current
$\Delta\Theta_t$ = temperature rise at test current
q = empirical factor (1.6) for AN (air natural) cooled air core reactors

1.2 Dry-type air-core reactors: basic aspects

The application fields for the use of reactors are various, such as in the neutral grounding systems, as short circuit (current) limiting reactors, as smoothing reactors, for harmonic filtering, as shunt reactors for compensating capacitive power, as line trap reactors, and so on. The main reason to

use reactors in power systems is to reduce or eliminate the effects of fault currents, to separate high frequency carrier signals for control purposes, to compensate capacitive power and to improve power quality.

Inductive reactors are mainly used as follows:

- **Current limiting reactors** are series connected to the transmission / distribution line or to the feeder in order to limit the short-circuit power on the load side of the reactor. The reactor limits the short-circuit current to a level which can be handled by the components installed in the electrical system, such as breakers, switches or fuses.

- **Neutral grounding reactors** are used for low-impedance grounding of the neutral point of three-phase networks in order to limit the fault current in the event of a phase-to-ground short-circuit.

- The harmonic currents have to be eliminated by filters. These harmonic filters, essentially consisting of reactors and capacitors, are usually installed close to the source of harmonics in order to provide a low impedance path for the harmonic currents. This is achieved by series connection of a **filter reactor** with a capacitor bank, forming a filter circuit tuned to the harmonic frequency, which needs to be eliminated. If several harmonic frequencies need to be eliminated, a number of filters with different resonance frequencies will be connected to the bus system, for instance the 3^{rd}, 5^{th} and 7^{th} harmonic of the fundamental frequency. If fine-tuning of the filter is required, the filter reactor may be equipped with taps for inductance adjustment.

- High voltage transmission lines and cables have an inherent capacitance, causing a capacitive charging current and, thus, capacitive power is generated. In lightly loaded lines or cables this capacitive current will increase the voltage at the end of the line. By the use of **shunt reactors,** the capacitive load will be compensated and the voltage increase at the end of the line will be limited. The shunt reactors are normally connected to the tertiary winding of the high voltage transformer (e.g. 400kV system) but can also be directly connected to lower voltage systems (e.g. 110kV).

- In order to optimize and to control the impedance of the transmission path, **load flow reactors** are connected in series to the high voltage transmission line. The use of load flow reactors in electric power grids is one the most cost-effective solutions, to ensure the required load balancing within the grid system under normal continuous load conditions.

1.3 Objectives of the study

The objective of this study is to find an accurate way to determine the hot-spot temperatures and their locations, to develop a solution algorithm for the current distribution between the coils for thermal modeling and to evaluate harmonic effects of a dry type air-cooled reactor. The model is made dynamic so that the effect of variable load and transient operation states can be analyzed.

Appropriate methods for determining the losses and hot-spot temperatures of air-core reactor windings have not been found in the literature.

The total inductance and current density of the reactor are the major figures required for calculating the reactor dimensions and number of cylinders. The hot-spot temperatures caused by the thermal losses (which can be different between the cylinders because of the out-of-step warming-up of the reactor cylinders caused by the different current distribution between the coils) and the eddy-current losses which are frequency dependent and are caused by the electrical and magnetic fields must also be considered, as well as the stray losses caused by magnetic flux in other metallic parts of the reactor and in the reactor support structure. The two eddy-current effects, the skin and proximity effects occur simultaneously in a conductor that carries an alternating current and is positioned in an external alternating field (Figure 1.1). This is exactly the situation that exists for the conductors in the layers of any winding. The essence of the combination of these effects is that the current in each conductor produces a skin effect in itself and a proximity effect in other conductors that are close to it. The circulating eddy currents due to skin and proximity effects cause the power losses in windings to increase dramatically with frequency.

If the conductor is composed of one or more concentric circular elements, then the centre portion of the conductor will be enveloped by a greater magnetic flux than those on the outside. Consequently the self induced back-emf will be greater towards the centre of the conductor, thus causing the current density to be less at the centre than the conductor surface. This extra concentration at the surface and change in the current density function in the wire is usually known as skin effect, and results in an increase in the effective resistance of the conductor.

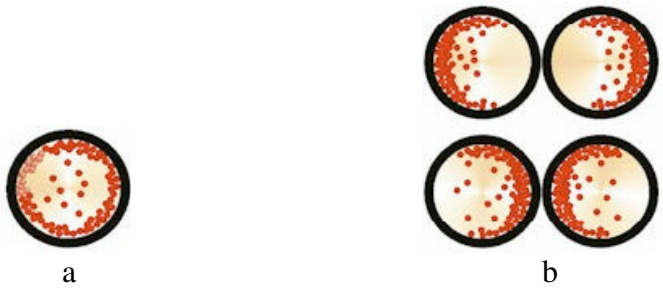

Figure 1.1: Skin effect (a) and proximity effect (b) (General Cable)

Proximity effect is caused by eddy currents induced by an externally applied magnetic field. Since the alternating current in some other nearby wires can cause this external field, this eddy-current phenomenon is often referred to as the proximity effect.

The time-varying field lines, which pass through the conductor, induce eddy currents in the conductor, and these eddy currents induce a field, which opposes the external magnetic field. This circulating current produces losses in the conductor even though it carries no net current.

The proximity effect also increases the effective resistance and is associated with the magnetic fields of two conductors, which are close together. Proximity effect is a special case of skin effect (Dwight, 1945). If each carries a current in the same direction, the halves of the conductors in close proximity are cut by more magnetic flux than the remote halves. Consequently, the current distribution is not even throughout the cross-section, a greater proportion being carried by the remote halves. If the currents are in opposite directions, the halves in close proximity will carry the greater density of current.

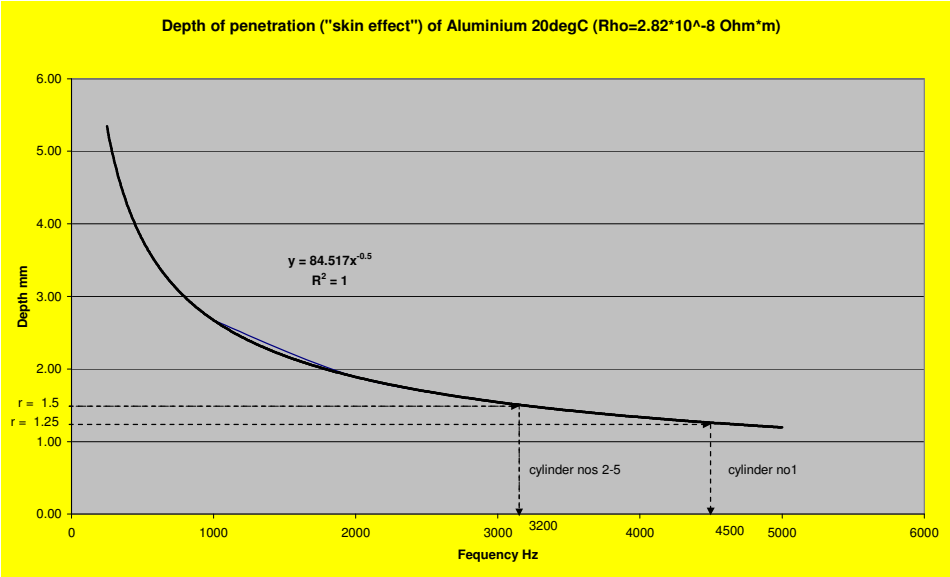

Figure 1.2 Depth of penetration of magnetic field with higher frequencies for aluminium wire

Skin depth is a physical material constant and cannot be dependent on geometry. The net instantaneous current in the conductor is unchanged by the eddy currents; it is the radial distribution of the current over the cross-section of the conductor that changes.

In addition to the phenomena above, the temperature rise leads to higher losses, as the resistance is temperature dependent as shown in Figure 1.3.

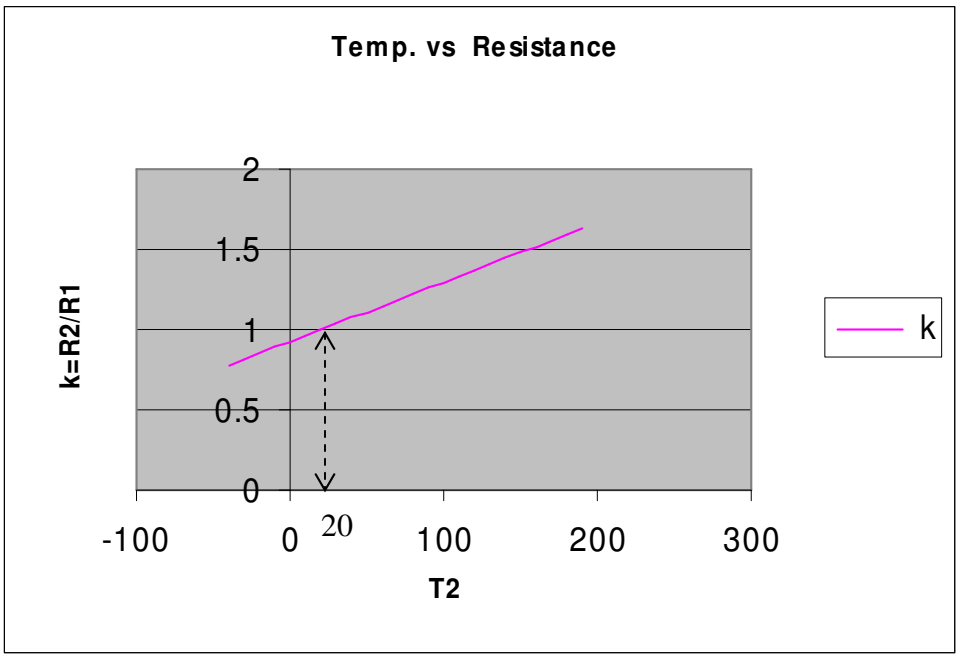

Figure 1.3: Resistance (Al) vs. temperature
(T2 in ^{o}C ; R1 = Resistance in Ohm by 20 ^{o}C and
R2 = Resistance in Ohm by T2 ^{o}C)

The mathematical equation for Figure 1.3 is:

$$k = (1+0.0037(T_2 - 20)) \qquad (1.1a)$$

Where

T_2 = Conductor temperature [^{o}C]

According to IEEE Std C57.110-1998 the load loss can be subdivided into thermal (I^2R) loss and "stray loss". Stray loss is determined by subtracting the thermal loss (calculated from the measured resistance) from the measured load loss (impedance loss). Stray loss can be defined as the loss due to stray electromagnetic flux in the windings, core, core clamps, magnetic shields, enclosure or tank walls, etc. (if any). Thus, the stray loss is subdivided into winding stray loss and stray loss in components other than the windings. The winding stray loss includes winding conductor's eddy-current losses and losses due to circulating currents between strands or parallel winding circuits. All of this loss may be considered to constitute winding eddy-current loss. The total load loss (P_{th}) can then be stated as

$$P_{th} = P_w + P_{ec} + P_{otherstray} \qquad (1.2)$$

The other stray losses ($P_{otherstray}$) in a dry-type air-core reactor (without enclosure, tank, etc.) are small and could be ignored. The winding losses (P_w) are caused only by the current (I) flowing through the reactor with resistance (R_{ac}):

$$P_w = I^2 R_{ac} \quad (1.3)$$

The total current (I) is a sum of harmonics (I_h) and can be calculated as follows:

$$I = (\sum (I_h)^2)^{0.5} \quad (1.4)$$

where

h = harmonic number (1...max)

AC-resistance (R_{ac}) is mathematically calculated from the ratio (R_{ac} / R_{dc}), which is called *skin-effect resistance ratio* and can be expressed as a Bessel's differential equation or with an a series approximation of powers of the actual frequency, diameter and resistivity of wires, as presented by Dwight among others (Dwight, 1945 pp. 159).

For example the skin-effect resistance ratio of a 3mm aluminium wire, as in our test coil's windings, at a frequency of 50 Hz, can be calculated with above mentioned Dwight's equation and is R_{ac}/R_{dc}= 1.093; that is, the AC-resistance at 50Hz is about 9% higher than the DC-resistance. The resistance R_{ac} is temperature and frequency dependent, as shown in Figures (1.4), (3.30) and (3.31). In the case of a significant amount of harmonics, the winding losses are better computed using the following equation:

$$P_w = \sum [(I_h)^2 R_{ac,h}] \quad (1.4a)$$

where the $R_{ac,h}$ is the AC-resistance for harmonic order h.

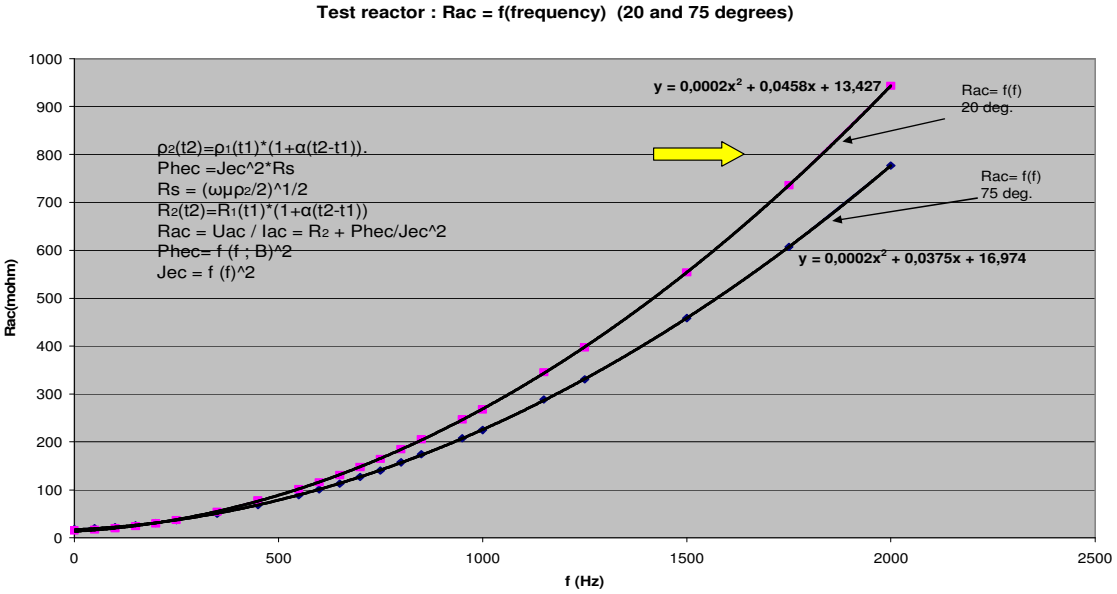

Figure 1.4: AC-resistance (R_{ac}) vs. frequency (f) and temperature (T) (source: NC)

When the stray losses ($P_{otherstray}$) on the spider arms, clamps and isolators of a reactor are ignored, the total losses can be calculated as follows:

$$P_{th} = P_w + P_{ec} \quad (1.5)$$

where P_w are the losses due to load current and winding resistance and P_{ec} the losses due to eddy currents in the windings. The eddy-current losses P_{ec} are also frequency and temperature dependent as presented in chapter 3.

The life of insulating materials commonly used in dry-type series reactors depends largely upon the temperatures to which they are subjected and the duration of such temperatures. Since the actual temperature is the sum of the ambient temperature and the winding temperature rise, it is apparent that the ambient temperature very largely influences the life of insulating materials used in dry-type reactors. According to IEEE standards *(IEEE Std C57.16-1996)* other factors upon which the life of insulating materials depends are as follows:

a) Dielectric stress and associated effects
b) Vibration or varying mechanical stress
c) Repeated expansions and contractions
d) Exposure to moisture, contaminants, etc.
e) Overloading (current) of the device

The questions, for what reason the reactor is needed and what are the ambient conditions, also influence the type and final design of the reactors.

Since energy costs are increasing, losses will become a more significant component of the total operating cost. Further, the proper current distribution between the coils would cause even temperatures in each coil and helps to optimize the manufacturing procedure, save costs and minimize the losses of the whole reactor. On the other hand, the reactor users, which are mostly utilities and electric power distributors, are interested in the behavior of reactors such as disturbing sound emissions or their correct operation in different climatic conditions, especially in the extreme temperatures accompanied by snow and ice that prevail in North-Finland.

For those reasons the research work was iniated with a group of reactor users and with the Finnish reactor manufacturer Nokian Capacitors Oy (NC), who has manufactured a test reactor. In the manufacturing process several optical wires (instead of wire optic probes, as mentioned in IEEE standards) were installed for temperature monitoring purposes, in the middle and at the surface of several cylinder windings. Through those optic wires it becomes possible to measure the dynamic temperature changes in several cylinders of the reactor because the temperatures depend on both location and time. The dynamic temperature behaviour in the middle of the windings over the whole length from bottom to top, could be determined. The same time, the surface temperatures, from bottom to top, could be measured with another set of optical wires. For comparative reasons some surface temperatures as well as cooling air temperatures in the air ducts were also measured by means of thermocouples and infrared cameras.

In this dissertation, the modeling methods for calculating the temperature distribution and hot-spot temperatures in large multi cylinder air-core reactors are studied.

Contributions of this research work:

Compared with the existing methods to determine the hot-spot region/location and surface temperatures, the major goals and contributions of this work are:

- An accurate measuring method to determine the temperature distribution and location for hot-spot areas in the windings of the separate cylinders of a reactor shall be developed and the test results, theoretically and through practical measurements via optical wires, shall be verified.

- An algorithm, with a matrix calculation complete with an iterating method to determine the impedance values of each coil in order to reach the desired current distribution and current density, which affect the coil's hot-spot temperatures, shall be proposed.

- The magnetic flux density will be calculated with a FEM model and used to predict reactor eddy current losses. Knowledge of the flux density in the reactor coils and their summation is used with the appropriate conductor dimensions to predict the eddy losses for a specific design.

- A hypothesized temperature distribution model of the cylinder of an air core reactor will be developed and verified through practical measurements. The exact temperature curvature on the inside- and outside-surface of the coil windings will be determined and mathematically modeled.

1.4 The test reactor

The air-core test reactor being used in this research work is a prototype of a new design based on a typical multi-cylinder and -wire construction, as shown in Figure 1.5.

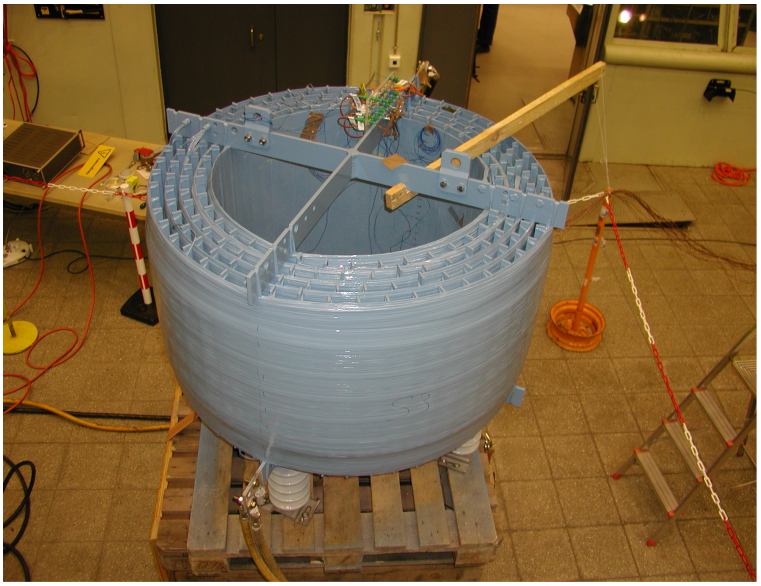

Figure 1.5: Test reactor

The reactor consists of five parallel connected cylinder coils. One coil is made of several coaxial winding groups or layers of 2.5/3.0 mm aluminium conductors of circular cross section and insulated by polyester film. The winding layers are embedded with resin impregnated filament wireglass. Between the cylinders there are spacers made of wireglass, separating the cylinders from each other. The spacers form cooling ducts between the coils.

The winding groups are different in each cylinder and vary from 5 to 7 layers. Each layer is made by two parallel connected and at the same time wound conductors which are individually insulated by polyester film. Thus, the test reactor resembles 62 coaxial and concentric parallel-connected winding coils.

On the top and bottom of the reactor are flat aluminium spider arms, which are used for the connecting of all the winding layers, fixing of the cylinders by wireglass roving and for optimizing the number of turns for correct inductance and current distribution. This is because the skin effect, proximity effect and mutual inductance among the parallel connected coils and layers of the reactor result in unequal current distribution among the layers and coils. The technique of dropping one or more turns at the ends of the outer layers of the coil combined with the application of spider arms is employed to ensure a uniform current distribution among layers. The current distribution of parallel connected layers or coils can be determined if the impedances of each layer and/or coil can be estimated.

The mean diameter of this reactor is about 1.0m and the height is 0.45m. The nominal rated current is 500A at 50Hz, and the inductance 4.3mH. The rated voltage is 22kV.

The detailed construction and manufacturing of an air core reactor is illustrated in appendix D.

1.5 Determining hot-spot temperature

An approach to determine the accurate hottest-spot ratio for dry-type reactors (hottest-spot rise/average rise) requires the accurate measurement of the average temperature rise and the adoption of a methodology that allows the measurement of hottest-spot temperature in a repeatable and accurate fashion. The average temperature rise can easily be measured using the well proven DC-resistance method. In order to accurately measure the hottest-spot temperature, knowledge of the location of the hottest spot is required.

According to the IEEE-standards (C57.134-2000) the applicable temperature measurement devices include, e.g.

- Optical temperature sensing device
- Thermocouples
- Resistance bridge
- Infrared temperature detector
- Temperature labels

The winding hottest-spot temperature rise and location is mainly affected by

- Amount and type of turn and layer insulation
- Vertical height of winding
- Radial build or thickness of winding
- Number of ventilating ducts in winding, size, thickness, and spacing
- Encapsulation thickness
- Coil configuration (round/rectangular)

Buoyancy driven flow in vertical ducts is of significance in many cooling applications. As an example, dry type air core reactors are cooled by air flowing through straight vertical ducts between the cylinders. In order to calculate the temperature rise of the windings, the Nusselt-numbers of the ducts are needed. For the calculation of duct outlet temperatures, also the flow rates in the ducts must be determined. Heat transfer equations for various duct geometries have been published extensively. However, equations for the calculation of flow rate have not received the same attention (Olsson 2004).

Correlations for natural convection heat transfer in open cooling ducts are not well known (Pierce 1994). The usual approach would be to calculate the air temperature at the hottest spot elevation similar to the methods used for liquid-filled transformers. This would require a calculation of the airflow rate, which complicates the heat transfer analysis.

Cooling air enters the bottom of the winding of each cylinder and it passes upwards through the cooling channels. The temperature of each cylinder is assumed to rise non-linear with the height, as shown in Figure 1.6. Winding length is the main parameter influencing the ratio of hottest spot to average winding temperature rise. This is due to the large thermal gradient from the bottom to the top of the winding due to natural convection air flow. The high heat transfer coefficients at the bottom of the winding before the flow becomes fully developed contribute to low temperatures at the bottom of the cylinder. At the top the flow becomes fully developed, the boundary layer is established, the heat transfer coefficients at the top of the coil are less, and the temperature of the air in the cooling ducts is high contributing to the hottest spot temperature rise in the top of the coil. Radiation from the ends of the coil ducts affects the hottest spot temperature rise and must also be considered (Pierce 1994).

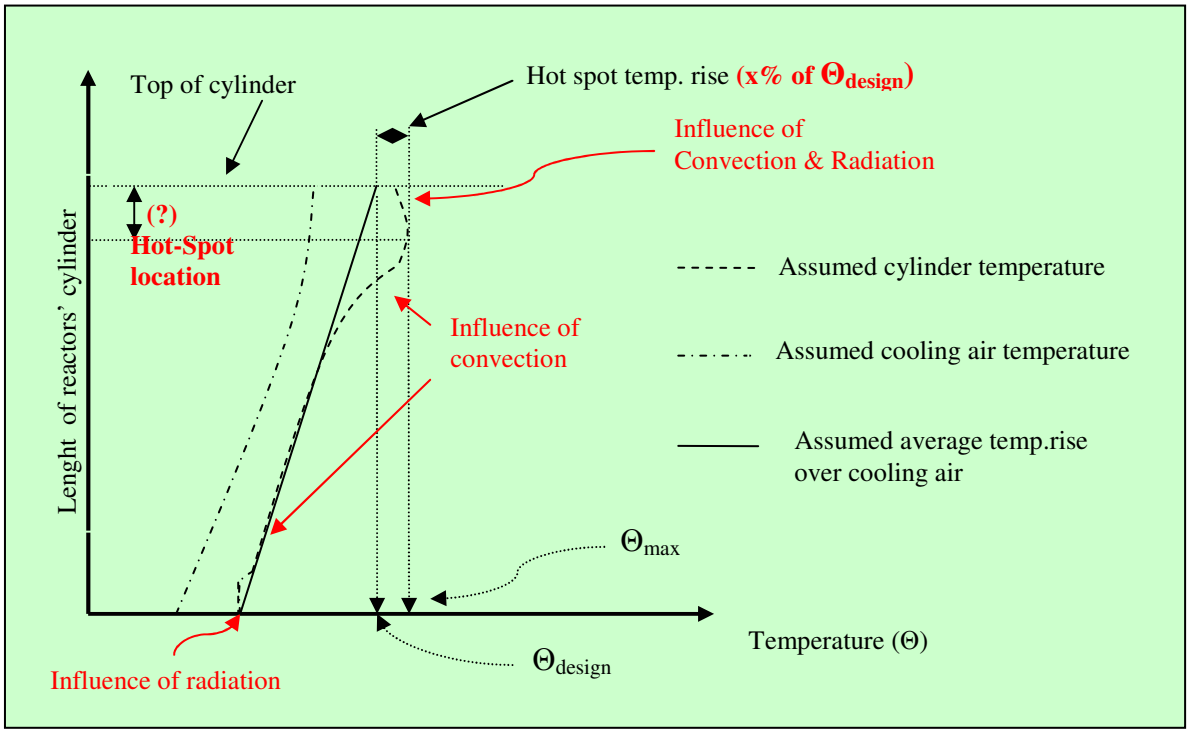

Figure 1.6: Temperature distribution model for one cylinder of an air core reactor hypothesized at the beginning of the research project

The maximum temperature (Θ_{max}) occurring in any part of the winding is called the "Hot-Spot-Temperature" and it will be the thermal limiting temperature of loading that cylinder of the reactor. Since the electrical impedances of each cylinder are different to each other, the current distribution is not even and so the heat losses are different. Therefore, each cylinder has its own hot spot temperature. The highest hot spot temperature of a single cylinder thus limits the electrical loading of the whole reactor and therefore design engineers try to keep the temperatures of all cylinders at the same level.

Accuracy in winding hottest-spot temperature measurement is dependent upon placing temperature sensors in the appropriate locations. The temperature difference between the winding hottest spot and coil surface may be determined by measurement or by calculation with a thermal model and added to the surface temperature for determining the winding hottest-spot temperature. If sufficient surface temperature measurements are made on a winding, coupled with an accurate temperature differential (proven by experiment on models or prototypes) relating surface (encapsulation) temperature to internal winding temperature, it is possible to determine the average winding temperature rise by taking the average of all surface temperature rises (with an external to internal correction factor). This is another means of verifying the surface temperature measurement methodology.

Embedded temperature sensors wound into the winding is the preferred method of determining the hottest spot location. The first step in determining hottest-spot location is to utilize a temperature measurement methodology where sufficient measurement points can be obtained along the surface of a winding. One simple method is to insert non-reversing temperature indicating labels into a number of cooling ducts for each winding, evenly spaced from top to bottom. Thermocouples, wire-optic probes, or other suitable temperature indicating devices can be used in a similar fashion. A proof of the validity of this approach can be demonstrated by taking the average of all label readings (after adding a known temperature differential value for the internal winding temperature and the measured surface temperature) for each particular test to ascertain if an average temperature rise close to the value derived from the DC-resistance method is yielded. Plotting the label readings vertically from bottom to top for each monitored cooling duct of a winding should yield a consistent definition of temperature profile and location of the hottest spot. A hot spot measurement has been made for each encapsulated winding group in the reactor under test. The hottest spot location and, hence, measurement point location, is typically in the last turns of the upper winding end. The exact location has been determined by the measurements during the tests.

Heat transfer theory

There are three physical mechanisms for heat transfer:

- Conduction
- Convection
- Radiation

Fourier Law describes the heat transferred by conduction. In very simple terms, the heat flux is proportional to the ratio of temperature over distance. In a reactor installation, heat conduction occurs everywhere inside the reactor's coil windings.

Based on Fourier's equation for one-dimensional thermal diffusion the thermal resistance for conduction heat transfer is given by

$$R_{thcond} = L/(kA) \qquad (1.6)$$

where L is the length of the heat flow path, k the thermal conductivity of the medium, and A the cross-sectional area for heat flow. The thermal conductivity is a thermo physical property of the material, which is, in general, a function of both temperature and location.

Convection of heat occurs in moving fluids (air, water, oil, etc.) and obeys **Newton's Law**. In a vacuum the convection is nil. The flow of heat is proportional to the temperature difference. In a dry–type reactor installation convection takes place in the air space inside and outside of the reactor cylinders.

Common dimensionless quantities that are used in the correlation of heat transfer data are the Nusselt number Nu, which relates the convective heat transfer coefficient to the conduction in the fluid, the Prandtl number (Pr), which is a fluid property parameter, the Grashof number (Gr), which accounts for the buoyancy effect and the Reynolds number (Re), which relates the momentum in the flow to the viscous dissipation.

In natural convection, fluid motion is induced by density differences resulting from temperature gradients in the fluid. The heat transfer coefficient for this regime can be related to the buoyancy and the thermal properties of the fluid through the Rayleigh number (Ra), which is the product of the Grashof and Prandtl numbers.

Natural convection flow over vertical cylinders is relevant to many practical applications, such as flow over cylindrical reactor coils. For large values of D/h, where D is the diameter of the cylinder and h its height, the flow can be approximated as that over a flat plate, since the boundary layer thickness is small compared to the diameter of the cylinder. However, since this result is based on the boundary layer thickness, which in turn depends on the Grashof number, the deviation of the results obtained for a vertical cylinder from those for a flat plate must be given in terms of D/h and the Grashof number. Sparrow and Gregg (1956) obtained the following criterion for a difference in heat transfer from a vertical cylinder of less than 5% from the flat plate solution, for Pr values of 0.72 and 1.0 (Jaluria 1995):

$$D/h = 35/G_r^{1/4} \qquad (1.7)$$

where G_r is the Grashof number based on height h.

Following the form of the conventional relations for convective heat transfer the thermal resistance in convective thermal transport can be written in the form of

$$R_{thconv} = 1/(\alpha_k A) \qquad (1.8)$$

where α_k is the coefficient of heat transfer.

The heat transfer literature contains many theoretical equations and empirical correlations that can be used to determine the heat transfer coefficient for specified fluids flowing within channels or along surfaces of various geometries. Many of these relations are expressed in nondimensional form as

$$Nu = C\, Re^{n}\ Pr^{m} \qquad (1.9)$$

where Nu is the Nusselt number, C a geometric constant, Re the Reynolds number and Pr the Prandtl number. The values of C, m and n are empirical constants and depend on whether the air flow is laminar or turbulent.

Several empirical models have been developed for the heat convection from vertical wall to surrounding air. In those models the heat transfer coefficient depends on ambient temperature, air pressure and velocity, surface temperature, dimensions, roughness of surface, etc. and is difficult to determine. Below are some empirical results from several authors to define the heat transfer coefficient α_k (Gotter 1954):

Jürgens	$\alpha_k = 6.55/\ h^{1/4}$	[W/m^2 ^{o}C]
Incropera:	$\alpha_k = 2...25$	[W/m^2 ^{o}C]
Mantsinger:	$\alpha_k = 2.17\ \Theta^{1/4}$	[W/m^2 ^{o}C]
Nusselt:	$\alpha_k = 2.55\Theta^{1/4}$	[W/m^2 ^{o}C]

where

Θ = temperature difference
h = height (m)

Heat transfer from a vertical surface may be expressed in terms of the commonly used Newton's law of cooling, which gives the relationship between the heat transfer rate Q and the temperature difference between the surface and the ambient as

$$Q = \alpha_k A(T_w - T_{amb}) \qquad (1.10)$$

where α_k is the average convective heat transfer coefficient, A is the total area of the vertical surface, T_w is the wall temperature and T_{amb} is the ambient temperature. The coefficient α_k depends on the flow configuration, cooling medium properties, dimensions of the heated surface, and generally also on the temperature difference, because of which the dependence of Q on $(T_w - T_{amb})$ is not linear. Since the fluid motion becomes zero at the surface due to the no-slip condition, which is generally assumed to apply, the heat transfer from the heated surface to the cooling medium in its immediate vicinity is by conduction.

The heat transfer coefficient represents an integrated value for the heat transfer rate over the entire surface, since, in general, the local value α_{kx} would vary with the vertical distance from the leading edge, x = 0, of the vertical surface. The local heat transfer coefficient α_{kx} is defined by the equation

$$\alpha_{kx} = Q_x / [A(T_w - T_{amb})] \qquad (1.11)$$

where Q_x is the rate of heat transfer per unit area per unit time at a location x, where the surface temperature difference is $(T_w - T_{amb})$, which may itself be a function of x (see Figure 3.39).

The average heat transfer coefficient α_k is obtained from equation (1.10) through integration over the entire surface area. Both α_k and α_{kx} are generally given in terms of a nondimensional parameter called the Nusselt number (Nu). An overall (or average) value Nu, and a local value Nu_x may be defined as

$$Nu = \alpha_k h/k, \text{ and } \quad Nu_x = \alpha_{kx} x/k \tag{1.12}$$

where h is the height of the vertical surface and k is the thermal conductivity of the cooling medium.

The **Stefan-Boltzmann Law** describes the radiation of heat phenomenon as being proportional to the difference of the absolute temperatures to the power of four ($T_2^4 - T_1^4$). In a reactor installation the radiation occurs mainly from the outer surface of the reactor's outermost cylinder facing and from the top and bottom of the cylinders. Thermal radiation is governed by the difference between the sources (T_1) and ambient temperatures (T_2), each raised to the fourth power

$$Q_{12} = \sigma \varepsilon A F_{12} (T_1^{\,4} - T_2^{\,4}) \tag{1.13}$$

Where σ is the Stefan–Boltzmann constant equal to $5.7*10^{-8} W/m^2K^4$, ε is the emissivity, A is the area and F_{12} the radiation view factor between surfaces 1 and 2. The emissivity of a material is the ratio of energy radiated by the material to energy radiated by a black body at the same temperature. It is a measure of a material's ability to absorb and radiate energy. A true black body would have an $\varepsilon = 1$ while any real object would have $\varepsilon < 1$. Emissivity is a numerical value and does not have units.

For two surfaces with aproximate same areas $A_1 \approx A_2$ and same emissivity factor (ε) the total emissivity factor (ε_{res}) is

$$\varepsilon_{res} = \varepsilon / (2 - \varepsilon) \tag{1.14}$$

For highly absorbing and emitting surfaces placed in close proximity to each other, F_{12} is close to unity. The value of F_{12} also approaches unity when determining the flow of radiant heat from a small, highly emitting surface to a large, highly absorbing surface that surrounds it on all sides. In our case with cylinders within each other and of practically the same hight, the radiation view factor is $F_{12} \approx 1$.

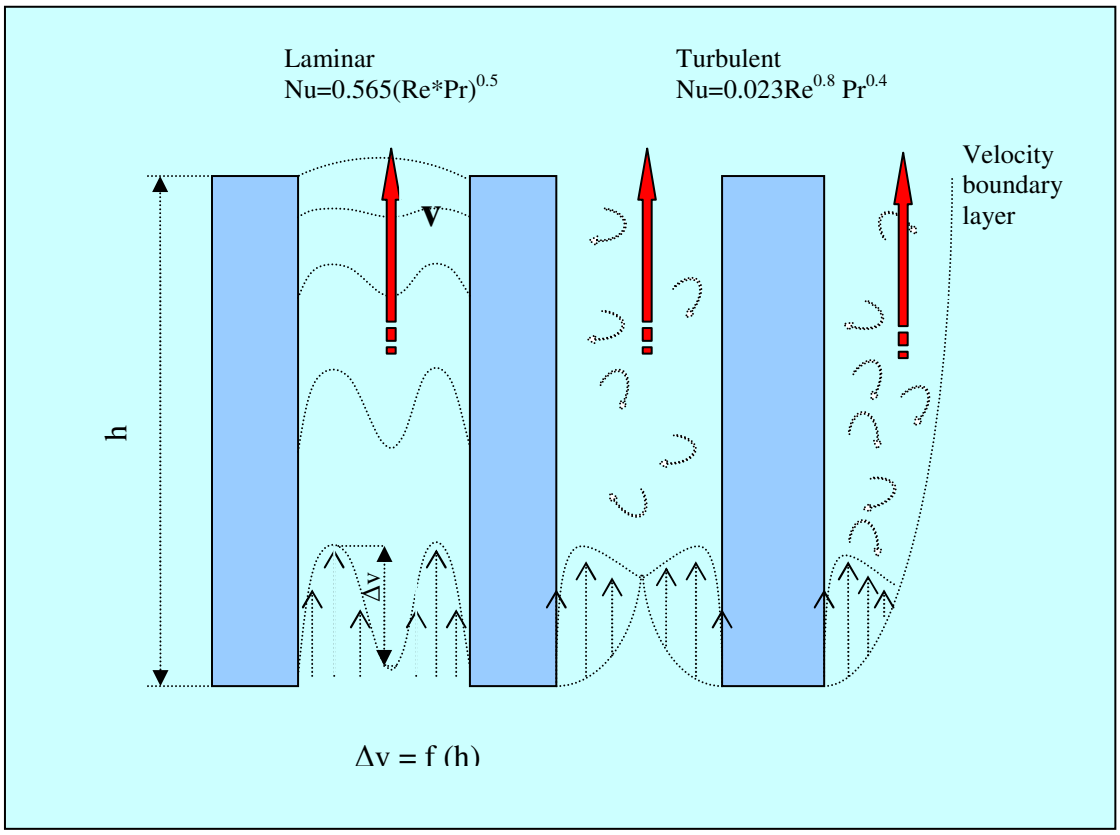

Figure 1.7: Air velocity between cylinders

Considering convection the cooling medium far from the vertical surface is stationary, since an extensive medium is considered. The fluid next to the surface is also stationary, due to the no-slip condition. Therefore, flow exists in a layer adjacent to the surface, with zero vertical velocity on either side, as shown in Figure 1.7. The temperature varies from T_w to T_{amb}. Therefore, the maximum vertical velocity occurs at some distance away from the surface. Its exact location and magnitude have to be determined through analysis or experimentation (Jaluria 1995).

The flow near the bottom or leading edge of the surface is laminar, as indicated by a well-ordered and well-layered flow, with no significant disturbance. However, as the flow proceeds vertically upward or downstream, the flow gets more and more disorderly and disturbed, because of flow instability, eventually becoming chaotic and random, a condition termed turbulent flow. The region between the laminar and turbulent flow regimes is termed the transition region. Its location and extent depend on several variables, such as the temperature of the surface, the fluid, and the nature and magnitude of external disturbances in the vicinity of the flow.

For laminar air flow between the cylinders the velocity arrows are as shown in Figure (1.7) above. Since there is no slip at the wall of cylinder, the velocity is there zero and increases towards the centerline of the cooling ducts. If the air velocity exceeds a critical Reynolds number ($Re_k \equiv v_m\ d/\nu_{kin.visk} \approx 2320$, were d is the hydraulic diameter depending on the dimensions of the cooling duct, and v_m is air velocity), the flow becomes turbulent (Schmitt and Beckmann, 1930).

At the outside wall of the cylinders, as long as the air velocity is low enough, the cooling air flow is laminar as shown in Figure 1.8 below (an example of velocity field at a vertical 120mm plate with ΔT to ambient of 10 degrees, modeled by FEMLAB®). When the air velocity increases, the air flow becomes also turbulent and then the cooling effect will be much better since the cooler ambient air will be mixed with the cooling air at the wall.

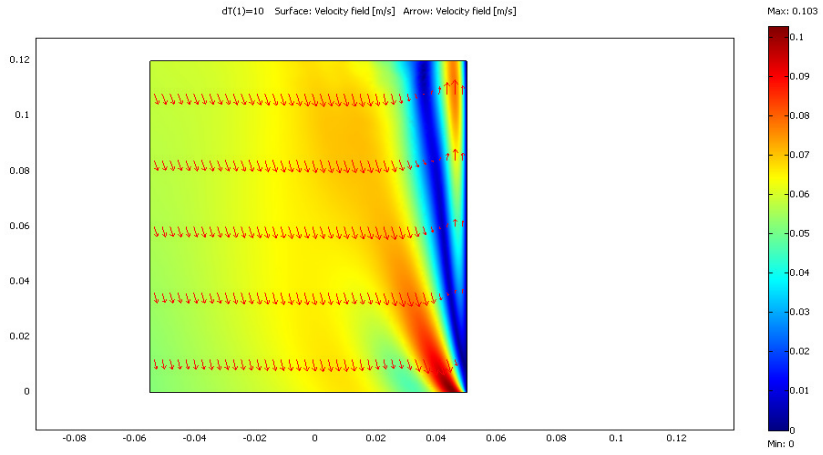

Figure 1.8: Free convection at a hot vertical plate with laminar air velocity field

1.6 Temperature sensing method

Conventional temperature sensing, such as thermocouples or platinum resistance thermometers provides information data at a single point. Using many of them could be interpreted as an average reading over a localized area.

As mentioned before, the temperatures of each cylinder are measured by means of optical wires embedded in the windings, so called Distributed wire-optic Temperature Sensors (DTS). Distributed temperature sensors use an optical wire, both as a temperature sensor and as a means of bringing the information back from the sensor to the terminal equipment. A laser source launches a pulse of light into optical wire. As the pulse travels down the wire, energy is lost through scattering. A fraction of the scattered signal is retained within the wire and a portion is directed back along the wire towards the laser source. This signal is called the backscatter-signal and can be optically filtered and handled with a detector. Moreover, the entire length of the wire is sensitive to temperature and each resolvable section of wire is equivalent to a point sensor. Depending on the wire length and the spatial resolution of the equipment, the wire can measure the temperature in several thousand locations, quasi-simultaneously. The position of each reading is calculated from the time taken for the light to travel out and back within the wire. This is possible because the speed of light propagation is known for each signal type.

A complete temperature profile of the optical wire is thus obtained and since the wire can be laid in contact with the object to be monitored, the length, surface or volume thermal profile of the object can be determined. Because distributed temperature sensors use optical wires as the sensing and communications element, they can be used in electrically noisy environments without any problems of interference. The fact that a single wire is able to replace many thousands of thermocouples simplifies wiring considerably and thus allows the technology to be used in applications where space, weight or wiring costs preclude traditional point sensors. An additional benefit of the technology is that the sensors can be made entirely from dielectric materials and in that sense are intrinsically safe. The operation of distributed temperature sensors is based on the optical time domain reflectometry (OTDR) technique, in which a short pulse of light is launched into the wire and the return signal is analyzed. The time from the launching of the pulse can be mapped directly into distance along the wire in a similar way to the measurement of target range in radars. The signal consists of light scattered by the glass in which the interrogating pulse is travelling. Some of the wavelength components (in particular the so called Raman anti-Stokes band) in the return signal are temperature-sensitive and these are used to determine the temperature along the wire. In order to separate the temperature variations from other factors which also influence the Raman backscatter signal, several referencing methods are used, including comparison with other wavelengths which are less sensitive to temperature and repeating the measurement, but launching into the opposite end of the wire (the latter then being installed in a loop configuration). In this way, an accuracy of +/- 0.3 ^{o}C can be achieved. (Appendix A)

In addition to this, the outside surface temperature of cylinder 5 and the inside surface temperature of cylinder 1 as well as of some cooling duct temperatures have been measured by thermocouples (TC) of type J.

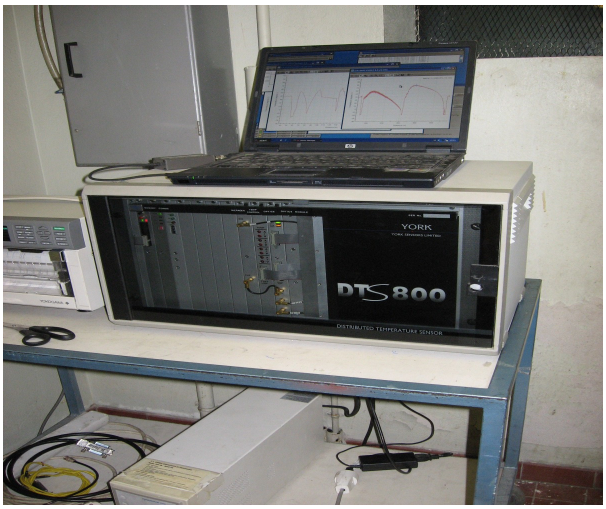

Figure 1.9: Measuring equipment for Optical Wires (OW) and the recorder of Thermocouples (TC) (left)

2 – Literature Review

There are not many research papers issued or published concerning the temperature behavior of an air core multi-cylinder reactor. It seems that this equipment is such a simple electrical machine that there is no interest to research them, or that the manufacturers are not willing to publish their research results.

However, even the simplest modern reactors are complicated, with many parallel winding layers and several cylinders within each other. Their precise design and optimization needs solid design, experiment and modern simulation programs.

The temperature behavior of reactor windings is in some cases similar to the windings of dry type transformers. Some articles about the temperature behavior of transformer windings are published. Gotter (1954) publishes one of the basic works, where the temperature behavior and designing of windings of transformers and rotating machines has been handled very fundamentally. In the same way Hak (1938) also wrote his basic work about the design and calculation of air core dry-type reactors. However, in those works multi-cylinder reactors and determining their hot-spot areas are not handled.

Steward & Whitman (1944) as well as Linden W.Pierce (1992, 1994) and Glenn Swift et.al. (2001) have published some works about hot-spot temperatures in dry-type transformers. Elmoudi (2006) presented an approach for computing the harmonic effects at winding temperatures and Yu (1996) the current distribution between cylinders.

Heat transfer problems, especially for determining the heat transfer coefficient and cooling air velocity in the case of symmetrically heated vertical parallel walls or ducts, has been researched by Schmidt & Beckmann (1930) and Sparrow & Gregg (1956) as well as Olsson (2004).

Dwight (1945) and Hak (1938) have presented the calculation of self- and mutual-inductances that are dependent on the physical dimensions of reactors. In addition, Grover (1937) has done basic research work, by determining the inductances, and published his famous handbook for the calculation of inductances in several different cases.

For example, Wien (1904), Black (1905), Emde (1912) and Rogowski (1918/1919) have made basic research work concerning the effect of different frequencies on resistances as well as their losses.

Dowell (1966) presented various methods for calculating the AC resistance of windings of inductors and transformers and effects of eddy currents. He has simplified the calculation by approximating the circular cross-section of a wire as a square and so using the trigonometric functions instead of Bessel-functions. The errors made by using trigonometric functions are marginal at lower frequencies. Perry (1979) and Ferreira (1994) have presented a similar simplified calculation method. Those methods operate more exact in the frequency band of 0.05-10kHz, which is where most of the high voltage reactors operate.

Burge and Fawzi (1978, 1991) as well as Putman (1979) have also handled eddy current effects in the design of reactors in their research work.

The simulation of the magnetic fields associated with monocylinder reactors (coils) and transformer windings by means of Finite Element Method (FEM)- electromagnetic analysis and simulating programs are presented in many research works, e.g. Chari & Csendes (1977), Konrad (1982), Preis & Stogner & Richter (1982), Chen & Konrad (1997), Malo (1993), Yu (1996), Elmoudi (2004) and Keitamo (2005).

However, works or articles about FEM-simulation for multi-layer and -cylinder reactors, where the proximity and skin effects of magnet fields and their losses with circular cross-section conductors inside or outside the reactor coil has been presented, are not available or have not yet been found in the public domain.

In addition, there are no articles available concerning mathematical handling or approach for optimizing the winding turns. The current distribution related to the temperatures of several cylinders is also lacking in the literature.

3 Research methods

3.1 Test reactor and measurements

The objective of this research work was to develop a dynamic thermal model for dry type air-core reactors, which could be used for optimizing the reactor construction for temperatures. This work involves the following research methods:

- Analytical calculations to define the currents in different coils of the reactor
- FEM-methods to obtain the magnetic fields and consequently the eddy current losses in windings
- Empirical model for temperature distribution
- Numerical calculation methods to find the required changes in the turn numbers of individual coil-windings needed for obtaining optimal temperature dissipation.

The above steps are arranged in the form of a solution algorithm described in 3.3.

A test reactor with wire optic temperature measurements was used to verify the developed model.

The test reactor in this research work was a five-cylinder reactor. During the manufacturing process, optical wire wires were installed into each cylinder to measure the temperatures, on the surface and/or in the middle, between the winding layers of each cylinder.

Figure 3.1: Optical wire-wire (OW) with 6.5 mm pitch

In addition, the optical wires have also been put into the cooling duct between each cylinder, as shown in Figure 3.2.

This, the so-called Distributed Temperature Sensing (DTS) system, allows the measurement of temperatures inside or at the surface of structures. The resolution of this DTS-system is 500mm. The configuration and method of this measuring system is represented in appendix A.

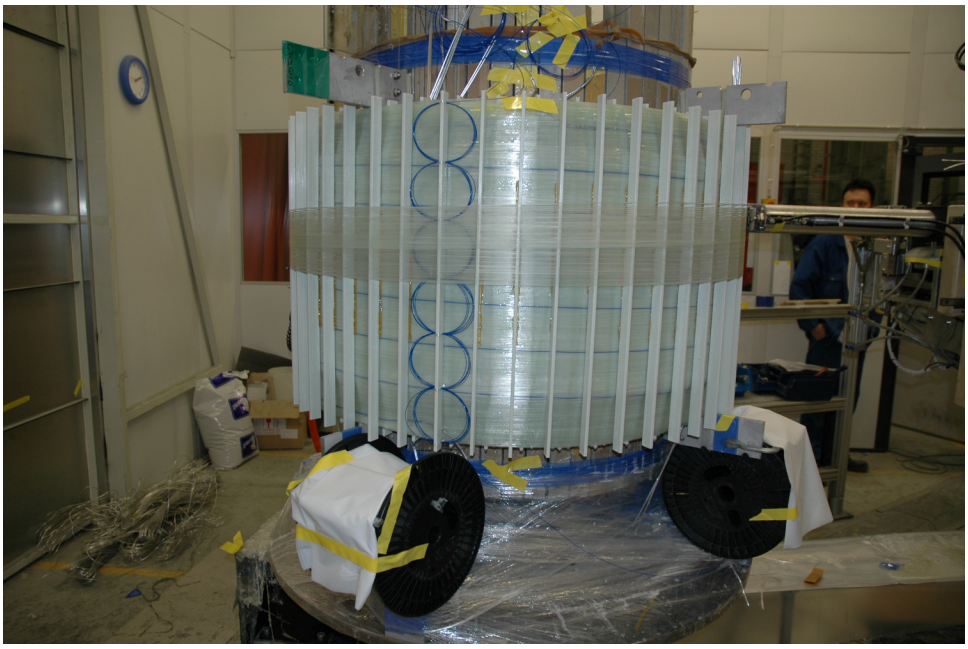

Figure 3.2: Optical wire-wire installed in cooling ducts between cylinders 1 and 2. (The OW at the outside surface of cylinder 1, with a pitch of 80mm, is shown as horizontal dark lines behind the spacers).

Table 3.1: Location of optical wires

	Outside surface	Inside Surface	In the windings
Cyl.1	X		
Cyl.2	X	X	X
Cyl.3	X		X
Cyl.4	X		
Cyl.5	X		X

There are four measuring loops (1...4) with lengths of 2*25m; 2*60m and 2*250m, which are formed as follows:

- The two shortest OWs, namely 2*25m, are in Loop 1 and installed in the cooling ducts so that one 25m wire was measuring the temperatures between cylinder 1 and 2 as well as between 2 and 3. The second OW was between 3 and 4 and between 4 and 5.

- The two 60m OWs (Loop 2) are used for surface temperature measuring with a pitch of 80mm. The first measured the outside surface of cylinder 1 and inside surface of cylinder 2, the second one the outside surfaces of cylinders 3, 4 and 5.

- The first 250m OW (Loop 3) in cylinder 2 was used for the measurement of the inside surface temperature and the temperatures in the winding between layers 3-4 of the 6 layer winding. The pitch of this OW was 6.5mm.

- The second 250m OW (Loop 4) was installed to measure the winding temperatures of cylinder 3 (between 3-4 of 5 layer winding) and cylinder 5 (between 3-4 of 7 layer windig) with the same pitch of 6.5mm.

All ends of the OWs were connected to a terminal plate made of plexi-glass (Figure 3.3), where several optical wires were connected in series with the measuring cables of the DTS-unit.

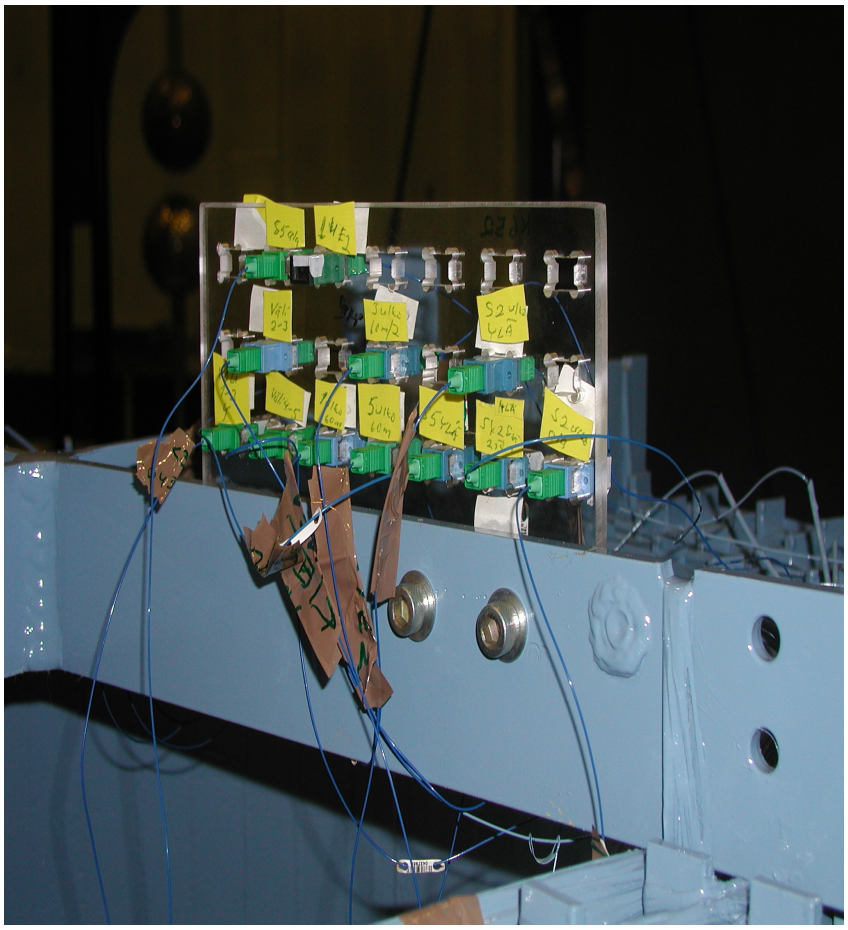

Figure 3.3: Terminal plate of OWs

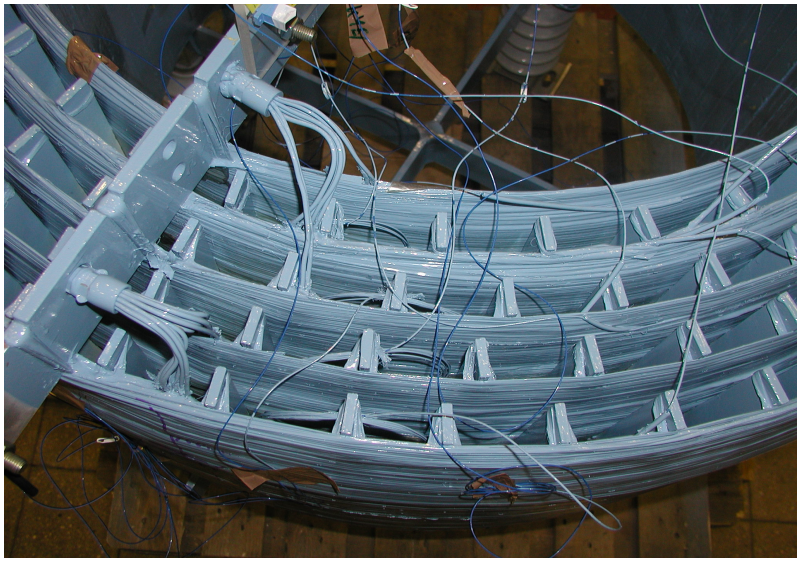

Figure 3.4: Several OW-connections and OWs in cooling ducts

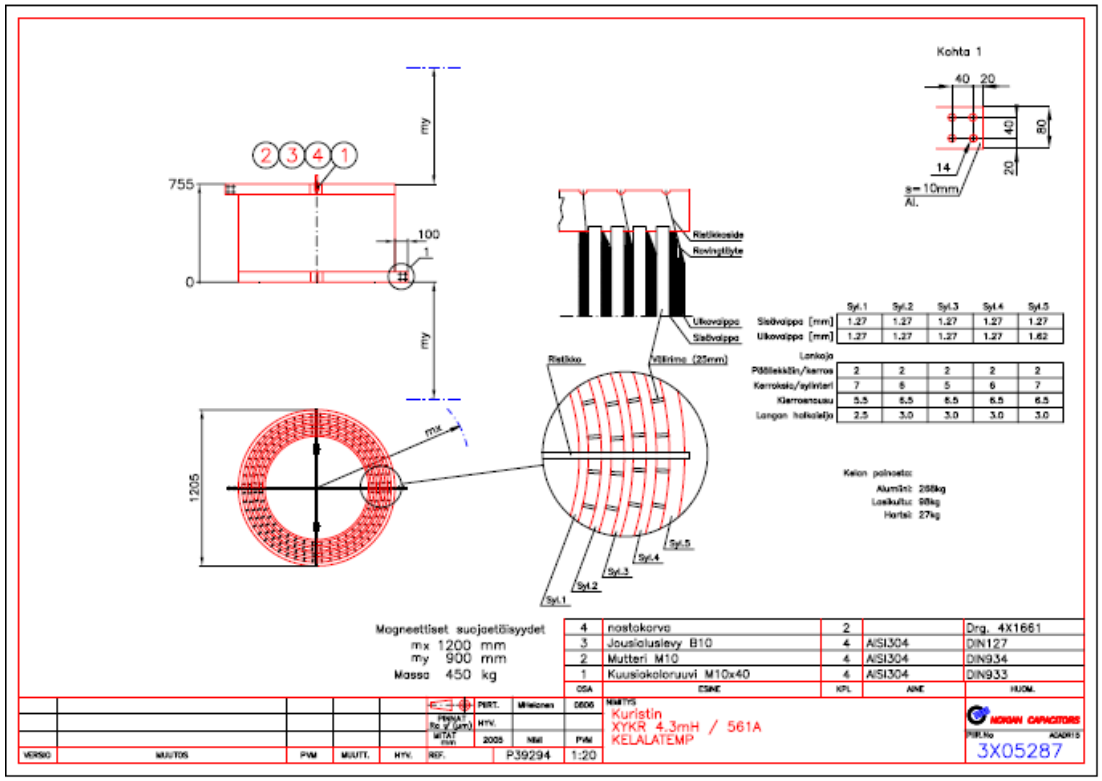

Figure3.5: Design drawing of test reactor

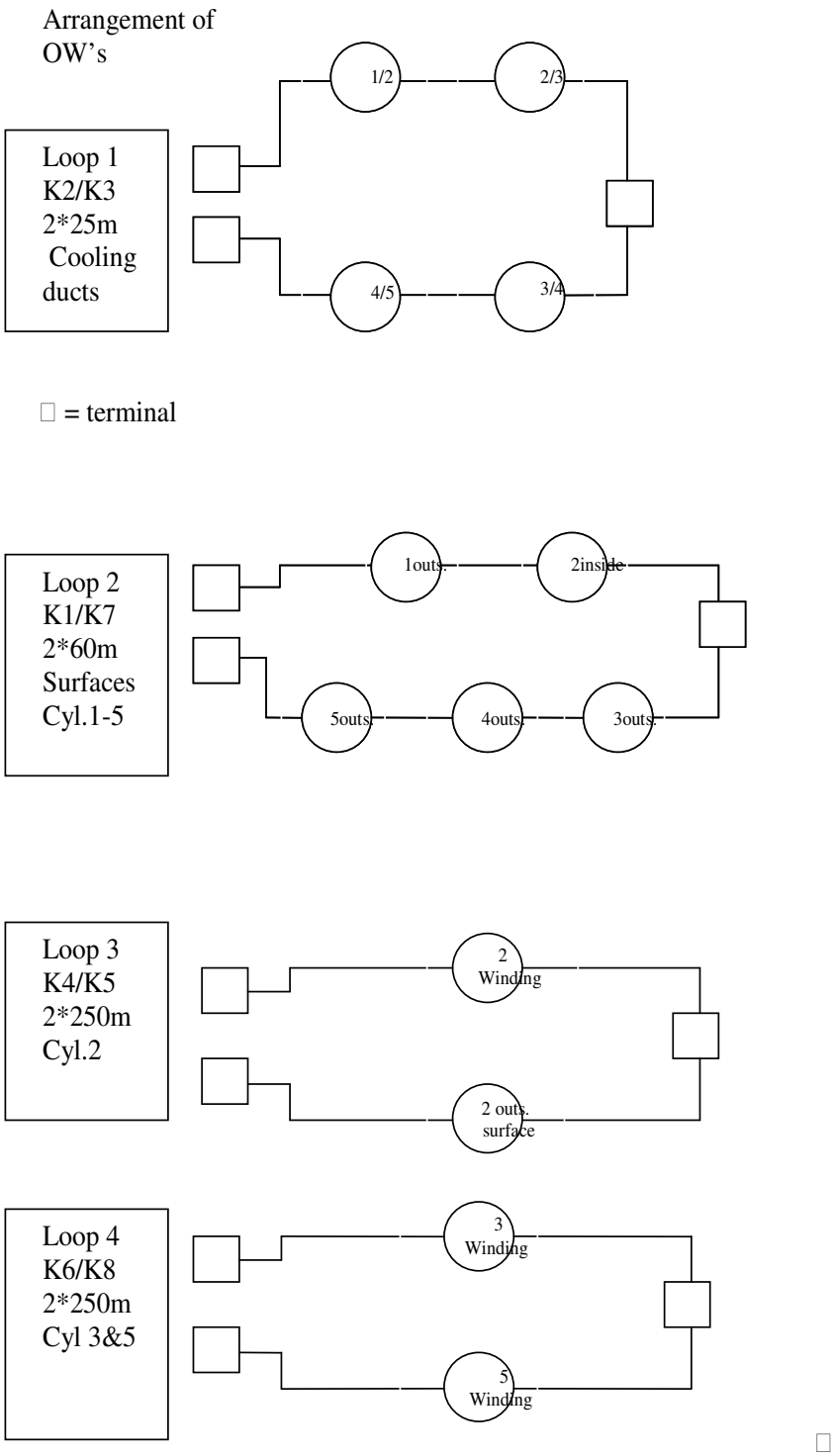

Figure 3.6: Measuring loops (L1...L4) of optical wires

Placing of optical wires on cylinders 1 to 5:

Cylinder 1. (Inner cylinder)

- Outside surface with a pitch of 80mm
- OW winding diameter 836 mm
- OW winding direction from top to bottom

Cylinder 2.

- Inner surface with a pitch of 80 mm
- OW winding diameter 891 mm
- OW winding direction from bottom to top (25.2m / 9 turns in roving at the top of cylinder).
- Inside cylinder between layers 3-4 with a pitch of 6.5mm (80 turns)
- OW winding diameter 909 mm
- OW winding direction from bottom to top (25.7m / 9 turns in roving at the top of cylinder).
- Outside surface with a pitch of 6.5mm (77 turns)
- OW winding diameter 925 mm
- OW winding direction from bottom to top (20.3m / 7 turns in roving at the top of cylinder).

Cylinder 3.

- Inside cylinder between layers 3-4 with a pitch of 6.5mm (69 turns)
- OW winding diameter 998 mm
- OW winding direction from bottom to top (28.2m / 9 turns in roving at the top of cylinder).
- Outside surface with a pitch of 80mm
- OW winding diameter 1009 mm
- OW winding direction from top to bottom

Cylinder 4.

- Outside surface with a pitch of 80mm
- OW winding diameter 1098 mm
- OW winding direction from bottom to top

Cylinder 5.

- Inside cylinder between layers 3-4 with a pitch of 6.5mm (62 turns)
- OW winding diameter 1171 mm
- OW winding direction from bottom to top (11.0m / 3 turns in roving at the top of cylinder).
- Outside surface with a pitch of 80mm
- OW winding diameter 1193 mm

- OW winding direction from top to bottom (Attn: The end of OW was too short and so only 4 turns are at the outside surface of cylinder 5)

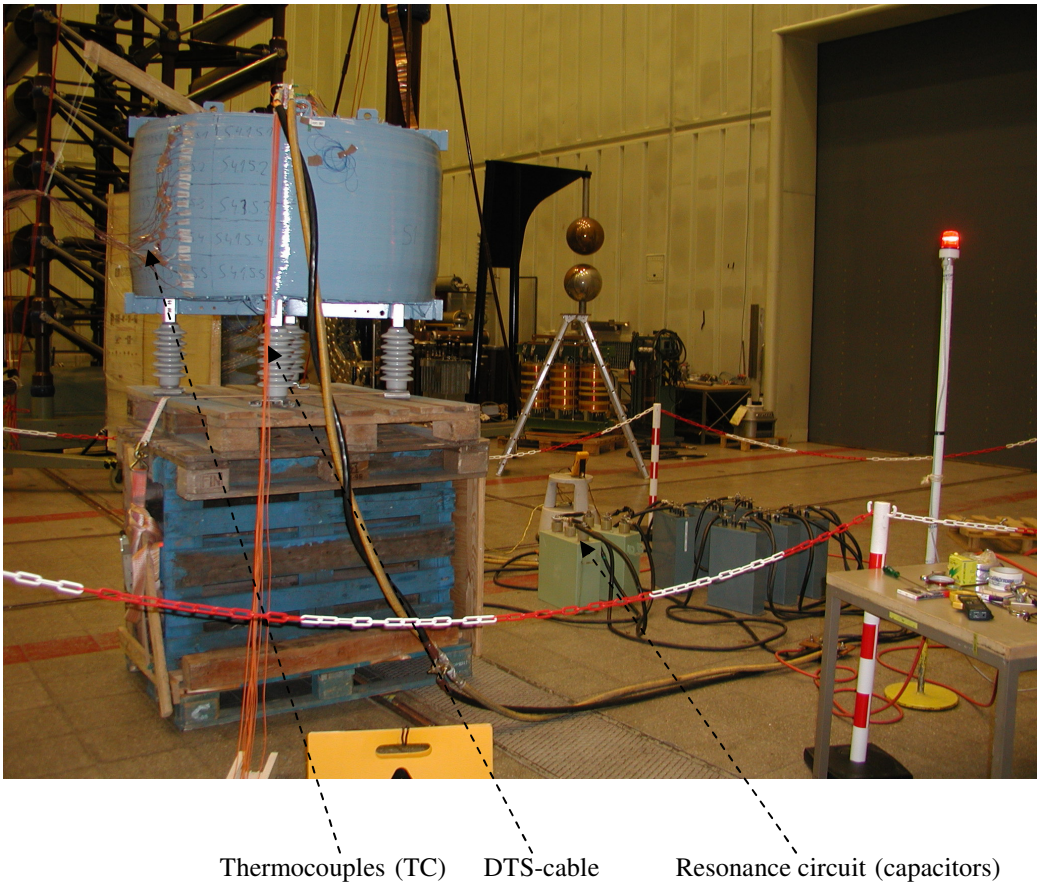

Figure 3.7: Measuring arrangement

In Figure 3.7 are shown the thermocouples (20 pcs / 30mm distance) at cylinder 5 for verifying the results of the OW-measurements as well as the connection cables of DTS-unit, which was located in a separate room because of the strong magnet field of the reactor. For the loading current (I=608A) needed in the temperature measurements, there was an 100% compensated resonance circuit with the test reactor and capacitors. The winding layers of cylinder 1 were made by 2.5mm PVC-insulated aluminium wire and the winding layers of cylinders 2 to 5 by 3.0mm aluminium wires. The example in Figure 3.8 shows a section of cylinder with two-layer winding.

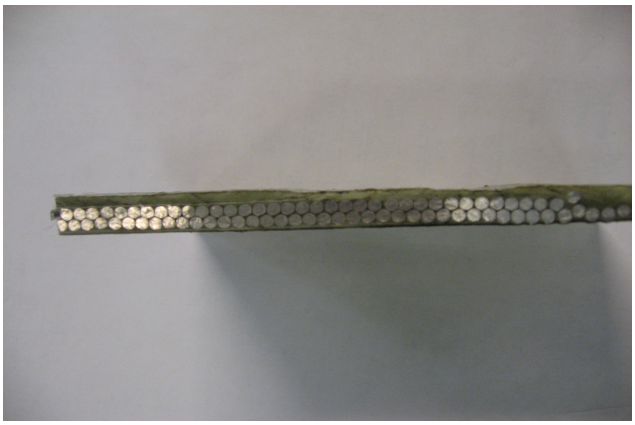

Figure 3.8: Two layer construction (3mm Al-wire without OW)

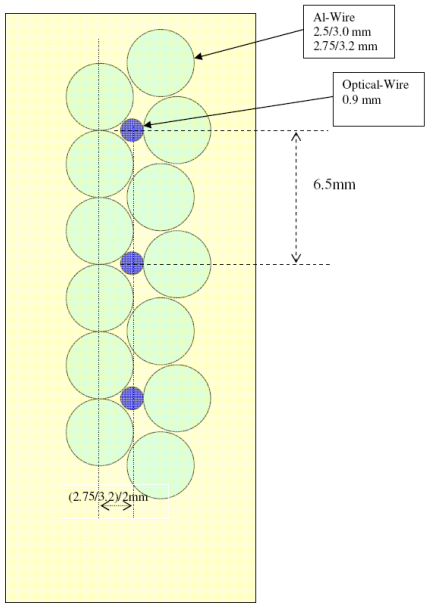

Figure 3.9: Location of embedded optical wires between layers

Temperature measurement over the whole length of the cylinder surface with thermocouples (TCs) was possible in our case on the inside surface of cylinder 1 and the outside surface of cylinder 5 (Figure 3.7) only.

For temperature measurement in the cooling ducts a wooden stick construction as shown in Figure 3.10 was used. The thermocouples were fixed at 30mm distances by a stick which was located in the cooling duct, as shown in Figure 3.10.

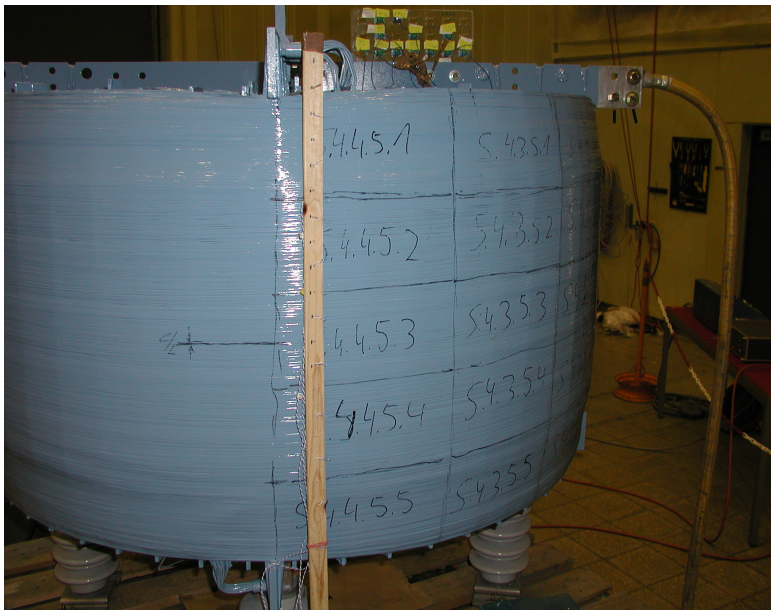

Figure 3.10: Wooden measuring stick with thermocouples (TCs)

Figure 3.11: Stick with thermocouples (TC) located in the cooling duct between cylinders 1 and 2

The result of this measurement was not ideal since the TCs normally need a good contact with the measured obstacle and therefore the measurement of air temperature by means of thermocouples is not very accurate.

As an example, the steady state temperature curves of loops 3 and 4 (cylinders 2, 3 and 5) measured by optical wires at a loading current of 608A are shown in the following Figures, 3.12 and 3.13.

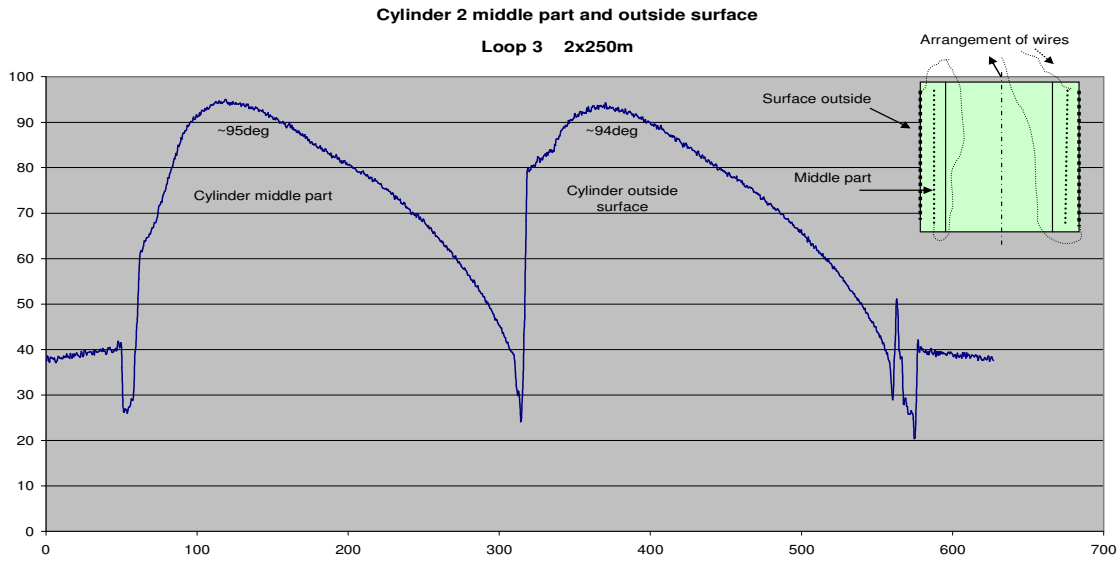

Figure 3.12: Temperature graph of loop 3 and OW arrangement

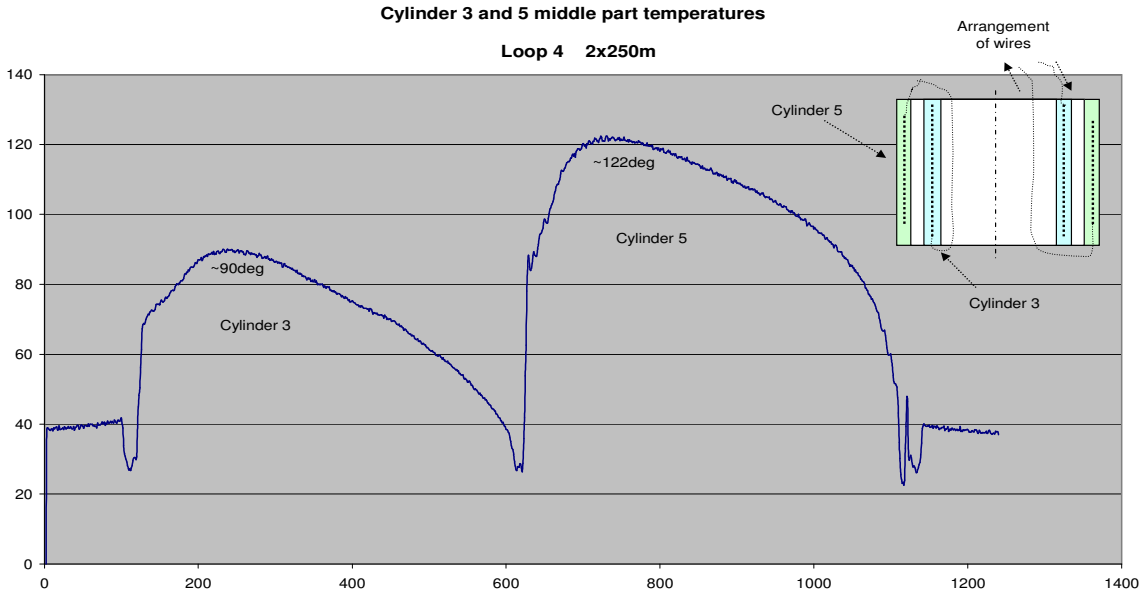

Figure 3.13: Temperature graph of loop 4 and OW arrangement

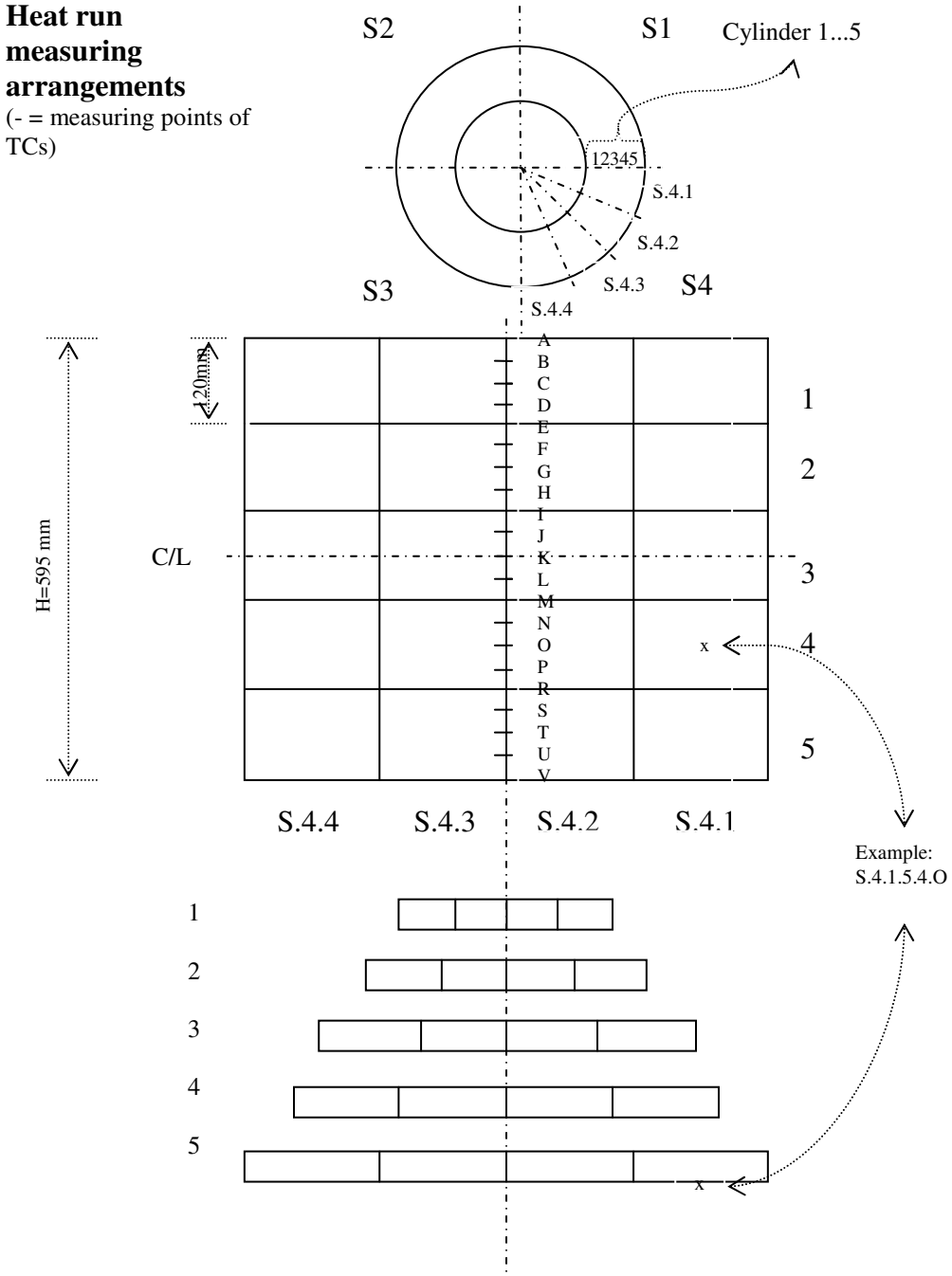

Figure 3.14: Measuring chart for surface temperature measurements by thermocouples (TCs)

3.2 - Cooling Room (arctic-) Tests

The motivation of this test was the fact that some air-core reactors installed in high voltage substations, which are located in very cold and snowy regions in Finland (like in Lapland), have had serious problems and failures. It was assumed that one reason would be the heavy and sustained snowfall combined with a cyclic reactor operation, which would lead to ice formation in the cooling ducts. To prove this the assumed situation was simulated and the different temperatures of our test reactor were measured by optical wires during this arctic test.

The reactor was installed in the cooling room and the temperature measuring equipment (York's DTS 800) was connected with the optical wires. Ten (10) thermocouples (TC type J) were also fixed to the outer side of cylinder 5 so that the first one was connected to the bottom spider arm and the last one (no 10) was on the top spider arm. Other TCs were fixed within approximately 7cm distance on the cylinder wall. The TCs were used for control purposes only.

The temperature in the room (as well as in the reactor) was + 20 $^{\circ}$C before the cooling equipment was switched on.

As soon as the ambient temperature in the room went below zero, the top of the reactor was covered with approximately 15...20 cm of very wet snow (Figure 3.15).

Fig 3.15: Reactor with snow cover

The room-coolers were running the whole night and in the morning the room (and reactor) temperature was – 37 °C.

After that the reactor was energized with a current of 608A and became warmer. At the same time the room-coolers were running with full power and kept the room temperature constant (-26, 5°C measured with a calibrated temperature meter by Vaisala) during the test.

The snow began to melt away and the water, which ran into the cooling ducts, froze again at the bottom of the reactor. Some of the cooling ducts were almost full of ice and long ice sticks were hanging out of cooling ducts. The proper circulation of cooling air was thus prevented.

Figure 3.16: Reactor about one hour from the beginning of test

After 6 hours the temperature rise of the reactor was stopped and the end temperature was reached (as measured by the TCs, which showed the maximum temperature of +53, 1°C at 22 cm from the top of cylinder 5) so that the current could be switched off. The room-coolers were still running keeping on the ambient temperature as low as possible.

The reactor got cooler but the snow was still melting on the top and more and more water was running down the cooling ducts.

The next morning the coolers were still running and the temperature of the reactor was -35.7 °C. The frozen water had filled some of the cooling ducts, but there was still snow on the top of reactor.

It is assumed that if the reactor had been powered again the melted water would have run down until finally, the frozen water would have plugged the ducts and the warmer water would have

filled the cooling ducts. After that, the water would have frozen on the top of the reactor (since on the top the temperature would have fallen down below zero degrees while the hot-spot area would have been warmer. The bottom temperature was -16.8°C and the top temperature at the same time +2.8°C, but the hot-spot temperature was +50.0 °C). Now the cooling ducts would have become be full of water but plugged at both ends by ice. When a reactor in this situation would be switched off again and remain at very deep ambient temperatures, the frozen water in cooling ducts could lead to strong tensions between the cylinders and later damage or bend the cylinder walls. That situation could be one of the reasons why some reactors have been damaged in Lapland.

(Because of our build-in optical wires in the test-reactor, we did not continue this scenario to the point of destruction).

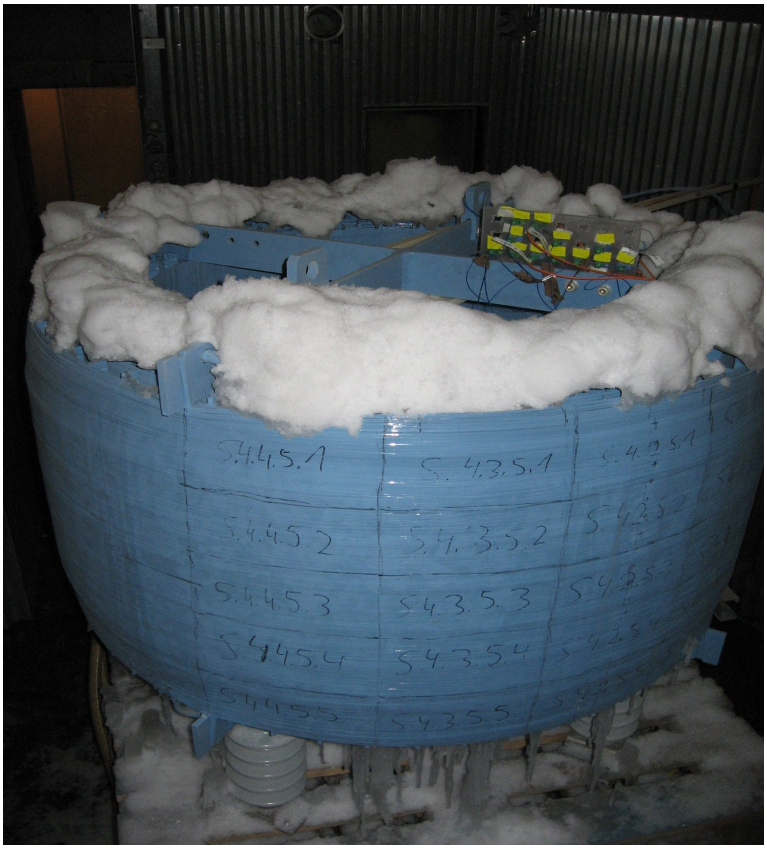

Figure 3.17: The reactor during the arctic test

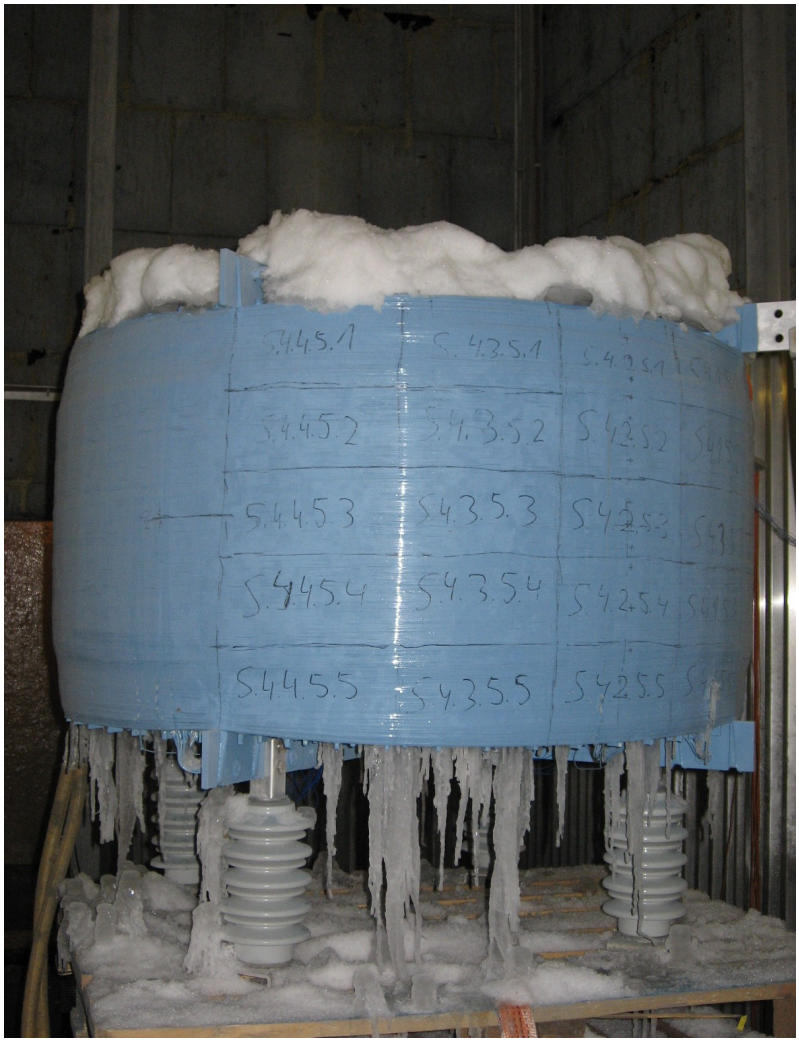

Figure 3.18: Icicles hanging on reactor

The results from the arctic test show that in spite of reduced cooling air flow the temperature rise in the reactor was not higher than that what was measured before with ambient temperature of +20 °C. That means that the sizes of the cooling ducts in our test reactor were sufficiently dimensioned.

The optical wires have well passed those extreme situations, as shown in Figure 3.19, where the wires are embedded in ice.

Figure 3.19: Optical wires embedded in ice

Figure 3.20: Cooling ducts with frozen water

The outer surface temperatures of Cylinder 5, measured by thermocouples (TC) as well as by optical wires (OW) during the arctic test, are shown in Figures 3.21 and 3.22:

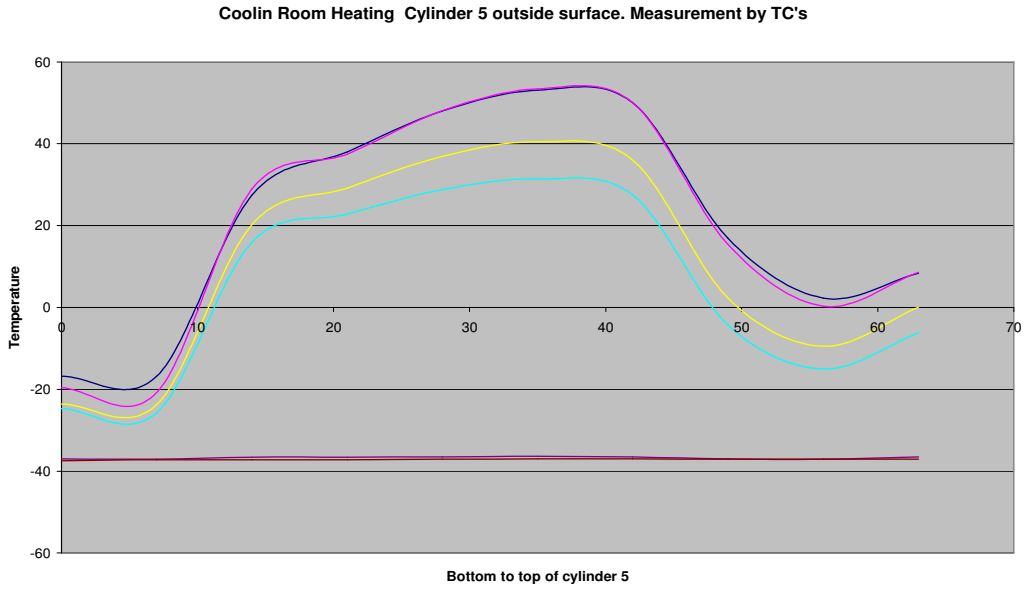

Figure 3.21: Temperatures measured by TCs on cylinder 5 at several points in time

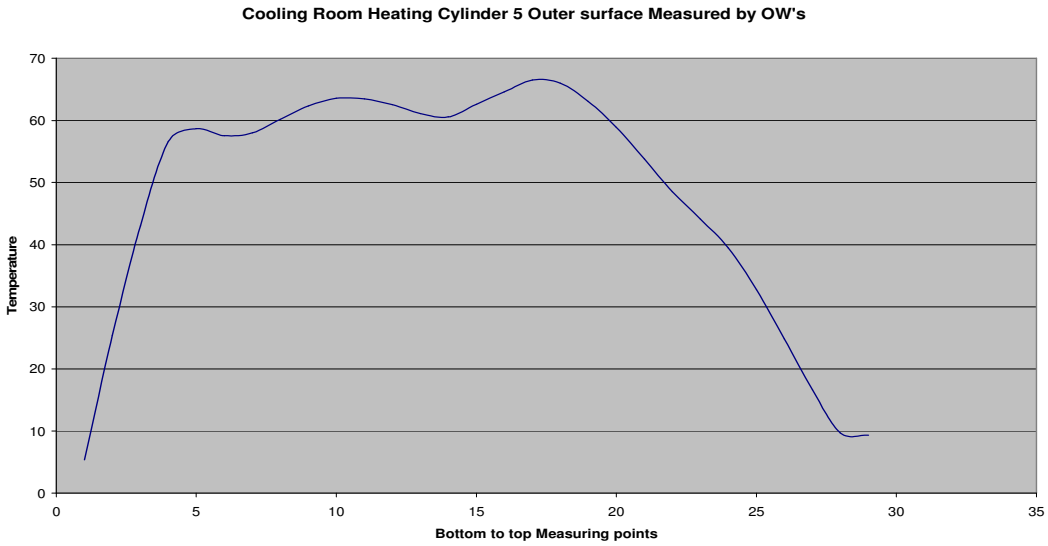

Figure 3.22: Temperatures measured by OW at cylinder 5

The shapes of these curves are almost identical with those measured in normal room temperatures. In the following figures the temperature curves show clearly, the warmer areas and the hot-spot place can exactly be calculated by means of counting of the layers of the optical wires when the location, pitch and dimensions of the embedded wires are known.

The different layers of OWs are shown in the temperature curves because the reactor was put in the test room under the cold air duct in the roof in such a manner, that the air flow from the duct of the cooler was not symmetrical but a little away from the center of reactor. In that way, one side becomes more cooled than the other side. Therefore, the opposite sides of the reactor had small temperature differences, which can be demonstrated in the curves.

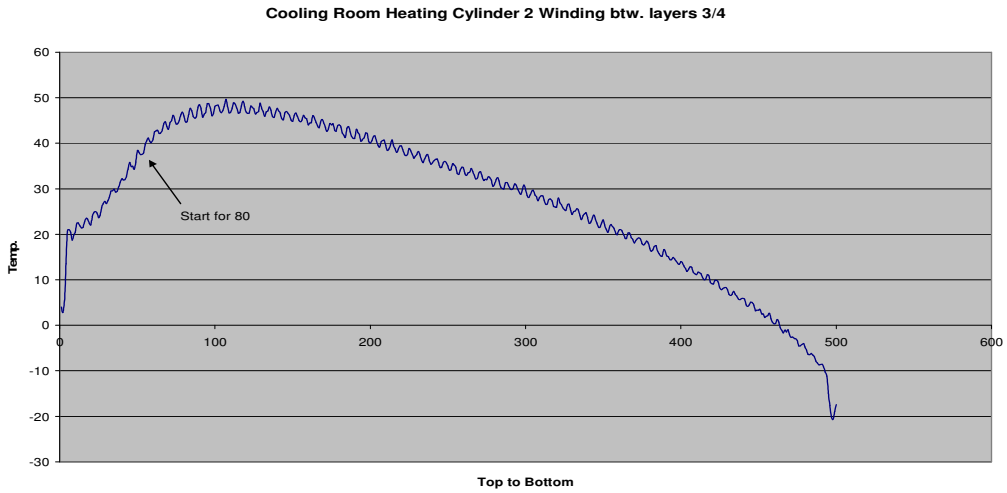

Figure 3.23: Cylinder 2 temperatures during the arctic test with an ambient temperature of about -37 °C

For comparison with Figure 3.23 above, Figure 3.24 below shows the test results from temperature measurements of the same cylinder with an ambient temperature of +20 °C.

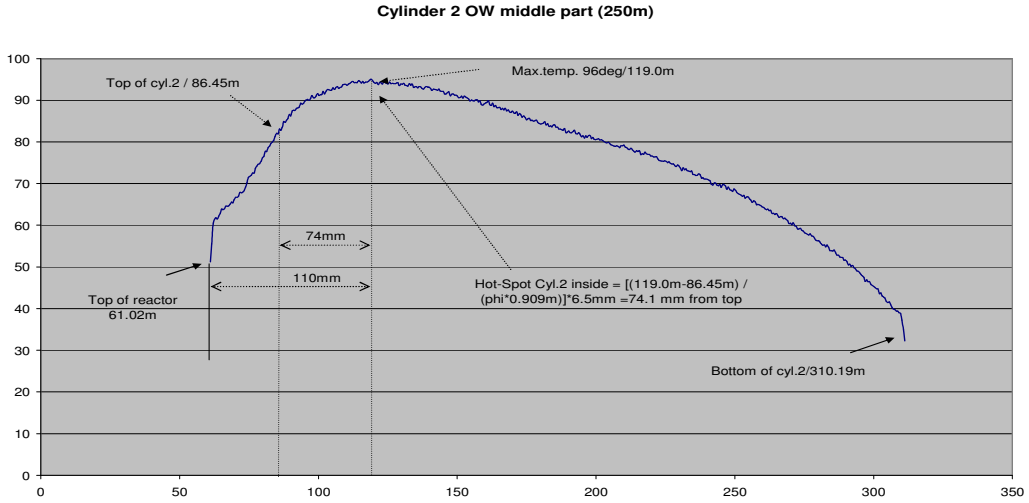

Figure 3.24: Cylinder 2 temperatures measured with an ambient temperature of +20 °C.

Further, in the following Figures 3.25 and 3.26 the temperature curves from the winding of Cylinder 5 during the arctic test with an ambient temperature of -37 °C and during another test with an ambient temperature of +20 °C are demonstrated.

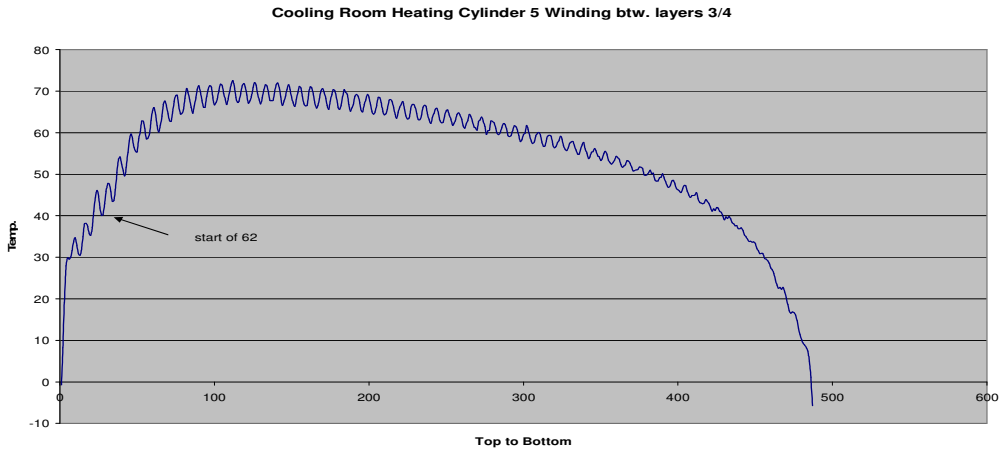

Figure 3.25: Cylinder 5 winding temperatures (between layers ¾) with OWs. Ambient temperature was about -37◦C

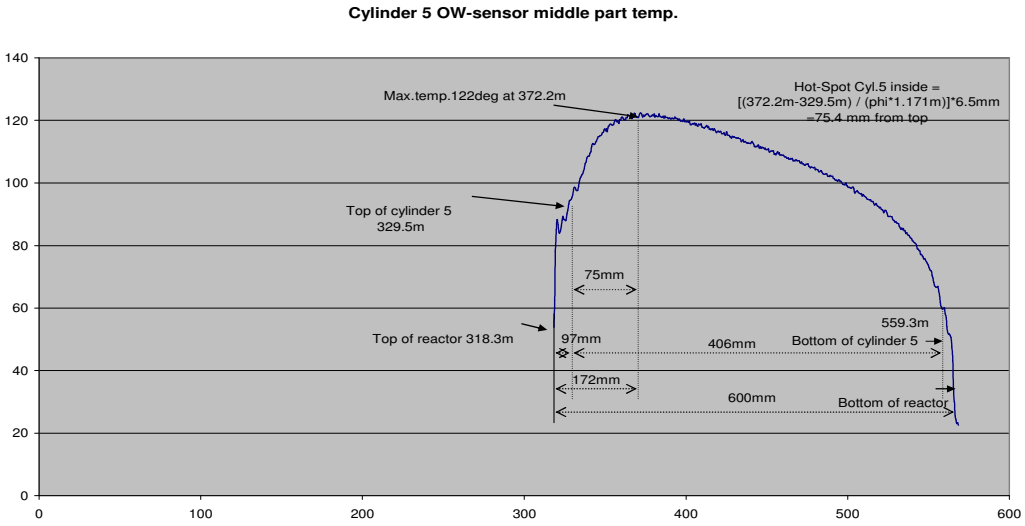

Figure 3.26: Cylinder 5 winding temperatures (between layers ¾) with OWs. Ambient temperature was +20◦C

3.3 - Developed solution method for dynamic thermal modeling and reactor optimization

This chapter will illustrate the dependence of several steps in this research work on each other.

In the following structural diagram of the analytical thermal model of the reactor, the different steps are shown with modules A and I...IV. The dependency of each module on the total number of turns in the reactor coil is also mentioned. The number of turns will establish the current distribution in the reactor as well as between the cylinders and in that way directly influence the total power losses and hot-spot temperatures of each cylinder.

After this diagram the internal calculation of each module will be demonstrated separately in simplified style.

The aim of this dynamic thermal modeling is:

The power losses shall be defined and optimized in each cylinder so that the final temperatures in each cylinder are as close as possible to each other and near to the rated limits, but will not exceed the temperature values given in the standards.

Modules A and I to V are as follows:

A -: Presumption

The rated current I_n and total impedance Z_n of the reactor are determined and known.

The current density $\mathbf{i_s}$ as well as the numbers of cylinders with their physical dimensions are fixed.

The optimal temperature design is now: $T_1 = T_2 = ... = T_i \leq T_{max}$

Where T_i is the temperature rise cylinder i and T_{max} is the maximum allowed hottest- spot temperature rise according to the standards.

The temperature (T) of a single cylinder in an air-core reactor is dependent on the following matters:

$T = f$ (losses (P_{th}); cooling)
Cooling = f (Conduction; Convection; Radiation; Ambient/ΔT)
$P_{th} = f$ (P_w; P_{ec})
$P_w = f$ (I^2; R)
$R_{dc} = f$ (ρ; l(N); r_{wire})
$R_{ac} = f$ (δ; r_{wire})
$P_{ec} = f$ (f^2; B^2; δ; ρ)
$R = f$ (R_{dc}; R_{ac})
B = f (I, Dimensions)
$\rho = f$ (ΔT)
$\delta = f$ ($\rho^{1/2}$; $(f^{-1})^{1/2}$)
$I_n = f$ (U; Z)
$Z = f$ (R; f; L; (C_s;C_m))
$L = f$ (L_{nn}; M_{mn}) = f (N^2; Dimensions, (T))

where,

T = Cylinder temperature
ΔT = Temperature difference
P_{th} = Total losses
P_w = Winding losses
R_{dc} = DC-resistance
R_{ac} = AC-resistance
P_{ec} = Eddy current losses
R = Resistance
B = Magnetic flux density
ρ = Resistivity of conductor material
δ = Depth of penetration
I = Current
Z = Impedance
L = Total inductance
L_{nn} = Self inductance
M_{mn} = Mutual inductance
f = frequency
N = Number of winding turns
C_s = Self capacitance
C_m = Mutual capacitance
U = Voltage
r_{wire} = Radius of conductor
Dimensions = The physical dimensions of cylinder

Assumptions:

The self and mutual capacitances (C_s / C_m) of the reactor are very small and can be ignored (Hak 1938) and it is assumed that the inductances (L) are independent from the coil temperatures (which is not really true since the dimensions slightly change when temperature changes) and from the proximity effect (which has an influence on the inductance in the reactors with thicker conductors).

I – Calculation of current/current distribution in and between cylinders

$$[\mathbf{J_{coil}}] = [\mathbf{V}][\mathbf{Z}]^{-1} \tag{3.1}$$

The impedances [Z] (or inductances [L]) of the cylinders will be determined (which, in an air core reactor operating at nominal frequency depend on their dimensions and numbers of turns only).

II – Calculation of losses in each cylinder

As stated before, the total losses of each cylinder can be calculated as follows,

$$\mathbf{P_{th} = P_w + P_{ec}} \qquad (3.2)$$

The influence of harmonic frequencies, especially the higher ones, on the total losses is considered later on (see Appendix C and FEM-results).

III – Calculation of temperatures in each cylinder

$$\mathbf{Q = (d\theta/dt)C_{th} + (\theta-\theta_{amb})/R_{th}} \qquad (3.3)$$

where,

Q = heat flow

θ = temperature

θ_{amb} = ambient temperature

R_{th} = thermal resistance

C_{th} = thermal capacity

Nusselt (Nu), Prandtl (Pr) and Grashof (Gr) numbers have to be determined empirically. Temperature transient coefficients and temperature resistances for conduction, convection and radiation will be determined. Analogous thermal circuits for calculating the heat flows and temperatures will be performed and the calculated results will be compared with measured values.

IV - Optimizing

By changing the outer dimensions or winding-turns (ΔN) the change in self- and mutual inductances has a direct influence to the current distribution in and between the cylinders, which further has influence on the losses and thus to the temperature rise.

Since the physical dimensions are fixed, as assumed before, the only way to determine the temperatures are to calculate and design the number of winding-turns in each cylinder in order to reach the required current distribution between cylinders.

V - Verification:

The calculated results of the current distributions will be verified with the measured values as well as the results of temperature measurements with the optical wires in each cylinder.

The structural diagram of the analytical thermal model of the reactor is as follows

(Figure 3.27):

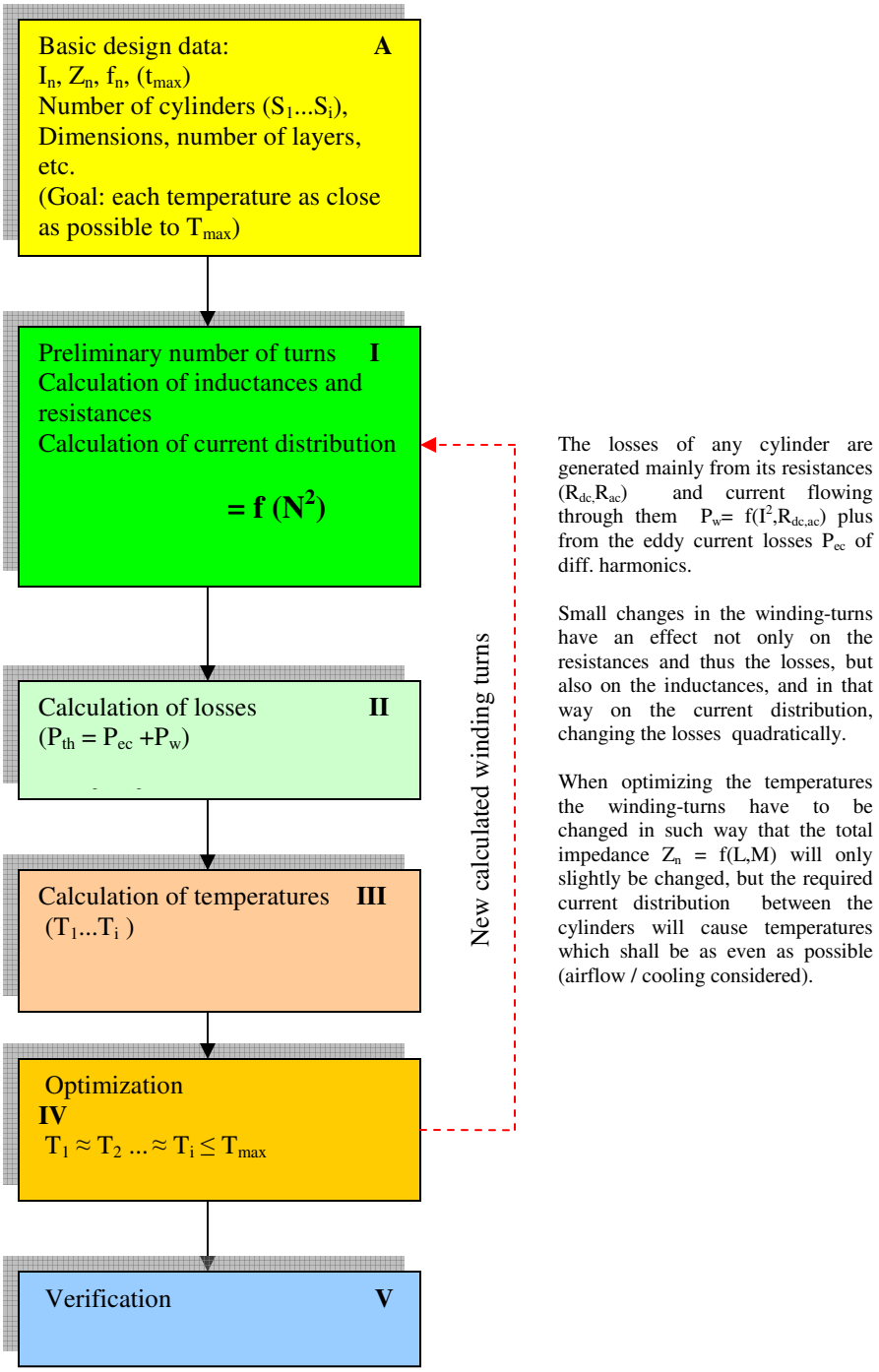

Figure 3.27: Structural diagram of the analytical thermal model of the reactor

The modules in Figure 3.27 are explained in more detail as follows:

I - Calculation of current distribution:

Self-inductances: L_{11}.... L_{nn}

$$L_{nn} = \mu_o N^2 \pi D^2 K/(4H), \qquad (3.4)$$

where:

μ_o = permeability of vacuum ($4\pi 10^{-7}$ Vs/Am)
H = height of cylinder
D = diameter of cylinder
N = number of winding turns
K = factor which takes the effects of cylinder ends into account (Grover 1973)

Mutual inductances: M_{12}...M_{mn}

$$M_{mn} = 2\pi^2 r^2 N_1 N_2 K/(R^2+H^2)^{1/2} \quad [\mu H] \qquad (3.5)$$

where:

r = radius of smaller cylinder (cm)
R = radius of larger cylinder (cm)
H = height of larger cylinder (cm)
K = f(r, R, H, H_p) (a factor calculated using a series of elliptic integrals) (Dwight 1945)
H_p = height of smaller cylinder (cm)

$$Z_{nn} = R_s + j\omega L_{nn} \qquad (3.6)$$

$$R_s = R_{dc} + R_{ac} \qquad (3.7)$$

$$Z_{mn} = j\omega M_{mn} = Z_{nm} \qquad (3.8)$$

R_s = total resistance, which also depend on N, f and T

Thus, the impedance matrix is:

(5 cylinders)

$$[Z] = \begin{vmatrix} Z_{11} & Z_{12} & Z_{13} & Z_{14} & Z_{15} \\ Z_{21} & Z_{22} & Z_{23} & Z_{24} & Z_{25} \\ Z_{31} & Z_{32} & Z_{33} & Z_{34} & Z_{35} \\ Z_{41} & Z_{42} & Z_{43} & Z_{44} & Z_{45} \\ Z_{51} & Z_{52} & Z_{53} & Z_{54} & Z_{55} \end{vmatrix} \qquad (3.9)$$

$$[Z][J_{coil}]^T = [U][V]^T \quad (3.10)$$

where

[U] = [1...1] uniform vector

[Z] = Impedance matrix from self- and mutual inductances
$[J_{coil}] = [J_1...J_n]$ current matrix from cylinder's currents

[V]= [V...V] voltage matrix over the cylinders

(Since the voltage over all cylinders is the same, and related to the impedances the currents are linearly distributed, the uniform vector can be used instead of voltage vector)

The total current (I) in the reactor is:

$$[U][J_{coil}]^T = I \quad (3.11)$$

and the current distribution between cylinders is: (Yu 1996)

$$J_{coil} = Z^{-1}U^T(UZ^{-1}U^T)^{-1}I \quad (3.12)$$

It can be shown, that the current distribution depends on the number of winding-turns to the power of two only **(N^2),** when the physical dimensions of reactor are kept unchanged.

The current distribution between the different winding-layers of the cylinders is calculated in same way.

II - Calculating of losses:

Winding loss at high frequencies is caused by eddy-current effects. Generally, eddy current effects are divided into skin effect and proximity effect. The classical definition of skin effect loss is the extra AC loss in a single isolated conductor which is carrying a time-varying current. And the corresponding definition of proximity-effect loss in a winding is defined as the total eddy-current loss minus the classical skin-effect loss (Sullivan 1999).

In the design and optimization of equipment such as reactors and transformers used in power applications, accurate prediction of high-frequency winding loss is very important. Eddy-current winding loss, which includes skin-effect loss and proximity-effect loss, increases rapidly with frequency.

An air-core reactor coil made of circular cross-section conductors generally can be modeled by an appropriate number of circular cylindrical conductor segments of finite length. The total magnetic field strength at a field point is the vectorial summation of the magnetic field strength of each conductor segment. For a large air-core reactor coil, the conductor size is normally much smaller than the coil diameter. Therefore, a large reactor coil can usually be modeled by circular cylindrical bar segments instead of general circular cylindrical segments to enhance the computation efficiency. In those cases where the coil conductor is not thin compared with the coil diameter, or the coil curvature is relatively sharp, the coil has to be modeled by segments with oblique end planes to reduce the number of segments used. (Yu 1996)

The calculation of steady-state skin effect problems in multiconductor systems is often of high importance to designers. Since in many problems the total currents in the conductors are given, the classical diffusion equation cannot be applied directly.

Another difficulty arises when the multiconductor system consists of some sub-systems with series connected conductors and given voltages. In this case the total currents in the respective sub-systems are of unknown values. Typical multiconductor systems of this kind are transformer windings and reactors. A finite element solution of such problems can be obtained using, for example, the superposition principle or the integrodifferential approach (Preis 1983).

The problem of electromagnetic analysis on a macroscopic level is the problem of solving Maxwell's equations subject to certain boundary conditions. Maxwell's equations are a set of equations, written in differential or integral form, stating the relationships between the fundamental electromagnetic quantities. These quantities are the electric field intensity E, the electric displacement or electric flux density D, the magnetic field intensity H, the magnetic flux density B, the current density J and the electric charge density ρ.

The equations can be equationted in differential or integral form. The differential form is presented here, because it leads to differential equations that the finite element method (FEM) can handle. For general time-varying fields, Maxwell's equations can be written as

$$\nabla \times \mathbf{H} = \mathbf{J} + \frac{\partial \mathbf{D}}{\partial t}$$

$$\nabla \times \mathbf{E} = -\frac{\partial \mathbf{B}}{\partial t}$$

$$\nabla \cdot \mathbf{D} = \rho$$

$$\nabla \cdot \mathbf{B} = 0$$

The first two equations are also referred to as Maxwell-Ampere's law and Faraday's law, respectively. Equation three and four are two forms of Gauss' law, the electric and magnetic form, respectively.

Another fundamental equation is the equation of continuity, which can be written as

$$\nabla \bullet \mathbf{J} = -\partial \rho / \partial t$$

.

Out of the five equations mentioned, only three are independent. The first two combined with either the electric form of Gauss' law or the equation of continuity form such an independent system (Comsol 2005).

Due to the complexity of winding geometries and interactions between conductors in windings, it is difficult to find a general analytical solution for the eddy current losses in windings. Several methods have been used to predict high-frequency winding losses in windings of round conductors. One of these methods, often called the Dowell method, is to use the analytical solution for a foil conductor as an equivalent to round conductors in the same layer with the same total cross-sectional area. Another type of method is called the Ferreira method or the Bessel-function method which is to use the analytical field solution of a single isolated round conductor which is subjected to an external uniform field (Sullivan 1999).

The winding- and eddy-current losses can be calculated as follows (Makarov2000, Elmoudi2006):

$$\mathbf{P_{th} = P_w + P_{ec}} \tag{3.13}$$

$$\mathbf{P_w = I_{coil}^2(4\rho DN/d^2)} \tag{3.14}$$

$$\mathbf{P_{ec} = (\pi fdB)^2 F(\xi)/(3\rho)} \tag{3.15}$$

$$\mathbf{F(\xi) = [3(\sinh(\xi) - \sin(\xi))]/[\xi(\cosh(\xi) - \cos(\xi))]} \tag{3.16}$$

$$\mathbf{\xi = d/\delta} \tag{3.17}$$

$$\mathbf{\delta = 1 / (\mu_o \pi f h/\rho)^{1/2}} \tag{3.18}$$

where

P_{th} = Total losses (W)
P_w = Winding losses (W)
P_{ec} = Eddy current losses (per volume) (Wm^{-3})
N = Number of turns
D = Diameter of turn (m)
d = Diameter of conductor (m)
δ = Depth of penetration (m)
ρ = Resistivity of conductor material ($m\Omega$)
f = Frequency (s^{-1})
h = Number harmonics
B = Magnetic flux density (T)
I_{coil} = Winding current (A)

It is seen from the above equations that eddy-current losses are also increasing with magnetic flux density (B) by the power of two. On the other hand when the temperature of a conductor increases the resistivity of the conductor material (ρ) will also increase so that the eddy-current losses (with the same frequencies but different temperatures) will be smaller (see Figures 3.30 and 3.31).

The test procedure and results used to check the theory for the effect of harmonics on eddy-current losses are described in more detail in appendix C. The results of these tests show that the harmonic frequencies have an increasing effect on the losses, as shown in equation (3.15).

The magnetic flux density to be used for the calculation of losses can be determined for complicated constructions with FEM calculations (Finite Element Methods).

The idea of finite elements is to break the problem down into a large number of regions, each with a simple geometry (e.g. triangles). For example, the advantage of breaking the domain down into a number of small elements is that the magnetic problem becomes transformed from a small but difficult to solve problem into a big but relatively easy to solve problem. Specifically, triangulation of the problem results in a linear algebra problem with perhaps tens of thousands of unknowns. However, techniques exist that allow a computer to solve for all the unknowns in only seconds.

In the following figures the test reactor is modeled with a FEM program (Comsol's FEMLAB) so that the aluminium wires (2.5 and 3.0mm) of each cylinder are replaced with solid cylinders with the same current densities as in original reactor, because the exact modeling of cylinders with thousands of turns and parallel wire-layers was not possible with the computer capacities available.

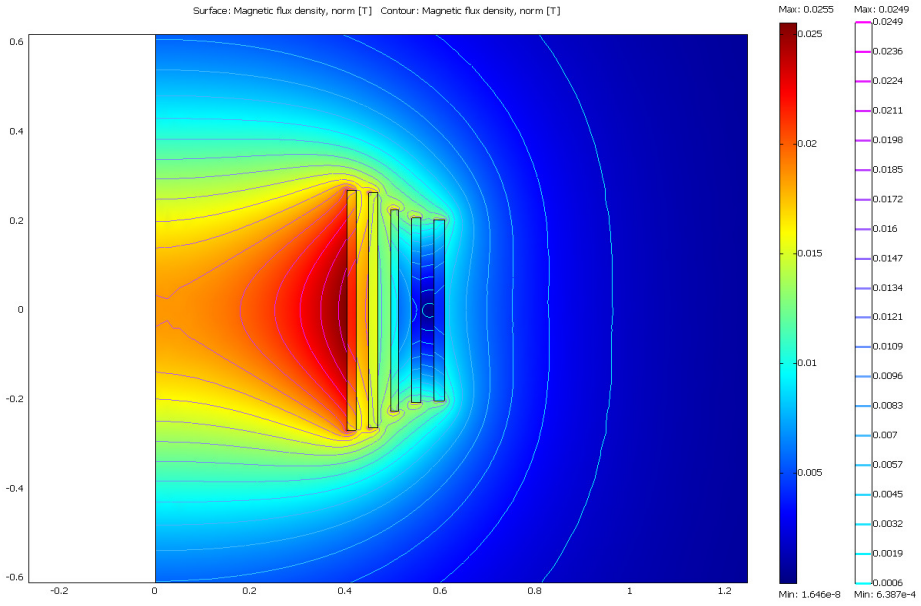

Figure 3.28: Reactor modeled with solid cylinders (0 Hz)

Figure 3.28 shows that the magnetic flux density is highest at the inside surface of the inner cylinder.

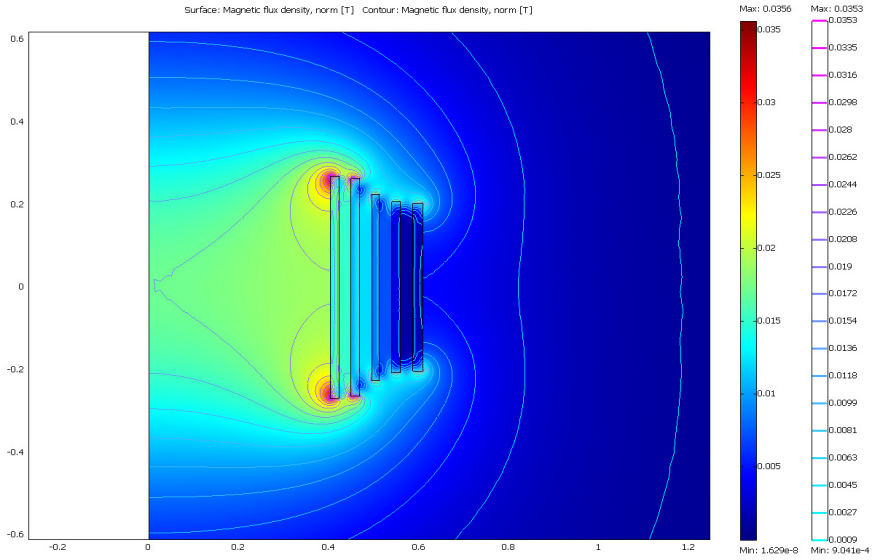

Figure 3.29: Reactor modeled with solid cylinders (50 Hz)

The average magnetic flux density in the above figures is about 20mT. Using the equations (3.15...3.18) it could be seen that the eddy current losses (P_{ec}) with low frequencies have only a minor influence to total losses, which are mainly caused by the winding losses (P_w).

For example in our test reactor the total winding losses of cylinder 1 at a temperature of 100 ^{0}C at 50Hz frequency and nominal current were 1736W but the calculated eddy current losses apprx. 9W (≈ 0.5%) only. Therefore, the eddy current losses can be neglected in the following calculations at lower harmonics.

In the next figures (Figures 3.30 and 3.31) the results from the calculation of eddy current losses of cylinder 1 at temperatures of +20 ^{0}C and +120 ^{0}C with constant magnetic flux densities are presented. It can be seen that if the current is rich in harmonics the eddy current losses are increased significantly.

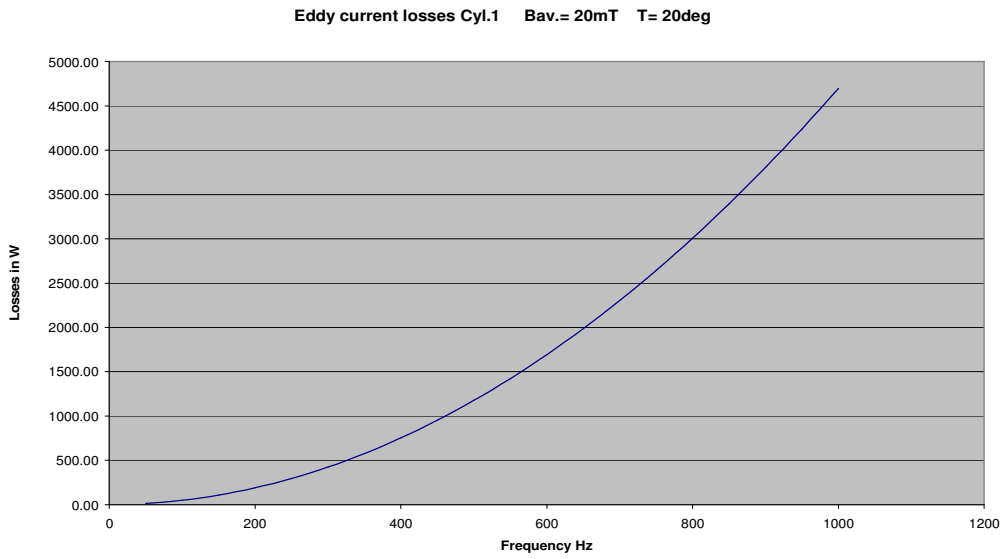

Figure 3.30: Eddy current losses vs. frequency on Cylinder 1 (T=20deg.C)

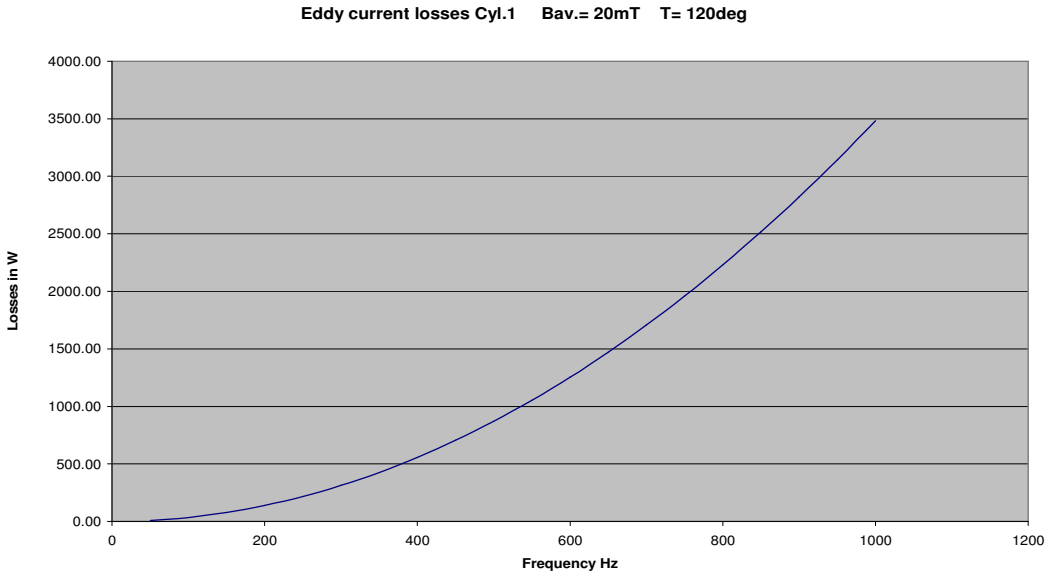

Figure 3.31: Eddy current losses vs. frequency on Cylinder 1 (T =120deg.C)

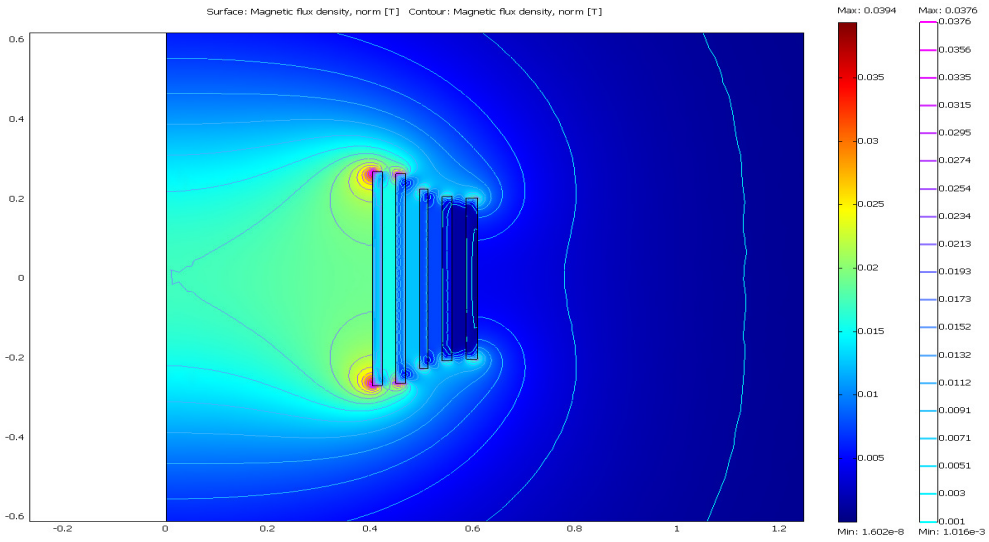

Figure 3.32: Reactor modeled with solid cylinders 100 Hz

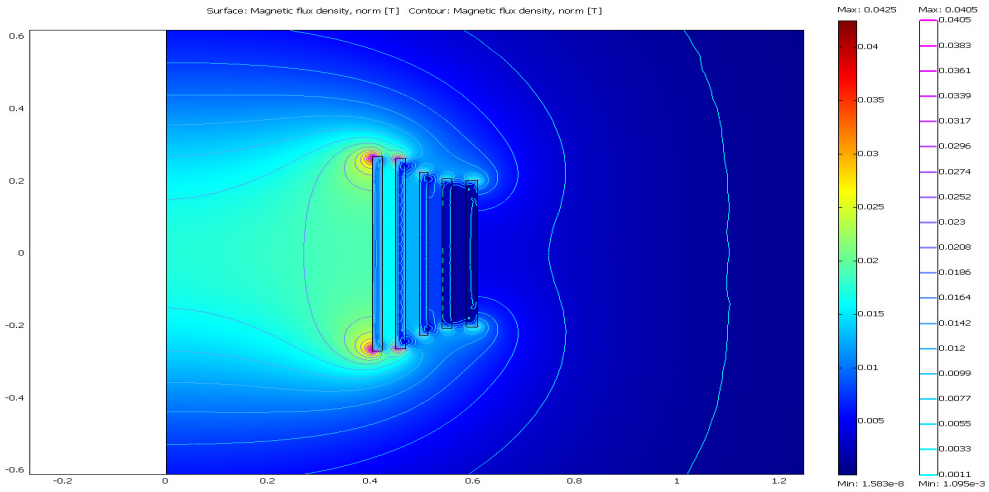

Figure 3.33: Reactor modeled with solid cylinders 150 Hz

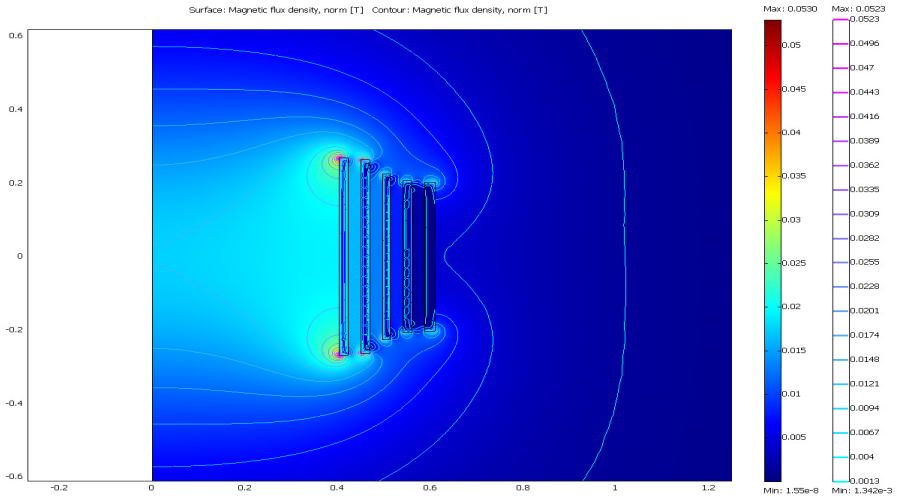

Figure 3.34: Reactor modeled with solid cylinders 450 Hz

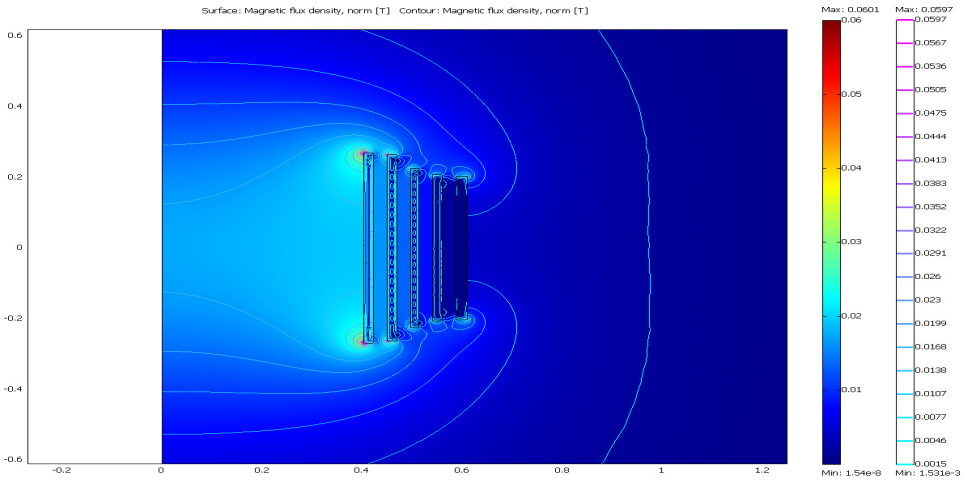

Figure 3.35: Reactor modeled with solid cylinders 900 Hz

In accordance with the figures shown above, the eddy current losses in the outer cylinders will be smaller than in inner cylinders because of the weaker magnetic flux densities.

It can also be seen that the extra losses caused by magnetic flux densities are straining the end regions of the cylinders more where the maximum values of magnetic flux densities are also shifted with increasing frequencies.

The proximity losses caused by the magnetic flux densities become lower at increased frequencies (the ac-resistance is increasing).

In the following Figure 3.36, the reactor's end part (taking a few layers of windings only) is simulated by FEMLAB.

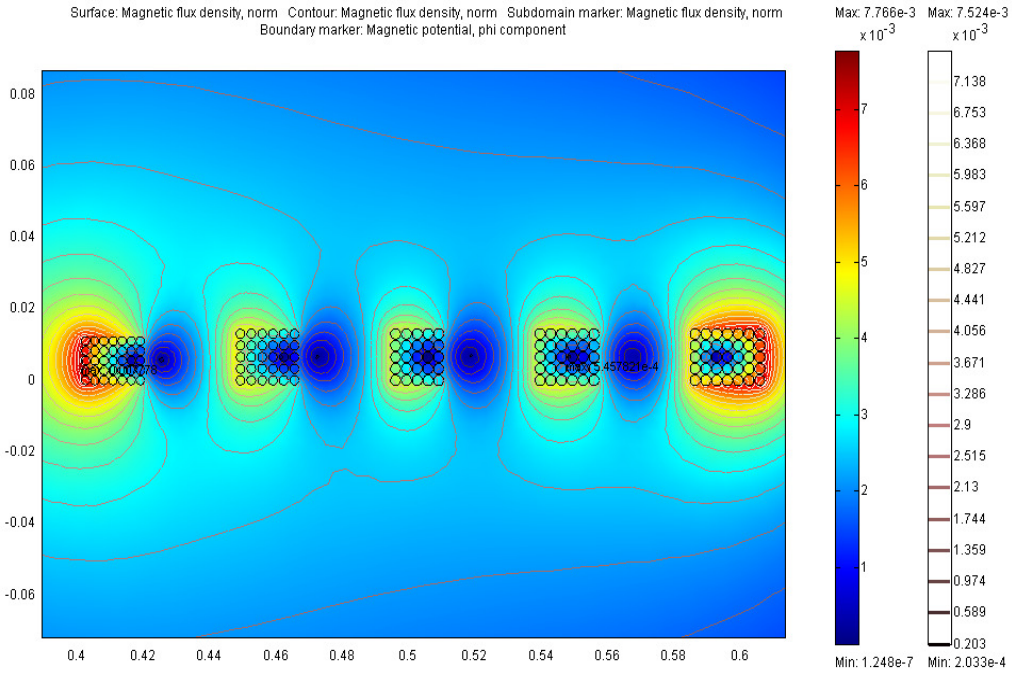

Figure 3.36: The lower parts of cylinders 1 to 5

The current values used for this simulation are as follows:

$$\mathbf{J_{s\varphi} = J_a A / s,} \qquad (3.19)$$

where

$J_{s\varphi}$ = Surface current density (A/m)
J_a = Current density (A/mm2)
A = Area
s = Circle

For simplicity the current densities of separate wires are supposed to be similar.

The calculated surface current densities for Figure 3.36 are as follows:

$J_{s\varphi 1}$ = 846 A/m
$J_{s\varphi 2}$ = 772 A/m
$J_{s\varphi 3}$ = 740 A/m
$J_{s\varphi 4}$ = 757 A/m
$J_{s\varphi 5}$ = 1090 A/m

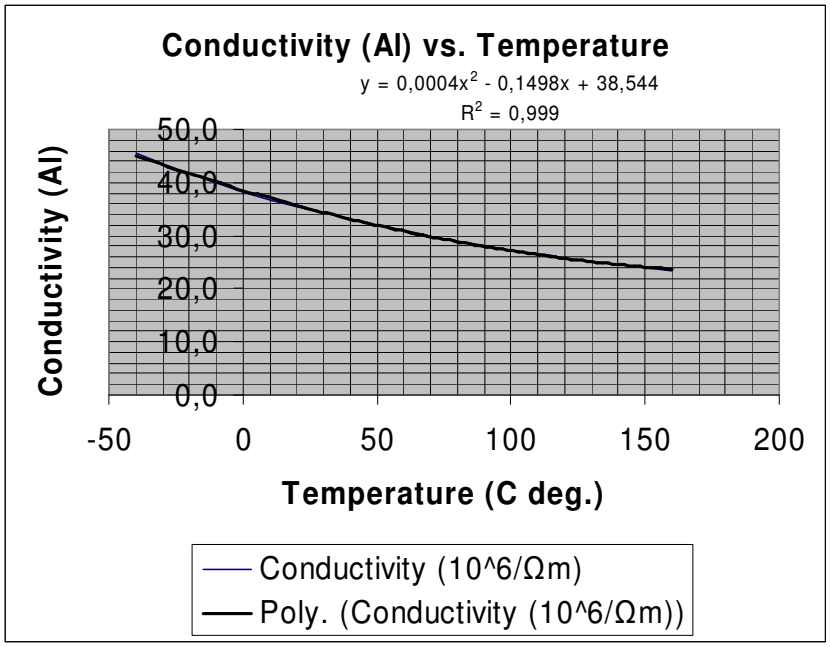

Figure 3.37: The conductivity (σ) of aluminium vs. temperature (t/^{o}C)

The equation for the conductivity of aluminium σ = f (t ($^{\circ}$C)) is:

$$\sigma = (0.0004t^2 - 0.1498t + 38.544)10^6 \Omega m \quad (3.20)$$

The thermal losses are:

$$P_w = J_{coil}^2 8RN/(\sigma d^2) \quad (3.21)$$

where

J_{coil} = current of coil
d = diameter of conductor (fixed)
R = radius of winding (fixed)
N = number of turns

Also in this case the number of turns determines the thermal losses of the coil (because small changes of turns have an effect on the current flow and therefore the losses in power of 2).

III - Calculation of temperatures

Dynamic thermal modeling of reactor:

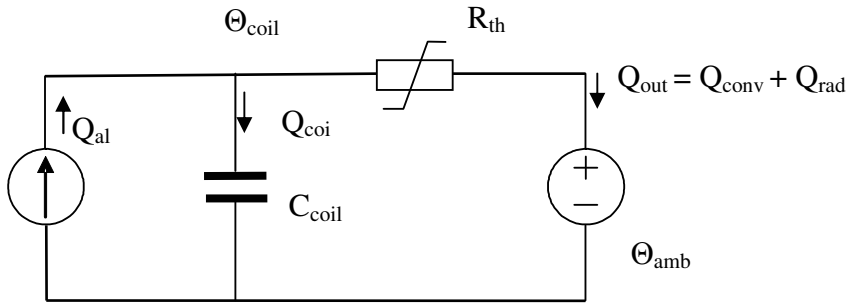

Figure 3.38: The analogous thermal model

The hot-spot temperature model is based on the thermal-electrical analogy. The thermal nonlinearity of the thermal resistance of a coil was described in Chapter 1.

A thermal process can be defined as follows: (Susa 2005)

$$\mathbf{Qdt = C_{th}d\Theta + (\Theta-\Theta_{amb})dt/R_{th}} \quad (3.21a)$$

Where

Q = heat flow

C_{th} = thermal capacity

Θ = temperature

R_{th} = thermal resistance

Thus, the equation for an air core reactor will be:

$$\mathbf{Q_{al} = C_{coil}d\Theta_{coil}/dt + \{[(\Theta_{coil} - \Theta_{amb})^{1.25}/R_{th}\,] + \varepsilon\sigma(\Theta_{wall}^{4} - \Theta_{amb}^{4})\}} \quad (3.22)$$

$$\mathbf{C_{coil} = m_{al}c_{al} + m_{resin+wire}\,c_{resin+wire} + m_{mylar}c_{mylar}} \quad (3.23)$$

$$\mathbf{m = \gamma V} \quad (3.24)$$

$$\mathbf{m_{al} = \gamma_{al}N(\pi/2)^2d^2D} \quad (3.25)$$

$$\mathbf{Q_{al} = Q_{coil} + Q_{out} = Q_{coil} + Q_{conv} + Q_{rad}} \quad (3.26)$$

where

R_{th} = thermal resistance of coil
C_{coil} = thermal capacitance of coil
Q_{al} = thermal losses of coil (= $P_w + P_{ec}$)
Q_{coil} = thermal energy (heat) stored in the coil
Q_{out} = thermal energy (heat) leaving out from the coil (convection and radiation)
m = weight of cylinder
c_p = specific heat (c_{al} = 920 Ws/kg °C ; $c_{resin+wire}$ = 840 Ws/kg°C ; c_{Mylar} = 1170Ws/kg°C)
γ = density (γ_{al} = 2.70 kg/dm^3)
N = number of turns of one cylinder (sum of each layer)
d = diameter of al-wire (2,5 or 3.0 mm)
D = mean diameter of one cylinder
Θ = temperature
V = volume
ε = emissivity of radiation ($\leq$ 1.0)
σ = Stefan-Boltzmann constant 5.7*10^{-8} W/m^{2}K^4

It is assumed that the thermal characteristics of the materials used in the manufacture of air core reactors are constant, that is, that the influence of temperature can be neglected. The only nonlinearity in this thermal dynamic modeling is the thermal resistance, which depends on the ambient conditions, such as cooling air velocity, ambient temperatures, geometrical dimensions and others, as mentioned in Chapter 1.

Table 3.2: Thermal properties of cooling air

Spec.heat (J/kg K)	Temp. (K)	Dens, (kg/m3)	Dyn.visc. (kg/m s)	Cond. (W/m K)
1027.0	100.00	3.56	6.92E-06	0.0093
1010.0	150.00	2.34	1.03E-05	0.0137
1006.0	200.00	1.75	1.33E-05	0.0181
1005.0	***250.00***	***1.39***	***1.60E-05***	***0.0223***
1006.0	***300.00***	***1.16***	***1.85E-05***	***0.0262***
1009.0	***350.00***	***1.00***	***2.08E-05***	***0.0300***
1014.0	***400.00***	***0.87***	***2.29E-05***	***0.0337***
1021.0	450.00	0.77	2.48E-05	0.0371
1030.0	500.00	0.70	2.67E-05	0.0404

For engineering calculations the heat flow through radiation (Stefan-Boltzmann law) can be simplified as follows:

$$Q_{rad} = 5.7\varepsilon[((273 + \Theta_{amb} + \Delta\Theta)/100)^4 - ((273 + \Theta_{amb})/100)^4] \; W/m^2 \qquad (3.26a)$$

For example:
If the emissivity ε is 0.85, the ambient temperature Θ_{amb} 20°C and the average temperature rise $\Delta\Theta$ between cylinder surface and ambient 85°C (as for cylinder 5), the radiated power density is 632W/m^2. The outer surface area of cylinder 5 is A = π*D*H = 1.5m^2, thus the radiated power losses between ambient and outer surface of cylinder 5 through radiation are 948W.

If the radiating cylinder with T_1, A_1 and ε_1 is surrounded by another cylinder with T_2, A_2 and ε_2 , the reduced emissivity can be calculated as follows:

$$\varepsilon_{red} = 1/(1 / \varepsilon_1 + (A_1 / A_2)(1 / \varepsilon_2 - 1)) \qquad (3.26b)$$

and the power transmitted between the cylinders is

$$Q_{12} = 5.7*10^{-8} \; \varepsilon_{red} \; ((273+T_{1x})^4 - (273+T_{2x})^4) W/m^2 \qquad (3.26c)$$

where T_{1x} and T_{2x} are the surface temperatures at the same height x in °C. Hence, if the cylinders are at same temperature, there is no heat transfer between them by radiation.

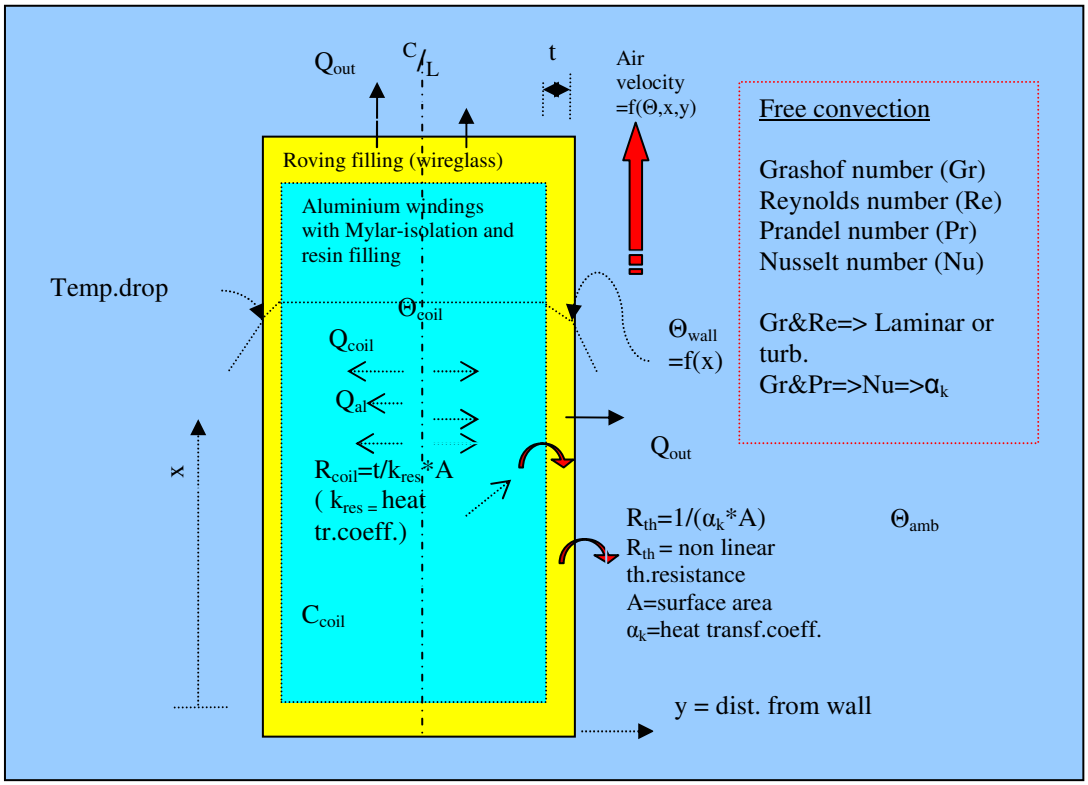

Figure 3.39: The factors affecting the heat transfer calculation

Considering convection (Figure 3.39) the equation for the heat transfer coefficient α_{kx} (Schmidt & Beckmann 1930) at an ambient air pressure of b (in mmHg) and vertical level x is as follows: (Schmidt and Beckmann, 1930 & Gotter, 1954)

$$\alpha_{kx} = 5.6[(\Theta_{wallx}-\Theta_{ambx})/(\Theta_{ambx})]^{0.25}(b/760)^{0.5} \quad [W/m^2 * K] \qquad (3.27)$$

where

x = the level of surface counted from bottom of cylinder [m]
Θ_{ambx} = ambient temperature [K] in level x
Θ_{wallx} = temperature at cylinder wall [K] in level x
b = air pressure (mmHg)

The thermal heat transfer coefficient of convection is dependent on temperature (Gotter, 1954) as shown in Figure 3.40:

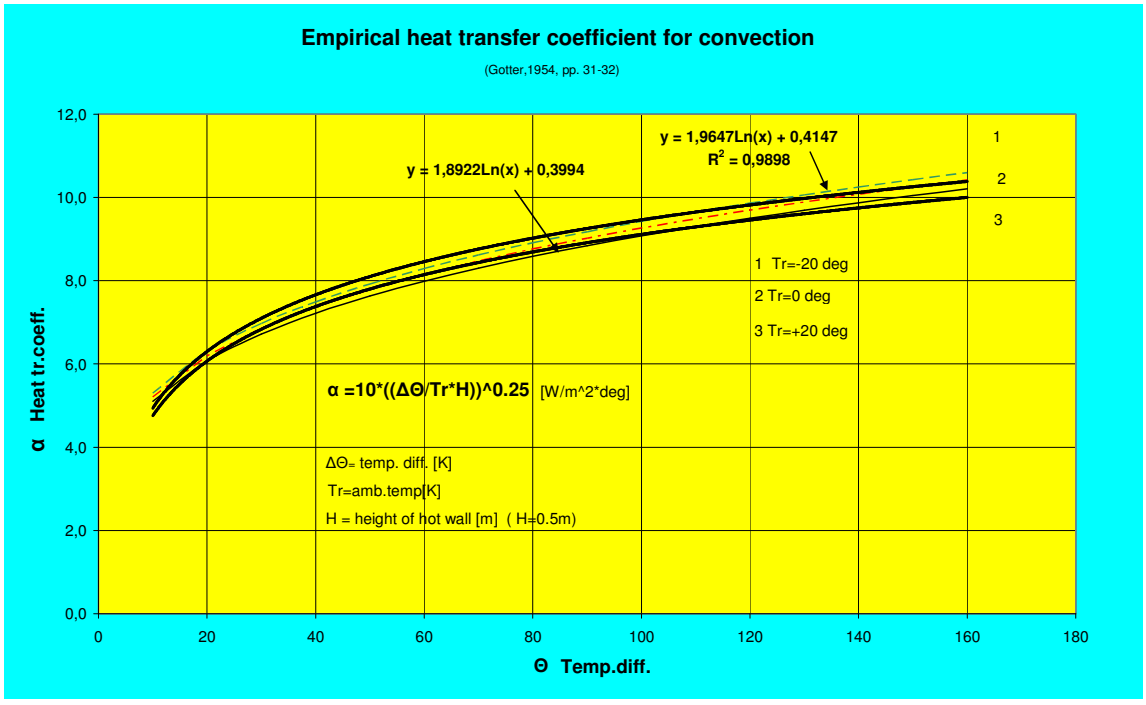

Figure 3.40: Thermal heat transfer coefficient of convection vs. temperature

The surface temperatures (Θ_{wall}) of some of the cylinders and the temperatures at different levels in the cooling ducts (Θ_{amb}) have been measured by optical wires. The thermal heat transfer coefficients at desired levels can be calculated when the wall- and ambient temperatures at the same level (x) are known. In addition to this the cooling air temperature and velocity, which are also dependent on x-level, must be known.

In the Figures 3.41 to 3.46 are the results of some measurements with optical wires for the temperatures in cooling ducts as well as in the surface and inside windings. The nominal current during those measurements was 608A.

Cooling ducts temperatures:

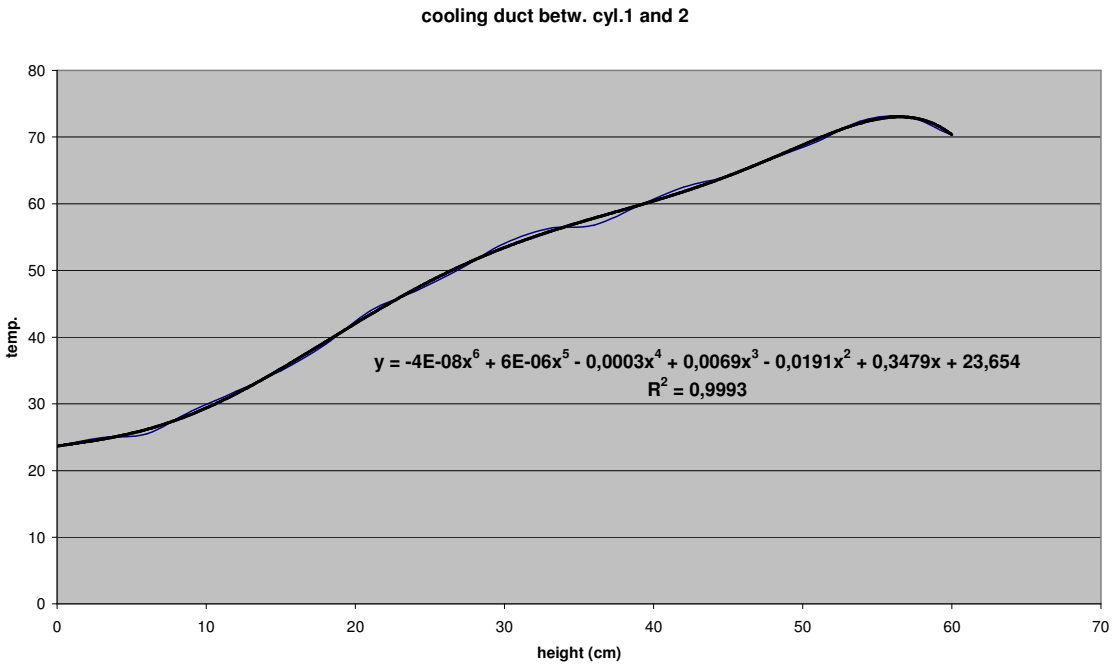

Figure 3.41: Air temperature in cooling duct between cylinders 1 and 2

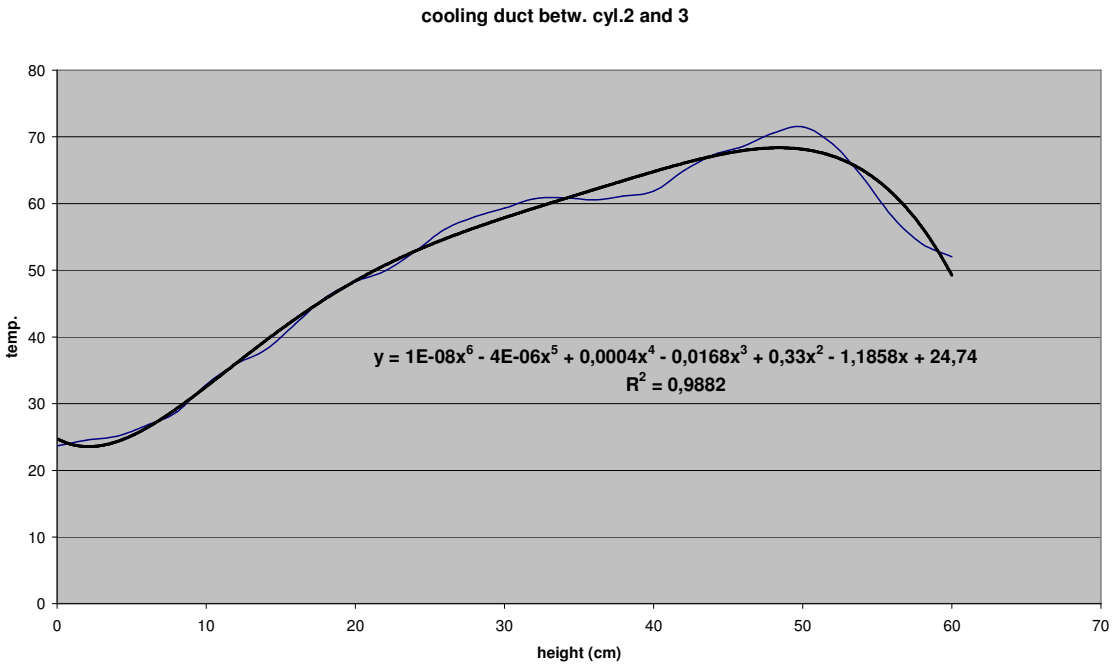

Figure 3.42: Air temperature in cooling duct between cylinders 2 and 3

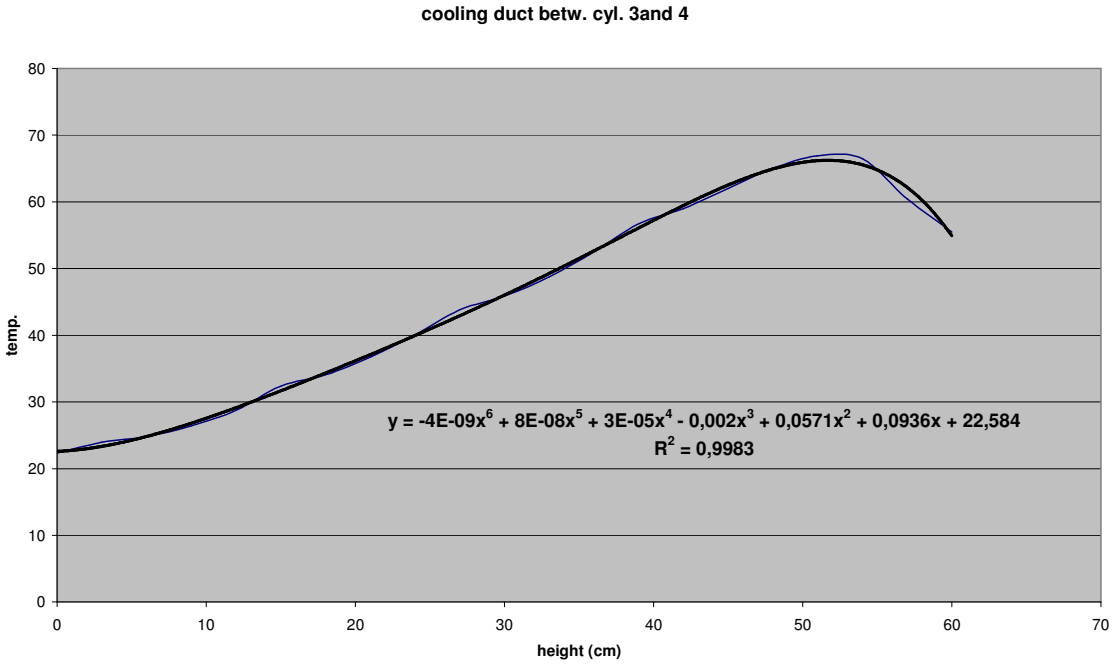

Figure 3.43: Air temperature in cooling duct between cylinders 3 and 4

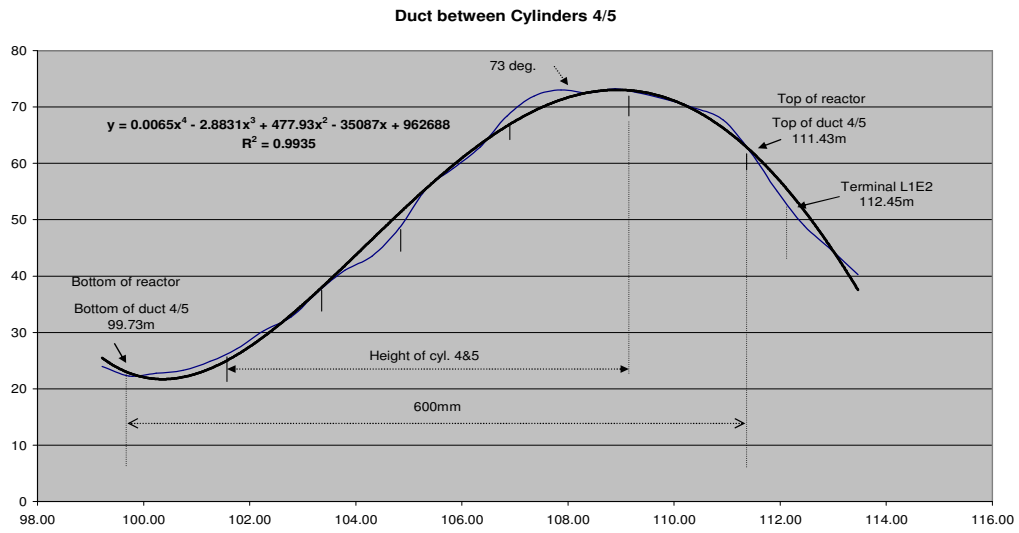

Figure 3.44: Air temperature in cooling duct between cylinders 4 and 5 by OWs. (Results from TC-measurement, see Figure 4.20b)

Surface and inside of winding temperatures:

As an example the following two figures (3.45 and 3.46) are from cylinder 2:

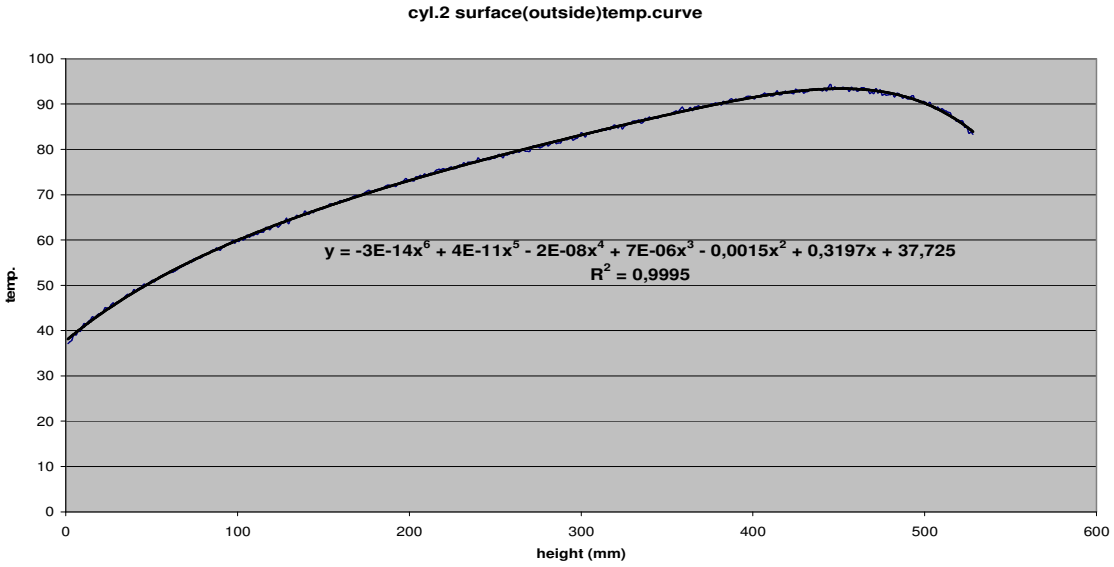

Figure 3.45: The temperature curve at outer surface of cylinder 2

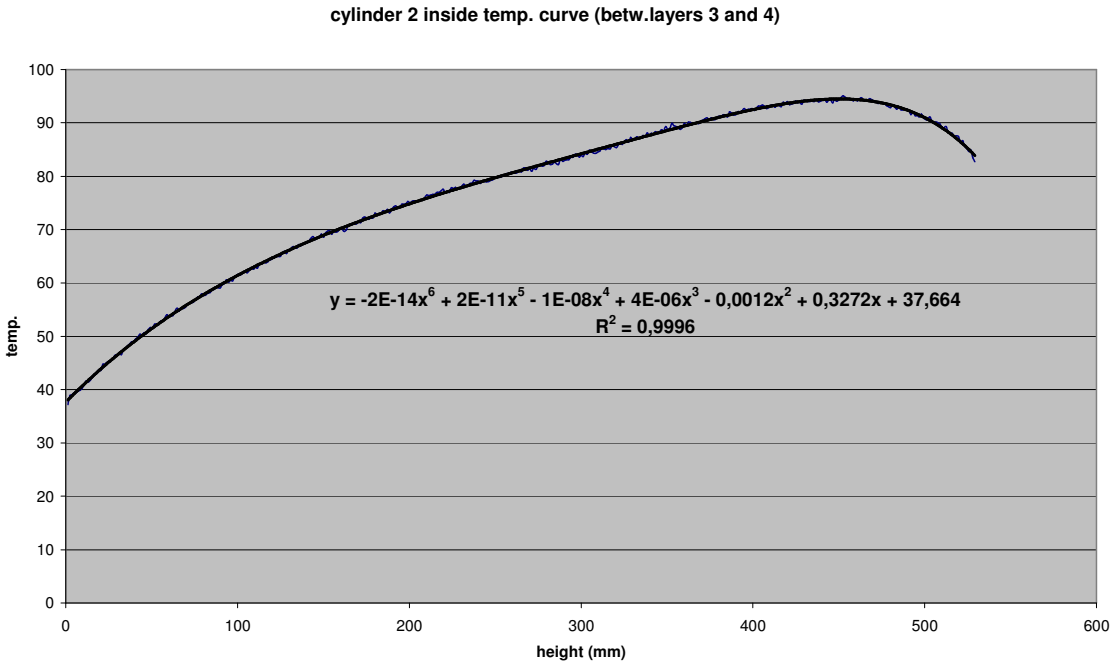

Figure 3.46: The temperature curve from inside of winding of cylinder 2

IV – Optimization

After determining the temperatures as per module III (conductance, convection and radiation with analytical & empirical solutions and with laminar or turbulent cooling airflow considered), the next step is to optimize the number of winding turns relative to the temperatures.

Winding turns have the following influence on other parameters:

Self-inductance:

$$L_{nn} = \mu_o N_{nn}^2 \pi D_{nn}^2 (K_{nn}/4) H_{nn} = k_{1nn} N_{nn}^2 \quad (3.28)$$

Mutual inductance:

$$M_{mn} = 2\pi^2 r_m^2 N_m N_n K_{mn} / (R_n^2 + H_n^2)^{1/2} = k_{2mn} N_m N_n \quad (3.29)$$

Resistance:

$$R_{snn} = \rho 8\pi R_{nn} N_{nn} / (\pi d^2) = k_{3nn} N_{nn} \quad (3.30)$$

Impedances:

$$Z_{nn} = R_{snn} + j\omega L_{nn} = k_{3nn} N_{nn} + j\omega k_{1nn} N_{nn}^2 \quad (3.31)$$

$$Z_{mn} = j\omega M_{mn} = j\omega k_{2mn} N_m N_n \quad (3.32)$$

For example the 5x5 matrix of a 5-cylinder reactor:

$$[\mathbf{Z}] = (j\omega)\begin{vmatrix} \{(j\omega)^{-1}k_{311}N_{11}+k_{111}N_{11}^2\} & k_{212}N_1N_2 & k_{213}N_1N_3 & k_{214}N_1N_4 & k_{215}N_1N_5 \\ k_{221}N_2N_1 & \{(j\omega)^{-1}k_{322}N_{22}+k_{122}N_{22}^2\} & k_{223}N_2N_3 & k_{224}N_2N_4 & k_{225}N_2N_5 \\ k_{231}N_3N_1 & k_{232}N_3N_2 & \{(j\omega)^{-1}k_{333}N_{33}+k_{133}N_{33}^2\} & k_{234}N_3N_4 & k_{235}N_3N_5 \\ k_{241}N_4N_1 & k_{242}N_4N_2 & k_{243}N_4N_3 & \{(j\omega)^{-1}k_{344}N_{44}+k_{144}N_{44}^2\} & k_{245}N_4N_5 \\ k_{251}N_5N_1 & k_{252}N_5N_2 & k_{253}N_5N_3 & k_{254}N_5N_4 & \{(j\omega)^{-1}k_{355}N_{55}+k_{155}N_{55}^2\} \end{vmatrix}$$

The optimizing of winding turns can be performed by means of a Jacobian-matrix, as shown below:

Jacobian-matrix [J]:

$$[J] = \begin{vmatrix} \partial I_1/\partial N_1 & \partial I_1/\partial N_2 & \dots & \partial I_1/\partial N_n \\ . & & & \\ . & & & \\ . & & & \\ \partial I_n/\partial N_1 & \partial I_n/\partial N_2 & \dots & \partial I_n/\partial N_n \end{vmatrix} \qquad (3.33)$$

The corrections of the winding turns (ΔN) can be determined when the corrections for coil currents (ΔI) are known.

$$[\,U\,] = [\,I\,][\,Z\,] \qquad (3.34)$$

$$[\,I\,] = [\,U\,][\,Z\,]^{-1} \qquad (3.35)$$

First the numerical calculation of $\partial I/\partial N$ for all I&N-pairs, making small changes to the numbers winding turns must be carried out.

The corrections to the winding turns are made as follows:

$$[\,\Delta N\,] = [\,J\,]^{-1}[\,\Delta I\,] \qquad (3.36)$$

Iteration using the Jacobian-matrix is demonstrated with the following examples:

First example:

Calculating the desired current distribution between cylinders (the nominal current of reactor is I = 487.07 A).

Jacobian-matrix [J] for one additional turn (+1) for each cylinder, one after the other:

$$[J] = \begin{matrix} 12.31237 & 12.80433 & 0.16303 & 1.00943 & 0.81753 \\ 10.85960 & -28.34640 & 16.48440 & 0.13670 & 1.31740 \\ 0.17201 & 14.43451 & -33.98599 & 17.97231 & 1.04511 \\ 0.73483 & 0.12693 & 16.49853 & -35.89377 & 17.28163 \\ 0.54602 & 0.98062 & 0.84012 & 16.77532 & -20.46168 \end{matrix}$$

Inverting the above matrix [J]:

```
>> inv(J)

ans =

1.0e+003 *

    7.3688    7.3688    7.3689    7.3689    7.3689
    6.3025    6.3024    6.3025    6.3024    6.3024
    5.5503    5.5502    5.5502    5.5502    5.5502
    5.0789    5.0789    5.0789    5.0788    5.0788
    4.8905    4.8904    4.8904    4.8904    4.8903
```

If the desired change in current distribution (ΔI) is, for example:

DI = [1 -0.5 -0.5 0 0]

(i.e. one amp more in cylinder 1 and half an amp less in cylinders 2 and 3, but the currents in cylinders 4 and 5 remain unchanged)

Now the changes to the number of winding turns (ΔN) must be calculated:

$DN = (inv(J))*I^T$

DN =

-0.0344
0.0392
0.0514
0.0401
0.0355

(i.e. The first coil has to have fewer (-0.0344) and the other coils more turns)

The turns will be changed accordingly and a new impedance matrix [Z] is ready:

Z =

1.9877	1.5392	1.2758	1.1051	0.9957
1.5392	1.7030	1.4036	1.2004	1.0834
1.2758	1.4036	1.6306	1.3777	1.2284
1.1051	1.2004	1.3777	1.6366	1.4335
0.9957	1.0834	1.2284	1.4335	1.7951

The new current distribution must now be calculated (Jcoil):

U = [1 1 1 1 1]

I = [487.07]

```
>> Jcoil=(inv(Z))*U'*(inv(U*(inv(Z))*U'))*I
```

New current distribution Original current distribution

Jcoil =

98.6410	97.610066
87.8265	88.333399
69.7166	70.237789
92.0991	92.113166
138.7868	138.77558

Second example:

The required current changes in the cylinders are:

DI= [-5 5 5 5 -10]

(i.e. five amps less in cylinder 1, five amps more in cylinders 2..4 and ten amps less in cylinder 5)

>> DN= (inv (J))*DI'

(The Jacobian-matrix [J] to be used now is the same as before (+1 turns))

DN =

0.2432

-0.1840

-0.2112

-0.0034

0.4749

Z =

1.9997	1.5396	1.2748	1.1077	1.0058
1.5396	1.6935	1.3943	1.1963	1.0881
1.2748	1.3943	1.6182	1.3714	1.2324
1.1077	1.1963	1.3714	1.6344	1.4427
1.0058	1.0881	1.2324	1.4427	1.8208

Jcoil = (inv(Z))*U'*(inv(U*(inv(Z))*U'))*I

New current distribution	Original current distribution
Jcoil =	
92.5194	**97.610066**
93.4243	**88.333399**
75.4288	**70.237789**
97.0644	**92.113166**
128.6331	**138.77558**

Small changes in the number of turns, as calculated above, is in practice not possible because the reactors have multi-branch spider arms (4-, 6-, 8- or 12- branches) and therefore the optimization of winding turns is possible in rough steps only.

V- Verifying

The results taken from the models and the results from measurements must be verified and after that some conclusions have to be made about the quality and accuracy of the model.

For comparative purposes the surface temperatures of cylinder 5 have been measured with an infrared camera (Figures 4.9 and 4.10) as well as with thermocouples (TC) fixed on the surface with a spacing of about 30mm (Figures 3.14 and 4.11) from top to bottom. In addition, a measuring stick (Figures 3.10, 3.11 and 4.12) measured the cooling air temperatures in the cooling duct.

Determination of the current distribution can be carried out by matrix-calculation (Qin Yu 1996) as follows:

$$[\mathbf{Z}][\mathbf{J}_{coil}]^{T} = [\mathbf{U}][\mathbf{V}]^{T}$$

where

$[\mathbf{V}] = [\mathbf{V...V}]$ voltage matrix over the cylinder
$[\mathbf{J}_{coil}] = [\mathbf{J}_1...\mathbf{J}_n]$ current matrix
$[\mathbf{U}] = [\mathbf{1...1}]$ unit matrix
$[\mathbf{Z}] =$ impedance matrix (self- and mutual-inductances)

Since the supply voltage over the coils is the same, the union matrix instead of voltage matrix can be used in calculations. The current distribution with the air-core reactors is a linear function related to their impedances.

The current is:

$$\mathbf{[U][J_{coil}]} = \mathrm{I}$$

and the relative current distribution is:

$$\mathbf{J_{coil}} = \mathbf{Z^{-1}U^{T}(UZ^{-1}U^{T})^{-1}}\mathrm{I}\ ,$$

The results and calculation methods presented in this work are verified by comparing them to measured temperature profiles of the test reactor. The results of the calculated current distributions by means of several different methods with comparison to measured values are shown in Appendix B.

The theoretical calculated results for changes to the winding turns and current distributions of our test reactor could not be verified because of the compact structure of the reactor (Figures 3.4 and 3.5). The changing or modifying of any winding connections was not possible without demolishing the cylinders of the reactor.

4 Results

Some results from the measurements by optical wires (OWs) and thermocouples (TCs) are presented and shown in the pictures below. It is possible to find the hot-spot locations as well as the temperature curves of all cylinders, which are then definable in the equations for loss calculations.

The measurements were performed in the high voltage hall of TKK, where the ambient temperature maintained during the tests was almost constant (+20...+21 degree). The rated test current in all tests was 608A, which was about 25% higher than the nominal current given from the manufacturer of our test reactor (i.e. 486.6A).

The temperatures presented in graphform for Loop1 are shown in Figures 4.1 and 4.2. Figure 4.3 shows, as an example, the temperatures in the cooling duct between cylinders 1 and 2, as calculated from the OW-measurement results.

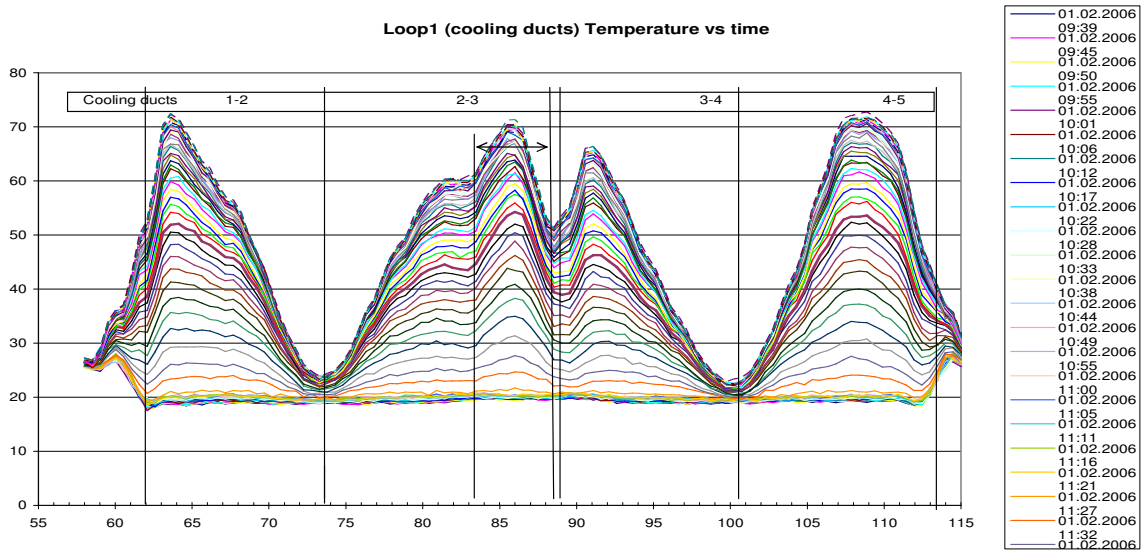

Figure 4.1: Temperature graph of Loop 1 vs. heating time.

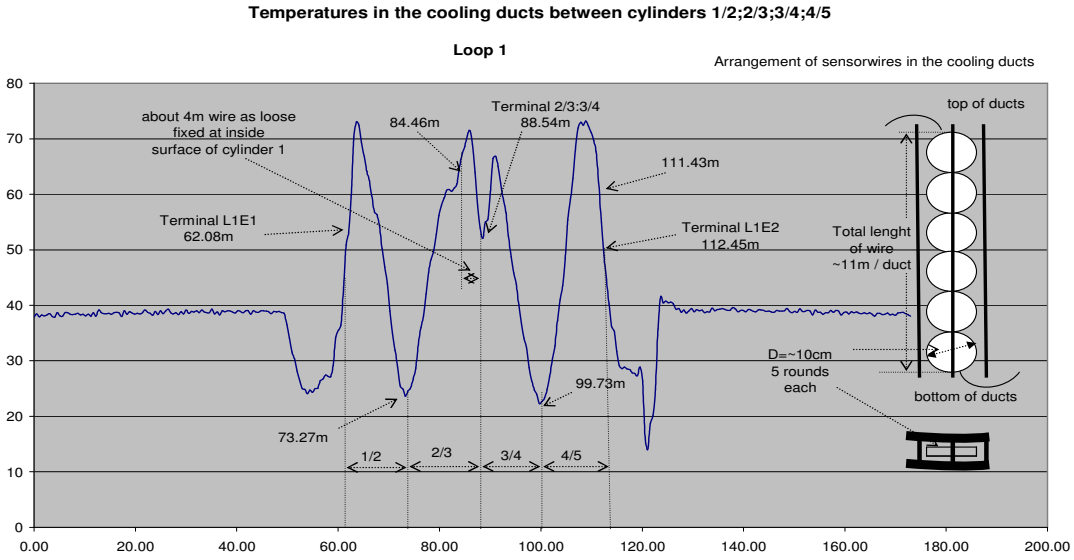

Figure 4.2: Temperature graph of Loop 1 (For arrangement see Figure 3.2)

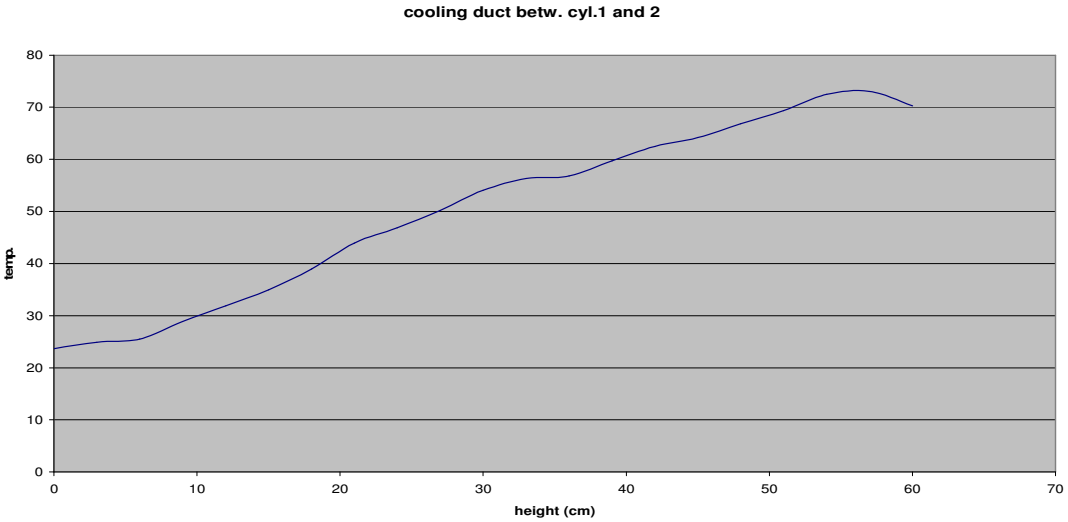

Figure 4.3: Temperature from bottom to top in cooling duct 1-2 by OW

The temperatures and OW arrangement for Loop 2 are shown in Figures 4.4 and 4.5.

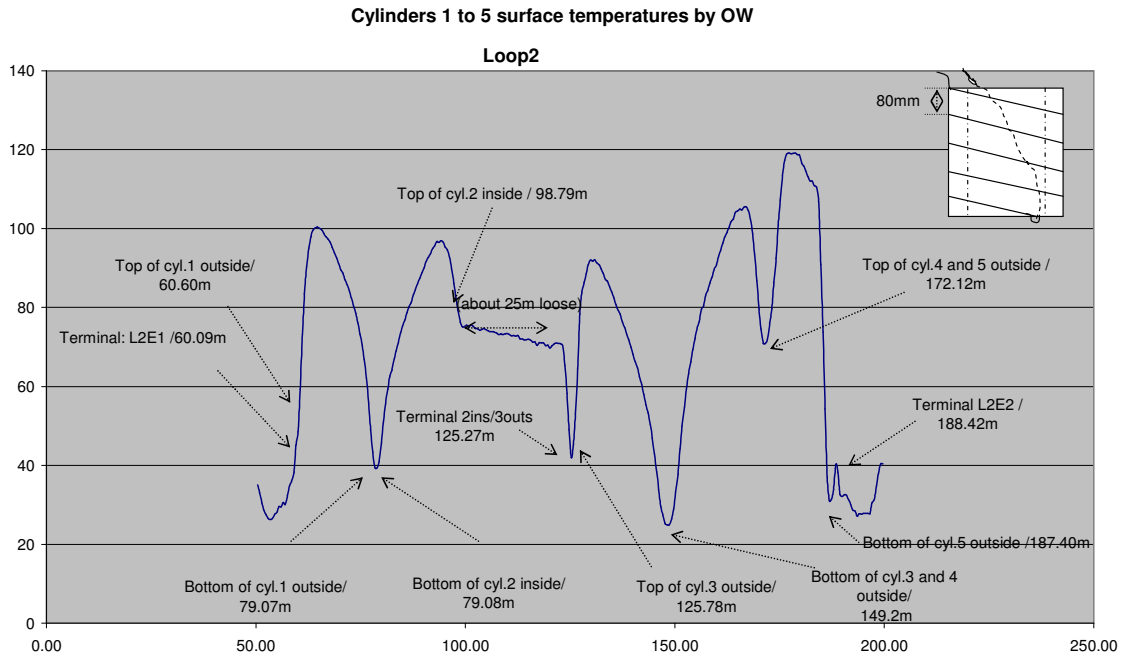

Figure 4.4: Temperature graph of Loop 2 and OW arrangement

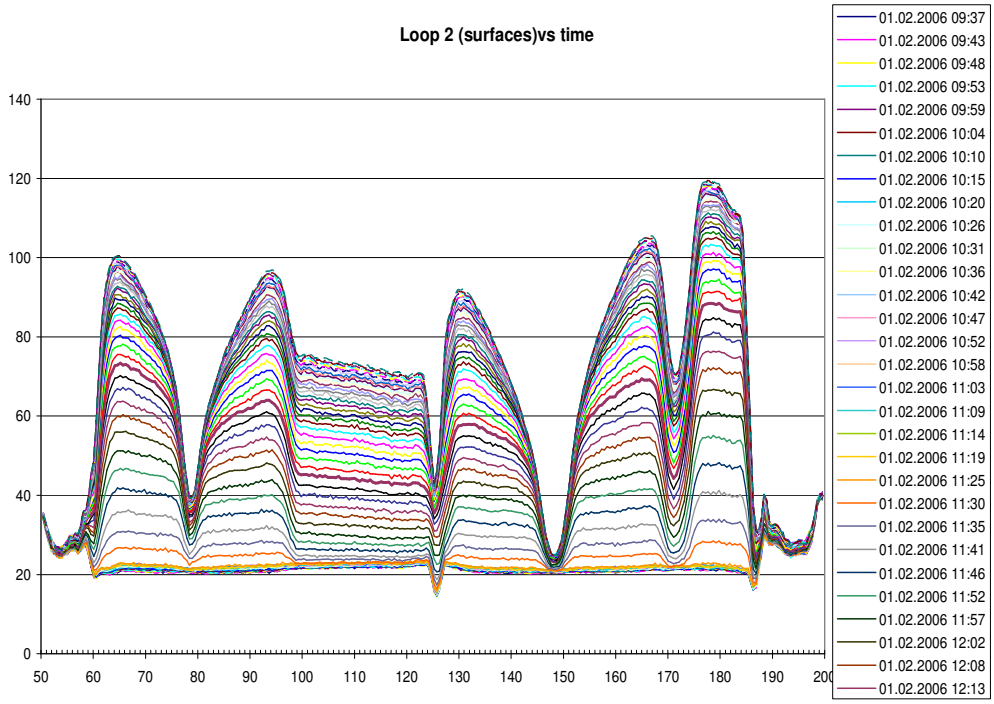

Figure 4.5: Temperature graph of Loop 2 vs. heating time.

The temperatures in Loop 3 are shown in Figures 4.6 and 4.7.

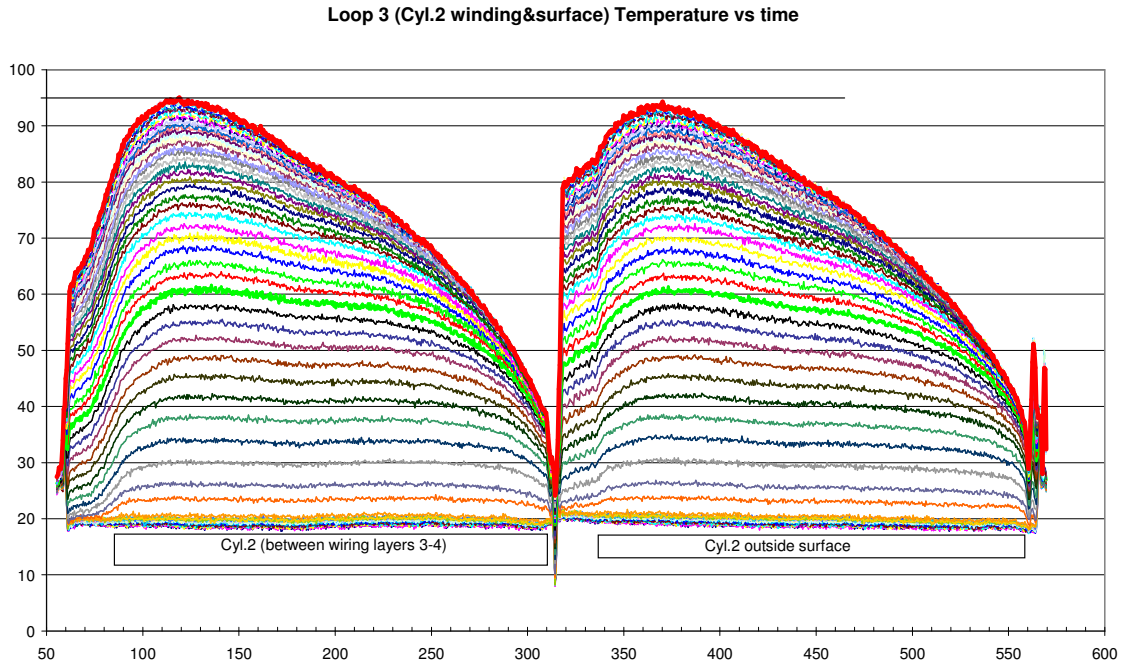

Figure 4.6: Temperature graph of Loop 3 vs. heating time
(time scale as per Figure 4.5)

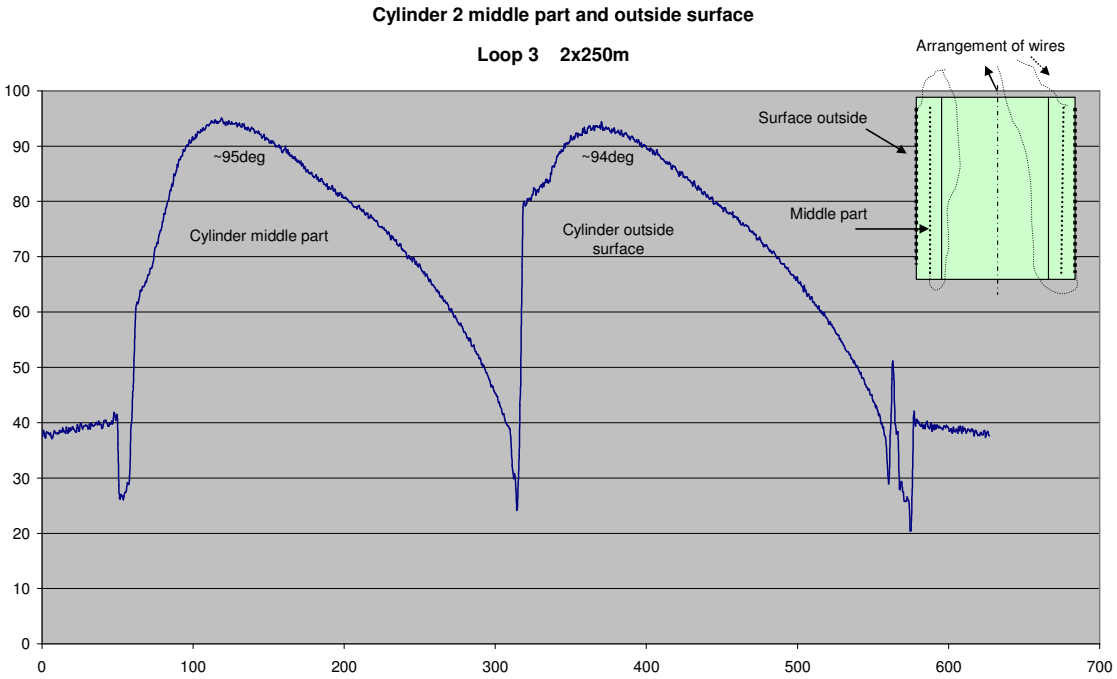

Figure 4.7: Temperature graph of Loop 3 and OW arrangement

The temperatures presented in Loop 4 are shown in Figure 4.8.

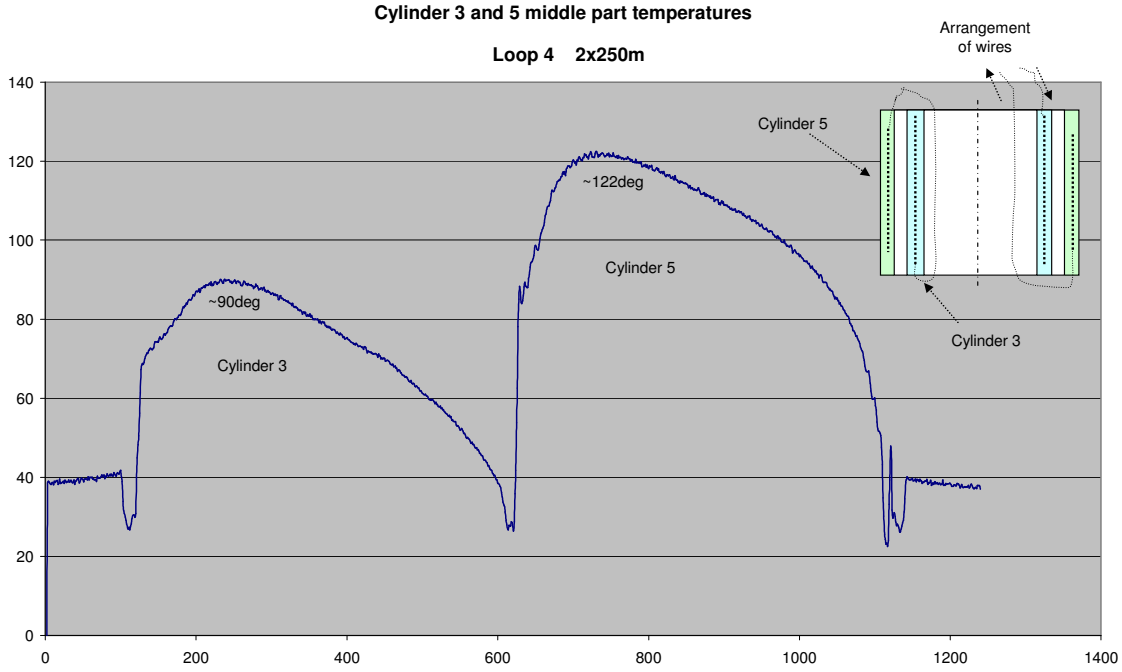

Figure 4.8: Temperature graph of Loop 4 and OW arrangement

The results of the surface measurements of cylinder 5 were possible to compare by means of an infrared camera, as shown in the Figures 4.9 and 4.10 below.

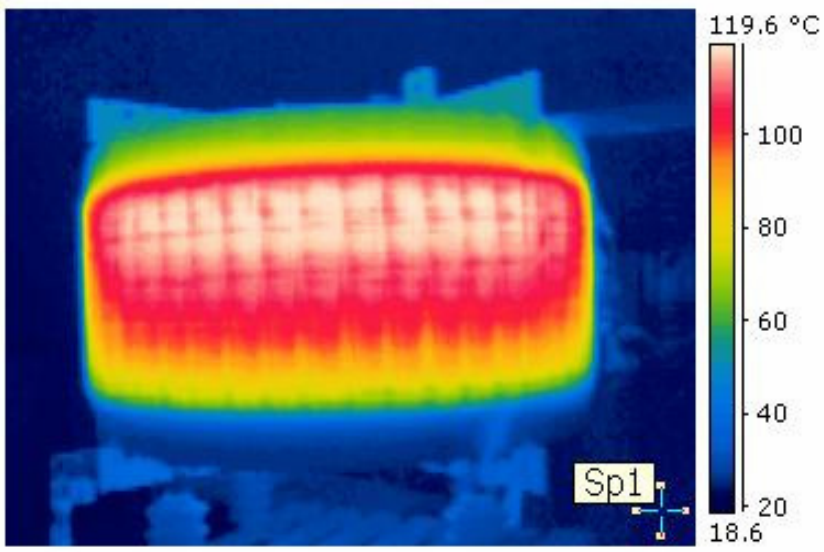

Figure 4.9: Surface temperatures of cylinder 5 by infrared camera

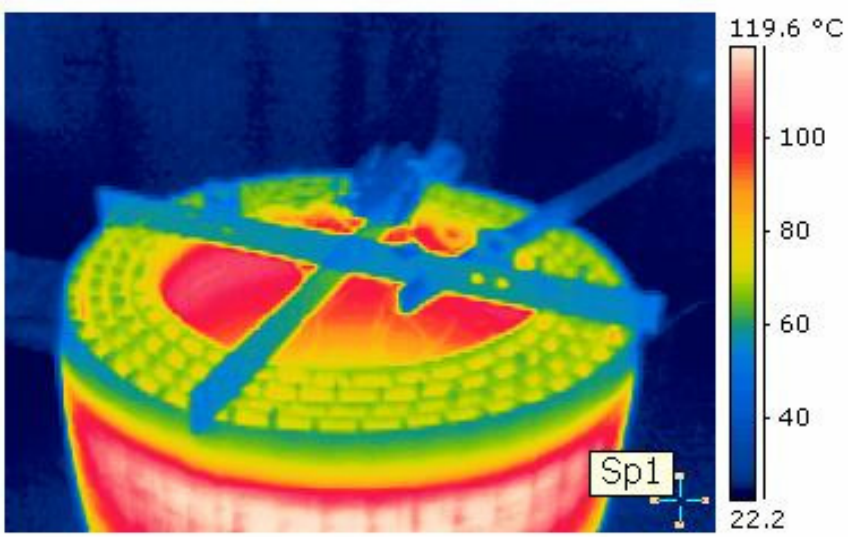

Figure 4.10: Temperatures at reactor by infrared camera

The temperatures measured by the OWs are similar to the temperatures shown in the above Figures 4.9 and 4.10, made by infrared camera..

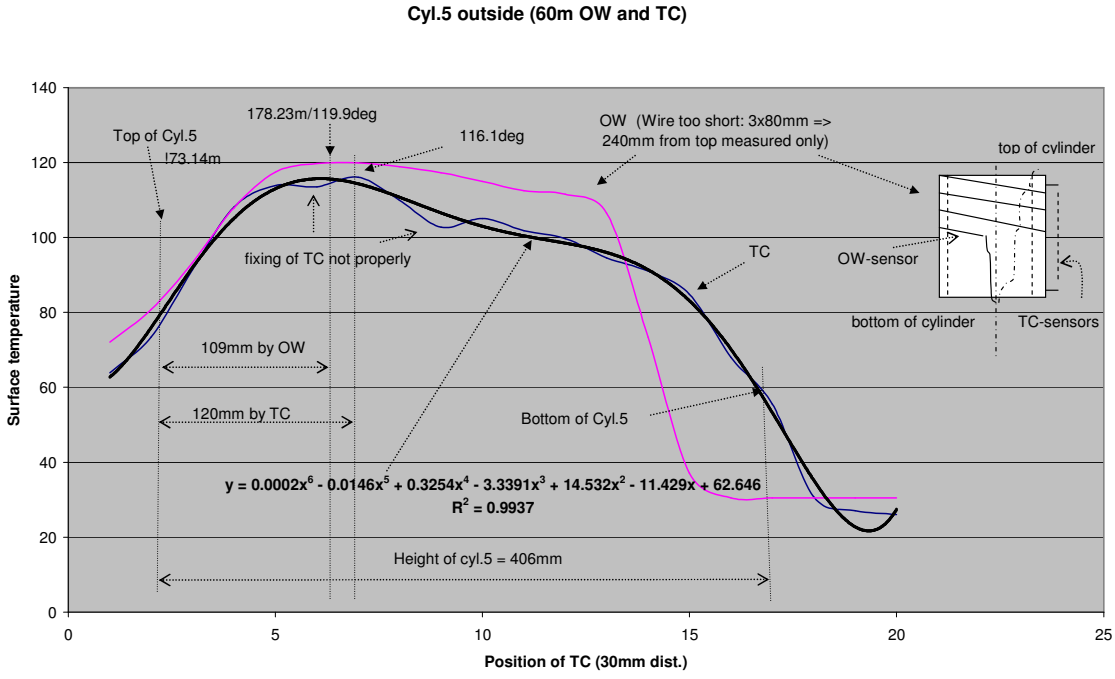

Figure 4.11: Comparison between thermocouples and optical wire at outside surface of cylinder 5

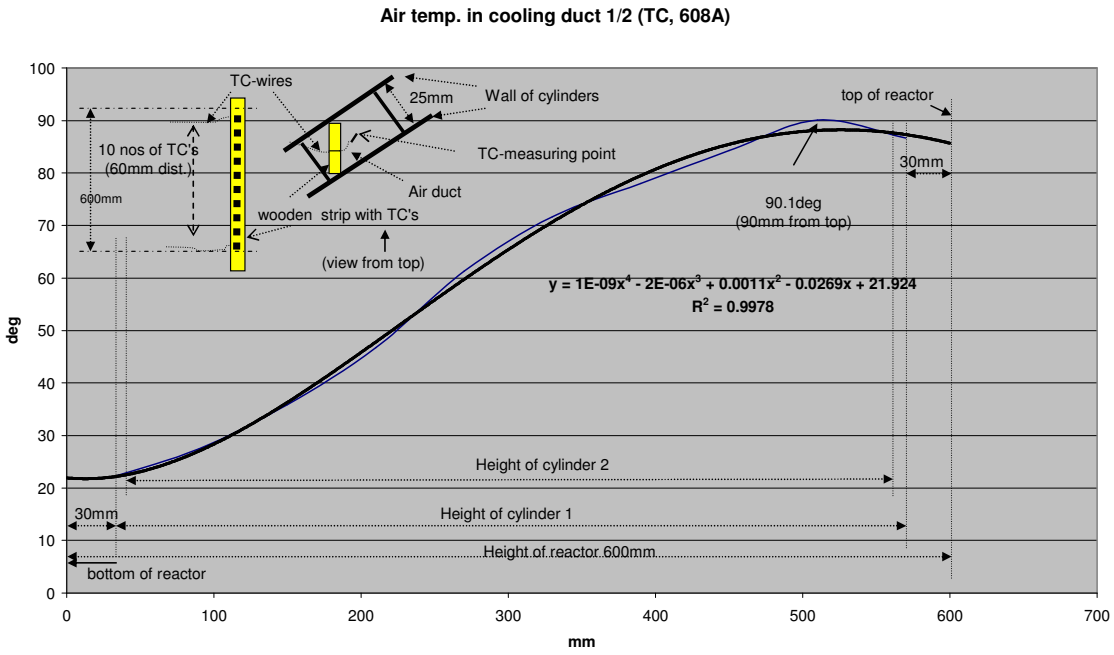

Figure 4.12: Temperature measurement in cooling duct between cylinders 1&2 by thermocouples (TCs) (by wooden stick)

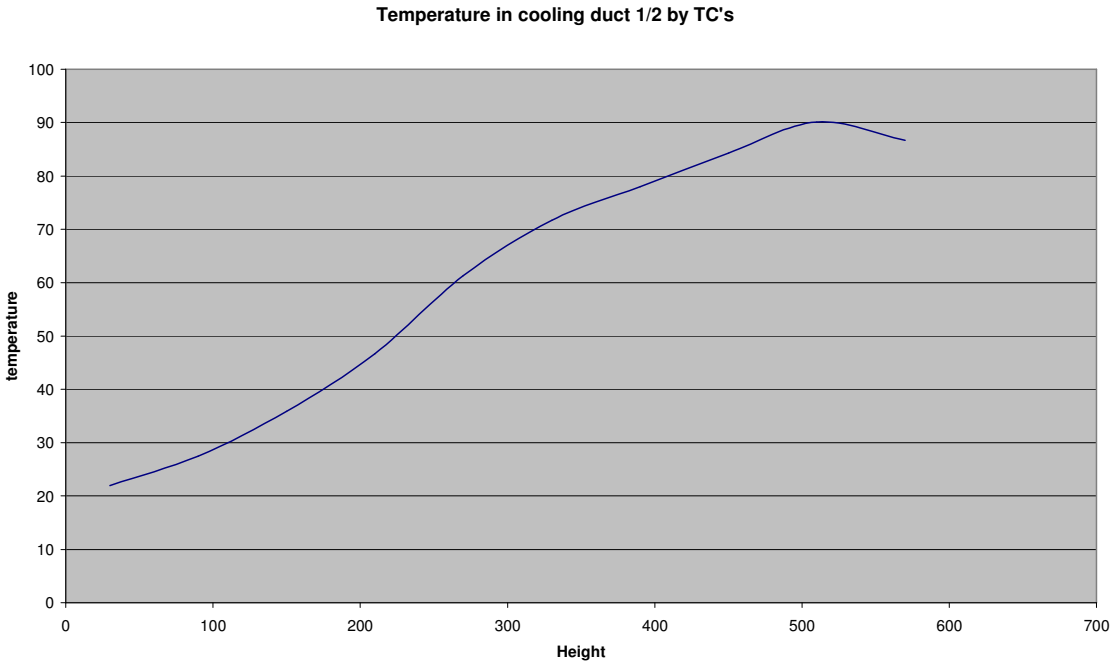

Figure 4.13: Temperature from bottom to top in cooling duct 1-2 by TCs

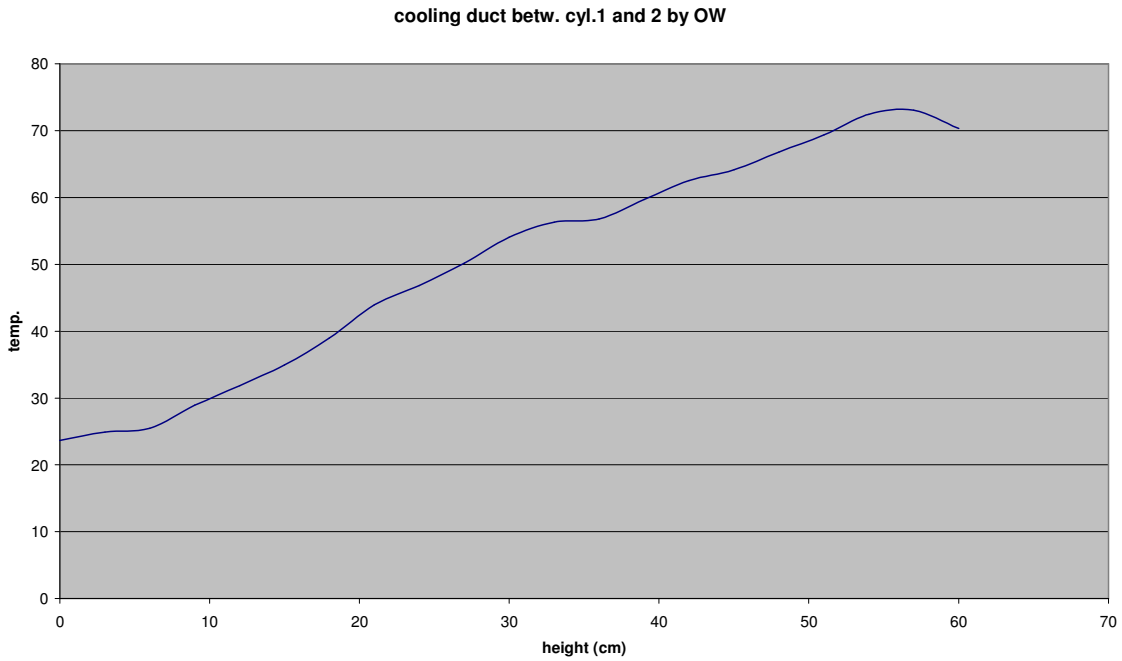

Figure 4.14: Cooling duct 1-2 temperatures by optical wires (OWs)

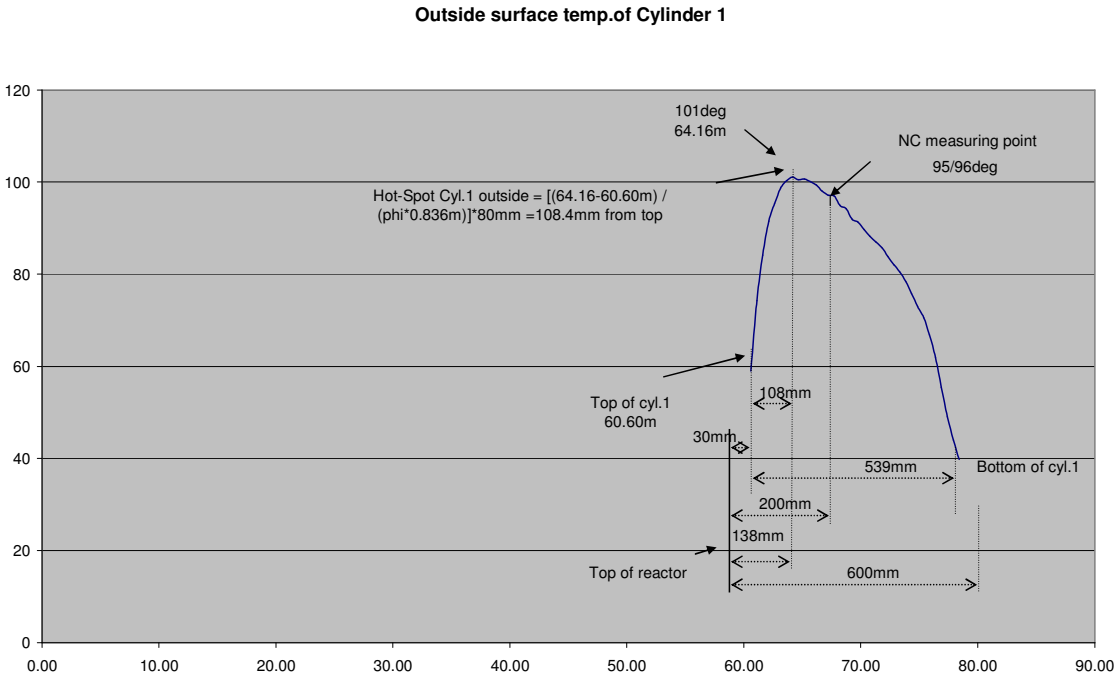

Figure 4.15: Surface temperature and hot-spot of cylinder 1 by OWs

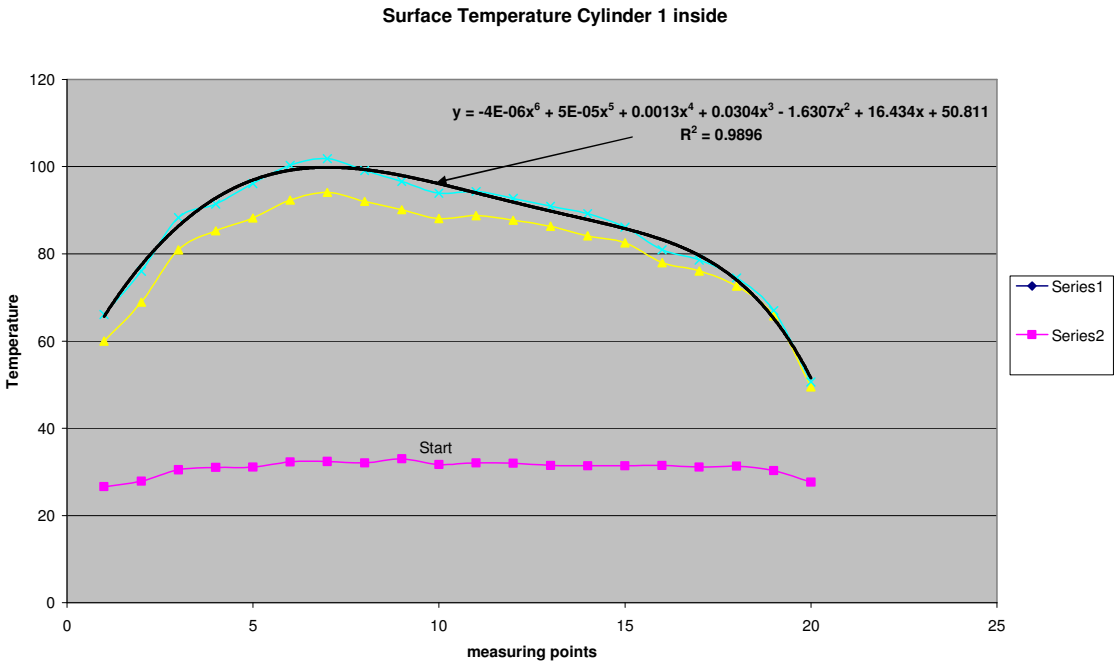

Figure 4.16: Temperatures at inside surface of cylinder1 measured by thermocouples (TCs)

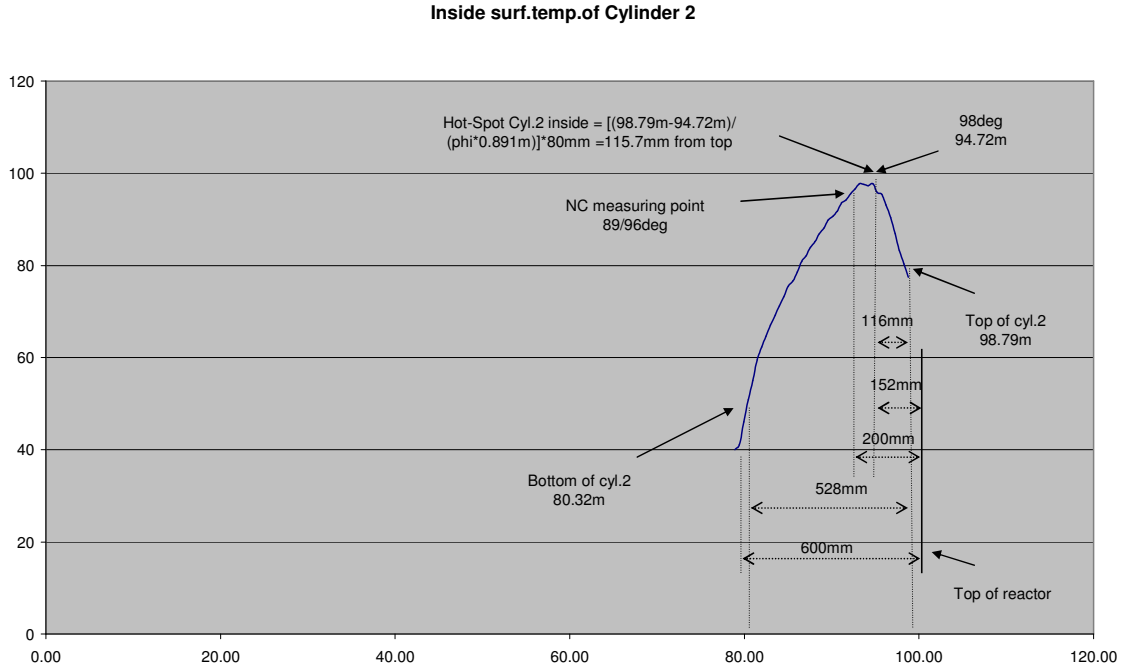

Figure 4.17: Winding temperature and hot-spot of cylinder2 by OWs

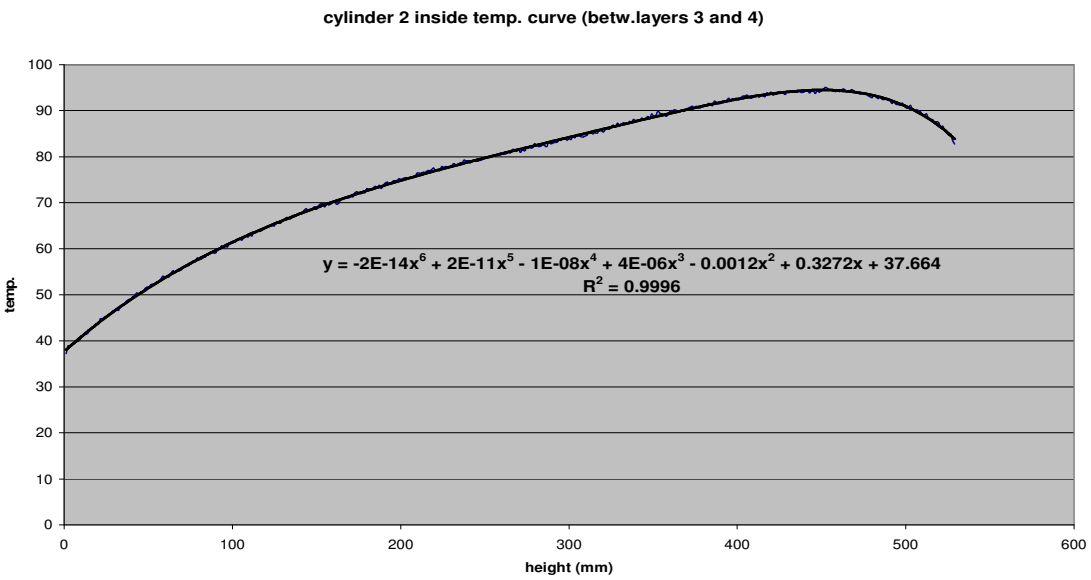

Figure 4.17a: Winding temperature of cylinder 2 (OWs)

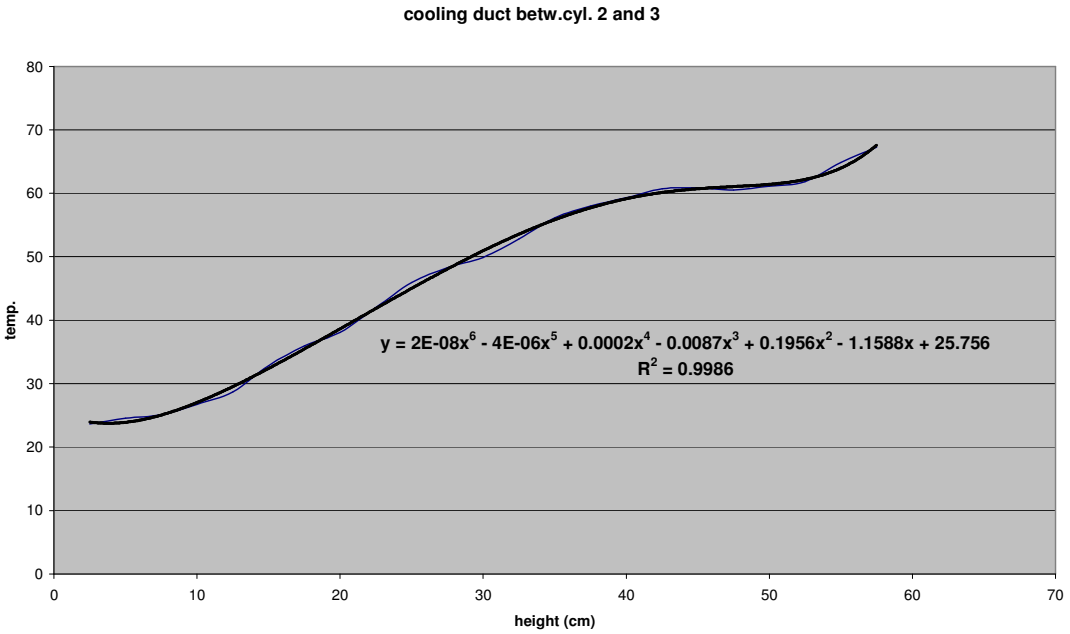

Figure 4.17 b: Cooling duct 2-3 temperatures by optical wires (OWs)

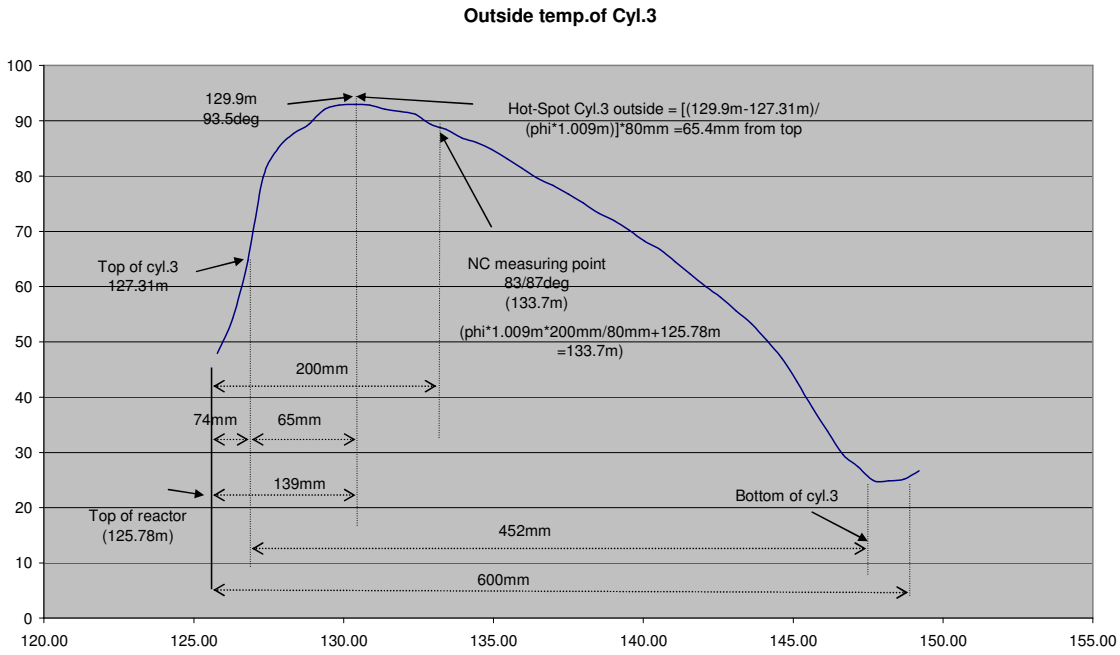

Figure 4.18: Surface temperature and hot-spot of cylinder 3 by OWs

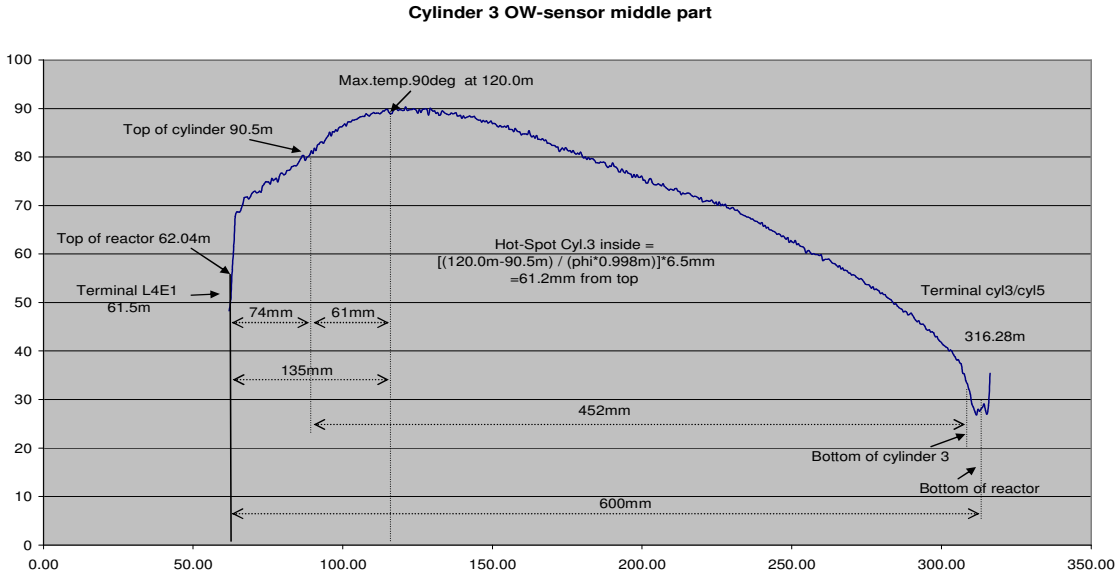

Figure 4.19: Winding temperature and hot-spot of cylinder 3 by OWs

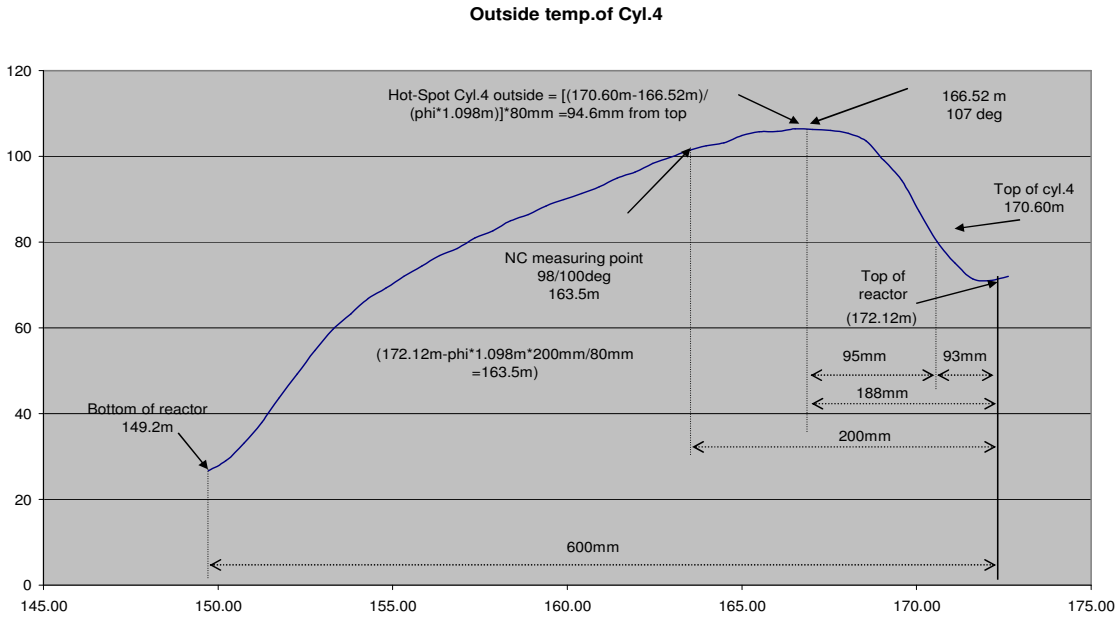

Figure 4.20: Surface temperature and hot-spot of cylinder 4 by OWs

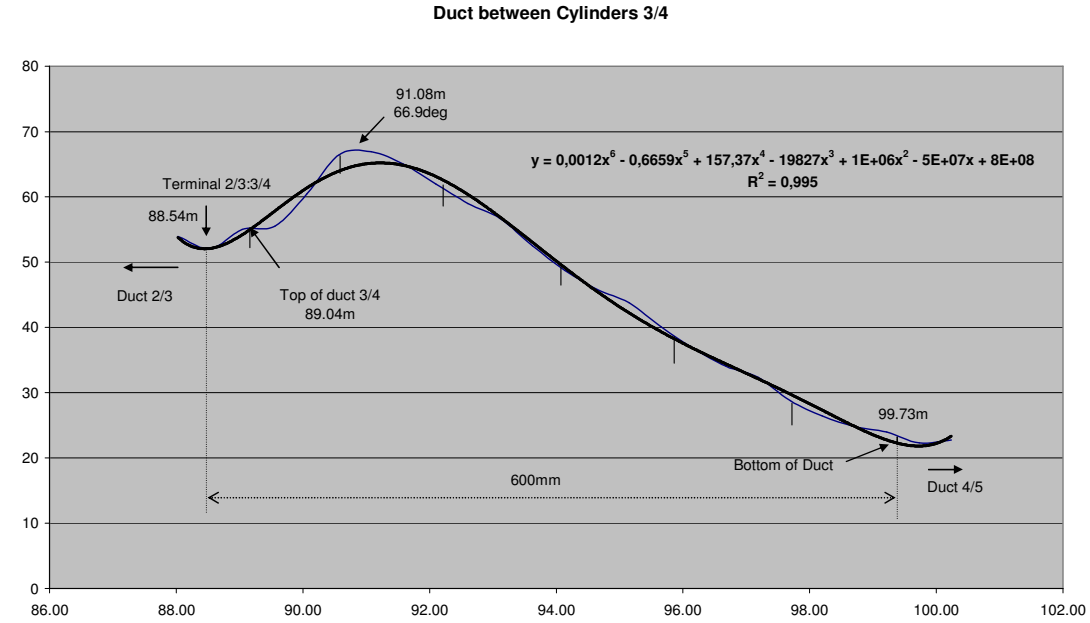

Figure 4.20a: Temperatures in cooling duct between cylinders 3 and 4 measured by OWs

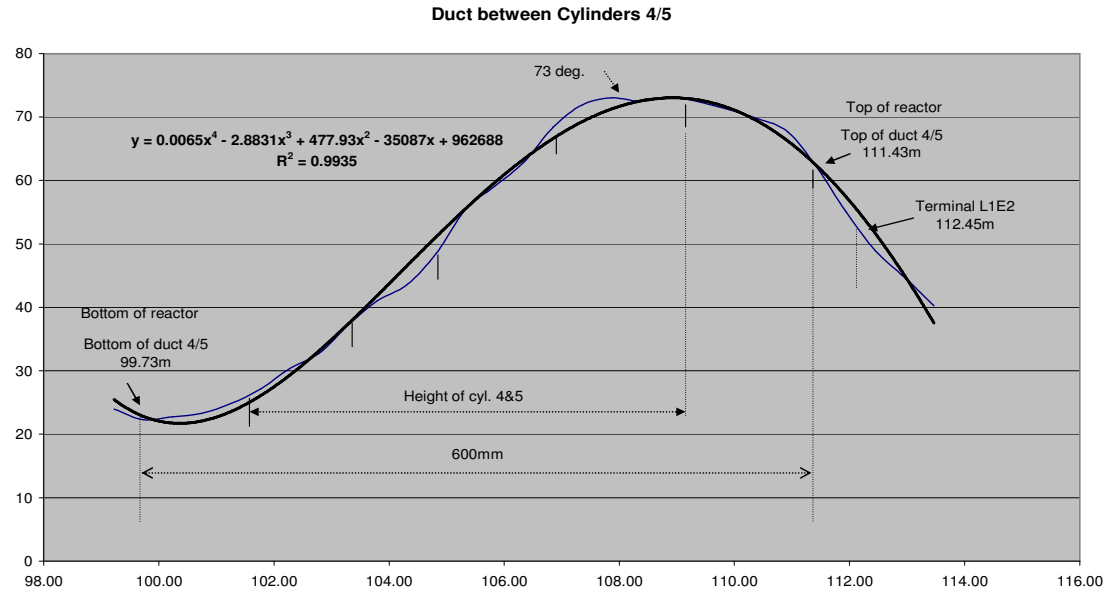

Figure 4.20 b: Temperatures in cooling duct between cylinders 4 and 5 measured by OWs

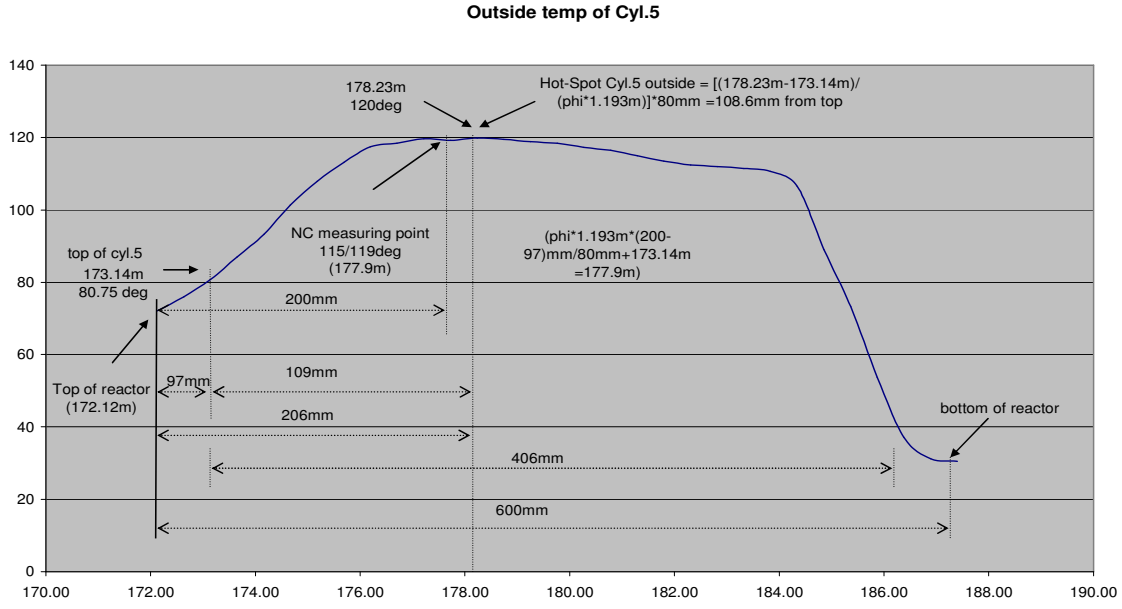

Figure 4.21: Surface temperature and hot-spot of cylinder 5 by OWs

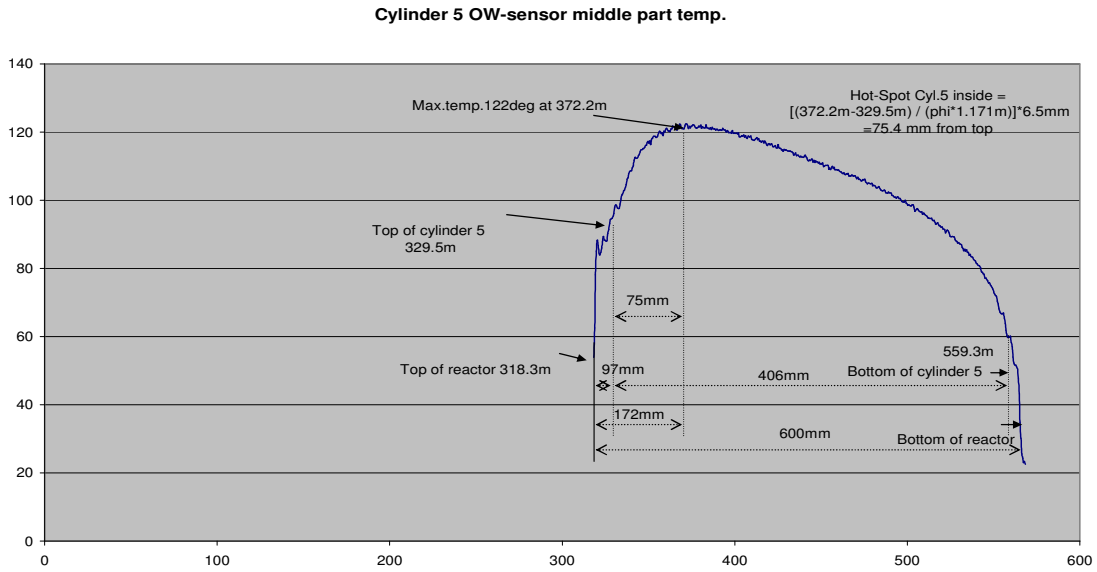

Figure 4.22: Winding temperature and hot-spot of cylinder 5 by OWs

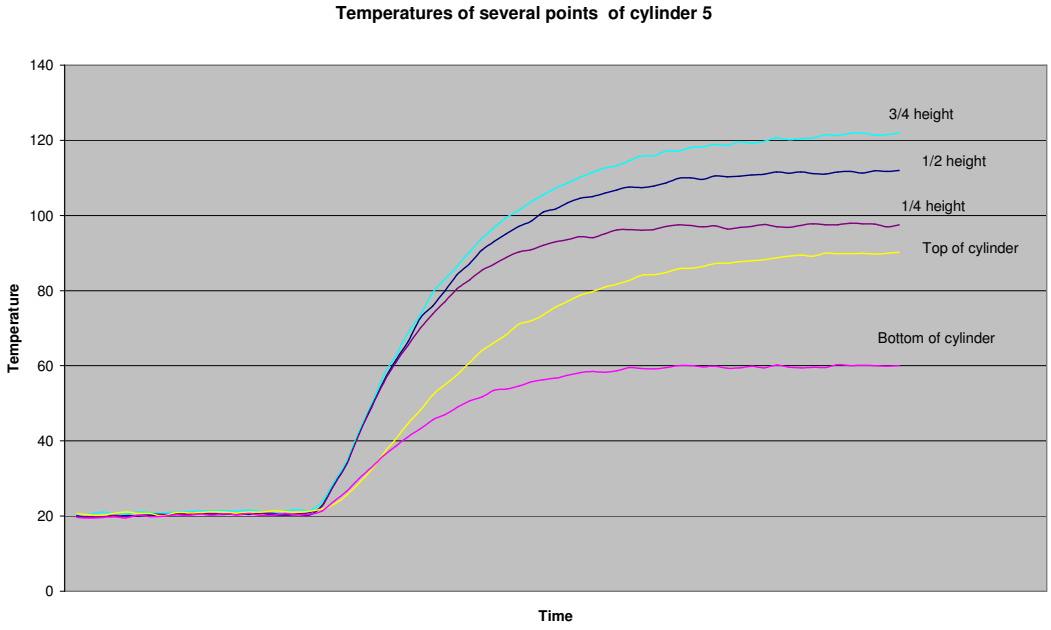

Figure 4.22a: Temperature curves of cylinder 5 vs. heating time (by OWs)

Time constants and losses

The thermal time constant (T) has also been defined by Richter (Richter, 1924), as the length of time required for the temperature to change from the initial value to the ultimate value if the initial rate of change is continued until the ultimate temperature is reached. The time constant is usually measured by determining the length of time required for a specific fraction of the change in temperature from initial value to ultimate value to take place. Generally, about 63 percent of the temperature change occurs in a length of time equal to the time constant, regardless of the relationship between the initial and final temperatures. After 4T the temperature rise has reached the value of approximately 98% of the final temperature.

The differential heat balance equation is:

$$\mathbf{Qdt - A\alpha_k \Delta\Theta dt = mcd\Theta_{winding}/dt} \qquad (4.1)$$

(Produced heat – heat flux to outside = in equipment stored heat)

where

Qdt = heat (P_h) produced in time dt
A = surface area
α_k = average heat transfer coefficient for convection
$\Delta\Theta dt$ = temperature rise in time dt
m = mass
c = specific heat
$d\Theta_{winding}$ = change of temperature in cylinder winding

In steady-state condition the right hand side of the above equation is zero, and the maximum temperature can be calculated

$$\mathbf{\Theta_{max} = Q/ (A\ \alpha_k)} \qquad (4.2)$$

The time constant is

$$\mathbf{T = mc / (A\ \alpha_k)} \qquad (4.3)$$

the differential equation is

$$\mathbf{dt = (T/ (\Theta_{max} - \Theta))d\Theta} \qquad (4.4)$$

and the solution when the boundary conditions at the beginning are t = 0 and $\Theta = \Theta_0 = 0$, is finally

$$\mathbf{\Theta/\Theta_{max} = 1- e^{-t/T}} \qquad (4.5)$$

Time constants and losses for cylinders 1 to 5, with a current of 608A/50Hz were measured and calculated as follows:

Calculated time constants (T) by means of weights and losses:

$$\mathbf{T = (C_{coil}/P_{hcoil})\Theta coil} \qquad (4.6)$$

where,

C = total thermal capacitance of one coil [Ws/°C]
P_h = electrical losses of one coil [W]
Θ_{coil} = temperature rise of one coil ($\upsilon_{end} - \upsilon_{amb}$) [°C]

$$\mathbf{C = mc} \qquad (4.7)$$

$$\mathbf{m = \gamma n(\pi/2)^2 d^2 D} \qquad (4.8)$$

where,

m = the weight of cylinder
c = the specific heat (c_{al} = 920 Ws/kg °C)
γ = density (γ_{al} = 2.70 kg/dm^3)
n = number of turns of one cylinder (sum of each layer)
d = diameter of aluminium wire (2,5 or 3.0 mm)
D = mean diameter of one cylinder

$$\mathbf{P_h = i_s^2 \rho n(\pi/2)^2 d^2 D} \qquad (4.9)$$

where,

i_s = mean current density [A/mm^2]
ρ = specific electrical resistance
(At reactor's mean over temperature of 82.4°C, $\rho_{al} = 0.0368*10^{-6}\Omega m$)

The time constant will be

$$\mathbf{T = (C/P_h)\,\Theta coil = [(\gamma n(\pi/2)^2 d^2 Dc)/(i_s^2 \rho n(\pi/2)^2 d^2 D)]\Theta_{coil}}$$

$$\mathbf{= (\gamma c/\rho)\,\Theta coil / i_s^2} \qquad (4.10)$$

Thus, (for aluminium winding)

$$\mathbf{T_{al} = 67.5\Theta coil/i_s^2\ sec.} \qquad (4.11)$$

$$\mathbf{T_{al} = 1.125\Theta coil / i_s^2\ min} \qquad (4.12)$$

Measured temperature rises (υ_{amb} =20°C)

Θ_1 = 81 °C
Θ_2 = 78 °C
Θ_3 = 74 °C

$\Theta_4 = 87$ °C
$\Theta_5 = 102$ °C

Current densities [A/mm^2] ($i_s = i_{s\,486}$* 608A/486,6A = 1.25* $i_{s\,486}$, where $i_{s\,486}$ is the current density at 486,6A, as per NC's specification)

$i_{s1} = 1.691$
$i_{s2} = 1.286$
$i_{s3} = 1.232$
$i_{s4} = 1.376$
$i_{s5} = 1.816$

Losses

$P_{h1} = 1736$ W	(d = 2.5mm; D = 0.821m; n = 1303)
$P_{h2} = 1166$ W	(d = 3.0mm; D = 0.915m; n = 943)
$P_{h3} = 854$ W	(d = 3.0mm; D = 1.005m; n = 685)
$P_{h4} = 1281$ W	(d = 3.0mm; D = 1.095m; n = 756)
$P_{h5} = 2788$ W	(d = 3.0mm; D = 1.192m; n = 868)

$\Sigma = 7825$ W	

Weights

$m_1 = 44{,}5$kg	Spider-arms: 4*(0.1*0.8*13.3) dm^3
$m_2 = 51{,}7$kg	$m = \gamma V = 11{,}5$kg
$m_3 = 41{,}3$kg	
$m_4 = 49{,}7$kg	
$m_5 = 62{,}1$kg	

$\Sigma = 249{,}3$kg	

The filling and supporting material is a mixture of wire glass (fg) with resin, in which the specific heat is $c_{fg} = 840$ Ws/kg°C. The total mass of the wire glass with resin is 125kg and it is assumed that each cylinder has 25 kg share.
The wires have a 0.1mm thin Mylar® polyester film layer of insulation, which has a specific heat $c_{Mylar} = 1170$Ws/kg°C and density $\gamma_{Mylar} = 1.39$ kg/dm^3.
Thus, in accordance with (4.7; 4.8) the thermal capacitance of wire glass with resin per cylinder is $C_{fg} = 21000$ Ws/°C and the thermal capacitances of Mylar® polyester film isolation per cylinder are:

$C_{1\,Mylar} = 4466$ Ws/°C
$C_{2\,Mylar} = 4294$ Ws/°C
$C_{3\,Mylar} = 3428$ Ws/°C
$C_{4\,Mylar} = 4118$ Ws/°C
$C_{5\,Mylar} = 5160$ Ws/°C

Time constants

The results for calculated and measured time constants are as follows:

	Calculated (Al.windings only)	Calculated (with fg/mylar)	Measured
T_1	31.9 min	51.6min	62.6 min
T_2	53.1 min	81.2min	82.3 min
T_3	54.9 min	90.2min	92.2 min
T_4	51.7 min	80.2min	79.5 min
T_5	34.8 min	50.8min	57.6min

It is assumed that the rather big differences between calculated and measured values of cylinders 1 and 5 are a consequence of better cooling from the outermost cylinders. The heat transfer through radiation is not taken into account here.

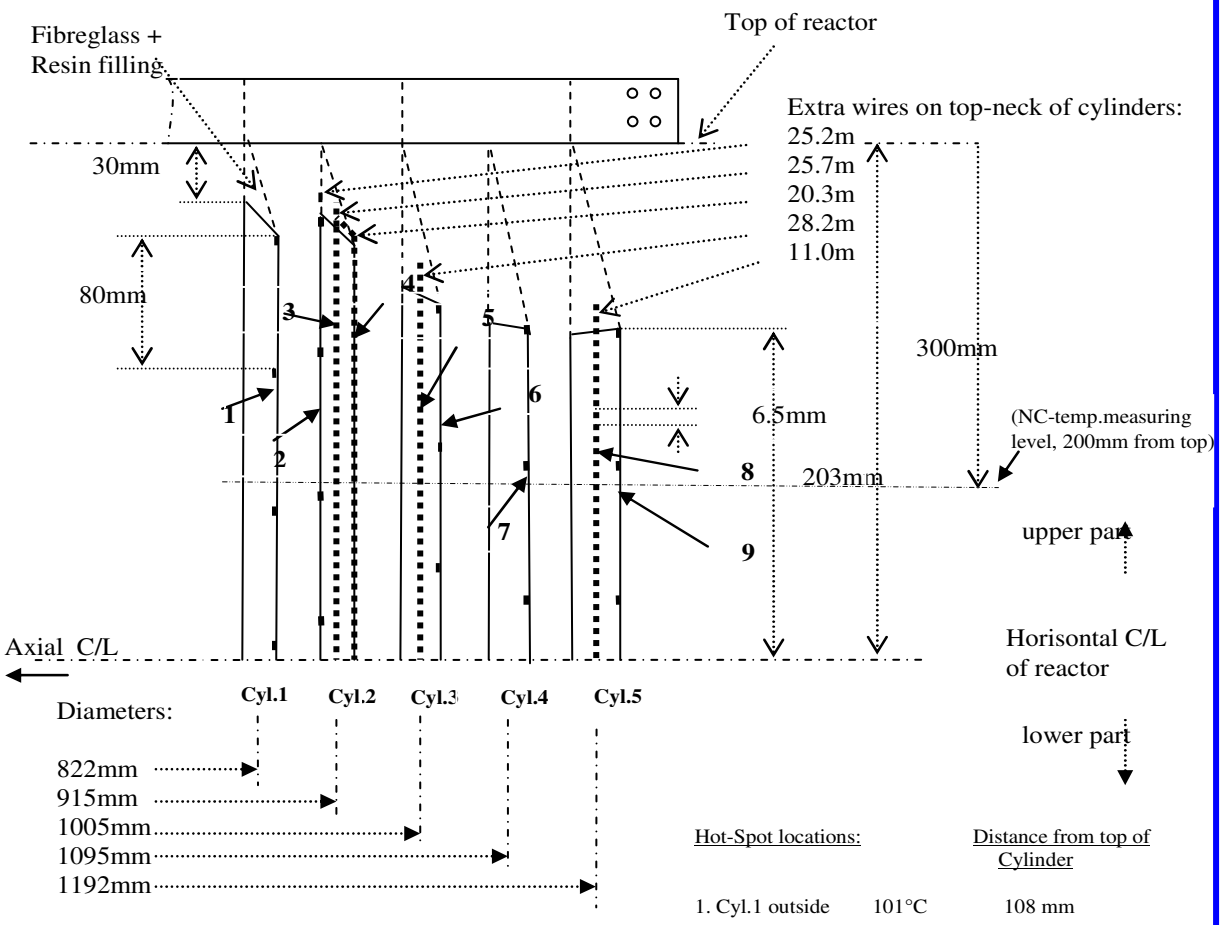

Calculated Time constants τ
(By: I = 608A, T_{amb} = 20°C)

$\tau = 1.125*\Theta_{max}/\sigma^2$ [min]
Θ_{max} = over temp. [°C]
σ = curr.dens. [A/mm^2]

τ_1 = 51.6min
τ_2 = 81.2min
τ_3 = 90.2min
τ_4 = 80.2min
τ_5 = 50.8min

Hot-Spot locations:		Distance from top of Cylinder
1. Cyl.1 outside	101°C	108 mm
2. Cyl.2 inside	98°C	116 mm
3. Cyl.2 middle part	96°C	74 mm
4. Cyl.2 outside	94°C	79 mm
5. Cyl.3 middle part	90°C	61 mm
6. Cyl.3 outside	94°C	77 mm
7. Cyl.4 outside	107°C	95 mm
8. Cyl.5 middle part	122°C	75 mm
9. Cyl.5 outside	120°C	109 mm

Hot-Spots and Arrangement of embedded optical sensor wires (OW)

Figure 4.23: Summary of hot-Spot values and locations from OW measurements

Temperature calculation from the outside (surface) to the inside of the winding:

The average inside temperature of a cylinder can be calculated if the temperature of outside surface is known.

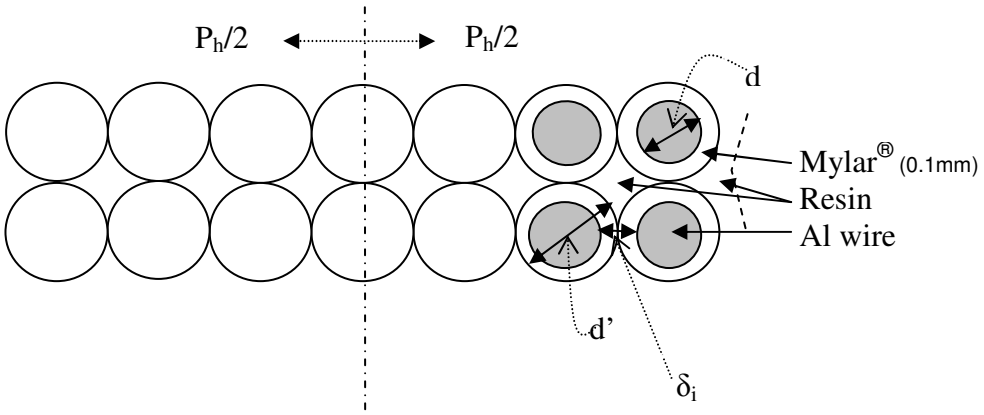

Figure4.24: Symmetrical arrangement of aluminium wires of cylinder

Resultant heat transfer coefficient λ_{res}: (Gotter,1954)

$\lambda i = \lambda_{resin} \approx \lambda_{mylar} = 0.155$ W/m ˚C

$\lambda_{res} = \lambda i(d_{wire}/\delta_i + \delta_i/d')$ (4.13.1)

$\lambda_{res} = 2.33$ or 1.95 W/m ˚C

where

d' = diameter of wire with insulation (d_{wire} + 2*0.1mm)

d_{wire} = diameter of wire (3.0mm or 2.5mm)

δ_i = d' – d_{wire} = 0.2mm

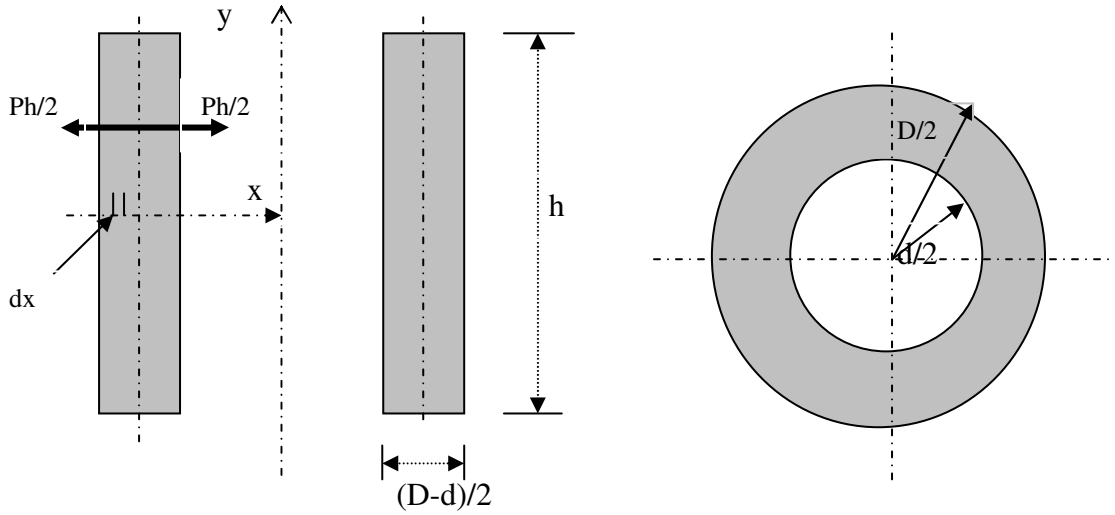

Figure 4.25: Dimensions of one cylinder

$$R_{th} = L/(\lambda_{res}A) \quad (4.13.2)$$

$$L = (D-d)/2 \quad (4.13.3)$$

$$r = R_{th}/L = 1/(\lambda_{res}A) \quad (4.13.4)$$

$$A = \pi(D+d)h/2 \quad (4.13.5)$$

$$p = Ph/L \quad (4.13.6)$$

where

Ph = total losses of cylinder
R_{th} = thermal resistance between inside core and outside surface of winding
λ_{res} = Resultant heat transfer coefficient
A= average area of jacket of cylinder
L = thickness of winding
p = losses of winding (per length)
r = thermal resistance (per length)

For calculating the inside temperature (Θa) when the outside temperature (Θb) is known, the following analogous thermal model can be used (Figure 4.27):

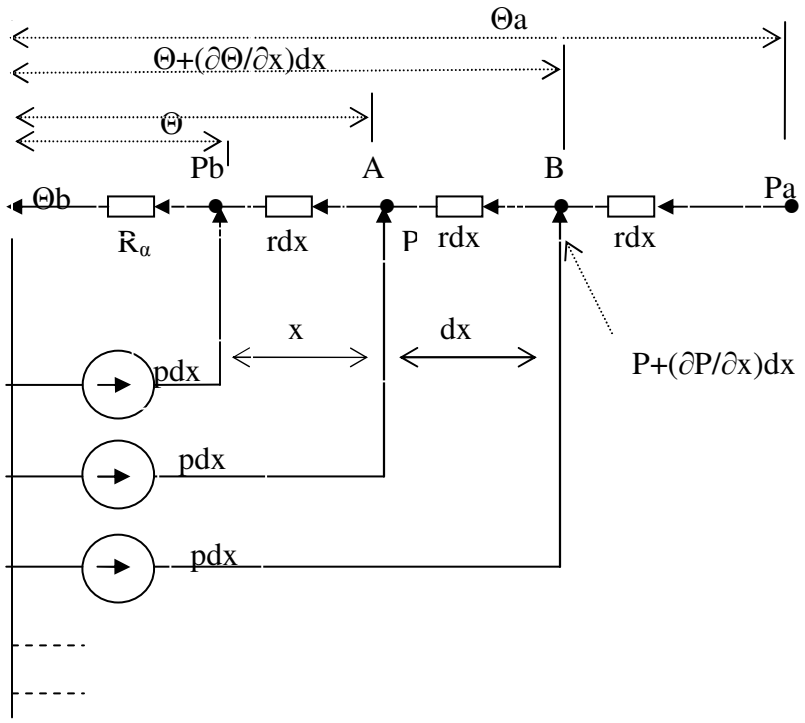

Figure 4.27: Analogous thermal model

where

Θa = inside temperature rise of cylinder
Θb = outside surface temperature rise of cylinder
R_α = thermal resistance from winding to ambient over the outer surface
dx = elementary unit in x-direction (i.e. between points A and B)
P = thermal flow in point A (in distance of x from surface)
Θ = temperature rise in point A
Pb = Thermal flow through the outer surface (= Ph/2)

The temperature change within horizontal direction dx is:

$$(\partial\Theta/\partial x)\, dx = Prdx$$

and so

$$\partial\Theta/\partial x = Pr \qquad (4.13.7)$$

The change of thermal flow within horizontal direction dx is:

$$\Delta P = P+(\partial P/\partial x)dx$$

and the thermal flow in point B is (Kirchoff's I law):

$$P = pdx + P + (\partial P/\partial x)dx$$

and so

$$\partial P/\partial x = -p \qquad (4.13.8)$$

By derivation of (4.13.7) and (4.13.8) with respect to x and substituting we will get

$$\partial^2\Theta/\partial x^2 = -rp \qquad (4.13.9)$$

The result from integrating (4.13.9) with following boundary conditions for the integrating constants

x = 0	x = 0
P = Pb	$\Theta = \Theta b$

is

$$\Theta = -rpx^2/2 + Pbrx + \Theta b \qquad (4.13.10)$$

$$P = -px+Pb \qquad (4.13.11)$$

Substituting (4.13.3 ... 4.13.6) with the middle point of winding (x = L/2) we will get

$$\Theta a = - [Ph(D-d)/8\lambda_{res}](D+d)\pi h + [Ph(D-d)/4\lambda_{res}](D+d)\pi h + \Theta b \qquad (4.13.12)$$

Thus, the temperature difference between the inside winding and surface is

$$\Delta\Theta = \Theta a - \Theta b = [Ph(D-d)/8\lambda_{res}](D+d)\pi h \qquad (4.13.13)$$

The results of measured and calculated temperature differences between outside and inside cylinders 2, 4 and 5 are as follows (inside temperatures of cylinders 1 and 4 were not measured by optical wires):

Table 4.1: Results of temperature calculations and –measurements

	Calculated $\Delta\Theta$ (°C)	Measured $\Delta\Theta$ (°C)
Cyl.1	3.9	not measured (no OWs available)
Cyl.2	1.95	2
Cyl.3	-1.23	-4 (Outside > Inside → Radiation)
Cyl.4	2.31	not measured (no OWs available)
Cyl.5	2.66	2

(Note: The technical data (i.e. heat transfer coefficients) of Mylar® and resin/glass wires are estimated since no exact data were available and may therefore cause some errors).

As shown in table 4.1, the thermal flow in cylinder 3 is from the outside surface to the inside of the winding because the temperature of cylinder 4 is higher and therefore the thermal flow is transferred by radiation to the lower temperature surface.

Calculation of heat flow and losses with known temperatures

When the temperatures of a vertical surface (such as the cylinder walls of the test reactor) are known the convective heat flow depending on the height (dx) can be calculated as follows:

$$\mathbf{dQ_{conv\,x} = \alpha_x \pi D (\Theta_{wall\,x} - \Theta_{ambx}) dx} \qquad (4.14)$$

where the elementary unit area is dA_x (= π D dx)

After integrating over the whole length (0...L) of the cylinder's surface the total heat flow is

$$\mathbf{Q_{conv} = \pi\, D_{o\text{-}L} \int [\alpha_x\, (\Theta_{wall\ x}(x) - \Theta_{ambx}(x))]\, dx} \qquad (4.15)$$

where

$Q_{conv\ x}$ = heat flow
Θ_{ambx} = ambient temperature on level x of outside reactor or in the cooling ducts, respectively.
$\Theta_{wall\ x}$ = wall temperature on level x
D = cylinder diameter
α_x = heat transfer coefficient on level x (equation 3.27)
dx = elementary highness unit
L = height of cylinder

The wall temperatures ($\Theta_{wallx}(x)=f(x)$) and ambient temperatures in the cooling ducts ($\Theta_{ambx}(x)=f(x)$) at level (x) can be determined for example in accordance with the temperature equations shown in figures 3.41-3.46 and in figures 4.11 and 4.12.

The radiation heat flow between the cylinders (q_{rad}) can be calculated with equations (3.26a)... (3.26c). The temperatures at different levels (x) are determined as shown above.

Thus,

$$\mathbf{dQ_{rad} = 5.7\varepsilon_{red}\pi D[((273 + \Theta_{1wall\ x})/100)^4 - ((273 + \Theta_{2wall\ x})/100)^4]dx\ \ [W]} \qquad (4.16)$$

and after integrating again over the whole length (0...L) of the cylinder

$$\mathbf{Q_{rad} = 5.7\varepsilon_{red}\pi D_{o\text{-}L} \int [((273 + \Theta_{1wall\ x}(x))/100)^4 - ((273 + \Theta_{2wall\ x}(x))/100)^4]dx\ \ [W]} \qquad (4.17)$$

in which (x) and (D) are in (meters) and ($\Theta_{1wall\ x}$) and ($\Theta_{2wall\ x}$) in ($^{\circ}$C).

The theoretical dynamic heat transfer model for each cylinder of our reactor is now:

$$\mathbf{P_w = I^2R_{ac} = mcd\Theta_{winding}/dt + \pi D_{o\text{-}L} \int [5.6[(\Theta_{wallx}(x) - \Theta_{ambx}(x))/(\Theta_{ambx}*x)]^{0.25}(b/760)^{0.5}(\Theta_{wallx}(x) - \Theta_{ambx}(x))]dx + 5.7\varepsilon_{red}\pi D_{o\text{-}L} \int [((273 + \Theta_{1wallx}(x))/100)^4 - ((273 + \Theta_{2wallx}(x))/100)^4]\, dx\ [W]} \qquad (4.18)$$

where the stored heat in the cylinder (mcdΘ/dt) is from equation (4.1) and the values of (Θ_{1wallx}) and (Θ_{2wallx}) are the respective temperatures of the cylinder walls on level (x). For the outside surface of cylinder 5 as well as for the inside surface of cylinder 1 the (Θ_{2wallx}) temperature is to be replaced with ambient temperature (Θ_{amb}).
In steady-state conditions, when the temperature changes in the reactor or cylinders are zero (theoretically $t \approx \infty$, but in practice after 4...5T) and the losses are transmitted from the reactor by natural convection and radiation only, the total losses can be calculated as follows:

$$\mathbf{P_w = I^2R_{ac} = \pi D_{o\text{-}L}\int[5.6[(\Theta_{wallx}(x) - \Theta_{ambx}(x))/(\Theta_{ambx}x)]^{0.25}(b/760)^{0.5}(\Theta_{wallx}(x) - \Theta_{ambx}(x))]dx +}$$

$$\mathbf{5.7\varepsilon_{red}\pi D_{o\text{-}L}\int[((273 + \Theta_{1wallx}(x))/100)^4 - ((273 + \Theta_{2wallx}(x))/100)^4]\,dx\ [W]} \qquad (4.19)$$

An unambiguous analytical solution for the above integral equations is not possible but the heat losses of the cylinders can be approximately calculated with equations (4.17...4.19) using the Riemann-Sum method, which means that the calculation is made for small (Δx) values assuming that the functions $\mathbf{\Theta_{wallx}}$ = f(x) and $\mathbf{\Theta_{ambx}}$ = f(x) have their average values and are unchanged between the boundaries of Δx.

For example, the losses calculations with measured temperatures for cylinder 5 are as follows:

The thickness of the thermal boundary layer (δ_{th}) in the cooling ducts is

$$\delta_{th} = \lambda_{air} / \alpha_{conv}$$

where

λ_{air} = thermal conductivity of cooling air (W/mK)
α_{conv} = heat transfer coefficient (W/m^2K)

With an average cooling air temperature of 50 °C and with average thermal conductivity (as shown below) α_{convav} = 6.5 W/m^2K, the thickness of thermal boundary layer for laminar flow will be δ_{th} = 4.3mm.

The height of cylinder 5 is h = 0.4m. The diameter of outer surface is D_{out5} = 1.21m and the inner surface D_{in5} = 1.17m. The assumed emissivity factor for radiation is ε = 0.85 for the outside of cylinder 5 and inside cylinder number 1. For other cylinders, the emissivity factor is calculated with equation (1.14).

Let's divide the height of cylinders 5 and 4 into four parts so that Δx = 0.1m. The average outer and inner temperatures of cylinders 5and 4 as well as the temperatures in cooling duct 4/5 for each part can be taken from Figures (4.22, 4.20 and 4.20b) and are, from bottom to top

$T_{51} = 78^{\circ}C$
$T_{52} = 106^{\circ}C$
$T_{53} = 118^{\circ}C$
$T_{54} = 110^{\circ}C$

$T_{41} = 62^{\circ}C$
$T_{42} = 90^{\circ}C$
$T_{43} = 101^{\circ}C$
$T_{44} = 97^{\circ}C$

$T_{cd14/5} = 36^{\circ}C$
$T_{cd24/5} = 49^{\circ}C$
$T_{cd34/5} = 61^{\circ}C$
$T_{cd44/5} = 78^{\circ}C$

The ambient temperature was $T_{amb} = 20^{\circ}C$

The heat transfer coefficients α_x (equation 3.27) on each level of Δx for the outer surface are

$\alpha_{xo1} = 6.6\ W/m^{2\circ}C$
$\alpha_{xo2} = 7.3\ W/m^{2\circ}C$
$\alpha_{xo3} = 7.6\ W/m^{2\circ}C$
$\alpha_{xo4} = 7.3\ W/m^{2\circ}C$

and for the inner surface (cooling duct temperature (Figure 4.20b) as ambient temperature)

$\alpha_{xi1} = 6.0\ W/m^{2\circ}C$
$\alpha_{xi2} = 6.4\ W/m^{2\circ}C$
$\alpha_{xi3} = 6.3\ W/m^{2\circ}C$
$\alpha_{xi4} = 5.4\ W/m^{2\circ}C$

The calculated losses (equations 4.14 and 4.16) will be than

Outer surface of cylinder 5:

Convection

$Q_{hconvx1} = 144W$
$Q_{hconvx2} = 236W$
$Q_{hconvx3} = 280W$
$Q_{hconvx4} = 236W$

896W

Radiation

$Q_{hradx1} = 152W$
$Q_{hradx2} = 240W$
$Q_{hradx3} = 304W$
$Q_{hradx4} = 240W$

936W

Inner surface of cylinder 5:

Convection

$Q_{hconvx1} = 126W$
$Q_{hconvx2} = 200W$
$Q_{hconvx3} = 267W$
$Q_{hconvx4} = 169W$

762W

The emissivity factor (ε_{res}) for the surfaces between the cylinders can be calculated with (1.14).

Radiation

$Q_{hradx1} = 55W$
$Q_{hradx2} = 72W$
$q_{hradx3} = 61W$
$Q_{hradx4} = 36W$

224W

The total losses of cylinder 5 are then

$Q_{h5} = 2818W$

The losses have been calculated for the other cylinders in a similar way, as per table 4.2 below.

Table 4.2: From the measured temperatures (with $\Delta x = 0.1m$) and with the supply current calculated losses (in Watts)

From temperatures calculated losses	**Cyl.1**	**Cyl.2**	**Cyl.3**	**Cyl.4**	**Cyl.5**	
Convection outside	411	403	306	508	896	
Convection inside	468	376	346	528	762	
Radiation outside	67	71	142	179	936	
Radiation inside	464	74	75	149	224	
Sum	1410	924	869	1364	2818	7385
With supply current calculated losses (Ph = I^2*Rac)	1736	1166	854	1281	2788	7825

In both methods some assumptions have been made. The ambient air pressure was at a normal level (760 mmHg) and for example, the emissivity factor and view factor for radiation were assumed to be 0.85 and 1.0 respectively. The back-reflection of radiated heat flow between the cylinders is not included in the calculations. The mean upper temperature used for the calculation of electrical losses was assumed the same for all cylinders, which is not exactly correct because the temperatures will influence to the specific electrical resistances and thus the losses, too. Because the ratio of the average cylinder length (L) to the average cylinder thicknes (s) was about L/s = 500mm/18mm the radiation and conduction from the end of the cylinders in the vertical direction have been ignored.

Determining the cooling air flow in the cooling ducts

The reactor was powered with the same current as before, namely with 608A. The temperature changes were measured by thermocouples (TCs) fixed to the outer side of cylinder 5.

When the end temperature had been reached, the power was switched off and the cooling airflow on the top of reactor in several places (on the cooling ducts, inside and outside of reactor at different locations) was measured.

The hot-spot temperature at the outside surface of cylinder 5 was 111.6 degrees and its location about 150mm from the top of the reactor.

The results at ambient conditions are as follows:

Ambient temperature: 21.1 degrees
Air pressure: 1019.19 hPa (or 765mmHg)
Humidity: 8.3%

The equipment used for the measurements was:

Flow Master Precision Anemometer type 54N60
Manufactured by Dantec/Denmark

The measured cooling air velocities were:

0.85...0.9 m/s at outer side and 2...3 cm horizontal away from the top of cylinder 5
0.7...0.8 m/s on top of the reactor above the cooling ducts
0.4 m/s above those cooling ducts in which optical wires were installed
0.5 m/s at the top of the reactor along the Z-axis

The measured maximum airflow rate was 0.9m/s
The average value was 0.8 m/s (= v_m)

The critical Reynolds number for a cooling duct of angular form with a hydraulic diameter of (d = 2ab / (a+b)) (Schmitt & Beckmann 1930) is

$$Re_k \equiv v_m\, d/\nu_{kin.visk} \approx 2320 \qquad (4.20)$$

The hydraulic diameter for our reactor is d = 2*6*2.5/(6+2.5) = 3.53cm and so the critical air flow velocity (v_{kr}) for an ambient temperature of T=20 degrees and kinetic viscosity of $\nu_{kin.visk\ 20C}$ = 0.15 cm^2/s is v_{kr} = 0.99m/s. When calculating the critical air flow in the cooling ducts, an average cooling duct temperature of T=50 degrees is used (Figure 4.20b). This correspondents to a kinetic viscosity $\nu_{kin.visk\ 50C}$ = 0.18 cm^2/s and the critical velocity before the air flow becomes turbulent will be v_{kr} = 1.18 m/s. Since the measured maximum air flow velocity was v_{mmax} = 0.9m/s, and so well below critical, it can be said that the air flows in the cooling ducts are laminar.

According to the above mentioned authors, the fully formed laminar flow starts from the bottom level of L = 0.029 $v_m d^2/\nu_{kin.visk}$ = 1.4cm, and after that the velocity is constant.

On the outer surface of cylinder 5 the Reynolds number is $R_e = v_m H / \nu_{kin.visk}$ = 0.8m/s * 0.6 m / 0.18 cm^2/s = $2.7*10^4$, which is below Reynolds number of $R_{ekr.} = 3*10^5$, the defined condition for turbulence. The air flows on the outer surfaces are also turbulence free (or laminar).

If the temperature (Θ_{cd}) in the cooling duct and the ambient temperature (Θ_{amb}) at the inlet of this duct are known, the air flow velocity (v) of the cooling air passing through the duct can be calculated using the following empirical equation (Sakonidou, 2007)

$$v_{cd} = C_{dc}\,(\rho_{aircd} / \rho_{airamb})\,[hg\,(\sin(s))^2(\Theta_{cd} - \Theta_{amb})/\Theta_{amb}]^{1/2} \qquad (4.21)$$

where

v_{cd} = cooling air flow velocity (m/s)
ρ_{aircd} = air density in cooling duct (e.g. $\Theta_{cd80deg}$: ρ_{aircd} = 0.986 kg/m^3)
ρ_{airamb} = ambient air density (e.g. $\Theta_{amb20deg}$: ρ_{airamb} = 1.188 kg/m^3)
C_{dc} = discharge coefficient for the opening
(C_{dc} in an empirical coefficient which gives the relation between real flow rate and the theoretical (ideal) flow rate and is ≤ 1)
g = gravitational acceleration (9.81 m/s^2)
s = slope of the cooling duct with respect to the horizontal plane ($\perp$)
h = height of cooling duct (0.6m)
Θ_{cd} = max.cooling duct temperature (K)
Θ_{amb} = ambient (inlet) temperature (K)

The height of the cooling ducts in our test reactor is 60cm (slope s = 90deg) and further the temperature in the cooling duct between cylinders 4/5 was +80°C. With an inlet temperature of +20°C, the velocity of the cooling air flow will be

$$v_{cd} = C_{dc} * 0.913 \text{ m/s} \quad (4.21)$$

As presented before the maximum air velocity from our test reactor was measured at the outlet openings between cylinders 4 and 5 and was 0.9 m/s. Thus, the discharge coefficient will be

$$C_{dc} = 0.9/0.913 = 0.986$$

When the air velocity (v_{cd}) is known, then the temperature rise ($\Delta\Theta = \Theta_{cd} - \Theta_{amb}$) in the cooling duct can roughly be calculated as follows (assuming that $\rho_{aircd(50...80deg)} \approx 1.0$ kg/m^3)

$$\Delta\Theta = \Theta_{amb} (v_{cd} \rho_{airamb} / \rho_{aircd} C_{dc})^2 / (hg) \ [K] \quad (4.22)$$

The calculated temperature rise, using (4.22), between cylinders 4 and 5 is then

$\Delta\Theta = \Theta_{amb} (v_{cd} \rho_{airamb} / \rho_{aircd} C_{dc})^2 / (hg)$ [K] $\approx 293(0.9*1.18/1.0*0.986)^2/0.6/9.81 = 57.7$K, which is close to the OWs measured values of $\Delta\Theta_{cd4\text{-}5} \approx 55$K (Figure 3.44).

The temperature in the cooling ducts at critical air velocity (v_{kr}) before turbulence will be

$$\Delta\Theta_{kr} = \Theta_{amb} (v_{kr} \rho_{airamb} / \rho_{aircd} C_{dc})^2 / (hg) \ [K] \quad (4.23)$$

With $\Theta_{amb} = 293$K and $v_{kr} = 1.18$m/s, the maximum critical temperature rise in the cooling duct before the cooling air flow becomes turbulent is

$$\Delta\Theta_{kr} = 101\text{K}$$

The average critical temperature (T_{kravcd} in °C) in the cooling duct will be then

$$T_{kravcd4/5} = (121 + 20)/2 = 70.5 \text{ °C}$$

The average air velocity inside a vertical duct (slope s = 90 deg) can also be calculated as follows (Sakonidou, 2007)

$$v_{cd} = [2hg(\rho_{airamb} - \rho_{aircd})/(k_{in} + k_{out} + fh/d)]^{1/2} \quad (4.24)$$

where

v_{cd} = air velocity inside a vertical duct (m/s)
k_{in} = inlet pressure coefficient (proposed value 1.5)
k_{out} = outlet pressure coefficient (proposed value 1.0)
d = hydraulic diameter (defined as d = 2ab/(a+b))
f = friction coefficient which is defined as

$$f = 0.316/Re^{1/4} \tag{4.25}$$

Re is the Reynolds number which is defined as

$$Re = dv_{cd}\rho_{aircd}/\mu_{aircd} \tag{4.26}$$

where

μ_{aircd} = dyn.viscosity of cooling air (kg/m s)

Thus, the calculated friction coefficient is then

$$f = 0.051$$

The calculated air velocity as per (4.24) will be

$$v_{cd4/5} = 0.84 \text{ m/s}$$

The result above corresponds well with the measured air velocity values from the cooling ducts between cylinders 4 and 5 (i.e. $v_{cd4/5measured} = 0.9$ m/s).

The turbulence of the cooling airflow on the outer surface of the cylinders has a better cooling effect because fresh air from ambient mixed with the cooling air and so the heat transfer will be better.

In relatively small cooling ducts the effect of turbulence is negative, contrary to free surfaces because the turbulence in the airflow will tend to down the cooling air velocity. Therefore, the cooling effect is inferior to the cooling effect with laminar airflow.

Figure 4.28 shows the critical airflow values using the kinetic viscosity for 50 ^{o}C as above and with a distance of 2.5cm (b) between cylinders, but different cooling duct widths (a).

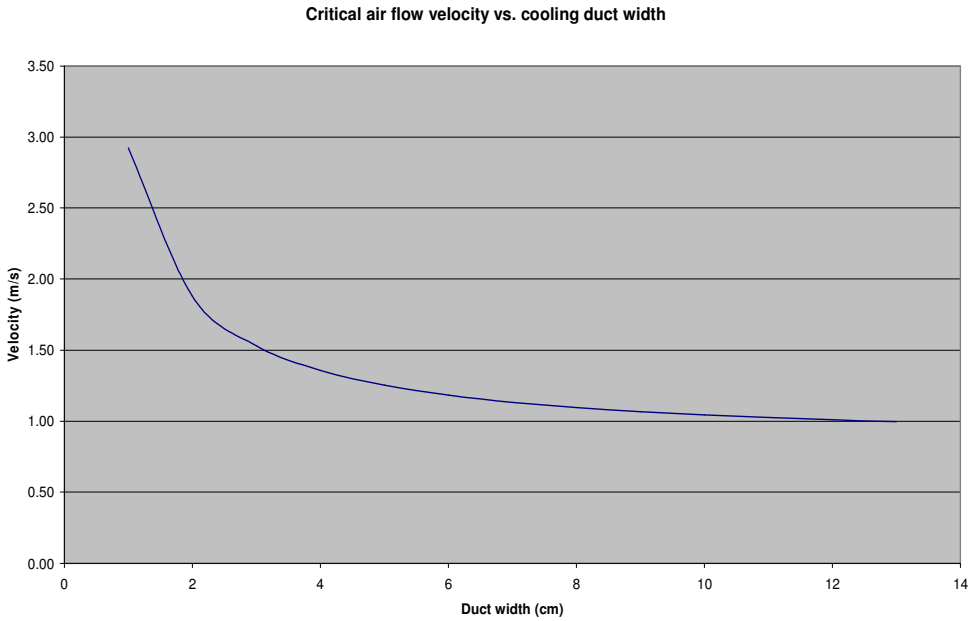

Figure 4.28: The influence of the width of cooling duct on the critical cooling air velocity

In Figure 4.28 the depths of the cooling ducts (distance between cylinders) are constant, namely 2.5cm, but the ducts widths do change. The respective critical airflow velocities are calculated before the flow becomes turbulent.

Determining the current distribution between cylinders

For determining the current distribution, the self- and mutual inductances have to be calculated. That has been done using the famous self-inductance equation by Nagaoga and the mutual inductances with the equation by H.B.Dwight (see Appendix B).

The influence of winding resistances and parallel winding layers in one cylinder has been examined and found to be so minimal that it can be ignored in this research work. However, they can be taken into account and calculated in the same manner. The matrices as well as the computing time for the calculations are then correspondingly greater.

In the following picture, Figure 4.29, the results of our calculated current distribution is compared with the manufacturer's data (which have been verified by their own measurements).

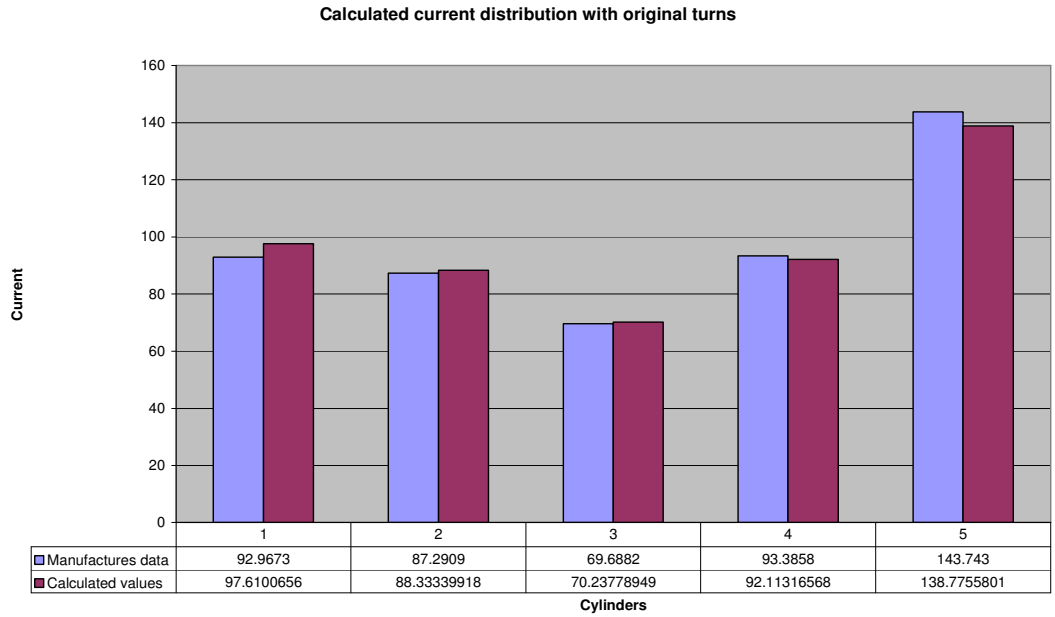

Figure 4.29: Calculated and manufacturer supplied current distribution

The small errors come from ignoring the resistances and parallel layers as mentioned before.

As an example, in the next picture (Figure 4.30), the winding turns on the 5th cylinder have been changed by -2 turns.

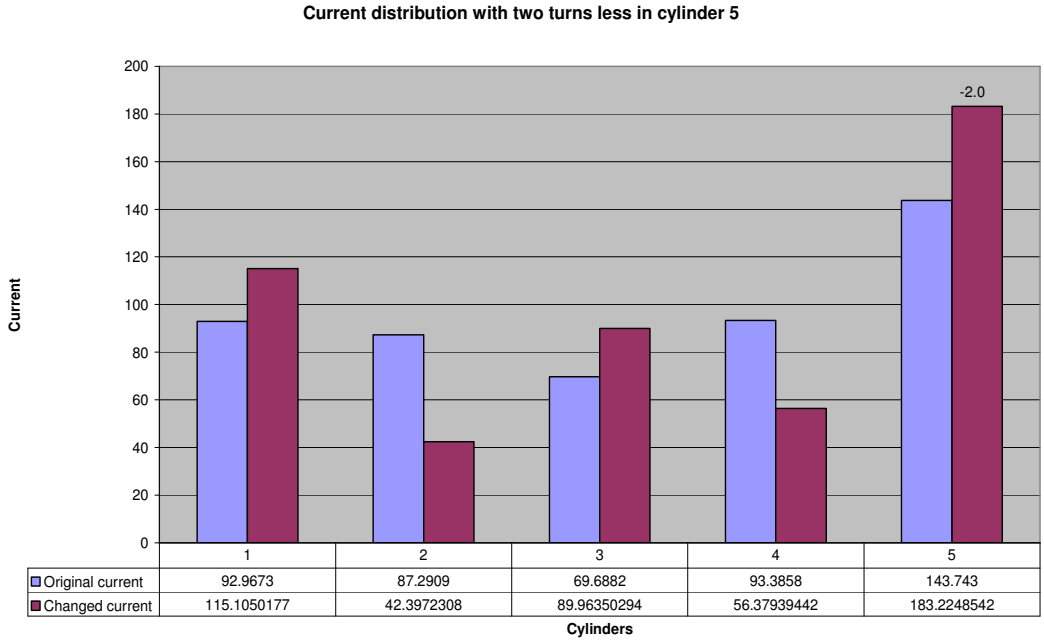

Figure 4.30: Current distribution when cylinder 5 has two turns less.

In the next example, Figure 4.31, the winding turns on the 5th cylinder have been changed by +2 turns.

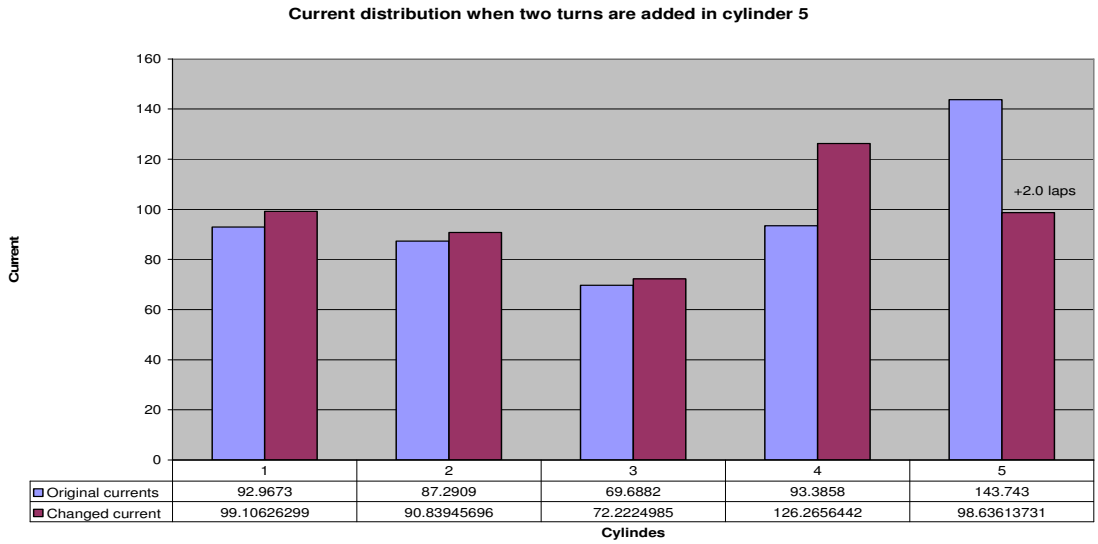

Figure 4.31: Current distribution when cylinder 5 has two turns more.

When the winding turns of each cylinder are changed one by one, the current distribution will change and the losses of cylinders will also be changed.

In the next table, Table 4.3, the winding turns have been changed cylinder by cylinder always by +/- 0.5 turns.

Table 4.3: Effects on cylinders when the winding turns have been changed +/- 0.5 turns

Changed	**N+0.5**	**Calculated current distribution and losses**				
			Curr./A	**Diff./A**	**Losses/W**	**Diff./W**
Cyl1	**93.54**		91.4103	-6.1998	863.71	-121.1
	78.58		93.7849	5.452	693.07	78.2
	68.50		70.3288	0.091	448.06	1.2
	62.96	**Z coil**	92.4876	0.374	646.83	5.2
	61.68	**1.362700**	139.0584	0.283	1336.09	5.4
					3987.77	**-31.1**
	93.04		104.06	6.4498	1119.30	134.5
Cyl2	**79.08**		74.02	-14.309	431.77	-183.1
	68.50		77.50	7.262	544.09	97.2
	62.96		92.19	0.080	642.73	1.1
	61.68	**1.363200**	139.29	0.517	1340.60	9.9
					4078.49	**59.6**
	93.04		97.72	0.108	987.03	2.2
	78.58		96.64	8.309	735.95	121.1

Cyl3	**69.00**		53.05	-17.193	254.89	-192.0
	62.96		100.43	8.319	762.73	121.1
	61.68	**1.363700**	139.23	0.457	1339.44	8.8
					4080.04	**61.2**
	93.04		98.15	0.537	995.71	10.9
	78.58		88.43	0.092	616.12	1.3
	68.50		79.29	9.056	569.56	122.7
Cyl4	**63.46**		73.96	-18.158	413.58	-228.0
	61.68	**1.364100**	147.25	8.473	1498.11	167.5
					4093.09	**74.2**
	93.04		98.04	0.428	993.50	8.7
	78.58		89.01	0.674	624.25	9.4
	68.50		70.77	0.536	453.75	6.8
	62.96		100.80	8.689	768.36	126.8
Cyl5	**62.18**	**1.364200**	128.45	-10.327	1140.00	-190.7
					3979.86	**-39.0**

Changed	**N- 0.5**					
Cyl1	**92.54**		103.9070	6.297	1116.01	131.2
	78.58		82.8288	-5.505	540.60	-74.2
	68.50		70.1377	-0.100	445.62	-1.3
	62.96		91.7239	-0.389	636.20	-5.4
	61.68	**1.356900**	138.4726	-0.303	1324.86	-5.8
					4063.29	**44.4**
	93.04		91.0810	-6.529	857.50	-127.3
Cyl2	**78.08**		102.8945	14.561	834.25	219.4
	68.50		62.8938	-7.344	358.33	-88.6
	62.96		91.9979	-0.115	640.00	-1.6
	61.68	**1.356300**	138.2027	-0.573	1319.70	-11.0
					4009.78	**-9.1**
	93.04		97.4581	-0.152	981.78	-3.1
	78.58		79.8895	-8.444	502.91	-111.9
Cyl3	**68.00**		87.8150	17.577	698.56	251.7
	62.96		83.6646	-8.449	529.31	-112.3
	61.68	**1.355800**	138.2428	-0.533	1320.47	-10.2
					4033.03	**14.2**
	93.04		97.0180	-0.592	972.94	-11.9
	78.58		88.1812	-0.152	612.72	-2.1
	68.50		61.0570	-9.181	337.70	-109.2
Cyl4	**62.46**		110.6721	18.559	926.19	284.6
	61.68	**1.355400**	130.1417	-8.634	1170.24	-160.4
					4019.80	**0.9**
	93.04		97.1541	-0.456	975.67	-9.2

	78.58		87.6184	-0.715	604.93	-9.9
	68.50		69.6754	-0.562	439.77	-7.1
	62.96		83.3340	-8.779	525.13	-116.5
Cyl5	**61.18**	**1.355300**	149.2881	10.513	1539.90	209.2
					4085.40	**66.5**

In Figure 4.32 the results of the current distribution can be seen when the winding turns have been changed simultaneously in each cylinder. The object was to try and find the winding combination where the currents are similar in all cylinders. The calculation was made using equations 3.33...3.36.

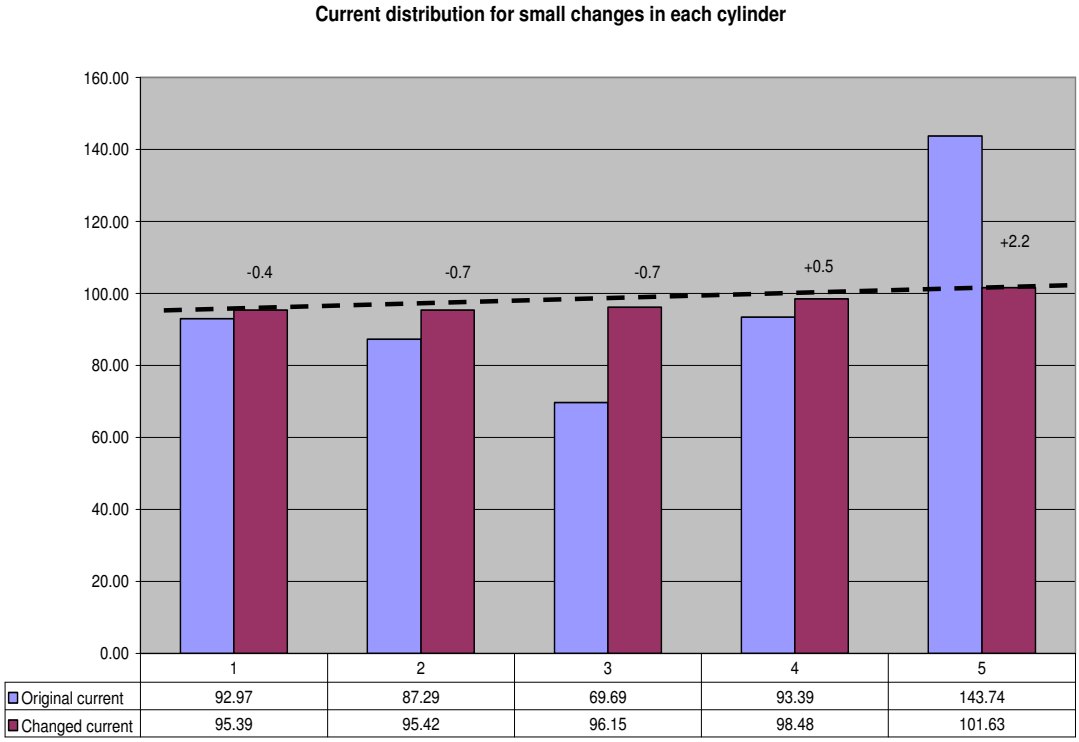

Figure 4.32: Current distribution for simultaneous winding changes

In this case the total impedance of the reactor was Z_{coil} = 1.37 Ω, while in the original case Z_{coil} = 1.36 Ω.

The current distribution shown in Figure 4.32 is not practical because the outer cylinders have better cooling and therefore can carry more current than the inner cylinders.

The numbers of the winding turns for the optimal current distribution at rated current should be designed so that the temperatures in each cylinder are at the same level and as close as possible to the maximum allowed temperatures.

The calculations of inductances, impedances, losses and current distributions as well as their optimization by an iterative method (Jacobian) are shown in more detail in appendix B.

5 –Discussions

For the design engineers of reactors as well as for the most economical use of that equipment, the temperatures of different parts of reactors should be known exactly, so the thermal losses can be optimized and minimized. Since energy costs are tending to increase, losses are becoming a more significant component of the total operating cost. Through conventional surface testing methods the exact locations of hot spots inside reactor coils can only be estimated by means of empirical mathematical calculations.

Therefore the ability to test the temperatures directly inside and between the wires of coils should lead to better results when designing reactors, and at the same time would show test engineers the exact locations of hottest-spot areas and temperatures. Further, the correct current distribution between the coils causes even temperatures at each coil and helps to optimize the manufacturing and losses of the whole reactor.

The maximum temperature occurring in any part of the winding is called the "Hot-Spot-Temperature" and is the thermally limiting temperature of loading for that cylinder of the reactor. Since the electrical impedances of each cylinder are different to each other, the current distribution is not even. That means the heat losses are also different and therefore each cylinder has its own hot spot temperatures. The highest hot spot temperature of one cylinder limits the electrical loading of the whole reactor and therefore design engineers are trying to keep the temperatures of all cylinders at the same level.

Accuracy in winding hottest-spot temperature measurement is dependent upon placing temperature sensors in the appropriate locations. The temperature differential between winding hottest spot and coil surface may be determined by measurement or by calculation with a thermal model and added to the surface temperature for determining the winding hottest-spot temperature. If sufficient surface temperature measurements are made on a winding, coupled with an accurate temperature difference (proven by experiment on models or prototypes) relating surface (encapsulation) temperature to internal winding temperature, it is possible to determine the average winding temperature rise by taking the average of all surface temperature rises (with the appropriate external to internal correction factors). This is another means of verifying the surface temperature measurement methodology.

According to IEEE- and IEC- standards there are several methods to determine the avarage temperature of reactor coils. In the ordinary methods embedded temperature sensors wound into the winding was the preferred method for determining the hottest spot location. For accurate results there are hundreds of embedded temperature sensors needed around the reactor's cylinders and in the cooling ducts. Other simple method is to insert non-reversing temperature indicating labels into a number of cooling ducts for each winding, evenly spaced from top to bottom. Thermocouples, wire-optic probes, or other suitable temperature indicating devices can be used in a similar fashion. A proof of the validity of this approach can be demonstrated by taking the average of all label readings (after adding a known temperature differential value for the internal winding temperature and the measured surface temperature) for each particular test to ascertain if an average temperature rise value close to the value derived from the DC-resistance method is yielded. Plotting the label readings vertically from bottom to top for each monitored cooling duct

of a winding should yield a consistent definition and location of the hottest spot. A hot spot measurement was made for each encapsulated winding group in the reactor under test. Hottest-Spot location and, hence, measurement point location, is typically in the last turns of the upper winding end. The exact location was determined by the measurements during the tests.

In our case, during the manufacturing of our test reactor the optical wires (so called Distributed Sensors, see Appendix A) for temperature measurements were installed in each coil of our reactor. Distributed sensors take advantage of the ability of optical wires to guide light signals over large distances and following sinuous paths. This allows the measurement of deformations and temperatures inside or at the surface of structures.

The accuracy of this method of temperature measurements was verified by using an infrared camera and with the thermocouples installed on the outer surfaces of cylinders 1 and 5, along with calculations presented in chapter 4, and is rather good. The errors result mainly from the assumption that the filling and supporting material which is a mixture of wire glass with resin and wiring insulating material, namely Mylar, were assumed to have similar heat transfer coefficient values of conduction because we had no better information about those materials. The influence of optical wires (0.9mm) on the heat transfer coefficient was neglected.

The time constants were measured and verified by calculation and those results were partly very good and partly sufficient. The errors between measured and calculated values occurred because exact information about the material volumes of all the different materials involved were not known by us. Also, the extra losses from the effect of radiation on the outer surfaces of cylinders 1 and 5 were not taken in to account. The actual losses in our test reactor can be determined by calculating the thermal losses with the actual current and the actual AC-resistance ($P_w = J^2R_{ac}$) at the rated frequency. The additional losses caused by external magnetic field density (B) can be neglected at fundamental frequency, as was shown in chapter 3.

The losses were also calculated using the measured surface temperatures and the temperatures in the cooling ducts, as shown in Table 4.2. For rough calculation the heights of all cylinders were divided into four segments and the average temperatures were estimated from the middle of each section which led to relative big errors between the temperature calculated and electrical current calculated losses. The accuracy of determining the average temperatures from the temperature curves of the cylinders and cooling ducts and thus the calculation results for losses would be better if the heights were to be divided into smaller parts and the temperatures fixed more accurately.

The current distribution between cylinders 1 to 5 is depends on the total impedances of each cylinder. The resistances and self-capacitances are very small and can therefore be neglected, so that only the self- and mutual- inductances affect the current distribution. The inductances and therefore the current distribution depends from the number of winding-turns to the power of two only**,** when the physical dimensions of the reactor will be kept unchanged.

The theoretical calculation for the right number of winding-turns on each cylinder, in order to obtain the desired current distribution and thus the desired heating power can be performed, as presented in this dissertation, by means of a matrix calculation coupled to an iteration method. In practice, the number of spider-arms only allows a rough approximation to the final calculated

number of winding-turns and therefore a completely exact and designer-desired current distribution is in principle not possible.

Because the thermal heat transfer coefficients of convection and radiation are depending on temperature differences, their exact prediction is not possible since the surface temperatures are not the same at different heights in cylinders. For that reason, the research work of Schmidt and Beckmann (Schmidt and Beckmann 1930) in determining thermal heat transfer coefficients of vertical heated plates and cooling ducts has been studied and their results were used in this research work.

Thermal heat transfer coefficients at the desired heights can be calculated when the wall and ambient temperatures at the same height are known. In addition to this, the cooling air temperature and velocity, which are also dependent on the height, must be known. The cooling air velocity was measured at the same rated current and frequency as all other measurements and the result was that the air flow inside the cooling ducts and at the surfaces is laminar.

The surface temperatures of all cylinders and temperatures at different heights in the cooling ducts were measured by optical wires. The results of the temperature measurements inside the windings and outer surface of each cylinder as well as of the cooling ducts have been plotted. The trend lines of the plotted temperature curves as well as the above-mentioned results from the calculation of heat transfer coefficients can be used in the theoretical dynamic thermal model.

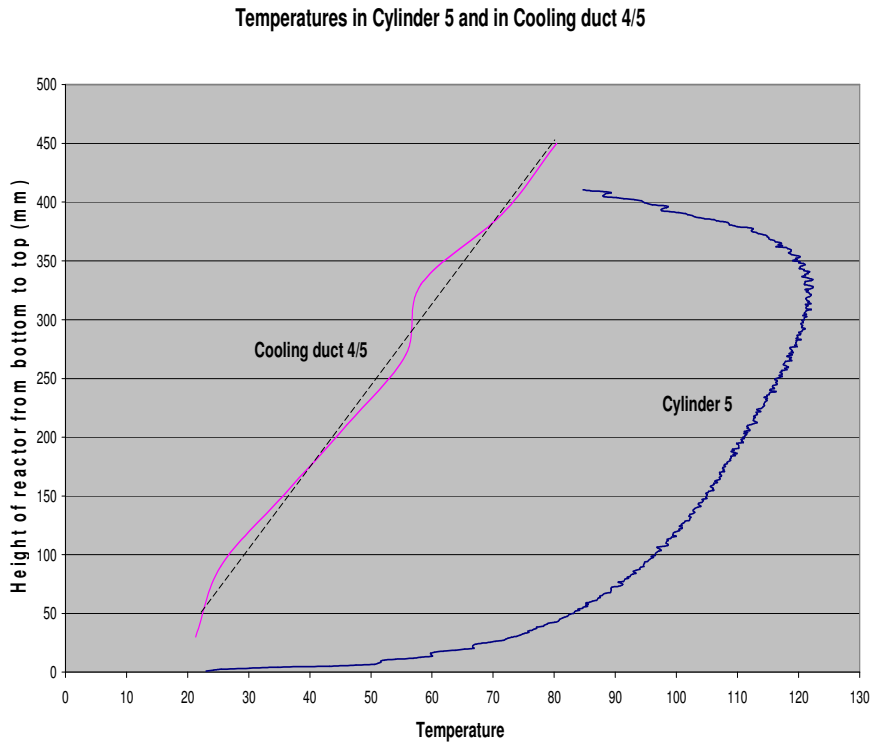

Figure 5.1 Temperature curves of cooling duct 4/5 and cylinder 5

At the beginning of this research work, a hypothesized temperature distribution model for one cylinder of an air core reactor was presented in Figure 1.6. The measured and therefore the real

situation are now shown in Figure 5.1 above. The “hot-spot” location is similar to the hypothetical location but the temperature rise in the bottom part of the cylinder is not linear as assumed before. At the bottom of the cylinder, the temperature increases exponentially. After that the temperature increase slows down and grows linearly up to the “hot-spot” location. It then drops off again very fast due to the better cooling effect. The above described phenomenon occurred for all the cylinders. The cooling air temperature rises in the middle of the cooling ducts are, as expected, quite linear.

Finally, by means of an arctic test it was possible to simulate the situations in which the reactors are installed in very cold and icy regions and confirm the hypothesis that snow and cold ambient temperatures coupled with the cyclic and discontinuous operation of reactors could lead to their damage.

6 - Conclusions

The total inductance and current density of a reactor are among the main figures reguired for calculating the reactor dimensions and number of cylinders. Not only this but also other things need to be considered, namely the hot-spot temperatures caused by the thermal losses (which can be different between the cylinders because of the out-of-step warming-up of the reactor cylinders caused by the different current distribution between the coils) and the eddy-current losses, which are frequency dependent and are caused by the electrical and magnetic fields as well as the stray losses caused by magnetic flux in other metallic parts of the reactor and in the reactor support structure.

In order to accurately ascertain the hottest-spot ratio for dry-type reactors (hottest-spot rise/average rise), accurate measurement of the average temperature rise and the adoption of a methodology that allows the measurement of hottest-spot temperature in a repeatable and accurate fashion are required. The average temperature rise can easily be measured using the well-proven DC-resistance method. In addition, the knowledge of the location of the hottest spot is required.

In this dissertation, the modeling methods for calculating the temperature distribution and hot-spot temperatures in large multi cylinder air-core reactors were studied.

The objective of this study was to find an accurate way to determine the hot-spot temperatures and their locations, to develop an algorithm to compute the current distribution between coils for thermal modeling and to evaluate harmonic effects of a dry type air cooled reactor. The model was made dynamic so that the effect of variable load and transient operation conditions could be analyzed and the results could be used for optimizing the reactor construction for temperatures. This work involved the following research methods:

- Analytical calculations to define the currents in different cores of the reactor
- FEM-methods to obtain the magnetic fields and consequently the eddy current losses in windings
- Analytical empirical models for heat transfer
- Numerical calculation methods to find the required changes in the turn numbers of individual coil-windings needed to achieve optimal power losses, which should be defined and optimized in each cylinder so that the final temperatures of each cylinder are as similar as possible and near to the rated limits but will not exceed the temperature values given in the standards

Compared with the existing methods to determine the hot-spot area and surface temperatures, the major contributions of this work are:

- An accurate measuring method to determine the temperature distribution and location for hot-spot areas in the windings of the separate cylinders of a reactor has been developed and the test results have been verified theoretically and through practical measurements via optical wires.

- An algorithm to determine the impedance values of each coil in order to reach the desired current distribution and current density affecting the coil temperatures has been proposed.

- With a FEM model, the magnetic flux densities were calculated and used to predict reactor eddy current losses. Knowledge of the flux densities of the reactor coils and their sum were used with the appropriate conductor dimensions to predict the eddy losses for a specific design.

- A hypothesized temperature distribution model at the cylinder of an air core reactor has been developed and through practical measurements verified. The exact temperature curvatures on the inside and outside surfaces of the coil windings were determined and mathematically modeled. In this model, the surface temperatures of some cylinders and temperatures at different levels in the cooling ducts were measured by optical wires and verified by thermocouples. The thermal heat transfer coefficients at desired levels can be calculated when the wall and ambient temperatures at the same height are known.

- For Nordic winter conditions, temperature tests and measurements have, for the first time, been carried out on a multi cylinder dry-type air-core reactor by means of the DTS-measuring method. The results show that the temperatures in the lower part of a reactor can be so low that melting snow from the upper part could form ice in the lower part of reactor, which may close the cooling ducts and thus lead to their partial damage.

References

Heat transfer

(Buchholz, 1934) Buchholz.H:
"Die Verteilung der Beharrungstemperatur in einer stromdurchflossenen Spule mit rechteckigem Querschnitt bei temperaturabhängigem Widerstand"
Archiv für Electrotechnik XXVIII Band 1934 s.122-130

(Gotter, 1954) Gotter.G:
"Erwärmung und Kühlung elektrischer Maschinen"
Springer-Verlag 1954

(Halacsy, 1958) Halacsy.A.A:
"Temperature Rise of Dry Type Transformers,"
AIEE Trans., Vol. 77, Part 111, pp. 456-462, August 1958.

(Higgins, 1944) Higgins, T. J.:
"Equations for calculating the temperature distribution in electric coils of general rectangular cross section,"
ASME Transactions, pp. 665–670, 1944.

(Higgins, 1945) Higgins, T. J.:
"Equations for calculating temperature distribution in transformer cores and other electrical apparatus of rectangular cross section,"
AIEE Transactions, Electrical Engineering, vol. 64, pp. 190–194, disc.Pp. 493–393, April 1945.

(Incropera and DeWitt, 1996) Incropera F. P. and DeWitt D. P.
"Fundamentals of Heat and Mass Transfer",
4th ed., John Wiley & Sons, 1996, pp. 886

(Jaluria, 1995) Jaluria. Yogesh
"Natural Convection"
Heat transfer handbook 2nd edition (Chapter 7) Wiley New York 1995

(Jokinen and Saari, 1997) Jokinen.T ,Saari.J:
"Modeling of the coolant flow with heat flow controlled Temperature sources in thermal networks"
IEE Electr.Power. App. Vol.44 No.5 pp.338-342 1997

(Ferreira, 1994) Ferreira, Jan A
"Improved Analytical Modeling of Conductive Losses in Magnetic Components"
IEEE Transactions on Power Electronics, Vol. 9, No. I, January 1994

(Millar, 2006) Millar, Robert:
"A Comprehensive Approach to Real Time Power Cable Temperature Prediction and Rating in Thermal Unstable Environments"
Helsinki University of Technology Doctoral Dissertation, 2006.

(Olsson, 2004) Olsson Carl-Olof:
"Prediction of Nusselt Number and Flow Rate of Buoyancy Driven Flow between Vertical Parallel Plates"
Transactions of the ASME 98/ Vol. 126, FEBRUARY 2004

(Pashkis and Baker, 1942) Pashkis.V and H. Baker:
"A method for determining the steady-state heat transfer by means of an electrical analogy",
ASME Transactions, Vol. 104, pp. 105-112, Feb.1942.

(Pierce, 1992) Pierce.W:
"An investigation of the temperature distribution in cast-resin transformer windings"
IEEE transactions on power delivery, Vol. 7, No. 2, April 1992

(Pierce, 1994) Pierce.W:
"Hottest Spot Temperatures in Ventilated Dry Type Transformers"
IEEE Transactions on Power Delivery, Vol. 9, No. 1, January 1994

(Pierce, 1994) Pierce.W:
"Predicting Hottest Spot Temperatures in Ventilated Dry Type Transformer Windings"
IEEE Transactions on Power Delivery, Vol. 9, No. 2, April 1994

(Pradhan and Ramu, 2004) Pradhan.M.K and T. S. Ramu:
"Estimation of the Hottest Spot Temperature (HST) in Power Transformers Considering Thermal Inhomogeniety of the Windings"

IEEE transactions on power delivery, vol. 19, no. 4, October 2004

(Radakovic and Feser, 2003) Radakovic.Z and K.Feser:
"A New Method for the Calculation of the Hot-Spot Temperature in Power Transformers with ONAN Cooling"
IEEE transactions on power delivery, vol. 18, no. 4, October 2003

(Richter, 1924) Richter R:
Elektrische Maschinen
Springer Verlag Berlin 1924

(Sakonidou, 2007) Sakonidou, E.P. et al., *"Modeling of the optimum tilt of a solar chimney for maximum air flow*"
Sol.Energy (2007) doi:10.1016/j.solener.2007.03.001

(Schmidt and Beckmann, 1930) Schmidt, E und Beckmann,W:
"Das Temperatur- und Geschwindigkeitsfeld vor einer Wärme abgebenden senkrechten Platte bei natürlicher Konvektion"
VDI-Zeitschrift Bd 1 Nr.10 Berlin 1930

(Schneider, 1954) Schneider, P. J.:
"Temperature fields in electrical coils: numerical solutions,"
AIEE Transactions-Pt. I, Communications and Electronics, vol. 73, pp. 768–771, 1954.

(Sparrow and Gregg, 1956) Sparrow.E.M. and J. L. Gregg:
"Laminar Free Convection from a Vertical Plate with Uniform Surface Heat Flux"
ASME Trans, Vol. 78, Feb. 1956, pp. 435-440.

(Stewart and Whitman, 1944) Stewart, H. C. and Whitman, L. C.:
"Hot-spot temperatures in dry-type transformer windings,"
AIEE Transactions, vol. 63, pp. 764–768 and 1445–1448, October 1944.

(Susa, 2005) Susa.D:
"Dynamic Thermal Modeling of Power Transformers"
Helsinki University of Technology Doctoral Dissertation 2005

(Swift, 2001) Swift.G:
"A Fundamental Approach to Transformer Thermal Modeling—Part I: Theory and Equivalent Circuit"
IEEE transactions on power delivery, vol. 16, no. 2, April 2001

(York Sensors) York Sensors, Ltd
Outline of Sensa Distributed Temperature Sensing (DTS) System
Gamma House, Chilworth Science Park, Southampton, Hampshire, SO16 7NS, United Kingdom

Electromagnetic and –losses/Inductance calculation

(Ala-Miekoja, 1979) Ala-Miekoja.E:
"Ilmasydämisen kuristimen vaihtovirtaresistanssin ja siihen vaikuttavien parametrien tutkiminen"
Tampere University of Technology Licentiate Thesis 1979 (in Finnish)

(Bayazitoglu and Sathuvalli, 1993) Bayazitoglu.Y and U. B. Sathuvalli:
"Field Gradient Analysis of a Conical Helix"
IEEE transactions on magnetics, vol. 29, no. 1. January 1993

(Black, 1905) Black.T.P:
"Über den Widerstand von Spulen für schnelle elektrische Schwingungen"
Annalen der Physik IV Band 19. s.157-169 1905

(Börner and Haist, 1965) Börner.S und Haist.W
"Die Frequenzabhängigkeit des Scheinwiderstands von einlagiger zylindrischen Luftspulen, Teil I und II"
Frequenz Bd. 19/1965 Nr.5

(Börner, 1967) Börner.S
"Die Frequenzabhängigkeitvon Verlustwiderstand und Induktivität einlagiger Ring-Luftspulen"
Frequenz Bd. 21/1967 Nr.8

(Burke and Fawzi, 1991) Burke.P.E and Fawzi.T.H :
"Effect of eddy losses on the design and modelling of air-cored reactors"
IEEE transactions on magnetics, vol. 27, no. 6, November 1991

(Chari and Csendes, 1977) Chari.M and Z.Csendes:

"Finite element analysis of the skin effect in current carrying conductors"
IEEE transactions on magnetics vol. Mac-13, no. 5, September 1977

(Chen and Konrad, 1997) Chen.Q, and A.Konrad,:
"A Review of Finite Element Open Boundary Techniques For Static and Quasi-Static Electromagnetic Field Problems"
IEEE transactions on magnetics, vol. 33, no. 1, January 1997

(Ciric, 1988) Ciric.I.R:
"Surface source models and equations for the magnetic f*ield of polygonal cross section conductors"*
IEEE transactions on magnetics, vol. 24, no. 6, November 1988

(Dowell, 1966) Dowell.P.L:
"Effects of eddy currents in transformer windings"
IEE Proc. Vol.113, No. 8 August 1966

(Dwight, 1945) Dwight.H.B:
"Electrical Coils and Conductors"
McGraw-Hill Book Company, inc. 1945 first edition

(Elmoudi, 2004) Elmoudi.A:
"Evaluation of Power Systems Harmonic Effects on Transformers"
Helsinki University of Technology Licentiate Thesis 2004

(Elmoudi, 2006) Elmoudi.A:
"Evaluation of power system harmonic Effects on transformers Hot Spot Calculation and Loss of Life Estimation"
Helsinki University of Technology Doctoral Dissertation, 2006

(Emde, 1912) Emde.F:
"Berechnung eisenfreier Drosselspulen für Starkstrom"
E. und M. XXX Jahrg. Heft 11 s.221-226 Wien, 1912

(Fawzi and Burge, 1978) Fawzi.T.H and Burge.P.E
"The accurate computation of self and mutual inductance of circular coils"
IEEE PAS-97 No.2 1978

(Ferreira, 1994) Ferreira J.A:
"Improved Analytical Modeling of Conductive Losses in Magnetic Components"
IEEE Power Electronics Vol.9 No.1 Jan.1994 ps.127-131

(Grover, 1973) Grover.F.W:
"Inductance calculations: Working equations and Tables"
Special edition prepared for Instrument Society of America 1973

(Haas, 1975) Haas.H:
"Ein Beitrag zur Berechnung der Gegeninduktivität koaxialer Zylinderspulen"
AfE 57 s.21-26 1975 Springer Verlag 1975

(Hak, 1938) Hak.J *:*
"Eisenlose Drosselspulen"
K.F.Koeler Verlag Leipzig 1938

(Hannakam, 1967) Hannakam.L
"Berechnung der Gegeninduktivität achsenparaleller Zylinderspulen"
AfE 51 Heft 3 s.142-154 Springer Verlag 1967

(Hwang, 1985) Hwang. Davis.
"Assessment of harmonic current effects in power system transformer"
The University of Texas at Austin Doctoral Dissertation 1985

(Keitamo, 2005) Keitamo.J:
"Suodatinkuristimen pyörrevirtahäviöiden tietokonemallinnus,
(Computational modeling of eddy currents in filter reactor)"
Tampere University of Technology Master Thesis 2005 (in Finnish)

(Konrad, 1981) Konrad.A:
"The Numerical Solution of Steady-State Skin Effect Problems. An Integrodifferential Approach"
IEEE transactions on magnetics, vol. Mag-17, no. 1, January 1981

(Konrad, 1982) Konrad.A:
"Integrodifferential Finite Element Equationtion of Two-Dimensional Steady- State Skin Effect Problems"

IEEE transactions on magnetics, vol. Mag-18, no. 1, January 1982

(Konrad et al. 1982) Konrad.A, M.Chari, Z.Csendes:
"New finite element techniques for skin effect problems"
IEEE transactions on magnetics, vol. Mag-18, no. 2, March 1982

(Lehner, 2003) Lehner.G:
"Elektromagnetische Feldtheorie"
Springer Verlag 2003

(Makarov, 2000) Makarov S . N, and Emanuel A. E.:
"Corrected Harmonic Loss Factor For Transformers supplying Non-sinusoidal Load current,"
Proc. of the 9th International conference on Harmonics and Power Quality, vol. 1, Oct. 2000,

(Malo, 1993) Malo.V.M:
"Eddy current and impedance evaluation using a two dimensiona finite element method"
IEEE Transactions on Energy Conversion, Vol. 8, No. 3, September 1993

(Moreau et al. 1998) Moreau.O, and L. Popiel, J. L. Pages:
"Proximity Losses computation with a 2D Complex Permeability Modeling"
IEEE transactions on magnetics, vol. 34, no 5, September 1998

(Murgatroyd, 1989) Murgatroyd, P.N.
"Calculation of proximity losses in multistranded conductor bunches"
IEE Proceedings, Vol. 136, Pt. A, No. 3, May 1989

(Nakata et al. 1990) Nakata.T, N.Takahashi, K.Fujiwara, H.Niinobe and K.Misawa:
"Finite element analysis of induced currents in axisymmetric Multi-conductors connected in parallel to voltage sources"
IEEE transactions on magnetics, vol. 26, no. 2, March 1990

(Nethe et al. 1998) Nethe.A, R. Quast and H. Stahlmann:
"*Boundary Condition for High Frequency Eddy Current Problems*"

IEEE transactions on magnetics, vol. 34, no. 5, September 1998

(Perry, 1979) Perry.M.P:
"Multiple layer parallel connected Air-Core inductor design"
IEEE Trans.PAS vol.98 No 4 July/Aug.1979

(Preis et al. 1982) Preis.K, H. Stogner, K.R. Richter:
"Calculation of eddy current losses in air coils by finite element method"
IEEE transactions on magnetics, vol. mag-18, no. 6, November 1982

(Preis, 1983) Preis.K:
"A contribution to eddy current calculations in plane an Axisymmetric multiconductor systems"
IEEE transactions on magnetics, vol. Mag-19, no. 6, November 1983

(Putman, 1979) Putman.T.H:
"*Eddy-current loss in large electrical reactors*"
IEEE transactions on magnetics, vol. Mag-15, no. 6, November 1979

(Rogowski, 1918/1919) Rogowski.W:
"Die Spule bei Wechselstrom"
A.f.E Band VII s.17-31 1918/1919

(Rogowski, 1918/1919) Rogowski.W:
" Ergänzung der Erwärmungsvorschriften"
A.f.E Band VII s. 41-47 1918/1919

(Shaikh and Yamashita 1988) Shaikh.Z.H and H.Yamashita:
"A three dimensional magnetic field analysis by a novel finite element method using magnetic flux density directly as an unknown variable"
IEEE Transactions on Power Delivery, Vol. 3, No. 1, January 1988

(Song, 2005) Song.C:
"A practical magnetic field evaluation method for 10kV air-core reactors"
CIRED 2005 Session 2 / Turin 6-9. June 2005

(Sonntag, 1975) Sonntag.J:
"Stromverdrängung bei Mehrleitersystemen mit dünnwandigen kreiszylindrischen Holleitern"
AfE 57 s.13-20 1975

(Sullivan, 1999) Sullivan.C.R:
" Winding Loss Calculation with Multiple Windings, Arbitrary Waveforms and Two-Dimensional Field Geometry"
IEEE Industry Applications Society Annual Meeting
Phoenix, AZ, 3-9 October, 1999

(Zuhrt, 1934) Zuhrt.H:
"Theoretische Behandlung ein- und mehrlagiger Spulen in beliebiger Schaltung"
AfE Band XXVII s.109-118 1934

(Urankar, 1984) Urankar.L.K:
"Vector Potential and Magnetic Field of Current-Carrying Finite Arc Segment in Analytical Form, Part IV: General Three- Dimensional Current Density"
IEEE transactions on magnetics, vol. Mag-20, no. 6, November 1984

(Urankar, 1990) Urankar.L:
"Vector Potential and Magnetic Field of Current-Carrying Circular Finite Arc Segment in Analytical Form-Part V: Polygon Cross Section"
IEEE transactions on magnetics, vol. 26, no. 3, May 1990

(Weggel and Schwartz, 1988) Weggel.C.F. and D. P. Schwartz:
" New analytical equations for calculating Magnetic field"
IEEE transactions on magnetics, vol. 24, no. 2, March 1988

(Weiss, 1985) Weiss.J:
"One step finite element equationtion of skin effect problems in Multiconductor systems with rotational symmetry"
IEEE transactions on magnetics, vol. Mag-21, no. 6, November 1985

(Weiss and Konrad, 1982) Weiss.J, and A.Konrad:
"Scalar Finite Element Solution of Magnetic Fields in Axisymmetric Boundaries"
IEEE transactions on magnetics, vol. Mag-18, no. 1, January 1982

(Welytschko, 1943) Welytschko.G:
"Die berechnung der Selbstinduktion von einlagiger Zylinderspulen"
AfE 37.Band Heft 11 s.520-533 1943

(Wien, 1904) Wien.M:
"Über den Durchgang schneller Wechselströme durch Drahtrollen"
Annalen der Physik/4.Folge Band 14 No.6 s.1-21 1904

(Yu, 1996) Yu.Q:
"Calculation of Three Dimensional Magnetic Field Distribution of Large Air- Core Reactor Coils"
Doctoral Dissertation in the Ohio State University 1996

(Yu, 1996) Yu.Q:
"Simplified Magnetic Field Modeling and Calculation of Large Air-Core Reactor Coils"
IEEE transactions on magnetics, vol. 32, no. 5, September 1996

(Yu, 1997) Yu.Q:
"Calculation Accuracy of the Planar Filament Current Loop Stack Model of Large Air-Core Reactor Coils"
IEEE transactions on magnetics, vol. 33, no. 5, September 1997

(Yu and Sebo, 1998) Yu.Q; S. A. Sebo:
"Accurate Evaluation of the Magnetic Field Strength of Large Substation Air-Core Reactor Coils"
IEEE transactions on Power Delivery, Vol. 13, No. 4, October 1998

Standards:

IEC 76-2 1993-4:
Power transformers Part 2: Temperature rise

IEC 289 1988:
Reactors

IEEE C57.16-1996:

IEEE Standard Requirements, Terminology and Test Code for Dry-Type Air-Core Series-Connected Reactors

IEEE C57.21-1990:
IEEE Standard Requirements, Terminology and Test Code for Shunt Reactors Rated over 500 kVA

IEEE Std C57.110-1998:
IEEE Recommended Practice for Establishing Transformer Capability when supplying nonsinusoidal Load Currents

IEEE Std C57.120-1991:
IEEE Loss Evaluation Guide for Power Transformers and Reactors

IEEE C57.125-1991:
IEEE Guide for Failure Investigation, Documentation, and Analysis for Power Transformers and Shunt Reactors

IEEE Std C57.134-2000:
IEEE Guide for Determination of Hottest-Spot Temperature in Dry-Type Transformers

IEEE Std C57.136-2000
IEEE Guide for Sound Level Abatement and Determination for Liquid-Immersed Power Transformers and Shunt Reactors Rated over 500 kVA

IEEE STD 62-1995:
IEEE Guide for Diagnostic Field Testing of Electric Power Apparatus
Part 1: Oil Filled Power Transformers, Regulators and Reactors

IEEE STD 1277-2000:
IEEE Trial-Use Standard General Requirements and Test Code for Dry-Type and Oil-Immersed Smoothing Reactors for DC Power

ANSI/IEEE STD 1-1986:
IEEE Standard General Principles for Temperature Limits in the Rating of Electric Equipment and for the Evaluation of Electrical Insulation

ANSI/IEEE C37.109-1988:
IEEE Guide for the Protection of Shunt Reactors

Finite Element Methods (FEM)

COMSOL™, 2005 FEMLAB®
Electromagnetic Module User's Guide
Multiphysics User's Guide.
COMSOL AB Stockholm

Appendix A

Description of Distributed Temperature Sensing (DTS) method
(York Sensors, Ltd)

Distributed sensors take advantage of the ability of optical wires to guide light signals over large distances and following sinuous paths. This allows the measurement of deformations and temperatures inside or at the surface of structures. The sensors can be arranged into a network that mimics the nervous system of our body and monitors the health of the structure. Long-gage and distributed sensors are ideal for the global monitoring of large structures, where they allow a good coverage of the structure with reduced number of sensors and little a priori knowledge on its degradation modes. Long-gage sensors give an integrated or average measurement of strain or temperature over lengths of typically a few tens of centimeters to a few tens of meters. On the other hand, distributed sensors allow the measurement of multiple points along a single wire. These sensors are mostly based on different types of light scattering including Rayleigh, Raman and Brillouin . Both types of sensors have already found niche applications where their characteristics and performance surpass those of conventional sensors.

Background
Distributed optical wire temperature sensing was first demonstrated in 1981 at Southampton University. Research and development by York Sensors, nowadays known as Sensa (a Schlumberger Company), has provided a technology able to measure temperature repeatedly and accurately over distances of up to 30 km. Distributed Temperature Sensing (DTS) instrumentation is used world-wide in the energy sector and other operational environments. Although the technology is sophisticated, the use of optical wires as sensors is very simple and opens many areas of measurement which have hitherto been impossible to address. Fast, accurate, high resolution measurements are now practical. The DTS system is based on optical wire technology which means that it can be used in a wide range of conditions including hazardous environments and EMI intensive areas such as cable monitoring.

The expression 'distributed sensing' is used to describe a technique whereby a single sensor can give data spatially distributed over many thousands of individual measurement points. In conventional sensing an individual sensor, such as a thermocouple, is needed for each point of interest. The following are the main advantages of distributed sensing over 'conventional' sensing when long distances and multiple measurements are required:
- DTS is cost effective.
- Many measurement points are acquired simultaneously.
- Data acquisition is conducted by a single processor.
- Installation and maintenance are simplified.

Basic Information about DTS

DTS systems offer:

- Measurement of temperature and position continuously over long distances using a single optical wire cable as the sensing element.
- Immunity to EMI radiation.
- User configurable zones with programmable alarms.
- Control interfaces & remote monitoring facilities.

Distributed sensing enables fast, accurate, high resolution measurements to be made. The DTS system is based on optical wire technology which means that it can be used in a wide range of conditions including hazardous environments and EMI intensive areas such as power cable installations and substations. The sensing optical cables are rugged, inexpensive, easy to install and low maintenance.

DTS systems are self-calibrating, and can be configured such that if the sensor wire is broken, they automatically identify a break has occurred and identify the location. Alternatively, if the sensor wire is configured in a loop, the system can switch to single-ended measurement from both ends thereby avoiding any loss of data. In all cases, measurement integrity is maintained and the fault location is flagged for attention. Zones comprising of one or more sampling points along the sensing wire can be assigned with up to four basic alarm levels, maximum, minimum, average or rate of change. The DTS may also be interfaced with a variety of monitoring and control systems.

Principles of DTS Operation

The optical wire distributed temperature sensor is based on Optical Time-Domain Reflectometry (OTDR, also referred to as backscatter). In this technique, a pulse of light is launched into the sensing wire through a directional coupler, as shown in *Figure 1*.

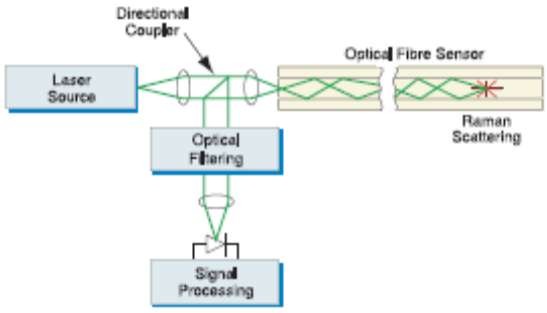

Figure 1 - Optical Time Domain Reflectometry

Light is scattered as the pulse passes down the wire through several mechanisms including density and composition fluctuations (Rayleigh scattering) as well as Raman and Brillouin scattering due to molecular and bulk vibrations respectively.
A proportion of this scattered light falls within the cone of acceptance of the wire (i.e. is retained within the wire core) and is guided back towards the source. The signal returned to the source is split off by the directional coupler to a suitable, highly sensitive receiver. In a uniform wire, the

intensity of this returned light shows an exponential decay with time (and therefore - knowing the speed of light in wire - the distance that the light has traveled down the wire), variations in temperature along the length of the wire show up in deviations from a 'perfect' exponential decay of intensity with distance. A profile of the wire temperature can then be produced, as shown in *Figure 2*.

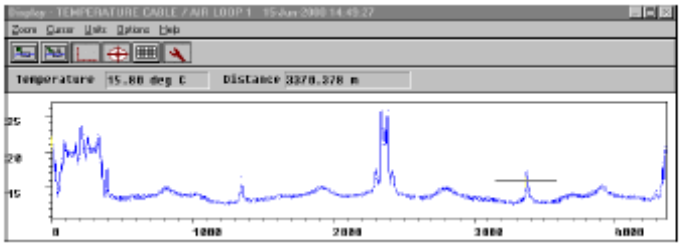

Figure 2 - Typical Temperature Profile

Components of Backscatter Signal

The OTDR technique is well established and used extensively in the optical telecommunications industry for qualification of a wire link or fault location. In OTDR, it is the Rayleigh backscatter signature which is examined. The signal is unshifted from the launch wavelength and is the one used by telecom engineers to verify integrity of a wire link. This signature gives information on loss, breaks, and variations in attenuation along the length of the wire and is very weakly sensitive to temperature differences along the wire. Two other backscatter components (i.e. Raman and Brillouin spectral lines, which are due to thermally driven molecular and bulk vibrations respectively) are temperature sensitive. The wavelength of these lines are shifted from the launch wavelength and the intensity of the signals is much lower than that of the Rayleigh trace, see *Figure 3*.

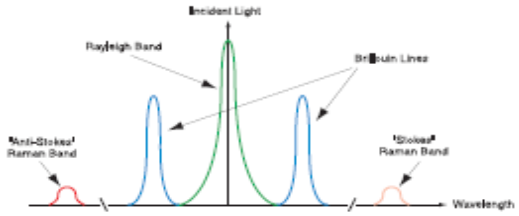

Figure 3 - Backscatter Spectrum

The Brillouin lines are separated from the launch wavelength by only a few tens of GHz and existing DTS systems do not separate this component from the Rayleigh signal. The Raman signal however is sufficiently strong and distinct to be used for temperature measurement. The Raman signal comprises two elements - the Stokes and anti-Stokes lines which are shifted in wavelength from the Rayleigh signal by 440 cm-1 in telecommunications grade optical wire and can therefore be filtered from the dominant constituent of the total backscattered light. The longer wavelength

Stokes line is only weakly temperature sensitive but the intensity of the backscattered light, at the shorter anti-Stokes wavelength, increases with an increase in temperature and vice versa.

DTS System Configuration

A DTS system comprises one or more sensors of optical wire cable, the optoelectronics unit with embedded processing software and a display unit. The DTS unit contains all necessary optics, electronics and data processing capability for interrogating the wires and generating temperature profiles and other important information such as zone and alarm data. The laser source used in multimode DTS systems is an optical wire (Neodymium doped) laser at 1064 nm supplying pulses of <10 ns width (equivalent to <1 m length). A directional coupler separates the launch pulse from the backscatter signal and a wire switch selects the sensing wire to be interrogated. The Raman backscatter signal is filtered and detected. This is then amplified and digitized by a high speed analogue-to-digital converter which samples the whole of the return signal at intervals programmable down to 2.5 ns. Digital averaging techniques improve the signal/noise ratio in a highly efficient manner prior to the data being sent to the display unit. DTS instruments are configured with a DTS PC, which also provides the temperature logging and data storage facility. PC Anywhere software is used to remotely communicate with the DTS PC via the PC's internal modem. DTS instruments can be configured in a variety of cabinet arrangements to suit the application. Since the DTS and PC are mains powered, UPS is normally provided in a fixed installation to provide backup in the event of a mains failure. Output relays are provided and are programmable to provide alarms for set temperature conditions in specified zones. Modbus protocol is used to communicate zone temperature analogue values.

.

Appendix B

Defining and optimizing current distributions and impedances

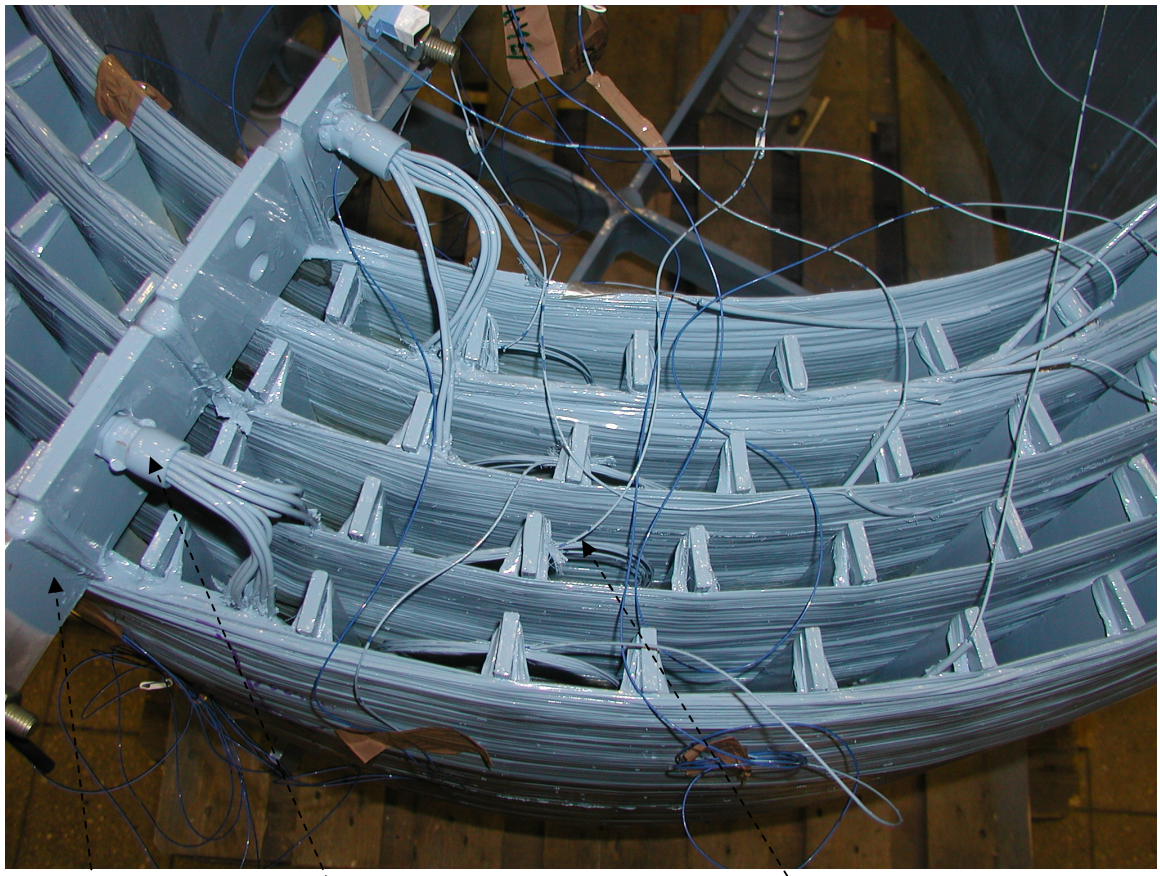

Figure 1: Spider Arm and Connections to cylinders no. 1...5

The impedances of the manufactured reactor as well as each individual cylinder can be determined by the measurement of the current distribution between the cylinders.

The results can be theoretically verified by mathematical calculations and vice versa.

A part of a spider arm and the winding connections to the cylinders are shown in Figure 1 above.

The current distribution between cylinders was determined by connecting a small AC- supply voltage over the reactor and then by measuring the currents flowing into each cylinder.

Supply voltage U = 71.3 V / 50Hz
Supply current J = 52.6A

$$\mathbf{Z_{tot\,i} = U/J_i\ ;\ (i = 1...5)} \qquad (1)$$

The values below are averages from the measurements between top and bottom measuring points.

	Current (J)	%	Z_{tot}/Ω	$L_{tot}/mH \approx Z_{tot}/\omega*10^3$
Syl.1	9.92A	18.75%	7.18	22.9
Syl.2	9.09A	17.18%	7.84	25.0
Syl.3	7.80A	14.74%	9.14	29.1
Syl.4	10.06A	19.01%	7.09	22.6
Syl.5	16.05A	30.32%	4.44	14.1
	52.92A	100%	$Z_{tot} = 1.350$	$L_{tot} = 4.30$

(Manufacturers data: $Z_{tot} = 1.363\Omega$ ja $L_{tot} = 4.34mH$)

$$\mathbf{L_{tot} = (\ Z_{tot}^{\ 2} - R_{ac}^{2})^{1/2}/\omega \approx Z_{tot}\ /\omega} \qquad (2)$$

The influence of resistance R_{ac} at 50Hz on the calculation of the impedances and inductances has been ignored ($R_{ac50hz} = 0.0164\Omega$ and $X_L = 1.3635\ \Omega$, thus $Z = (R_{ac}^2 + X_L^2)^{1/2} = 1.3636\ \Omega \approx X_L$), or at other frequency e.g. f = 2 kHz: $X_L = 54.5\Omega$ and $R_{ac} = 0.95\Omega$, thus $Z = (R_{ac}^2 + X_L^2)^{1/2} = 54.51\ \Omega \approx X_L$). For the loss calculations the AC- resistance cannot be ignored, but must be accurately determined.

The impedance of the reactor calculated with the supply voltage and currents (50Hz and 246.6Hz) used during the heat run tests are :

$Z_{tot50} = U/J = 815V/608A = 1.3405\Omega$ => $L_{tot} = 4.267$ mH

$Z_{tot50} = U/J = 670V/500A = 1.340\Omega$ => $L_{tot} = 4.265$ mH

$Z_{tot246.6} = U/J = 1702V/252A = 6.754\Omega$ => $L_{tot} = 4.358$ mH

One reason for the differences is inaccuracy in the measurements, because the voltage in the 246.6Hz test was measured on the low voltage side and then converted with the voltage ratio of transformer to the high voltage side.

For determining the current distribution between the coils of the reactor the mutual inductances between coils and their self inductances must be calculated.

The self-inductance of a solenoid type cylinder can be calculated with the following equation from Nagaoga (1909):

$$\mathbf{L_{self} = \mu_o N^2 \pi D^2 (K/4) H,} \qquad (3)$$

where,

μ_o = permeability of vacuum ($4\pi 10^{-7}$ Vs/Am)
H = Height of cylinder,
D = Diameter of cylinder
N = Number of winding turns
K = Nagaoga-Factor, which takes the end turns in to account

For simple calculations the factor K can be evaluated as follows:

$$\mathbf{K = [(1+(D/2H)^2)^{1/2} - D/2H]} \qquad (4)$$

With an air core solenoid type cylinder the equation (3) can be written as follows, when the diameters are in cm:

$$\mathbf{L_{self} = 0.004\pi^2 a^2 b n^2 K \ [\mu H] = 0.002\pi^2 a(2a/b) N^2 K \ [\mu H]} \qquad (5)$$

where,

a = radius/cm (= D/2)
b = length/cm (=H)
n = turns per length/cm
N = number of winding turns
K = Nagaoga-Factor which takes the end turns in account (= *f* (b/2a))

The shape of the conductors in the winding has no influence on the results, as shown with those equations above.

Grower (1945, Table 36*:"Values of K for short or long single layer coils"*) has published the K-factors, which were calculated by Nagaoga earlier, but it is not said how the factors are calculated. The factors can be found from the tables of Grover by calculating the relation of "length/diameter" of the cylinder and then by interpolation. The difference to the K-factors calculated with equation (4) is that the relation is now "diameter/2*length".

For the test reactor with given dimensions the K-factors were defined in both cases as follows:

Grower (table 36):		$K = [(1+(D/2H)^2)^{1/2} - D/2H]$
Cyl.1: b/2a = 0.656 =>	K1 = 0.591	K1 = 0.495
Cyl 2: b/2a = 0.577 =>	K2 = 0.559	K2 = 0.457
Cyl 3: b/2a = 0.450 =>	K3 = 0.500	K3 = 0.384
Cyl 4: b/2a = 0.378 =>	K4 = 0.458	K4 = 0.335
Cyl 5: b/2a = 0.341 =>	K5 = 0.434	K5 = 0.308

Table 1: Self-inductances calculated with K-factors from Grower

	N	D	H	Kgrover	pii^2		Lself	H/D
Cyl1	93.04	0.821456	0.539	0.591	9.8696	10000	**6.32**	0.656152
Cyl2	78.58	0.914666	0.528	0.559	9.8696	10000	**5.40**	0.5772599
Cyl3	68.5	1.00497	0.452	0.500	9.8696	10000	**5.17**	0.44976467
Cyl4	62.96	1.09528	0.414	0.458	9.8696	10000	**5.19**	0.37798554
Cyl5	61.68	1.19199	0.406	0.434	9.8696	10000	**5.70**	0.34060688

Table 2: Self-inductances calculated with K-factors with equation (4)

	N	D	H	pii^2		K(4)	Lself	H/D
Cyl1	93.04	0.821456	0.539	9.8696	10000	0.4952	**5.30**	0.656152
Cyl2	78.58	0.914666	0.528	9.8696	10000	0.4568	**4.41**	0.5772599
Cyl3	68.5	1.00497	0.452	9.8696	10000	0.3836	**3.97**	0.44976467
Cyl4	62.96	1.09528	0.414	9.8696	10000	0.3355	**3.80**	0.37798554
Cyl5	61.68	1.19199	0.406	9.8696	10000	0.3082	**4.05**	0.34060688

The influence of the winding layers on the self-inductance of a cylinder

The self-inductances shown in tables 1 and 2 were calculated with average winding turns (N) of each cylinder. Since the cylinders have several parallel layers, the influence of the self and mutual inductances of each layer must be taken into account.

The K-factors used in the following tables were first calculated with equation (4) and were then calculated with the K-factors from Grower's table 36.

Table 3: Calculation of inductance of Cylinder 1

Cylinder 1 / 7 layers

N	D/m	H/m	K (4)	pii	10^-4	L/mH
98	0,80525	0,539	0,501208	3,1416	10000	5,715377
96	0,81065	0,528	0,493015	3,1416	10000	5,581321
94,25	0,81605	0,51838	0,4855	3,1416	10000	5,468135
92,75	0,82146	0,51013	0,478699	3,1416	10000	5,37631
91,25	0,82686	0,50188	0,471839	3,1416	10000	5,282334
90	0,83226	0,495	0,465748	3,1416	10000	5,21016
89	0,83766	0,4895	0,460464	3,1416	10000	5,16013

L11	L12	L13	L14	L15	L16	L17
5,598736	5,598736	5,496676	5,409196	5,321715	5,248815	5,190495
5,496676	5,479579	5,479579	5,39237	5,305162	5,232489	5,17435
5,409196	5,39237	5,381109	5,381109	5,294083	5,221561	5,163544
5,321715	5,305162	5,294083	5,289361	5,289361	5,216904	5,158939
5,248815	5,232489	5,221561	5,216904	5,209974	5,209974	5,152085
5,190495	5,17435	5,163544	5,158939	5,152085	5,152269	5,152269
5,715377	5,581321	5,468135	5,37631	5,282334	5,21016	5,16013
37,98101	37,76401	37,50468	37,22419	36,85471	36,49217	36,15181

Parallel

18,9361	18,68196	18,33627	36,15181

9,404084	12,16577

Cyl.1 inductance (mH)

5,304066

The K-factor used in table 3 was calculated with equation (4).

When the same calculation is made with Grower's K-factor the result is : L_{self1} = 6.365 mH, which is almost the same as calculated with the average number of winding turns namely: L_{self1} = 6.322 mH

The small error may occur from the iteration error.

The same procedure was followed for cylinder 5.

Table 4: Calculation of inductance of Cylinder 5

Cylinder5 / 7 layers

N	D/m	H/m	K	pii	10^-4	L/mH
61,5	1,1728	0,39975	0,308427	3,1416	10000	3,961536
61,25	1,1792	0,39813	0,306011	3,1416	10000	3,957317
61,25	1,1856	0,39813	0,30464	3,1416	10000	3,98247
61,5	1,192	0,39975	0,304306	3,1416	10000	4,037626
61,75	1,1984	0,40138	0,303981	3,1416	10000	4,093265
62	1,2048	0,403	0,303653	3,1416	10000	4,149424
62,5	1,2112	0,40625	0,304344	3,1416	10000	4,237058

L11	L12	L13	L14	L15	L16	L17
3,945432	3,945432	3,945432	3,961536	3,977639	3,993743	4,025951
3,945432	3,957317	3,957317	3,97347	3,989622	4,005774	4,038079
3,961536	3,97347	3,998725	3,998725	4,01498	4,031235	4,063745
3,977639	3,989622	4,01498	4,054039	4,054039	4,070452	4,103279
3,993743	4,005774	4,031235	4,070452	4,109837	4,109837	4,142981
4,025951	4,038079	4,063745	4,103279	4,142981	4,182887	4,182887
3,961536	3,957317	3,98247	4,037626	4,093265	4,149424	4,237058
27,81127	27,86701	27,9939	28,19913	28,38236	28,54335	28,79398

Parallel

13,91956	14,04807	14,23132	28,79398

6,991759	9,524077

Cyl.5 Inductance (mH)

4,031891

With the average turns (N) the calculated value was: L_{self5} = 4.05mH. Using Grover's K-factors the inductances are L_{self5} = 5.69mH and with the average turns, L_{self5} = 5.703mH.
The same calculations have been carried out for each other cylinder and the results are very close to those ones shown in tables 1 and 2. In the following calculations the average values of each cylinder has been used for the number of winding turns, N.

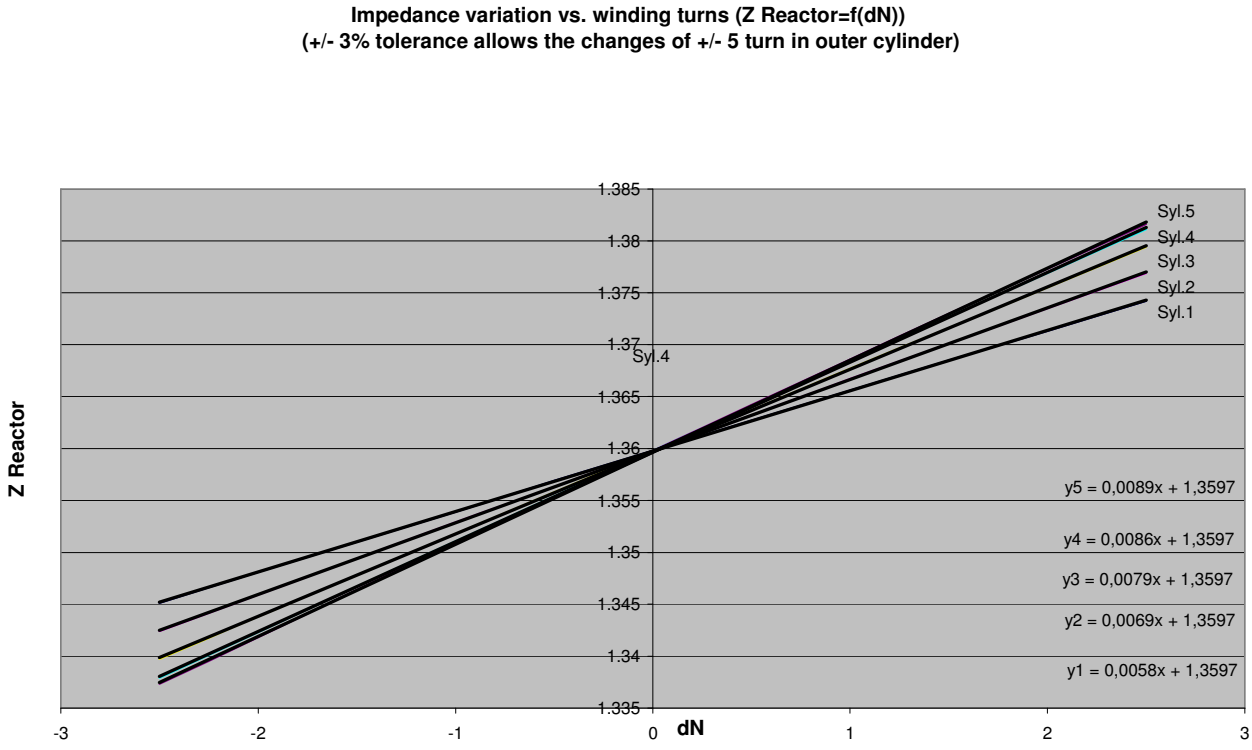

Figure 2: Changes in reactor impedance, when the winding turns have been changed

The following calculation is based on the method of Professor Dwight. It was founded and published in 1937 by him and Grover. In this method the influence of winding thickness is clarified.

Table 5: Results from the calculation of inductances

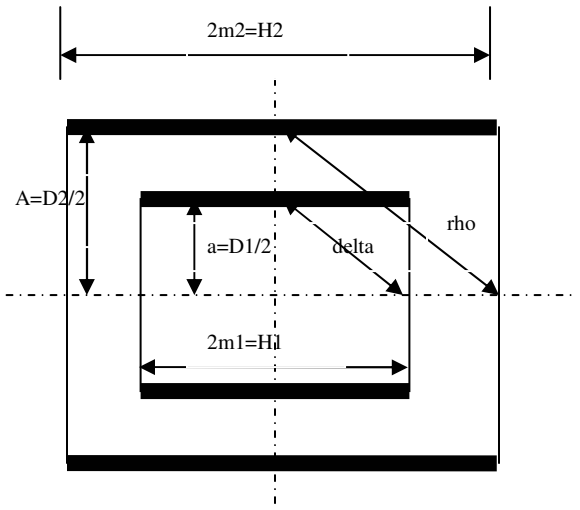

Diagonals:
delta=(a^2+m1^2)^1/2
rho=(A^2+m2^2)^1/2

	H	D	N	D/2	n=N/H	pi^2
syl1	53,9	82,1	93,0	41,1	1,7	9,870
syl2	52,8	91,5	78,6	45,7	1,5	9,870
syl3	45,2	100,5	68,5	50,2	1,5	9,870
syl4	41,4	109,5	63,0	54,8	1,5	9,870
syl5	40,6	119,2	61,7	59,6	1,5	9,870

	delta	rho	x=a/delta	y=A/rho	H/2	H/D
syl1	49,1	0,0	0,836	0,000	27,0	0,656
syl2	52,8	52,8	0,866	0,866	26,4	0,577
syl3	55,1	55,1	0,912	0,912	22,6	0,450
syl4	58,6	58,6	0,935	0,935	20,7	0,378
syl5	63,0	63,0	0,947	0,947	20,3	0,341

	pi
z=delta/rho	3,1415927

3,1415927

	cyl1	cyl2	cyl3	cyl4	cyl5	3,1415927
syl1	1					3,1415927
syl2	0,93	1,00				3,1415927
syl3	0,89	0,96	1,00			
syl4	0,84	0,90	0,94	1,00		
syl5	0,78	0,84	0,87	0,93	1,00	

	lamda/eta2	lamda/eta4	lamda/eta6	lamda/eta8	lamda/eta10
syl1	-0,22	-0,13	0,15	-0,02	-0,07
syl2	-0,31	-0,05	0,15	-0,08	-0,02
syl3	-0,46	0,11	0,08	-0,13	0,09
syl4	-0,53	0,22	-0,02	-0,09	0,11
syl5	-0,57	0,28	-0,08	-0,05	0,10

M=K1*K2

K1=2*pi^2*a^2*N1*N2/rho*

K1.12	4610091					
K1.13	3852225	K1.23	4033763			
K1.14	3331330	K1.24	3488321	K1.34	3670930	
K1.15	3034852	K1.25	3177871	K1.35	3344229	
					K1.45	3650921,6

K2=[1-A^2*delta^2/2/rho^4*
{lamda2+z^2*lamda4*eta2+z^4*lamda6*eta4+z^6*lamda8*eta6+z^8*lamda10*eta8}]

K2.12	1,063					
K2.13	1,054	K2.23	1,11			
K2.14	1,056	K2.24	1,09	K2.34	1,1929334	
K2.15	1,044	K2.25	1,08	K2.35	1,1676193	
					K2.45	1,2482816

kerr. 10^-6
0,000001
0,000001
0,000001
0,000001

M=K1*K2*10^-6 mH

M12	4,90	M21	4,90	M31	4,06
M13	4,06	M23	4,46	M32	4,46
M14	3,52	M24	3,82	M34	4,38
M15	3,17	M25	3,44	M35	3,90
M1	15,64	M2	16,62	M3	16,81

M41	3,52	M51	3,2
M42	3,82	M52	3,4
M43	4,38	M53	3,9
M45	4,56	M54	4,6
M4	16,27	M5	15,1

K2=[(ln(4/a))(1+a^2/8-a^4/64+5a^6/1024-35a^8/16384)-1/2+a^2/32+a^4/96-109a^6/24576+431a^8/196608…]

a=H/D

K1=2*pi*D*N^2/10^9	**K2**
0,0045	1,42
0,0035	1,52
0,0030	1,75
0,0027	1,90
0,0028	2,00

Lself

Thickness of winding (∆L)

D1	**D2**	**t**
80,5	83,8	1,6205
89,9	93,1	1,6005
99,2	101,8	1,2815
107,9	110,5	1,2800
117,3	121,1	1,92

∆L = K1*K3*10^3 mH

K3= (Pi*t/3/b-25*t^2/72/b^2-t^2/8/d^2+19*b^2*t^2/768/d^4-t^4/180/b^4+67*t^4/7200/b^2/d^2-17*t^4/3840/d^4-(ln(4*d/b))*(t^2/24/d^2+7*b^2*t^2/384/d^4+11*t^4/2880/d^4)-(ln(b/t))*(t^2/6/b^2-t^4/120/b^2/d^2)-1/q/N*(ln(p/w)+0,15))

t	b	d	q	w	p	N
1,6205	53,9	82,1	7	0,25	0,55	93,0
1,6005	52,8	91,5	6	0,3	0,65	78,6
1,2815	45,2	100,5	5	0,3	0,65	68,5
1,2800	41,4	109,5	6	0,3	0,65	63,0
1,92	40,6	119,2	7	0,3	0,65	61,7

K3	**∆L/mH**
0,029122	0,1301136
0,028859	0,1024129
0,026218	0,0776809
0,028989	0,0790752

0,045382 0,1293033

	Ls=K1*K2-∆L		
	Ls	**Lm**	**L/mH**
syl1	6,194	15,645	21,839
syl2	5,308	16,624	21,931
syl3	5,097	16,806	21,903
syl4	5,116	16,270	21,386
syl5	5,574	15,076	20,65

	Ls1= K1s*K2s-∆L	**M**	**Ls2= K1s*K2s**	**L/mH = Ls2+M**
syl1	6.2260806	15.685954	6.35689221	22.042846
syl2	5.2829341	16.610085	5.38485178	21.994936
syl3	5.0655797	16.784206	5.14275777	21.926963
syl4	5.1152657	16.291353	5.19433201	21.485685
syl5	5.6601105	15.17987	5.79145987	20.97133

(L)
11.009433
7.3293819
5.465085
4.3353118

Rac(Ω)				**Z(Ω)**		
Rac = 1,05* Rdc[Ω]				**Zm=ωM/1000**		
Rs=2ρDN/d^2 =k3DN				**Zs=(Rac^2+ (ω(Ls2) /1000)^2)^1/2**		
	k3=2ρ/d^[Ω/cm] (2 cond./turn)					
k3:d=2.5mm		**k3:d=3.0mm**				
0.00009024		6.267E-05				
	Rdc	**Rac**	**Rac/no.of layer**	**ω=2πf**	**Zs**	**Zm**
syl1	0.6914915	0.726066	0.1037237	314.159265	2.1249675	4.9278877
syl2	0.4493586	0.4718265	0.0674038	314.159265	1.7562667	5.218212
syl3	0.43007	0.4515735	0.0645105	314.159265	1.6775659	5.2729137
syl4	0.432107	0.4537123	0.064816	314.159265	1.6937477	5.1180794
syl5	0.4642745	0.4874882	0.0696412	314.159265	1.8836161	4.7688968
Rac			**(Z)**			**Z/cyl**
0.04085475				3.45984163		6.9276376
0.025013564				2.30337598		6.9117472
0.018048395				1.71750483		6.8910963
	0.0143336				**1.3624106**	6.7524393
						6.5896491
					(Per layer)	
				Rac cyl	**Zs cyl**	
				0.1033664	1.9997499	
				0.07879747	1.6935352	
	Resist. Per layer			0.09058706	1.6181826	
				0.09058706	1.6343599	
R=k3/ (sum(1/DN))				0.06909425	1.8207522	**Rac reac.**
N	**D/cm**	**1/DN**	**Sum 1/DN**	**Rdc cyl**	**Rdc reac.**	0.0447125
98	80.525	0.0001267			0.0425834	0.0299364
96	81.065	0.0001285			0.0285108	0.0214461
94.25	81.605	0.00013			0.0204249	**0.0163662**
92.75	82.146	0.0001313			0.0155869	
91.25	82.686	0.0001325				
90	83.226	0.0001335			**N/aver.**	
89	83.766	0.0001341	0.0009167	0.09844419	0.1033664	93.035714
81.25	89.866	0.000137				
80	90.506	0.0001381				
79	91.146	0.0001389				
78	91.787	0.0001397				
77	92.427	0.0001405				
76.25	93.067	0.0001409	0.0008351	0.07504521	0.0787975	78.583333
69.5	99.217	0.000145				
69	99.857	0.0001451				
68.5	100.5	0.0001453				
68	101.14	0.0001454				

67.5	101.78	0.0001456	0.0007264	0.08627339	0.0905871	68.5
63.75	107.93	0.0001453				
63.25	108.57	0.0001456				
63	109.21	0.0001453				
62.75	109.85	0.0001451				
62.5	110.49	0.0001448				
62.5	111.13	0.000144	0.0008702	0.07201722	0.0756181	62.958333
61.5	117.28	0.0001386				
61.25	117.92	0.0001385				
61.25	118.56	0.0001377				
61.5	119.2	0.0001364				
61.75	119.84	0.0001351				
62	120.48	0.0001339				
62.5	121.12	0.0001321	0.0009523	0.06580405	0.0690943	61.678571

Z-matrix

N						
93.2832	**1.9997499**	1.5395947	1.2748028	1.10769725	1.0057929	
78.396	1.5395947	**1.6935352**	1.3943096	1.19625088	1.0880567	
68.2888	1.2748028	1.3943096	**1.6181826**	1.37144274	1.2323586	
62.9549	1.1076973	1.1962509	1.3714427	**1.63435993**	1.4426885	**Zreact.**
62.1535	1.0057929	1.0880567	1.2323586	1.44268853	**1.8207522**	**1.3624106**

6.9043652
6.923966
6.907976

Matlab

Results of Jacobian matr.

Jcoil=(inv(Z))*U'* (inv(U* (inv(Z))*U'))*I

6.74603
6.529326

Z1
With orig.turns

-0.0392						
0.0344		1.989364	1.539185	1.2754412	1.104869	0.995506
0.0514		1.539185	1.701477	1.401904	1.199123	1.082277
0.0401		1.275412	1.401904	1.628176	1.375759	1.226725
0.0355		1.104869	1.199123	1.375759	1.634536	1.431743
		0.995506	1.082277	1.226725	1.431743	1.793075

New curr.	measured	Jcoil=	error%	calculated	Jcoil=	error%
98.641	9.92	10.605302	6.4618851	92.9673	97.610066	-4.993977
87.8265	9.09	9.5973956	5.2868053	87.2909	88.333399	-1.1942816
69.7166	7.8	7.6313134	-2.210453	69.6882	70.237789	-0.7886407
92.0991	10.06	10.008066	-0.518921	93.3858	92.113166	1.3627707
138.7868	16.05	15.077922	-6.4470257	143.743	138.77558	3.4557648
	52.92			487.0752	487.07	

				925.194	92.5194
				934.243	93.4243
				754.288	75.4288
Z3 Cyl5 + 5 turns					
				970.644	97.0644
				1.286.331	128.6331
	1.9893642	1.5391849	1.27541158	1.104869	1.0762068
	1.5391849	1.701477	1.40190449	1.1991233	1.1700126
	1.2754116	1.4019045	1.628176	1.3757586	1.3261696
	1.104869	1.1991233	1.37575856	1.634536	1.5478074
	1.0762068	1.1700126	1.32616962	1.5478074	2.0951541
				Jcoil=	Error%
			NC's values		
			92.9673	100.39917	-7.994071
			87.2909	93.65639	-7.2922723
			69.6882	74.446428	-6.8278825
			93.3858	174.01197	-86.336654
			143.743	44.556035	69.002988
			487.0752	487.07	
	Z3 cyl.5 + 2 turns				
	1.9893642	1.5391849	1.27541158	1.104869	1.0277862
	1.5391849	1.701477	1.40190449	1.1991233	1.1173715
	1.2754116	1.4019045	1.628176	1.3757586	1.2665027
	1.104869	1.1991233	1.37575856	1.634536	1.4781685
	1.0277862	1.1173715	1.26650266	1.4781685	1.9110753
			92.9673	99.106263	-6.6033573
			87.2909	90.839457	-4.0652084
			69.6882	72.222498	-3.636625
			93.3858	126.26564	-35.208612
			143.743	98.636137	31.380215
				487.07	
	Z4 cyl5 -2 turns				
	1.9893642	1.5391849	1.27541158	1.104869	0.9632253
	1.5391849	1.701477	1.40190449	1.1991233	1.1173715
	1.2754116	1.4019045	1.628176	1.3757586	1.1869467
	1.104869	1.1991233	1.37575856	1.634536	1.3853167
	0.9632253	1.0471833	1.18694673	1.3853167	1.6788508
			92.9673	115.10502	-23.81237

87.2909	42.397231	51.429953
69.6882	89.963503	-29.094313
93.3858	56.379394	39.627444
143.743	183.22485	-27.466975
	487.07	

Pac=Rac*Jcoil^2

Rac/cyl.	**Pnc**	**PDwight**	**P+2**	**P+5**	**P-2**
0.103366404	893.38745	984.84667	1015.27013	1041.9327	1369.5186
0.078797471	600.41319	614.84007	650.221518	691.17355	141.64044
0.090587059	439.93109	446.8974	472.51019	502.05801	733.16019
0.075618084	659.45832	641.60698	1205.58008	2289.7282	240.36237
0.069094251	1427.6289	1330.6628	672.224016	137.16869	2319.5871
0.016366204	**4020.8189**	**4018.8539**	**4015.80594**	**4662.0612**	**4804.2686**

Ph=J^2*Rac
3882.755

2 turns less.
changes%
53.29503
-76.409506
66.653416
-63.551545
62.478298
19.48483

Current distrib.

	Chart4	Chart2	
NC	Changed turns	Changed turns	**Dwight+Qin +Matlab**
92.97	95.39	94.52	97.6100656
87.29	95.42	90.41	88.3333992
69.69	96.15	92.6	70.2377895
93.39	98.48	93.14	92.1131657
143.74	101.63	116.4	138.77558
487.0752	487.07	487.07	487.07

Changed Z of reactor with changed turns

Zreact. = f(∆N)

∆N/Syl	**1**	**2**	**3**	**4**	**5**
-2.5	1.3451	1.3424	1.3397	1.3379	1.3373
-2	1.3481	1.3459	1.3438	1.3423	1.3418
-1.5	1.351	1.3494	1.3478	1.3467	1.3464
-1	1.3539	1.3529	1.3518	1.3511	1.3509
-0.5	1.3569	1.3563	1.3558	1.3554	1.3553
0	**1.3598**	**1.3598**	**1.3598**	**1.3598**	**1.3598**
0.5	1.3627	1.3632	1.3637	1.3641	1.3642

	1	1.3656	1.3667	1.3677	1.3684	1.3686
	1.5	1.3685	1.3701	1.3716	1.3727	1.373
	2	1.3713	1.3735	1.3755	1.3769	1.3773
	2.5	1.3742	1.3769	1.3794	1.3811	1.3816

Chart 1

92.97	94.11	941.061	92.97	95.39	953.868
87.29	98.54	985.388	87.29	97.41	974.063
69.69	94.72	947.226	69.69	94.69	946.942
93.39	100.07	1.000.685	93.39	99.99	999.893
143.74	99.63	996.341	143.74	99.59	995.934
487.08	487.07				

Matrix calc. results

	120.70	-107.86	1.26	-3.35	-0.22	
	-107.86	241.83	-123.02	1.86	-3.28	
	1.26	-123.02	256.35	-125.07	-1.80	
	-3.35	1.86	-125.07	250.23	-113.87	
	-0.22	-3.28	-1.80	-113.87	134.24	
Sum	**10.54**	**9.53**	**7.72**	**9.80**	**15.08**	**52.67**
U	73.10	73.10	73.10	73.10	73.10	
Omega	314.16	314.16	314.16	314.16	314.16	
L=U*1000/J /Omega [mH]	**22.08**	**24.41**	**30.13**	**23.74**	**15.43**	

Matrix calc. results with winding thickness

	136.33	-130.55	9.35	-4.43	0.11	
	-130.55	286.12	-150.91	9.14	-4.24	
	9.35	-150.91	293.45	-148.21	3.75	
	-4.43	9.14	-148.21	286.85	-134.19	
	0.11	-4.24	3.75	-134.19	150.53	
	10.82	**9.58**	**7.43**	**9.17**	**15.97**	**52.96**
L=U*1000/J /Omega [mH]	**21.50**	**24.29**	**31.33**	**25.38**	**14.57**	

In Table 6 the results of the self inductance calculations using Dwight's method are compared with the results calculated with Nagaoga's as well as Hak's methods.
(The winding thickness is used in the results from Dwight and Hak but not in the results from Nagaoga. The advantages for using Dwight's and Hak's equations are that it is not necessary to interpolate the K-factors, but the calculations can be carried out with series developments.

Table 6: Comparison of results for self inductance calculation

		Self inductance/mH:	
	Nagaoga	Dwight	Hak
L_{itse1}	6.322	6,194	6,250848
L_{itse2}	5.398	5,308	5,341642
L_{itse3}	5.174	5,097	5,04605
L_{itse4}	5.192	5,116	5,017937
L_{itse5}	5.703	5,574	5,473817

Matrix calculation with Dwight's method

L =

6.1937	4.8994	4.0598	3.5169	3.1688
4.8994	5.3078	4.4624	3.8169	3.4450
4.0598	4.4624	5.0969	4.3792	3.9048
3.5169	3.8169	4.3792	5.1158	4.5574
3.1688	3.4450	3.9048	4.5574	5.5740

>> LmH=(L)/1000

LmH =

0.0062	0.0049	0.0041	0.0035	0.0032
0.0049	0.0053	0.0045	0.0038	0.0034
0.0041	0.0045	0.0051	0.0044	0.0039
0.0035	0.0038	0.0044	0.0051	0.0046
0.0032	0.0034	0.0039	0.0046	0.0056

>> inv(LmH)

```
ans =

  1.0e+003 *

    0.5999   -0.5763    0.0439   -0.0225    0.0027
   -0.5763    1.2681   -0.6755    0.0481   -0.0222
    0.0439   -0.6755    1.3062   -0.6584    0.0158
   -0.0225    0.0481   -0.6584    1.2622   -0.5877
    0.0027   -0.0222    0.0158   -0.5877    0.6610

>> omega=[314.15926]

omega =

  314.1593

>> u=[71.3]

u =

   71.3000

>> inv(omega)

ans =

    0.0032

>> J=(u)*(inv(omega))*(inv(LmH))

J =

  136.1410  -130.7854    9.9727   -5.1035    0.6224
 -130.7854   287.8047  -153.3062   10.9062   -5.0463
    9.9727  -153.3062   296.4429  -149.4278    3.5864
   -5.1035    10.9062  -149.4278   286.4687  -133.3814
    0.6224    -5.0463    3.5864  -133.3814   150.0245
```

Current distribution:

10.8472	**9.573**	**7.268**	**9.4622**	**15.8056**	**Sum: 52.956A**

Measured:

```
>> Jmit=[9.92 9.09 7.80 10.06 16.05]
```

Jmit =

9.9200 9.0900 7.8000 10.0600 16.0500 Sum: 52.92A

>> Ucalc.=(Jmit)*(omega)*(LmH)

Ucalc. =

70.3348 70.7947 71.4145 71.7390 71.7907

(Utest = 71.3V)

For comparative reasons the current distribution in table 8 was calculated with and without the winding thicknesses.

The results from the calculations of Dwight's method are very close to those calculated earlier with the [Jmit] matrix.

Table 7: Current distribution

	Results of current distribution (without thickness of winding)					
	120,6966	-107,857	1,2619	-3,3492	-0,2158	
	-107,857	241,8322	-123,023	1,8569	-3,2762	
	1,2619	-123,023	256,3491	-125,067	-1,7996	
	-3,3492	1,8569	-125,067	250,2277	-113,868	
	-0,2158	-3,2762	-1,7996	-113,868	134,2396	
Sum	**10,5367**	**9,5331**	**7,7216**	**9,8005**	**15,0799**	**52,6718**
U	73,1	73,1	73,1	73,1	73,1	
Omega	314,16	314,16	314,16	314,16	314,16	
L=U*1000/J/Omega [mH]	**22,08319**	**24,40801**	**30,13417**	**23,74205**	**15,43007**	

Results of current distribution (with thickness of winding)

136,3344	-130,548	9,3466	-4,4273	0,1149
-130,548	286,1249	-150,907	9,1447	-4,2362
9,3466	-150,907	293,4514	-148,211	3,7476

	-4,4273	9,1447	-148,211	286,8521	-134,191	
	0,1149	-4,2362	3,7476	-134,191	150,5313	
	10,821	**9,5787**	**7,4274**	**9,1671**	**15,9663**	**52,9605**
L=U*1000/J/Omega [mH]	**21,503**	**24,29181**	**31,32778**	**25,38251**	**14,57344**	

The results of the calculation of self-inductance shown in table 8 are calculated with Hak's equations (56...58, page 19 and values from table III):

Table 8: Self-inductances calculated by Hak's equations

Hak's equation 56 page19 and table III	
	Ls
cyl1	**6,265994**
cyl2	**5,342263**
cyl3	**5,048774**
cyl4	**5,015658**
cyl5	**5,470949**

Hak's equations 56...58 page19	
	Ls
cyl1	**6,250848**
cyl2	**5,341642**
syl3	**5,04605**
cyl4	**5,017937**
cyl5	**5,473817**

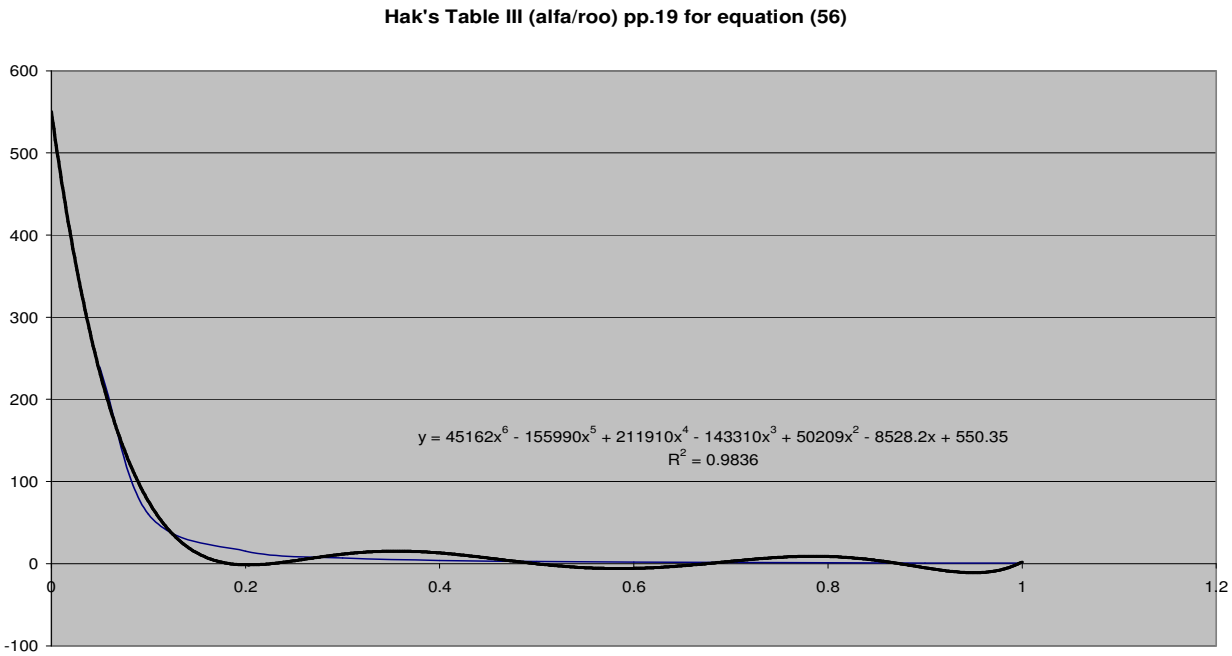

Figure 3: Alpha/roo values for equation 56 (Hak, 1938)

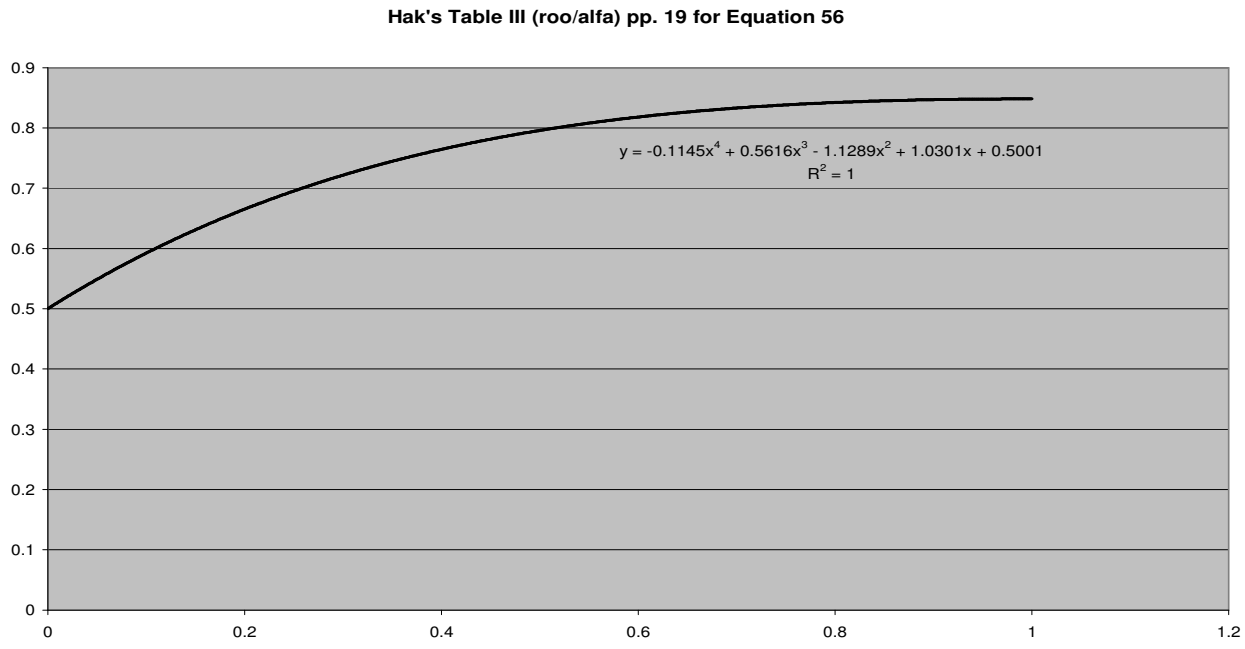

Figure 4: Roo/alpha values for equation 56 (Hak, 1938)

Current distribution using the mutual inductances from Dwight and self-inductances from Hak:

L =

6.2508	4.8994	4.0598	3.5169	3.1688
4.8994	**5.3416**	4.4624	3.8169	3.4450
4.0598	4.4624	**5.0461**	4.3792	3.9048
3.5169	3.8169	4.3792	**5.0179**	4.5574
3.1688	3.4450	3.9048	4.5574	**5.4738**

>> J=(u)*(inv(omega))*(inv(LmH))

J =

129.3604	**-121.5935**	**7.7523**	**-5.7647**	**0.9085**
-121.5935	**277.4196**	**-158.3614**	**18.2351**	**-6.4196**
7.7523	**-158.3614**	**326.3535**	**-183.6912**	**15.3090**
-5.7647	**18.2351**	**-183.6912**	**344.8627**	**-164.2277**
0.9085	**-6.4196**	**15.3090**	**-164.2277**	**170.7884**

>> Ucalc=(Jmit)*(omega)*(LmH)

Ucalc =

70.5129	**70.8915**	**71.2898**	**71.4297**	**71.2856**

129,36	**-121,59**	**7,7523**	**-5,7647**	**0,9085**	
-		**-**			
121,59	**277,42**	**158,361**	**18,2351**	**-6,4196**	
7,7523	**-158,36**	**326,354**	**-183,69**	**15,309**	
-		**-**			
5,7647	**18,2351**	**183,691**	**344,863**	**-164,23**	
0,9085	**-6,4196**	**15,309**	**-164,23**	**170,788**	
10,663	**9,2802**	**7,3622**	**9,4142**	**16,3586**	**53,0782**

Voltages				
71,3	**71,3**	**71,3**	**71,3**	**71,3**
(Z=U/J)				
6,686674	**7,683024**	**9,684605**	**7,573665**	**4,358564**
Ind.(=Z/Omega*10^3 mH)				
21,28429	**24,45577**	**30,82698**	**24,10767**	**13,87371**

The determination of the current distribution can be carried out by matrix- calculation (Qin Yu 1996) as follows:

$$[\mathbf{Z}][\mathbf{J}_{coil}]^{T} = [\mathbf{U}][\mathbf{V}]^{T}$$

where

$[\mathbf{V}] = [\mathbf{V...V}]$ voltage matrix over the cylinder
$[\mathbf{J}_{coil}] = [\mathbf{J}_1...\mathbf{J}_n]$ current matrix
$[\mathbf{U}] = [\mathbf{1...1}]$ unit matrix
$[\mathbf{Z}] =$ impedance matrix (self- and mutual-inductances)

Since the supply voltage over the coils is the same, the unit matrix instead of the voltage matrix can be used in the calculations. The current distribution in air-core reactors is a linear function related to the impedances of each coil.

The current is:

$$[\mathbf{U}][\mathbf{J}_{coil}] = \mathrm{I}$$

and the relative current distribution is:

$$\mathbf{J}_{coil} = \mathbf{Z}^{-1}\mathbf{U}^{T}(\mathbf{U}\mathbf{Z}^{-1}\mathbf{U}^{T})^{-1}\mathrm{I}\,,$$

The current distribution is next calculated for the reactor using the inductance matrix [L] with Dwight's mutual inductances and Hack's self-inductances:

L =

6.2508	4.8994	4.0598	3.5169	3.1688
4.8994	5.3416	4.4624	3.8169	3.4450
4.0598	4.4624	5.0461	4.3792	3.9048
3.5169	3.8169	4.3792	5.0179	4.5574
3.1688	3.4450	3.9048	4.5574	5.4738

```
>> omega=[314.15926]

>> LmH=(L)/1000
```

LmH =

0.0063	0.0049	0.0041	0.0035	0.0032
0.0049	0.0053	0.0045	0.0038	0.0034
0.0041	0.0045	0.0050	0.0044	0.0039
0.0035	0.0038	0.0044	0.0050	0.0046
0.0032	0.0034	0.0039	0.0046	0.0055

```
>> U=[1 1 1 1 1]

>> Z=(omega)*(LmH)
```

Z =

1.9638	1.5392	1.2754	1.1049	0.9955
1.5392	1.6781	1.4019	1.1991	1.0823
1.2754	1.4019	1.5853	1.3758	1.2267
1.1049	1.1991	1.3758	1.5764	1.4317
0.9955	1.0823	1.2267	1.4317	1.7197

Supply current

```
>> I=52.6

>> Jcoil=(inv(Z))*U'*(inv(U*(inv(Z))*U'))*I
```

Jcoil =	error/%
10.5670	6.6
9.1965	1.1
7.2959	6.4
9.3294	7.3
16.2112	1.0

measured currents are:

9.92A
9.09A
7.80A
10.06A
16.05A

Now the calculation with rated current
I=486.6A

```
>> I=486.6

>> Jcoil=(inv(Z))*U'*(inv(U*(inv(Z))*U'))*I
```

Jcoil =	error/%
97.7549	5.1
85.0768	2.5
67.4937	3.2
86.3054	7.6
149.9692	4.2

Current distribution calculated by the manufacturer:

92.9673
87.2909
69.6882
93.3858
143.743

Next the calculation with Dwight's results:

L =

6.1937	4.8994	4.0598	3.5169	3.1688
4.8994	5.3078	4.4624	3.8169	3.4450
4.0598	4.4624	5.0969	4.3792	3.9048
3.5169	3.8169	4.3792	5.1158	4.5574
3.1688	3.4450	3.9048	4.5574	5.5740

>> Z=(omega)*(L)/1000

Z =

1.9458	1.5392	1.2754	1.1049	0.9955
1.5392	1.6675	1.4019	1.1991	1.0823
1.2754	1.4019	1.6013	1.3758	1.2267
1.1049	1.1991	1.3758	1.6072	1.4317
0.9955	1.0823	1.2267	1.4317	1.7511

>> Jcoil=(inv(Z))*U'*(inv(U*(inv(Z))*U'))*I

Jcoil =	error/%
99.6727	7.2
87.9635	0.8
66.7835	1.4
86.9457	7.0
145.2346	1.0

Current distribution calculated by the manufacturer:

92.9673
87.2909
69.6882
93.3858
143.743

The errors are smaller but the divergence is larger then in the earlier calculations.

The current distribution with the test current of I=52.6 and Dwight's impedances:

```
>> Jcoil=(inv(Z))*U'*(inv(U*(inv(Z))*U'))*I

Jcoil =                 error/%

   10.7743              8.6
    9.5086              4.6
    7.2191              7.4
    9.3986              6.5
   15.6994              2.2
```

Measured values:

9.92A
9.09A
7.80A
10.06A
16.05A

Errors are between 2...8% but the divergence is still too large.

It seems that the errors are caused because, as mentioned before, the self and mutual inductances of several winding layers within and between the cylinders are not included in the results.

The current distribution was also calculated with the inductances from Grower, as follows:

```
L =
   6.3213   5.3389   4.6540   4.2776   4.1906
   5.3389   5.3980   4.7055   4.3249   4.2370
   4.6540   4.7055   5.1739   4.7555   4.6588
   4.2776   4.3249   4.7555   5.1921   5.0866
   4.1906   4.2370   4.6588   5.0866   5.7029

>> Z=L*Omega/1000

Z =

   1.9859   1.6773   1.4621   1.3439   1.3165
```

```
    1.6773    1.6958    1.4783    1.3587    1.3311
    1.4621    1.4783    1.6254    1.4940    1.4636
    1.3439    1.3587    1.4940    1.6312    1.5980
    1.3165    1.3311    1.4636    1.5980    1.7916

>> I=[486.6]
I =

  486.6000

>> Jcoil=(inv(Z))*U'*(inv(U*(inv(Z))*U'))*I

Jcoil =

   24.4512
  164.0443
   67.7612
  164.6735
   65.6698


>> I=52.92

I =

   52.9200

>> Jcoil=(inv(Z))*U'*(inv(U*(inv(Z))*U'))*I

Jcoil =

    2.6592
   17.8406
    7.3693
   17.9090
    7.1419



L =

    6.3210    4.8444    4.0532    3.4686    3.0959
    4.8444    5.3966    3.6183    3.0837    2.7966
    4.0532    3.6183    5.1768    2.9460    2.6444
    3.4686    3.0837    2.9460    5.1871    2.4527
    3.0959    2.7967    2.6444    2.4527    5.6992
```

```
>> Z=L*Omega/1000

Z =

    1.9858    1.5219    1.2734    1.0897    0.9726
    1.5219    1.6954    1.1367    0.9688    0.8786
    1.2734    1.1367    1.6263    0.9255    0.8308
    1.0897    0.9688    0.9255    1.6296    0.7705
    0.9726    0.8786    0.8308    0.7705    1.7905

>> I=[486.6]

I =

  486.6000

>> Jcoil= (inv (Z))*U'*(inv (U*(inv (Z))*U'))*I

Jcoil =

  -64.0013
  118.9954
  131.1852
  154.7346
  145.6862

>> I=52.92

I =

   52.9200

>> Jcoil=(inv(Z))*U'*(inv(U*(inv(Z))*U'))*I

Jcoil =

   -6.9604
   12.9413
   14.2670
   16.8281
   15.8440
```

The inductances calculated with Grover's equation and the values from table 36 are incorrect since the amounts and directions of currents are wrong.

In the table 8 the winding turns have been changed, one by one.

Table 8: Optimizing of winding turns in relation to impedances and current distribution

(Changing of turns will affect Z_S;Z_M;Z_{coil})

(N = average number of turns):

		At the beginning				
	N					
		1.989364	1.539185	1.275412	1.104869	0.995506
	78.58	1.539185	**1.701477**	1.401905	1.199123	1.082277
	68.50	1.275412	1.401905	**1.628176**	1.375759	1.226725
	62.96	1.104869	1.199123	1.375759	**1.634536**	1.431743
	61.68	0.995506	1.082277	1.226725	1.431743	**1.793075**
Changed	N+0.5	**Changed impedances**				
cyl1	**93.54**	**2.010746**	1.547457	1.282266	1.110807	1.000856
	78.58	1.547457	**1.701477**	1.401905	1.199123	1.082277
	68.50	1.282266	1.401905	**1.628176**	1.375759	1.226725
	62.96	1.110807	1.199123	1.375759	**1.634536**	1.431743
	61.68	1.000856	1.082277	1.226725	1.431743	**1.793075**
	93.04	**1.989364**	1.548979	1.275412	1.104869	0.995506
cyl2	**79.08**	1.548979	**1.723152**	1.410825	1.206753	1.089164
	68.50	1.275412	1.410825	**1.628176**	1.375759	1.226725
	62.96	1.104869	1.206753	1.375759	**1.634536**	1.431743
	61.68	0.995506	1.089164	1.226725	1.431743	**1.793075**
	93.04	**1.989364**	1.539185	1.284721	1.104869	0.995506
	78.58	1.539185	**1.701477**	1.412137	1.199123	1.082277
cyl3	**69.00**	1.284721	1.412137	**1.651958**	1.385801	1.235679
	62.96	1.104869	1.199123	1.385801	**1.634536**	1.431743
	61.68	0.995506	1.082277	1.235679	1.431743	**1.793075**
	93.04	**1.989364**	1.539185	1.275412	1.113644	0.995506
	78.58	1.539185	**1.701477**	1.401905	1.208646	1.082277
	68.50	1.275412	1.401905	**1.628176**	1.386685	1.226725
cyl4	**63.46**	1.113644	1.208647	1.386685	**1.660522**	1.443113
	61.68	0.995506	1.082277	1.226725	1.443113	**1.793075**

	93.04	**1.989364**	1.539185	1.275412	1.104869	1.003576
	78.58	1.539185	**1.701477**	1.401905	1.199123	1.091051
	68.50	1.275412	1.401905	**1.628176**	1.375759	1.236669
	62.96	1.104869	1.199123	1.375759	**1.634536**	1.443349
cyl5	**62.18**	1.003576	1.091051	1.236669	1.443349	**1.822221**

N+1

cyl1	**94.04**	**2.032243**	1.555728	1.289120	1.116744	1.006206
	78.58	1.555728	**1.701477**	1.401905	1.199123	1.082277
	68.50	1.289120	1.401905	**1.628176**	1.375759	1.226725
	62.96	1.116744	1.199123	1.375759	**1.634536**	1.431743
	61.68	1.006206	1.082277	1.226725	1.431743	**1.793075**
	93.04	**1.989364**	1.558772	1.275412	1.104869	0.995506
cyl2	**79.58**	1.558772	**1.744966**	1.419745	1.214383	1.096050
	68.50	1.275412	1.419745	**1.628176**	1.375759	1.226725
	62.96	1.104869	1.214383	1.375759	**1.634536**	1.431743
	61.68	0.995506	1.096050	1.226725	1.431743	**1.793075**
	93.04	**1.989364**	1.539185	1.294031	1.104869	0.995506
	78.58	1.539185	**1.701477**	1.422370	1.199123	1.082277
cyl3	**69.50**	1.294031	1.422370	**1.675915**	1.395843	1.244633
	62.96	1.104869	1.199123	1.395843	**1.634536**	1.431743
	61.68	0.995506	1.082277	1.244633	1.431743	**1.793075**
	93.04	**1.989364**	1.539185	1.275412	1.122418	0.995506
	78.58	1.539185	**1.701477**	1.401905	1.218170	1.082277
	68.50	1.275412	1.401905	**1.628176**	1.397610	1.226725
cyl4	**63.96**	1.122418	1.218170	1.397611	**1.686714**	1.454484
	61.68	0.995506	1.082277	1.226725	1.454484	**1.793075**
	93.04	**1.989364**	1.539185	1.275412	1.104869	1.011646
	78.58	1.539185	**1.701477**	1.401905	1.199123	1.099824
	68.50	1.275412	1.401905	**1.628176**	1.375759	1.246614
	62.96	1.104869	1.199123	1.375759	**1.634536**	1.454956
cyl5	**62.68**	1.011646	1.099824	1.246614	1.454956	**1.851603**

N+1.5

cyl1	**94.54**	**2.053855**	1.564000	1.295974	1.122682	1.011555
	78.58	1.564000	**1.701477**	1.401905	1.199123	1.082277
	68.50	1.295974	1.401905	**1.628176**	1.375759	1.226725
	62.96	1.122682	1.199123	1.375759	**1.634536**	1.431743
	61.68	1.011555	1.082277	1.226725	1.431743	**1.793075**
	93.04	**1.989364**	1.568566	1.275412	1.104869	0.995506

cyl2	**80.08**	1.568566	**1.766917**	1.428665	1.222013	1.102937
	68.50	1.275412	1.428665	**1.628176**	1.375759	1.226725
	62.96	1.104869	1.222013	1.375759	**1.634536**	1.431743
	61.68	0.995506	1.102937	1.226725	1.431743	**1.793075**
	93.04	**1.989364**	1.539185	1.303340	1.104869	0.995506
	78.58	1.539185	**1.701477**	1.432603	1.199123	1.082277
cyl3	**70.00**	1.303340	1.432603	**1.700045**	1.405885	1.253587
	62.96	1.104869	1.199123	1.405885	**1.634536**	1.431743
	61.68	0.995506	1.082277	1.253587	1.431743	**1.793075**
	93.04	**1.989364**	1.539185	1.275412	1.131193	0.995506
	78.58	1.539185	**1.701477**	1.401905	1.227693	1.082277
	68.50	1.275412	1.401905	**1.628176**	1.408536	1.226725
cyl4	**64.46**	1.131193	1.227693	1.408536	**1.713114**	1.465854
	61.68	0.995506	1.082277	1.226725	1.465854	**1.793075**
	93.04	**1.989364**	1.539185	1.275412	1.104869	1.019716
	78.58	1.539185	**1.701477**	1.401905	1.199123	1.108598
	68.50	1.275412	1.401905	**1.628176**	1.375759	1.256558
	62.96	1.104869	1.199123	1.375759	**1.634536**	1.466562
cyl5	**63.18**	1.019716	1.108598	1.256558	1.466562	**1.881221**
	N+2					
cyl1	**95.04**	**2.075582**	1.572272	1.302828	1.128619	1.016905
	78.58	1.572272	**1.701477**	1.401905	1.199123	1.082277
	68.50	1.302828	1.401905	**1.628176**	1.375759	1.226725
	62.96	1.128619	1.199123	1.375759	**1.634536**	1.431743
	61.68	1.016905	1.082277	1.226725	1.431743	**1.793075**
	93.04	**1.989364**	1.578360	1.275412	1.104869	0.995506
cyl2	**80.58**	1.578360	**1.789007**	1.437585	1.229643	1.109823
	68.50	1.275412	1.437585	**1.628176**	1.375759	1.226725
	62.96	1.104869	1.229643	1.375759	**1.634536**	1.431743
	61.68	0.995506	1.109823	1.226725	1.431743	**1.793075**
	93.04	**1.989364**	1.539185	1.312650	1.104869	0.995506
	78.58	1.539185	**1.701477**	1.442836	1.199123	1.082277
cyl3	**70.50**	1.312650	1.442836	**1.724350**	1.415927	1.262542
	62.96	1.104869	1.199123	1.415927	**1.634536**	1.431743
	61.68	0.995506	1.082277	1.262542	1.431743	**1.793075**
	93.04	**1.989364**	1.539185	1.275412	1.139967	0.995506
	78.58	1.539185	**1.701477**	1.401905	1.237216	1.082277
	68.50	1.275412	1.401905	**1.628176**	1.419462	1.226725

cyl4	**64.96**	1.139968	1.237216	1.419462	**1.739720**	1.477225
	61.68	0.995506	1.082277	1.226725	1.477225	**1.793075**
	93.04	**1.989364**	1.539185	1.275412	1.104869	1.027786
	78.58	1.539185	**1.701477**	1.401905	1.199123	1.117372
	68.50	1.275412	1.401905	**1.628176**	1.375759	1.266503
	62.96	1.104869	1.199123	1.375759	**1.634536**	1.478169
cyl5	**63.68**	1.027786	1.117372	1.266503	1.478169	**1.911075**

N+2.5

cyl1	**95.54**	**2.097425**	1.580543	1.309682	1.134557	1.022255
	78.58	1.580543	**1.701477**	1.401905	1.199123	1.082277
	68.50	1.309682	1.401905	**1.628176**	1.375759	1.226725
	62.96	1.134557	1.199123	1.375759	**1.634536**	1.431743
	61.68	1.022255	1.082277	1.226725	1.431743	**1.793075**
	93.04	**1.989364**	1.588154	1.275412	1.104869	0.995506
cyl2	**81.08**	1.588154	**1.811235**	1.446506	1.237273	1.116710
	68.50	1.275412	1.446506	**1.628176**	1.375759	1.226725
	62.96	1.104869	1.237273	1.375759	**1.634536**	1.431743
	61.68	0.995506	1.116710	1.226725	1.431743	**1.793075**
	93.04	**1.989364**	1.539185	1.321959	1.104869	0.995506
	78.58	1.539185	**1.701477**	1.453069	1.199123	1.082277
cyl3	**71.00**	1.321959	1.453069	**1.748828**	1.425969	1.271496
	62.96	1.104869	1.199123	1.425969	**1.634536**	1.431743
	61.68	0.995506	1.082277	1.271496	1.431743	**1.793075**
	93.04	**1.989364**	1.539185	1.275412	1.148742	0.995506
	78.58	1.539185	**1.701477**	1.401905	1.246739	1.082277
	68.50	1.275412	1.401905	**1.628176**	1.430388	1.226725
cyl4	**65.46**	1.148742	1.246739	1.430388	**1.766533**	1.488595
	61.68	0.995506	1.082277	1.226725	1.488595	**1.793075**
	93.04	**1.989364**	1.539185	1.275412	1.104869	1.035856
	78.58	1.539185	**1.701477**	1.401905	1.199123	1.126145
	68.50	1.275412	1.401905	**1.628176**	1.375759	1.276447
	62.96	1.104869	1.199123	1.375759	**1.634536**	1.489775
cyl5	**64.18**	1.035856	1.126145	1.276447	1.489775	**1.941165**

N- 0.5

cyl1	**92.54**	**1.968098**	1.530913	1.268558	1.098931	0.990156
	78.58	1.530913	**1.701477**	1.401905	1.199123	1.082277
	68.50	1.268558	1.401905	**1.628176**	1.375759	1.226725
	62.96	1.098931	1.199123	1.375759	**1.634536**	1.431743

	61.68	0.990156	1.082277	1.226725	1.431743	**1.793075**
	93.04	**1.989364**	1.529391	1.275412	1.104869	0.995506
cyl2	**78.08**	1.529391	**1.679940**	1.392984	1.191493	1.075391
	68.50	1.275412	1.392984	**1.628176**	1.375759	1.226725
	62.96	1.104869	1.191493	1.375759	**1.634536**	1.431743
	61.68	0.995506	1.075391	1.226725	1.431743	**1.793075**
	93.04	**1.989364**	1.539185	1.266102	1.104869	0.995506
	78.58	1.539185	**1.701477**	1.391672	1.199123	1.082277
cyl3	**68.00**	1.266102	1.391672	**1.604568**	1.365717	1.217771
	62.96	1.104869	1.199123	1.365717	**1.634536**	1.431743
	61.68	0.995506	1.082277	1.217771	1.431743	**1.793075**
	93.04	**1.989364**	1.539185	1.275412	1.096094	0.995506
	78.58	1.539185	**1.701477**	1.401905	1.189600	1.082277
	68.50	1.275412	1.401905	**1.628176**	1.364833	1.226725
cyl4	**62.46**	1.096094	1.189600	1.364833	**1.608757**	1.420372
	61.68	0.995506	1.082277	1.226725	1.420372	**1.793075**
	93.04	**1.989364**	1.539185	1.275412	1.104869	0.987436
	78.58	1.539185	**1.701477**	1.401905	1.199123	1.073504
	68.50	1.275412	1.401905	**1.628176**	1.375759	1.216780
	62.96	1.104869	1.199123	1.375759	**1.634536**	1.420136
cyl5	**61.18**	0.987436	1.073504	1.216780	1.420136	**1.764165**

N-1

cyl1	**92.04**	**1.946947**	1.522642	1.261703	1.092994	0.984806
	78.58	1.522642	**1.701477**	1.401905	1.199123	1.082277
	68.50	1.261703	1.401905	**1.628176**	1.375759	1.226725
	62.96	1.092994	1.199123	1.375759	**1.634536**	1.431743
	61.68	0.984806	1.082277	1.226725	1.431743	**1.793075**
	93.04	**1.989364**	1.519597	1.275412	1.104869	0.995506
cyl2	**77.58**	1.519597	**1.658541**	1.384064	1.183863	1.068505
	68.50	1.275412	1.384064	**1.628176**	1.375759	1.226725
	62.96	1.104869	1.183863	1.375759	**1.634536**	1.431743
	61.68	0.995506	1.068505	1.226725	1.431743	**1.793075**
	93.04	**1.989364**	1.539185	1.256792	1.104869	0.995506
	78.58	1.539185	**1.701477**	1.381439	1.199123	1.082277
cyl3	**67.50**	1.256792	1.381439	**1.581133**	1.355674	1.208816
	62.96	1.104869	1.199123	1.355675	**1.634536**	1.431743
	61.68	0.995506	1.082277	1.208816	1.431743	**1.793075**
	93.04	**1.989364**	1.539185	1.275412	1.087320	0.995506

	78.58	1.539185	**1.701477**	1.401905	1.180077	1.082277
	68.50	1.275412	1.401905	**1.628176**	1.353907	1.226725
cyl4	**61.96**	1.087320	1.180077	1.353907	**1.583185**	1.409002
	61.68	0.995506	1.082277	1.226725	1.409001	**1.793075**
	93.04	**1.989364**	1.539185	1.275412	1.104869	0.979366
	78.58	1.539185	**1.701477**	1.401905	1.199123	1.064730
	68.50	1.275412	1.401905	**1.628176**	1.375759	1.206836
	62.96	1.104869	1.199123	1.375759	**1.634536**	1.408530
cyl5	**60.68**	0.979366	1.064730	1.206836	1.408530	**1.735491**

N-1.5

cyl1	**91.54**	**1.925910**	1.514370	1.254849	1.087056	0.979456
	78.58	1.514370	**1.701477**	1.401905	1.199123	1.082277
	68.50	1.254849	1.401905	**1.628176**	1.375759	1.226725
	62.96	1.087056	1.199123	1.375759	**1.634536**	1.431743
	61.68	0.979456	1.082277	1.226725	1.431743	**1.793075**
	93.04	**1.989364**	1.509804	1.275412	1.104869	0.995506
cyl2	**77.08**	1.509804	**1.637279**	1.375144	1.176233	1.061618
	68.50	1.275412	1.375144	**1.628176**	1.375759	1.226725
	62.96	1.104869	1.176234	1.375759	**1.634536**	1.431743
	61.68	0.995506	1.061618	1.226725	1.431743	**1.793075**
	93.04	**1.989364**	1.539185	1.247483	1.104869	0.995506
	78.58	1.539185	**1.701477**	1.371206	1.199123	1.082277
cyl3	**67.00**	1.247483	1.371206	**1.557873**	1.345632	1.199862
	62.96	1.104869	1.199123	1.345633	**1.634536**	1.431743
	61.68	0.995506	1.082277	1.199862	1.431743	**1.793075**
	93.04	**1.989364**	1.539185	1.275412	1.078545	0.995506
	78.58	1.539185	**1.701477**	1.401905	1.170554	1.082277
	68.50	1.275412	1.401905	**1.628176**	1.342981	1.226725
cyl4	**61.46**	1.078545	1.170554	1.342981	**1.557819**	1.397631
	61.68	0.995506	1.082277	1.226725	1.397631	**1.793075**
	93.04	**1.989364**	1.539185	1.275412	1.104869	0.971295
	78.58	1.539185	**1.701477**	1.401905	1.199123	1.055957
	68.50	1.275412	1.401905	**1.628176**	1.375759	1.196891
	62.96	1.104869	1.199123	1.375759	**1.634536**	1.396923
cyl5	**60.18**	0.971295	1.055957	1.196891	1.396923	**1.707053**

N-2

cyl1	**91.04**	**1.904990**	1.506098	1.247995	1.081119	0.974106
	78.58	1.506098	**1.701477**	1.401905	1.199123	1.082277

	68.50	1.247995	1.401905	**1.628176**	1.375759	1.226725
	62.96	1.081119	1.199123	1.375759	**1.634536**	1.431743
	61.68	0.974106	1.082277	1.226725	1.431743	**1.793075**
	93.04	**1.989364**	1.500010	1.275412	1.104869	0.995506
cyl2	**76.58**	1.500010	**1.616156**	1.366224	1.168604	1.054732
	68.50	1.275412	1.366224	**1.628176**	1.375759	1.226725
	62.96	1.104869	1.168604	1.375759	**1.634536**	1.431743
	61.68	0.995506	1.054732	1.226725	1.431743	**1.793075**
	93.04	**1.989364**	1.539185	1.238173	1.104869	0.995506
	78.58	1.539185	**1.701477**	1.360973	1.199123	1.082277
cyl3	**66.50**	1.238173	1.360973	**1.534787**	1.335590	1.190908
	62.96	1.104869	1.199123	1.335590	**1.634536**	1.431743
	61.68	0.995506	1.082277	1.190908	1.431743	**1.793075**
	93.04	**1.989364**	1.539185	1.275412	1.069771	0.995506
	78.58	1.539185	**1.701477**	1.401905	1.161031	1.082277
	68.50	1.275412	1.401905	**1.628176**	1.332055	1.226725
cyl4	**60.96**	1.069771	1.161031	1.332055	**1.532661**	1.386260
	61.68	0.995506	1.082277	1.226725	1.386260	**1.793075**
	93.04	**1.989364**	1.539185	1.275412	1.104869	0.963225
	78.58	1.539185	**1.701477**	1.401905	1.199123	1.047183
	68.50	1.275412	1.401905	**1.628176**	1.375759	1.186947
	62.96	1.104869	1.199123	1.375759	**1.634536**	1.385317
cyl5	**59.68**	0.963225	1.047183	1.186947	1.385317	**1.678851**
	N-2,5					
cyl1	**90.54**	**1.884184**	1.497827	1.241141	1.075181	0.968756
	78.58	1.497827	**1.701477**	1.401905	1.199123	1.082277
	68.50	1.241141	1.401905	**1.628176**	1.375759	1.226725
	62.96	1.075181	1.199123	1.375759	**1.634536**	1.431743
	61.68	0.968756	1.082277	1.226725	1.431743	**1.793075**
	93.04	**1.989364**	1.490216	1.275412	1.104869	0.995506
cyl2	**76.08**	1.490216	**1.595171**	1.357303	1.160974	1.047845
	68.50	1.275412	1.357303	**1.628176**	1.375759	1.226725
	62.96	1.104869	1.160974	1.375759	**1.634536**	1.431743
	61.68	0.995506	1.047845	1.226725	1.431743	**1.793075**
	93.04	**1.989364**	1.539185	1.228864	1.104869	0.995506
	78.58	1.539185	**1.701477**	1.350740	1.199123	1.082277
cyl3	**66.00**	1.228864	1.350740	**1.511875**	1.325548	1.181954
	62.96	1.104869	1.199123	1.325548	**1.634536**	1.431743
	61.68	0.995506	1.082277	1.181954	1.431743	**1.793075**

	93.04	**1.989364**	1.539185	1.275412	1.060996	0.995506
	78.58	1.539185	**1.701477**	1.401905	1.151508	1.082277
	68.50	1.275412	1.401905	**1.628176**	1.321129	1.226725
cyl4	**60.46**	1.060996	1.151508	1.321129	**1.507709**	1.374890
	61.68	0.995506	1.082277	1.226725	1.374890	**1.793075**
	93.04	**1.989364**	1.539185	1.275412	1.104869	0.955155
	78.58	1.539185	**1.701477**	1.401905	1.199123	1.038410
	68.50	1.275412	1.401905	**1.628176**	1.375759	1.177002
	62.96	1.104869	1.199123	1.375759	**1.634536**	1.373710
cyl5	**59.18**	0.955155	1.038410	1.177002	1.373710	**1.650885**

	Turns		**Impedances**				
	93.28	**1.999750**	1.539595	1.274803	1.107697	1.005793	
	78.40	1.539595	**1.693535**	1.394310	1.196251	1.088057	
	68.29	1.274803	1.394310	**1.618183**	1.371443	1.232359	
	62.95	1.107697	1.196251	1.371443	**1.634360**	1.442689	**Zreactor**
	62.15	1.005793	1.088057	1.232359	1.442689	**1.820752**	**1.3624**
			current(I/A)			**P=Rac*I^2**	
	N	**(Dwight)**		**Rac/cyl.**	**Rac/cyl.**	**Losses/W**	
	93.04		**97.6101**	0.1033664	0.103366	984.85	
	78.58		**88.3334**	0.0787975	0.078797	614.84	
	68.50		**70.2378**	0.0905871	0.090587	446.90	
	62.96	**Zreactor**	**92.1132**	0.0756181	0.075618	641.61	
	61.68	**1.359800**	**138.7756**	0.0690943	0.069094	1330.66	
						4018.85	

Changed N+0.5

			Currents/A	**Diff./A**	**Losses/W**	**Diff./W**
cyl1	**93.54**		91.4103	-6.1998	863.71	-121.1
	78.58		93.7849	5.452	693.07	78.2
	68.50		70.3288	0.091	448.06	1.2
	62.96		92.4876	0.374	646.83	5.2
	61.68	**1.362700**	139.0584	0.283	1336.09	5.4
					3987.77	**-31.1**
	93.04		104.06	6.4498	1119.30	134.5
cyl2	**79.08**		74.02	-14.309	431.77	-183.1
	68.50		77.50	7.262	544.09	97.2

	62.96		92.19	0.080	642.73	1.1
	61.68	**1.363200**	139.29	0.517	1340.60	9.9
					4078.49	**59.6**
	93.04		97.72	0.108	987.03	2.2
	78.58		96.64	8.309	735.95	121.1
cyl3	**69.00**		53.05	-17.193	254.89	-192.0
	62.96		100.43	8.319	762.73	121.1
	61.68	**1.363700**	139.23	0.457	1339.44	8.8
					4080.04	**61.2**
	93.04		98.15	0.537	995.71	10.9
	78.58		88.43	0.092	616.12	1.3
	68.50		79.29	9.056	569.56	122.7
cyl4	**63.46**		73.96	-18.158	413.58	-228.0
	61.68	**1.364100**	147.25	8.473	1498.11	167.5
					4093.09	**74.2**
	93.04		98.04	0.428	993.50	8.7
	78.58		89.01	0.674	624.25	9.4
	68.50		70.77	0.536	453.75	6.8
	62.96		100.80	8.689	768.36	126.8
cyl5	**62.18**	**1.364200**	128.45	-10.327	1140.00	-190.7
					3979.86	**-39.0**
	N+1					
cyl1	**94.04**		85.30	-12.312	752.06	-232.8
	78.58		99.19	10.860	775.31	160.5
	68.50		70.41	0.172	449.09	2.2
	62.96		92.85	0.735	651.88	10.3
	61.68	**1.365600**	139.32	0.546	1341.15	10.5
					3969.50	**-49.4**
	93.04		110.41	12.804	1260.17	275.3
cyl2	**79.58**		59.99	-28.346	283.55	-331.3
	68.50		84.67	14.435	649.45	202.6
	62.96		92.24	0.127	643.38	1.8
	61.68	**1.366700**	139.76	0.981	1349.53	18.9
					4186.09	**167.2**
	93.04		97.77	0.163	988.14	3.3
	78.58		104.82	16.484	865.73	250.9
cyl3	**69.50**		36.25	-33.986	119.05	-327.8
	62.96		108.61	16.499	892.03	250.4
	61.68	**1.367700**	139.62	0.840	1346.82	16.2
					4211.77	**192.9**
	93.04		98.62	1.009	1005.32	20.5
	78.58		88.47	0.137	616.74	1.9
	68.50		88.21	17.972	704.86	258.0
cyl4	**63.96**		56.22	-35.894	239.00	-402.6
	61.68	**1.368400**	155.55	16.775	1671.81	341.1
					4237.74	**218.9**

	93.04		98.43	0.818	1001.41	16.6
	78.58		89.65	1.317	633.32	18.5
	68.50		71.28	1.045	460.30	13.4
	62.96		109.39	17.282	904.94	263.3
cyl5	**62.68**	**1.368600**	118.31	-20.462	967.19	-363.5
					3967.16	**-51.7**
	N+1.5					
cyl1	**94.54**		79.28	-18.334	649.63	-335.2
	78.58		104.55	16.219	861.35	246.5
	68.50		70.48	0.244	450.00	3.1
	62.96		93.19	1.081	656.76	15.1
	61.68	**1.368500**	139.57	0.790	1345.85	15.2
					3963.60	**-55.3**
	93.04		116.67	19.062	1407.07	422.2
cyl2	**80.08**		46.23	-42.106	168.39	-446.5
	68.50		91.75	21.512	762.56	315.7
	62.96		92.25	0.141	643.57	2.0
	61.68	**1.370100**	140.17	1.391	1357.47	26.8
					4339.06	**320.2**
	93.04		97.78	0.170	988.29	3.4
	78.58		112.85	24.514	1003.45	388.6
cyl3	**70.00**		19.87	-50.367	35.77	-411.1
	62.96		116.64	24.531	1028.84	387.2
	61.68	**1.371600**	139.93	1.152	1352.84	22.2
					4409.19	**390.3**
	93.04		99.0324	1.422	1013.76	28.9
	78.58		88.4658	0.132	616.68	1.8
	68.50		96.9764	26.739	851.92	405.0
cyl4	**64.46**		38.9226	-53.191	114.56	-527.0
	61.68	**1.372700**	163.6729	24.897	1850.95	520.3
					4447.87	**429.0**
	93.04		98.7834	1.173	1008.67	23.8
	78.58		90.2614	1.928	641.97	27.1
	68.50		71.7657	1.528	466.55	19.7
	62.96		117.8846	25.771	1050.85	409.2
cyl5	**63.18**	**1.373000**	108.3749	-30.401	811.52	-519.1
					3979.56	**-39.3**
	N+2					
cyl1	**95.04**		73.3471	-24.263	556.09	-428.8
	78.58		109.8619	21.529	951.06	336.2
	68.50		70.5438	0.306	450.80	3.9
	62.96		93.5266	1.413	661.45	19.8
	61.68	**1.371300**	139.7905	1.015	1350.20	19.5
					3969.59	**-49.3**
	93.04		122.8293	25.219	1559.49	574.6

cyl2	**80.58**		32.7531	-55.580	84.53	-530.3
	68.50		98.7267	28.489	882.95	436.1
	62.96		92.2364	0.123	643.32	1.7
	61.68	**1.373500**	140.5245	1.749	1364.41	33.8
					4534.71	**515.9**
	93.04		97.7420	0.132	987.51	2.7
	78.58		120.7234	32.390	1148.41	533.6
cyl3	**70.50**		3.9147	-66.323	1.39	-445.5
	62.96		124.5204	32.407	1172.48	530.9
	61.68	**1.375500**	140.1695	1.394	1357.53	26.9
					4667.32	**648.5**
	93.04		99.3874	1.777	1021.04	36.2
	78.58		88.4144	0.081	615.97	1.1
	68.50		105.5820	35.344	1009.82	562.9
cyl4	**64.96**		22.0797	-70.033	36.86	-604.7
	61.68	**1.376900**	171.6065	32.831	2034.74	704.1
					4718.44	**699.6**
	93.04		99.1063	1.496	1015.27	30.4
	78.58		90.8394	2.506	650.22	35.4
	68.50		72.2225	1.985	472.51	25.6
	62.96		126.2657	34.153	1205.58	564.0
cyl5	**63.68**	**1.377300**	98.6361	-40.139	672.22	-658.4
					4015.81	**-3.0**
	N+2.5					
cyl1	**95.54**		67.5102	-30.100	471.11	-513.7
	78.58		115.1202	26.787	1044.28	429.4
	68.50		70.5973	0.360	451.48	4.6
	62.96		93.8453	1.732	665.96	24.4
	61.68	**1.374200**	139.9970	1.221	1354.19	23.5
					3987.02	**-31.8**
	93.04		128.8812	31.271	1716.95	732.1
cyl2	**81.08**		19.5703	-68.763	30.18	-584.7
	68.50		105.5982	35.360	1010.13	563.2
	62.96		92.1882	0.075	642.65	1.0
	61.68	**1.376900**	140.8321	2.057	1370.39	39.7
					4770.31	**751.5**
	93.04		97.6596	0.050	985.85	1.0
	78.58		128.4390	40.106	1299.89	685.0
cyl3	**71.00**		-11.6082	-81.846	12.21	-434.7
	62.96		132.2348	40.122	1322.26	680.7
	61.68	**1.379400**	140.3448	1.569	1360.93	30.3
					4981.13	**962.3**
	93.04		99.6863	2.076	1027.19	42.3
	78.58		88.3180	-0.015	614.63	-0.2
	68.50		114.0174	43.780	1177.63	730.7
cyl4	**65.46**		5.7034	-86.410	2.46	-639.1

	61.68	**1.381100**	179.3450	40.569	2222.39	891.7
					5044.29	**1025.4**
	93.04		99.3969	1.787	1021.23	36.4
	78.58		91.3854	3.052	658.06	43.2
	68.50		72.6539	2.416	478.17	31.3
	62.96		134.5329	42.420	1368.62	727.0
cyl5	**64.18**	**1.381600**	89.1009	-49.675	548.54	-782.1
					4074.62	**55.8**
	N- 0.5					
cyl1	**92.54**		103.9070	6.297	1116.01	131.2
	78.58		82.8288	-5.505	540.60	-74.2
	68.50		70.1377	-0.100	445.62	-1.3
	62.96		91.7239	-0.389	636.20	-5.4
	61.68	**1.356900**	138.4726	-0.303	1324.86	-5.8
					4063.29	**44.4**
	93.04		91.0810	-6.529	857.50	-127.3
cyl2	**78.08**		102.8945	14.561	834.25	219.4
	68.50		62.8938	-7.344	358.33	-88.6
	62.96		91.9979	-0.115	640.00	-1.6
	61.68	**1.356300**	138.2027	-0.573	1319.70	-11.0
					4009.78	**-9.1**
	93.04		97.4581	-0.152	981.78	-3.1
	78.58		79.8895	-8.444	502.91	-111.9
cyl3	**68.00**		87.8150	17.577	698.56	251.7
	62.96		83.6646	-8.449	529.31	-112.3
	61.68	**1.355800**	138.2428	-0.533	1320.47	-10.2
					4033.03	**14.2**
	93.04		97.0180	-0.592	972.94	-11.9
	78.58		88.1812	-0.152	612.72	-2.1
	68.50		61.0570	-9.181	337.70	-109.2
cyl4	**62.46**		110.6721	18.559	926.19	284.6
	61.68	**1.355400**	130.1417	-8.634	1170.24	-160.4
					4019.80	**0.9**
	93.04		97.1541	-0.456	975.67	-9.2
	78.58		87.6184	-0.715	604.93	-9.9
	68.50		69.6754	-0.562	439.77	-7.1
	62.96		83.3340	-8.779	525.13	-116.5
cyl5	**61.18**	**1.355300**	149.2881	10.513	1539.90	209.2
					4085.40	**66.5**
	N-1					
cyl1	**92.04**		110.2894	12.679	1257.32	272.5
	78.58		77.2838	-11.050	470.64	-144.2
	68.50		70.0273	-0.210	444.22	-2.7
	62.96		91.3202	-0.793	630.61	-11.0
	61.68	**1.353900**	138.1493	-0.626	1318.68	-12.0

					4121.47	**102.6**
	93.04		84.4677	-13.142	737.50	-247.3
cyl2	**77.58**		117.7076	29.374	1091.75	476.9
	68.50		55.4738	-14.764	278.77	-168.1
	62.96		91.8473	-0.266	637.91	-3.7
	61.68	**1.352900**	137.5736	-1.202	1307.71	-23.0
					4053.63	**34.8**
	93.04		97.2499	-0.360	977.59	-7.3
	78.58		71.3324	-17.001	400.95	-213.9
cyl3	**67.50**		105.7581	35.520	1013.20	566.3
	62.96		75.0971	-17.016	426.45	-215.2
	61.68	**1.351800**	137.6326	-1.143	1308.83	-21.8
					4127.02	**108.2**
	93.04		96.3588	-1.251	959.76	-25.1
	78.58		87.9783	-0.355	609.91	-4.9
	68.50		51.7641	-18.474	242.73	-204.2
cyl4	**61.96**		129.6100	37.497	1270.29	628.7
	61.68	**1.351100**	121.3588	-17.417	1017.62	-313.0
					4100.30	**81.4**
	93.04		96.6585	-0.952	965.74	-19.1
	78.58		86.8729	-1.460	594.68	-20.2
	68.50		69.0854	-1.152	432.35	-14.5
	62.96		74.4725	-17.641	419.39	-222.2
cyl5	**60.68**	**1.350900**	159.9807	21.205	1768.39	437.7
					4180.54	**161.7**
	N-1.5					
cyl1	**91.54**		116.7600	19.150	1409.18	424.3
	78.58		71.6965	-16.637	405.05	-209.8
	68.50		69.9066	-0.331	442.69	-4.2
	62.96		90.9017	-1.211	624.84	-16.8
	61.68	**1.351000**	137.8053	-0.970	1312.12	-18.5
					4193.89	**175.0**
	93.04		77.7800	-19.830	625.34	-359.5
cyl2	**77.08**		132.7572	44.424	1388.76	773.9
	68.50		47.9854	-22.252	208.59	-238.3
	62.96		91.6601	-0.453	635.31	-6.3
	61.68	**1.349400**	136.8873	-1.888	1294.70	-36.0
					4152.70	**133.8**
	93.04		96.9874	-0.623	972.32	-12.5
	78.58		62.6699	-25.663	309.48	-305.4
cyl3	**67.00**		124.0475	53.810	1393.93	947.0
	62.96		66.4221	-25.691	333.62	-308.0
	61.68	**1.347800**	136.9432	-1.832	1295.75	-34.9
					4305.11	**286.3**
	93.04		95.6353	-1.975	945.40	-39.4
	78.58		87.7193	-0.614	606.32	-8.5

	68.50		42.3746	-27.863	162.66	-284.2
cyl4	**61.46**		148.9011	56.788	1676.57	1035.0
	61.68	**1.346700**	112.4397	-26.336	873.54	-457.1
					4264.49	**245.6**
	93.04		96.1263	-1.484	955.13	-29.7
	78.58		86.0927	-2.241	584.04	-30.8
	68.50		68.4680	-1.770	424.66	-22.2
	62.96		65.5365	-26.577	324.78	-316.8
cyl5	**60.18**	**1.346400**	170.8464	32.071	2016.76	686.1
					4305.38	**286.5**
	N-2					
cyl1	**91.04**		123.3174	25.707	1571.91	587.1
	78.58		66.0686	-22.265	343.96	-270.9
	68.50		69.7755	-0.462	441.03	-5.9
	62.96		90.4682	-1.645	618.90	-22.7
	61.68	**1.348100**	137.4402	-1.335	1305.18	-25.5
					4280.97	**262.1**
	93.04		71.0244	-26.586	521.43	-463.4
cyl2	**76.58**		148.0301	59.697	1726.68	1111.8
	68.50		40.4366	-29.801	148.12	-298.8
	62.96		91.4358	-0.677	632.21	-9.4
	61.68	**1.345900**	136.1432	-2.632	1280.66	-50.0
					4309.10	**290.2**
	93.04		96.6694	-0.941	965.96	-18.9
	78.58		53.9143	-34.419	229.04	-385.8
cyl3	**66.50**		142.6611	72.423	1843.64	1396.7
	62.96		57.6520	-34.461	251.34	-390.3
	61.68	**1.343800**	136.1732	-2.602	1281.22	-49.4
					4571.21	**552.4**
	93.04		94.8466	-2.763	929.87	-55.0
	78.58		87.4030	-0.930	601.96	-12.9
	68.50		32.9049	-37.333	98.08	-348.8
cyl4	**60.96**		168.5171	76.404	2147.40	1505.8
	61.68	**1.342300**	103.3983	-35.377	738.70	-592.0
					4516.01	**497.2**
	93.04		95.5569	-2.053	943.85	-41.0
	78.58		85.2778	-3.056	573.04	-41.8
	68.50		67.8229	-2.415	416.70	-30.2
	62.96		56.5344	-35.579	241.69	-399.9
cyl5	**59.68**	**1.341800**	181.8779	43.102	2285.61	954.9
					4460.88	**442.0**
	N-2,5					
cyl1	**90.54**		129.9606	32.351	1745.83	761.0
	78.58		60.4022	-27.931	287.49	-327.4
	68.50		69.6339	-0.604	439.25	-7.7

	62.96		90.0196	-2.094	612.77	-28.8
	61.68	**1.345100**	137.0537	-1.722	1297.85	-32.8
					4383.19	**364.3**
	93.04		64.2080	-33.402	426.15	-558.7
cyl2	**76.08**		163.5126	75.179	2106.76	1491.9
	68.50		32.8355	-37.402	97.67	-349.2
	62.96		91.1734	-0.940	628.58	-13.0
	61.68	**1.342400**	135.3405	-3.435	1265.60	-65.1
					4524.76	**505.9**
	93.04		96.2946	-1.315	958.48	-26.4
	78.58		45.0792	-43.254	160.13	-454.7
cyl3	**66.00**		161.5747	91.337	2364.90	1918.0
	62.96		48.8001	-43.313	180.08	-461.5
	61.68	**1.339700**	135.3215	-3.454	1265.25	-65.4
					4928.84	**910.0**
	93.04		93.9925	-3.618	913.20	-71.6
	78.58		87.0280	-1.305	596.80	-18.0
	68.50		23.3724	-46.865	49.48	-397.4
cyl4	**60.46**		188.4273	96.314	2684.81	2043.2
	61.68	**1.337900**	94.2498	-44.526	613.77	-716.9
					4858.06	**839.2**
	93.04		94.9498	-2.660	931.90	-53.0
	78.58		84.4280	-3.905	561.68	-53.2
	68.50		67.1502	-3.088	408.47	-38.4
	62.96		47.4751	-44.638	170.43	-471.2
cyl5	**59.18**	**1.337300**	193.0669	54.291	2575.48	1244.8
					4647.95	**629.1**

Changed turns (+/-)	
N1	0.50
N2	1.00
N3	1.50
N4	2.00
N5	2.50

Current changes when the turns have been changed

More Turns

Δ**I**

	N1	**N2**	**N3**	**N4**	**N5**
cyl1	-6.19977	-12.31237	-18.33367	-24.26297	-30.09987
cyl2	-14.30950	-28.34640	-42.10590	-55.58030	-68.76310
cyl3	-17.19259	-33.98599	-50.36669	-66.32309	-81.84599
cyl4	-18.15787	-35.89377	-53.19057	-70.03347	-

					86.40977
cyl5	-10.32658	-20.46168	-30.40068	-40.13948	-49.67468

Less turns

∆I

	N1	**N2**	**N3**	**N4**	**N5**
cyl1	6.29693	12.67933	19.14993	25.70733	32.35053
cyl2	14.56110	29.37420	44.42380	59.69670	75.17920
cyl3	17.57721	35.52031	53.80971	72.42331	91.33691
cyl4	18.55893	37.49683	56.78793	76.40393	96.31413
cyl5	10.51252	21.20512	32.07082	43.10232	54.29132

Jacobian-matrix

:

J1=∂I/∂N **More turns**

cyl1	-12.3995	-24.6247	-36.6673	-48.5259	64.7011
cyl2	-14.3095	-28.3464	-42.1059	-55.5803	75.1792
cyl3	-11.4617	-22.6573	-33.5778	-44.2154	60.8913
cyl4	-9.0789	-17.9469	-26.5953	-35.0167	48.1571
cyl5	-4.1306	-8.1847	-12.1603	-16.0558	21.7165

J2=∂I/(-∂N) **Less turns**

cyl1	-12.5939	-25.3587	-38.2999	-51.4147	-64.7011
cyl2	-14.5611	-29.3742	-44.4238	-59.6967	-75.1792
cyl3	-11.7181	-23.6802	-35.8731	-48.2822	-60.8913
cyl4	-9.2795	-18.7484	-28.3940	-38.2020	-48.1571
cyl5	-4.2050	-8.4820	-12.8283	-17.2409	-21.7165

test reactor (I/N)

1.05
1.12
1.03
1.46
2.25

Calculated value (I/N)
More turns

0.9772	0.9070	0.8385	0.7717	0.7066
0.9361	0.7538	0.5773	0.4065	0.2414
0.7688	0.5216	0.2839	0.0555	-0.1635
1.1654	0.8790	0.6038	0.3399	0.0871
1.6011	1.8876	1.7154	1.5490	1.3883

DN=(inv(J1))*(DI)

DN =

1.0e+005 *

0.5406	1.0905	1.6493	2.2165	2.7917
-1.5552	-3.1367	-4.7436	-6.3746	-8.0285
1.4465	2.9173	4.4116	5.9283	7.4663
-0.4496	-0.9067	-1.3710	-1.8424	-2.3204
-0.0057	-0.0115	-0.0175	-0.0235	-0.0295

DN=(inv(J2))*(DI)

DN =

1.0e+006 *

0.0381	0.0768	0.1161	0.1559	0.1964
-0.1751	-0.3532	-0.5341	-0.7177	-0.9038
0.2746	0.5538	0.8375	1.1254	1.4173
-0.1881	-0.3794	-0.5738	-0.7711	-0.9712
0.0482	0.0972	0.1470	0.1975	0.2488

Changed syl5 +0.5 Syl3 -0.5 turns

Rac/50Hz	Curr.distr.		Dwight	Losses
0.10337	978800.00	97.88	97.6101	990.30
0.07880	805273.00	80.53	88.3334	510.97
0.09059	884282.00	88.43	70.2378	708.35
0.07562	922951.00	92.30	92.1132	644.14
0.06909	1279393.00	127.94	138.7756	1130.96
				3984.72

Jacobian matrix (N+1)

-12.31237	12.80433	0.16303	1.00943	0.81753
10.85960	-28.34640	16.48440	0.13670	1.31740
0.17201	14.43451	-33.98599	17.97231	1.04511
0.73483	0.12693	16.49853	-35.89377	17.28163
0.54602	0.98062	0.84012	16.77532	-20.46168

DN		Changed curr.	Orig.curr.
-0.0788	1076097.00	107.61	**97.6101**
0.0005	799984.00	80.00	**88.3334**
0.0215	695805.00	69.58	**70.2378**
0.0128	915458.00	91.55	**92.1132**
0.0093	1383355.00	138.34	**138.7756**

Appendix C

"Test setup and results for assessing the losses of a conductor due to a varying magnetic field at different harmonics"

(by John Millar, Matti Lehtonen, Asaad Elmoudi and Kari Nurminen)

Part 1

This relates the test procedure and results used to check TKK's theory for the effect of harmonics on eddy losses induced in a current by an external magnetic field. Professor Lehtonen suggested making a simple air coil, or solenoid, to create a homogeneous magnetic field whose flux density would be proportional to the current in the coil, regardless of the frequency. The coil and a power supply are shown in Figure 1 below.

Figure 1 The AC power supply and coil

Construction details

The coil consists of 205 turns of copper wire wound on a 16 cm PVC pipe. The diameter of the copper conductor is 1.8 mm, but the layer of insulating lacquer gives the wire an overall diameter of about 1.9 mm. The coil has an overall length of 405 mm and a radius of 80.95 mm. A scale drawing of the coil and sample holder is shown in Figure 2.

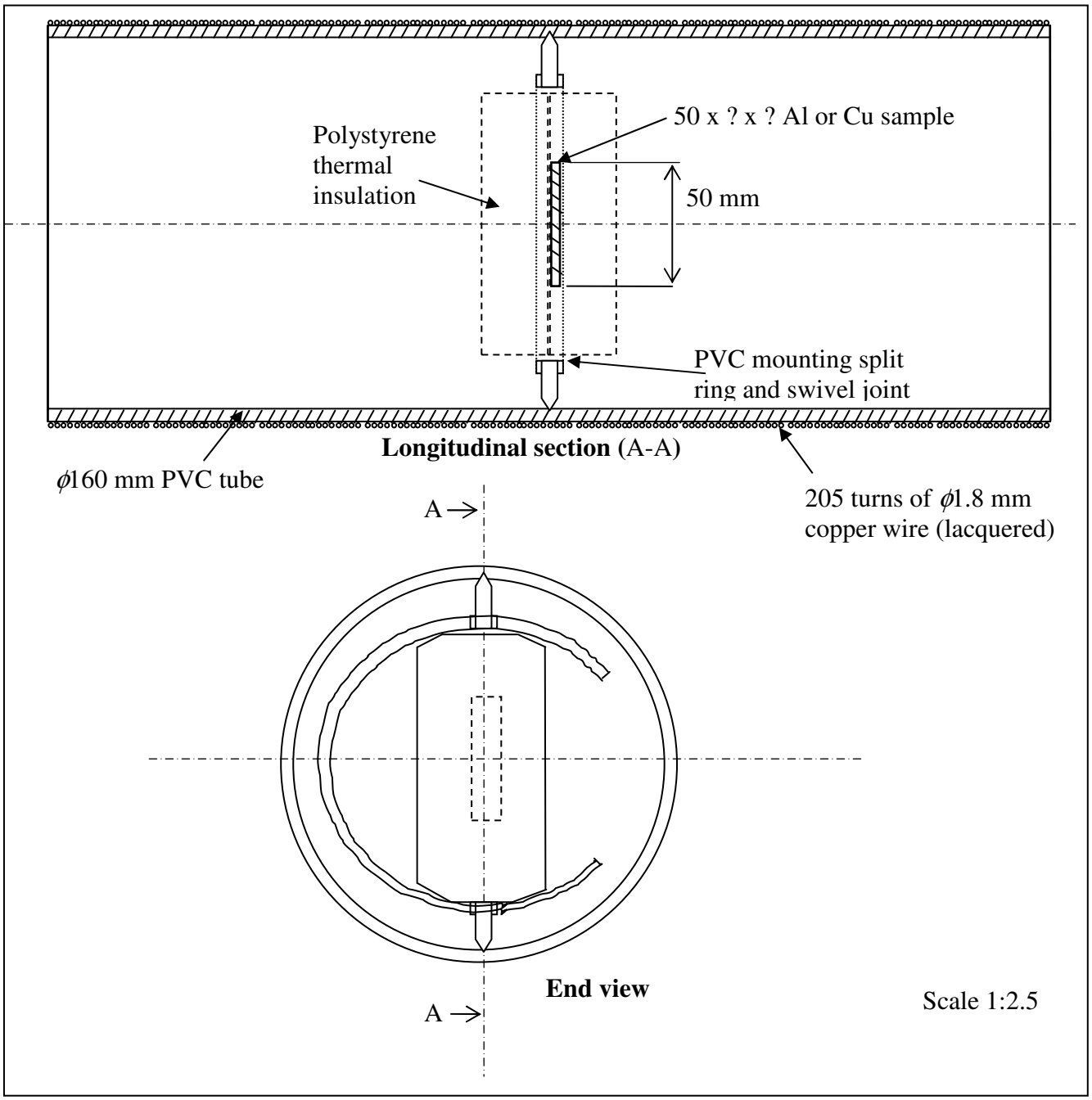

Figure 2 Air coil and sample mounting arrangement.

Electrical details

The inductance of a solenoid of infinite length is:

$$L_{coil} = \mu_0 N^2 A_{coil} \text{ (H/m)}$$

Grower (Grower, 1973) provides a correction factor, *K*, for the effect of finite length, which gives:

$$L_{coil} = \frac{\mu_0 N^2 A_{coil}}{Coil\_length} K \text{ (H)} \qquad (1)$$

For our coil, $K = 0.85$, so:

$$L_{coil} = \frac{4\pi 10^{-7} 205^2 \pi 0.08095^2}{0.405} 0.85 = 2.28 \text{ mH}$$

Other circuit elements are the resistance of the coil itself, a series resistance necessary for the stable operation of the power supply and a series measurement resistance for shunt measurement of the current.

The resistance of the coil is:

$$R_L = \frac{\rho_{cu} N \pi D}{\pi 0.00095^2}$$

$$\approx 0.63 \ \Omega \text{ at } 20^{\circ} C$$

The series load resistor depends on the voltage range being used. The measurement resistor is 0.01 Ω.

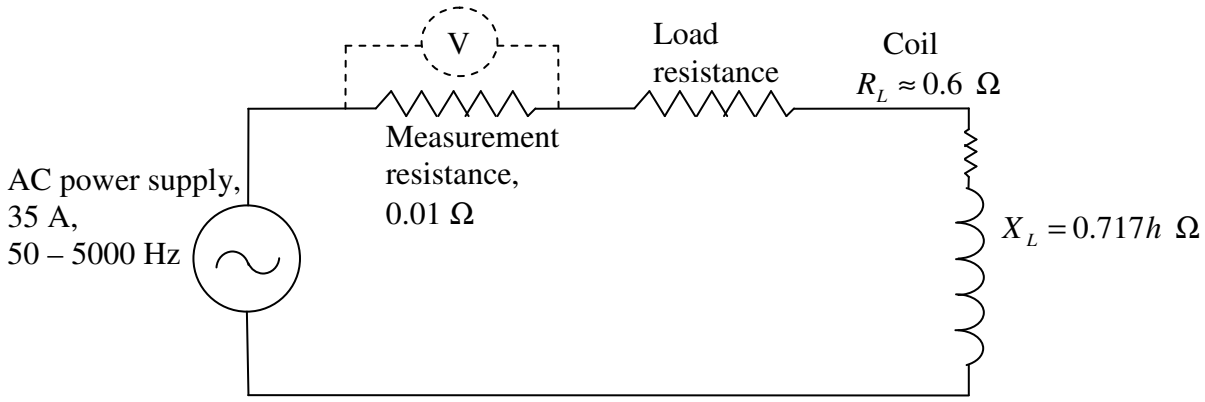

Figure 3 Circuit diagram

The magnetic field in the coil, which should be homogeneous and parallel to the centre line of the coil near the middle of the coil is:

$$B_{coil} = \frac{N\mu_0 I}{Coil\_length} K \qquad (2)$$
$$= 0.54 I \quad \text{mT}$$

where I is the current in the coil (in A).

This relationship has been roughly verified with measurements, at safe field strengths, as can be seen in Table 1.

Table 1 Measured vs. calculated magnetic field density

		Magnetic field density	
Freq (Hz)	Current (A)	measured (μT)	calculated (μT)
50	0.512	**291**	277
100	0.502	**289**	271
150	0.487	**281**	263
200	0.465	**272**	251
250	0.456	**264**	247
300	0.438	**254**	237
350	0.423	**244**	229
400	0.407	**234**	220
450	0.39	**224**	211
500	0.373	**215**	202

The calculated values from equation (1) are probably more trustworthy than our field measurements, but the main point to note is that the magnetic field is proportional to the coil current. When corrected for current there was less than 3 % variation in the measured field over the 50-500 Hz range.

We can thus assume that the coil, when situated away from metal objects, provides a homogeneous field that is proportional to the supplied current, and that we can estimate the field density (from the supply current) to an absolute accuracy of within 5%, and a relative accuracy of better than 3%.

Thermal details

The geometry and heat flux from the coil itself make steady-state tests impractical without a lot of temperature sensors, which may affect the field. The process we have adopted, then, is to measure the temperature rise of the samples with a single sensor when subjected to a magnetic field in order to determine the relationship of losses to frequency. There is likely to be some error in this procedure, but the main aim at this stage is to establish the relationship between eddy current losses and frequency. In this report, frequency is represented by the harmonic order, h, where 50 Hz corresponds to $h = 1$.

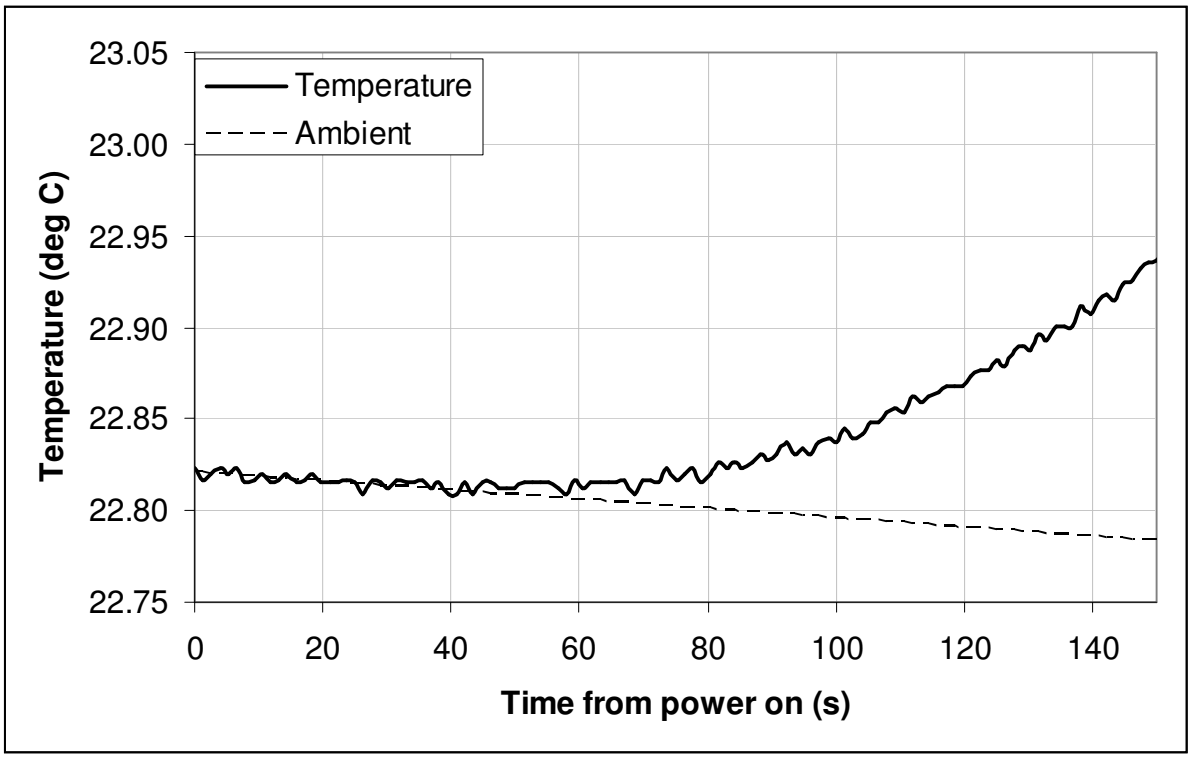

Figure 4 Temperature rise at sample position due to the heat from the coil showing why the test time should be limited to 40 s...

If we assume the conductor sample to be a perfect thermal conductor with perfectly insulating boundary conditions, then the transient form of the heat equation simplifies to:

$$q = \rho c \frac{d\theta_{sample}}{dt} \text{ W/m}^3 \qquad (3)$$

where ρ is the density of the sample, c is the specific heat capacity and θ_{sample} is the temperature rise of the sample.

The ideal conditions are impossible to achieve, but are approximated by attaching a tiny Pt100 sensor to the conductor sample, and packing the sample in polystyrene. The thermally insulated sample is then suspended in the heating tube in a swivel bracket, which minimizes the thermal contact between the sample and the solenoid. The 4-wire connection to the Pt100 is suspended down the centre-line of the tube, to minimize the flux change across the connection wires. Fans are directed at and through the coil but even so, we have only about 40 s before the heat flux from the coil starts noticeably affecting the sample, as Figure 4 shows.

Photographs of the test set-up are shown in Figure 5. The losses at fundamental frequency are problematic to measure, as the field must be very strong to produce a measurable temperature rise in samples with small conductor sections. Nevertheless, by controlling the ambient conditions and using as high a supply current as possible, we have obtained results that are at least indicative of

trends, and show the relationship of losses with frequency, even if the absolute values for the losses that we obtain are not to be fully trusted.

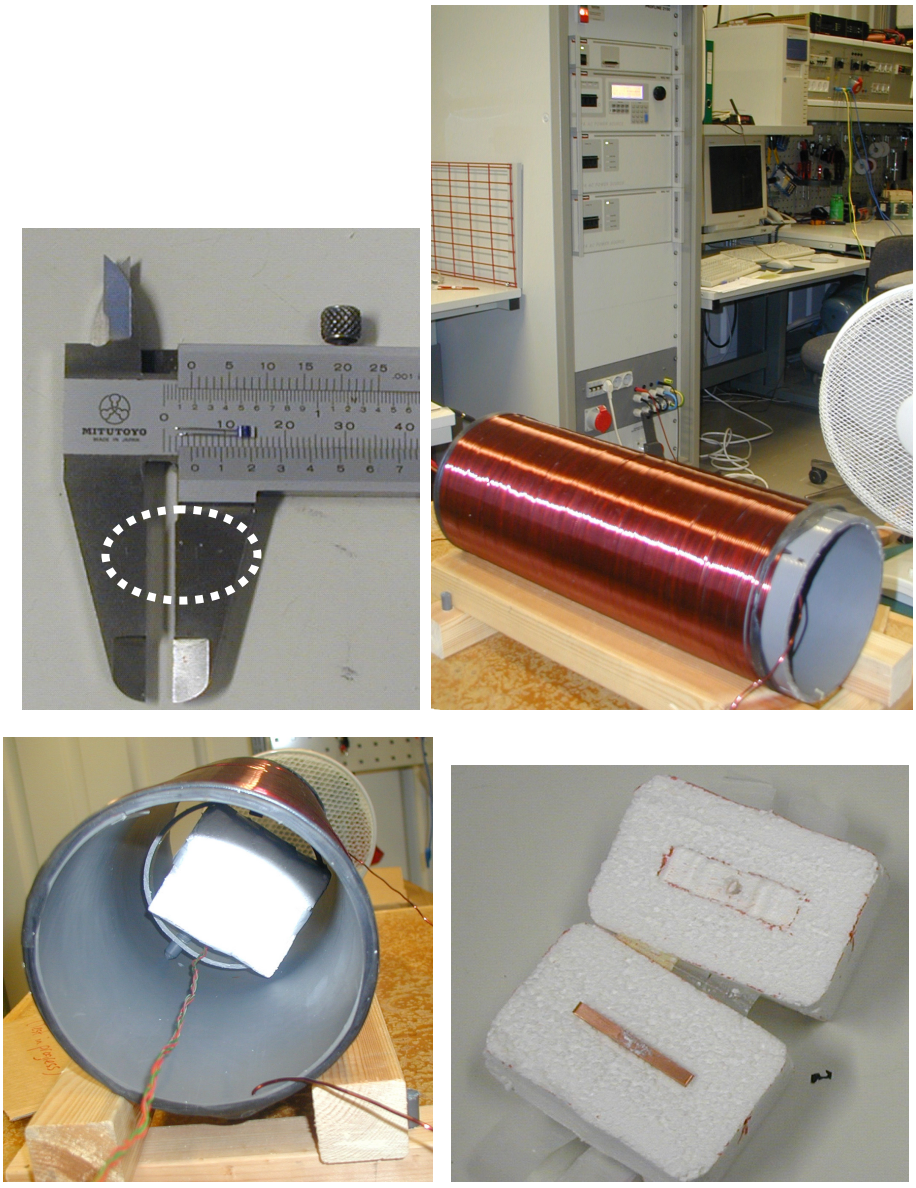

Figure 5 Photographs of the test equipment, which includes a tiny Pt100 temperature sensor (top left) attached with thermal paste to the thermally insulated sample (bottom right), a coil wound on a PVC tube, a high quality AC power supply (top right), capable of supplying a good sinusoidal current at a range of frequencies, and suitable cooling.

Naturally, we do not have perfect thermal insulation around our conductor samples and what is more, the leads to the temperature sensor will also conduct some heat away from the sensor itself. During each test, however, we do not touch the test setup, so that whatever thermal imperfections that exist (in terms of contact resistance between the sensor and sample and heat dissipation through the polystyrene and sensor wires) are consistent for all frequencies.

Experimental procedure

We are faced with very small temperature rises at the fundamental (50 Hz) and so it is necessary to ensure constant ambient temperatures before and during each test, or model the change in ambient temperature before each test and trust that the conditions in the room will not change their behavior during the 40 s test period at each frequency. Fortunately, the Shaffner voltage generator can be programmed to make voltage and frequency steps automatically, so the procedure has been to run the tests at night time, when nobody is coming and going from the room. For frequencies higher than 500 Hz, the lower power HP6834B power supply was used manually, noting that at higher frequencies the eddy current losses are much higher, and so lower coil currents are permissible. The temperature gradients obtained at each frequency were scaled by the inverse square of the currents to enable comparison with the fundamental response, the current of which was used as a base. The entire test period is logged, which means that the temperature behavior at the sensor on the sample can be modeled prior to each power step. The temperature rise above ambient can then be estimated.

Figure 6 illustrates the procedure:

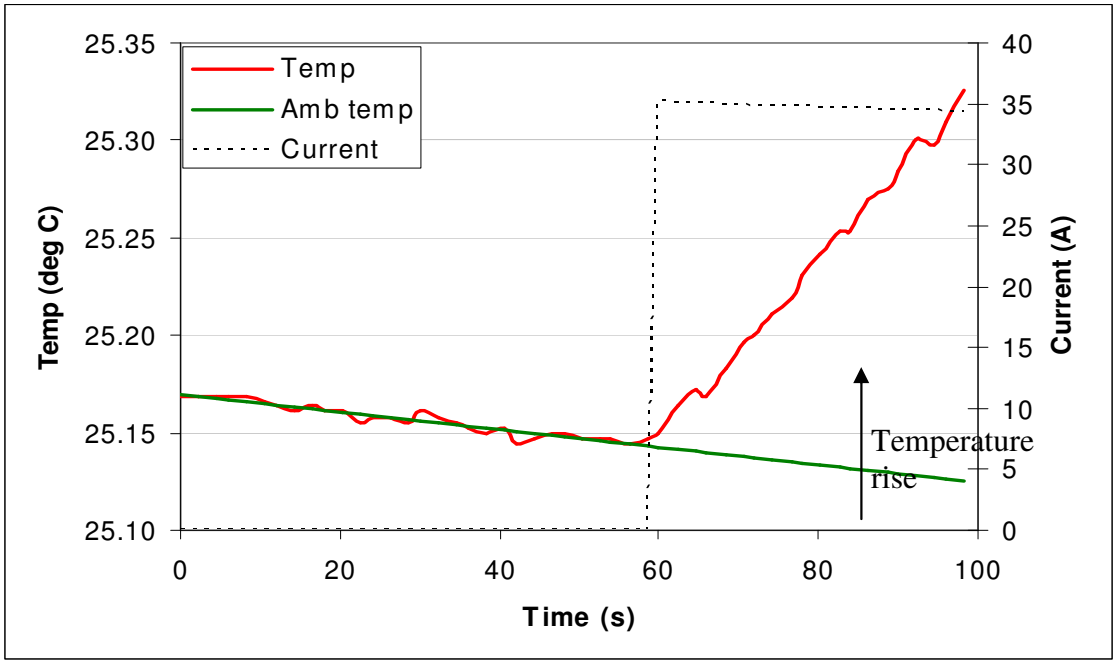

Figure 6 Measurement of the temperature rise at 50 Hz for a 12mm sample. The ambient temperature is extrapolated from the sample temperature sensor 60 s before the coil is switched on, so that the temperature rise can be accurately estimated without waiting for the coil and sample to cool completely between tests.

Results for solid copper conductor samples

The test samples were 50 cm long, to ensure good clearance from the hot coil, and are shown in Figure 7.

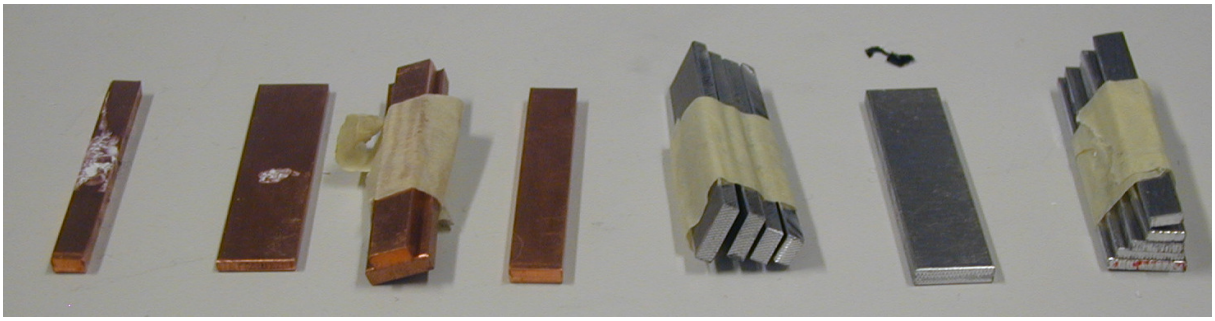

Figure 7 Solid conductor sample

Figure 8 shows the measured response and fitted gradient for the 12 mm x 2mm x 50 mm copper sample at 50 Hz, while Figure 9 collates the gradients from the tests at each harmonic order. The gradients are scaled by the ratio of the currents squared, to match the current and hence magnetic field strength in the 50 Hz test.

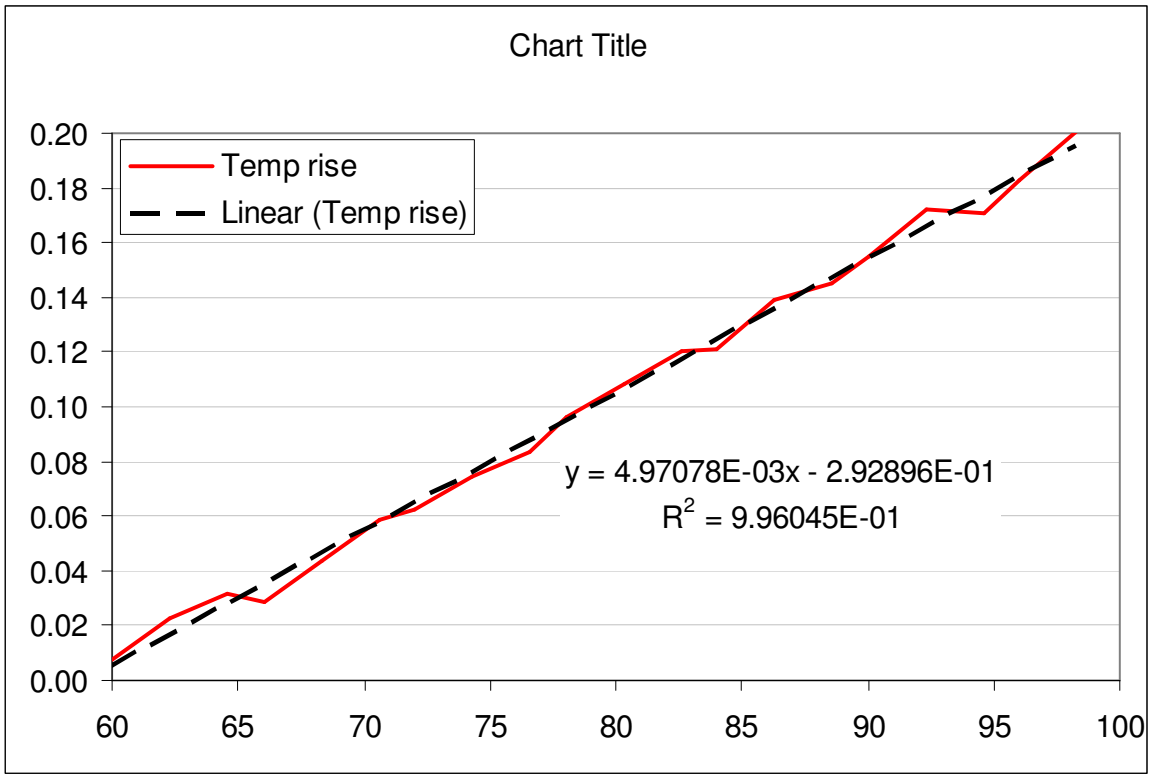

Figure 8 The line of best fit (using the least squares method) gives a gradient of $4.97 \cdot 10^{-3}$ K/s at 50 Hz

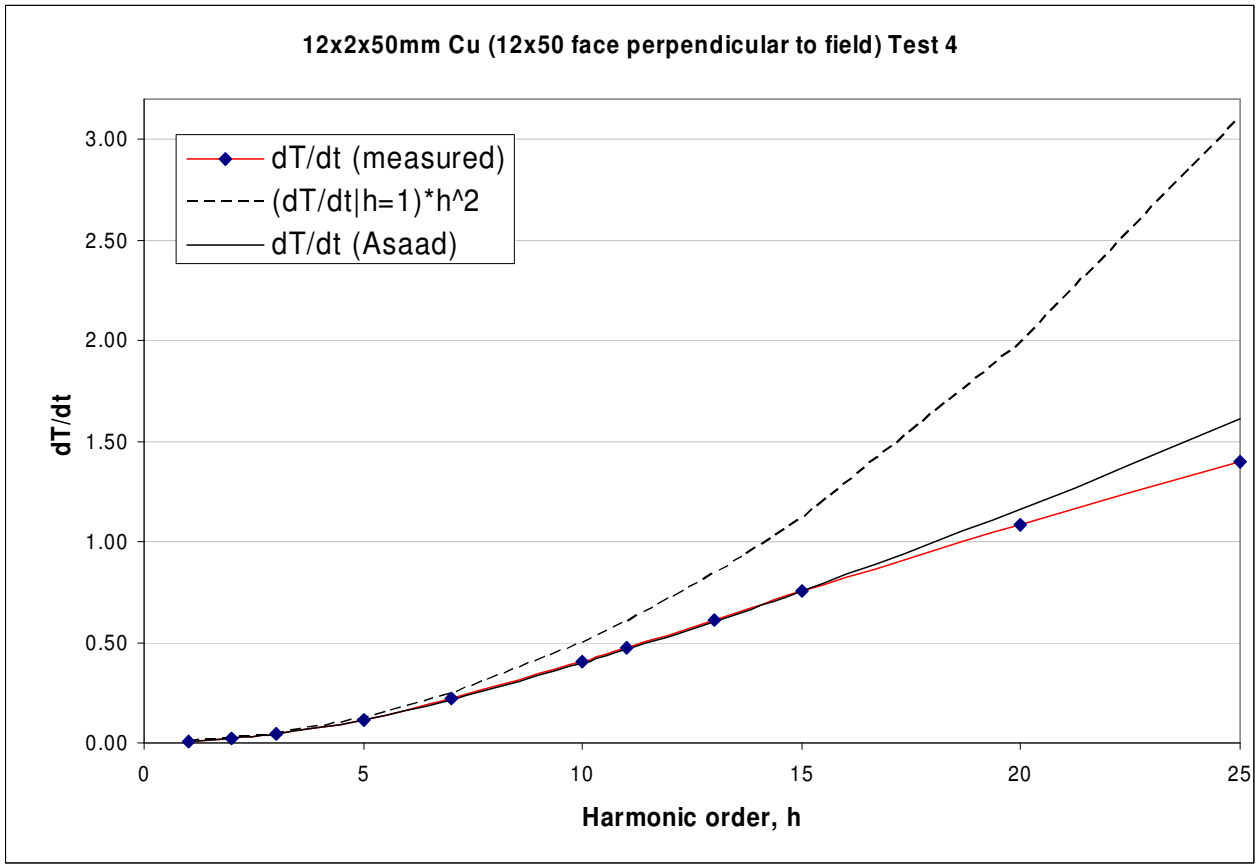

Figure 9 Responses from 50 to 1250 Hz. The measured temperature gradients (red line) are related to the current used at 50 Hz (using a ratio of the square of the currents). The dashed line is generated by multiplying the measured 50 Hz gradient by the square of the harmonic order. This is what is generally used in the standards, and can be seen to be conservative at high harmonics. The solid black line applies the correction factor based on skin-effect theory. (Asaad refers to Elmoudi's PhD-Thesis (Elmoudi 2006) and to eq. 3.15/3.16 of this thesis. h^2- refers to the conventionally used h-squared rule).

The results shown in Figure 9 are extremely encouraging, showing a near perfect fit with the response predicted in Figure 9 up to the 15th harmonic. This holds true for smaller conductors as well, although it must be admitted that the temperature response becomes so small for small sections, that the gradient at 50 Hz can only be estimated. The losses at higher harmonics are greater, and thus give rise to temperature gradients that are high enough to be accurately measured. When the sample that generated the results in Figure 6 to Figure 9 is turned 90° so that the narrow edge faces the field, the losses, which are much lower, show a quadratic relationship with harmonic order, as is predicted, see Figure 10.

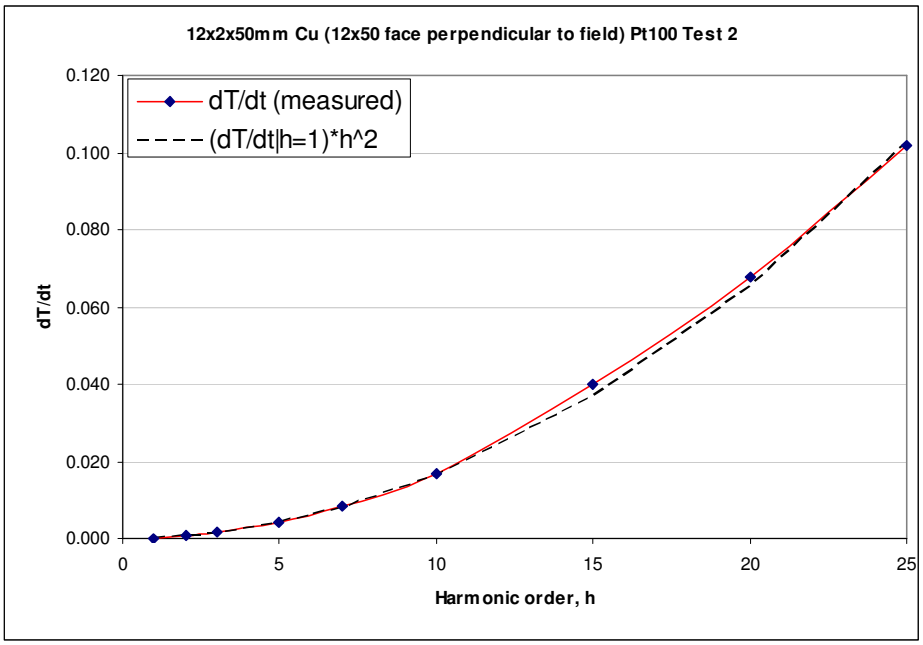

Figure 10 The response of the 12mm conductor with the 2 mm edge facing the field

The following chart, Figure 11, shows results for various sizes of conductor up to the 10th harmonic.

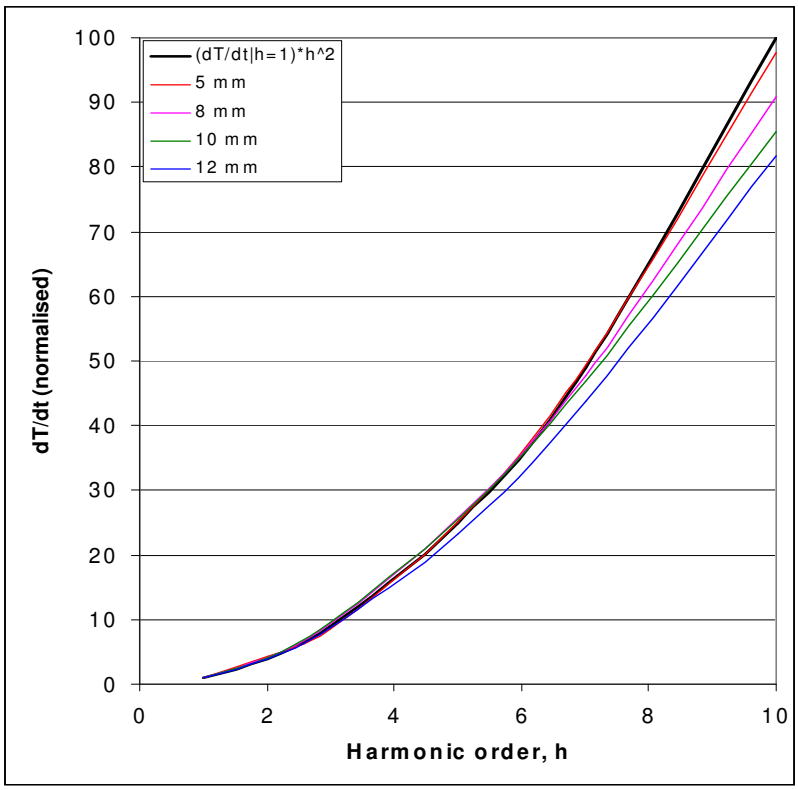

Figure 11 Responses for different conductor sizes (related to unity at the fundamental)

The effect of the angle of incidence of the magnetic field on the losses, adjusted to the same current base (34.7 A), is shown for the 12 mm conductor in Figure 12.

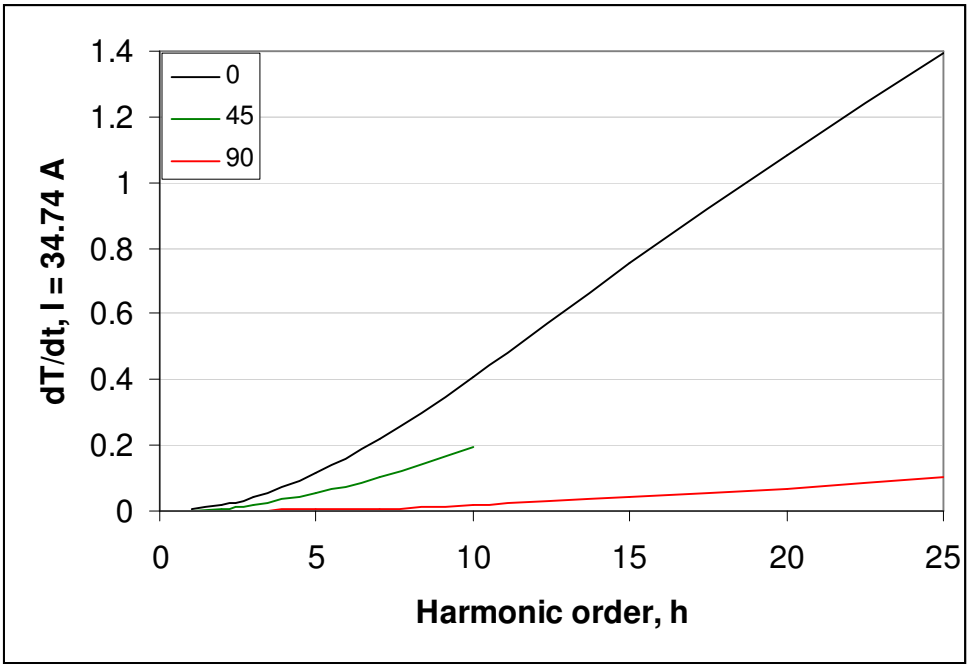

Figure 12 Effect of angle of incidence of magnetic field on losses for a 12 mm copper conductor

While the results up to this point are very encouraging, there is one significant cause for concern, and that concerns the absolute value of losses that should occur at the fundamental according to equation (4), and the value obtained from our measurements.

$$q = \frac{\pi^2 B^2 f^2 T^2}{3\rho} \qquad (4)$$

where B is the flux density, f is the frequency, T is the dimension of the sample perpendicular to the field and ρ is the electrical resistivity of the sample material.

For example, for the 12x2mm copper sample, the gradient at the fundamental is 4.97e-3 K/s for a current of 34.74 A, which corresponds to a field density of 0.0188 T. Equation (4) gives a value of 23.76 kW/m^3 for the losses but equation (3) implies that the losses should be:

$$q = mc\frac{d\theta_{sample}}{dt} = 8700 \cdot 385 \cdot 4.97\text{e-}3 = 16.65\ \text{kW/m}^3$$

which is some 30 % lower than they "should" be.

There are various explanations for this. Firstly, equation (3) implies that the sample is perfectly thermally insulated, which is not strictly the case. In addition, some heat is transferred through the wires to the temperature sensor. Another contributing factor is that equation (4) is a 1-dimensional equation, and implicitly assumes that the conductor is infinitely long. This equation should be

derived in 2 dimensions, to more accurately model the finite length of our conductors. If such a derivation is too demanding, then our experimental setup could be simulated using finite element analysis, although this is not a trivial exercise.

A solid aluminium conductor

The correction factor seems to also apply for aluminium conductors, allowing for the change in electrical conductivity

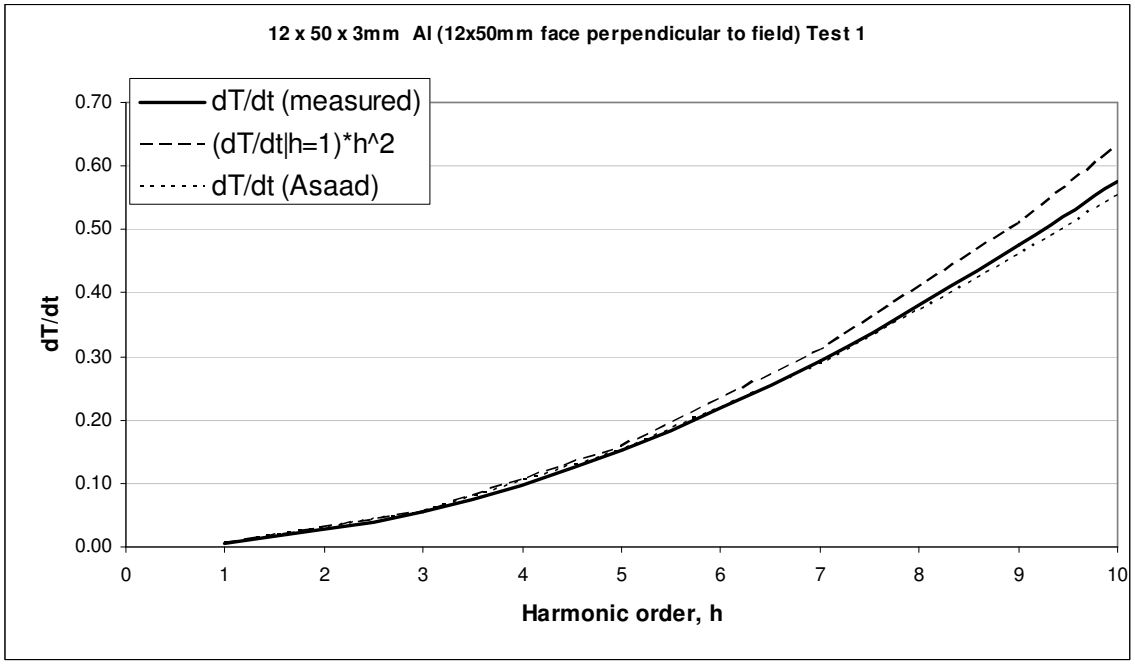

Figure 13 The response of a 12 x 3mm aluminium conductor with the 12 mm faces perpendicular to the field

The losses implied by the 50 Hz temperature gradient are 15.3 kW/m^3 whereas theory suggests they should be 28.8 kW/m^3....

Insulated stranded aluminium coil conductors

We now turn our attention to stranded conductors, see Figure 14, such as are used in air coils.

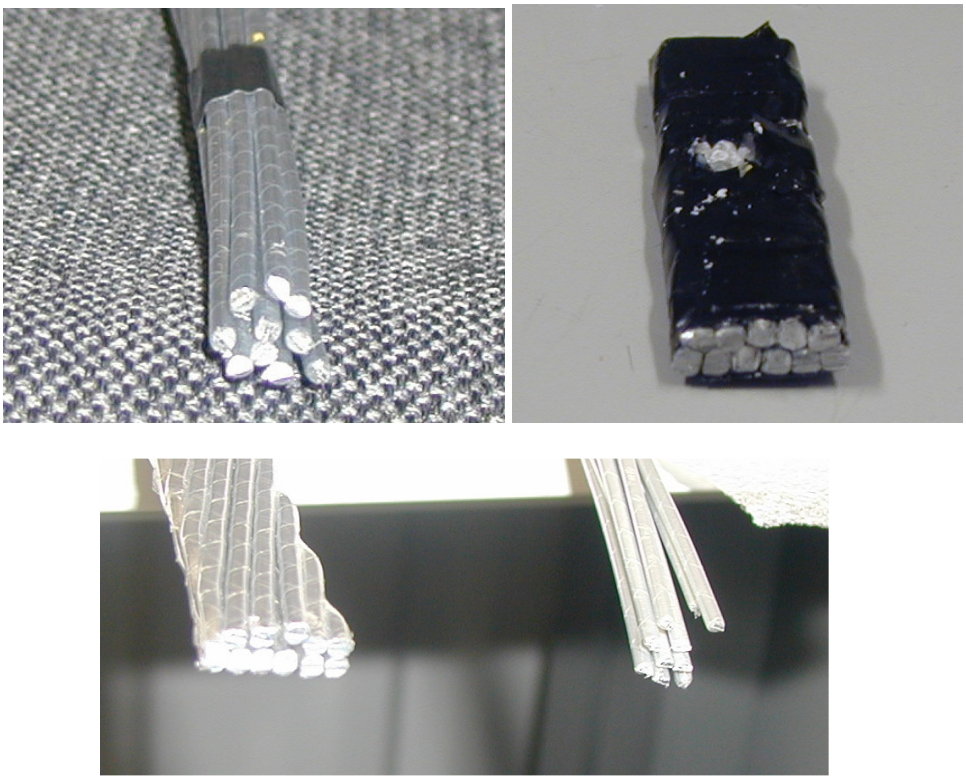

Figure 14 Stranded aluminium conductors

We have some samples of coil conductors where each 3mm strand is individually insulated and continuously transposed, presumably to limit the effect of eddy currents and circulating currents. Our preliminary measurements indicate that the induced losses in these conductors are very much lower that they would be if the conductors were solid, or if the strands were not insulated from each other. This is indicated by the equation for eddy current losses in a single round conductor of diameter *d*:

$$q = \frac{\pi^2 B^2 f^2 d^2}{3\rho} \qquad (5)$$

Very roughly, the eddy current losses per unit length in, say, 11 individual strands would be, at low frequencies:

$$Q = 11 \cdot \frac{\pi^2 B^2 f^2 0.003^2}{3\rho} \cdot \pi 0.0015^2 = 2.30 \cdot 10^{-9} \frac{B^2 f^2}{\rho} \text{ W/m},$$

whereas a rectangular conductor of the same area, say 15.8 mm x 4.9 mm would have losses per unit length of:

$$Q = \frac{\pi^2 B^2 f^2 0.0158^2}{4\rho} \cdot 0.0158 \cdot 0.0049 = 4.795 \cdot 10^{-8} \frac{B^2 f^2}{\rho} \text{ W/m}$$

i.e., some 20 times greater than the stranded conductor at the fundamental.

Following the same logic, the low frequency eddy current losses per unit length of a solid round conductor with the same cross-sectional area (of conductor) would be *n* times the losses of a conductor made up of *n* insulated strands.

Figure 15 shows the response (up to the 25th harmonic) of an 18x5.6x70mm sample, consisting of 11 insulated 3mm aluminium stands, 2 deep. The field is perpendicular to the 18mm face.

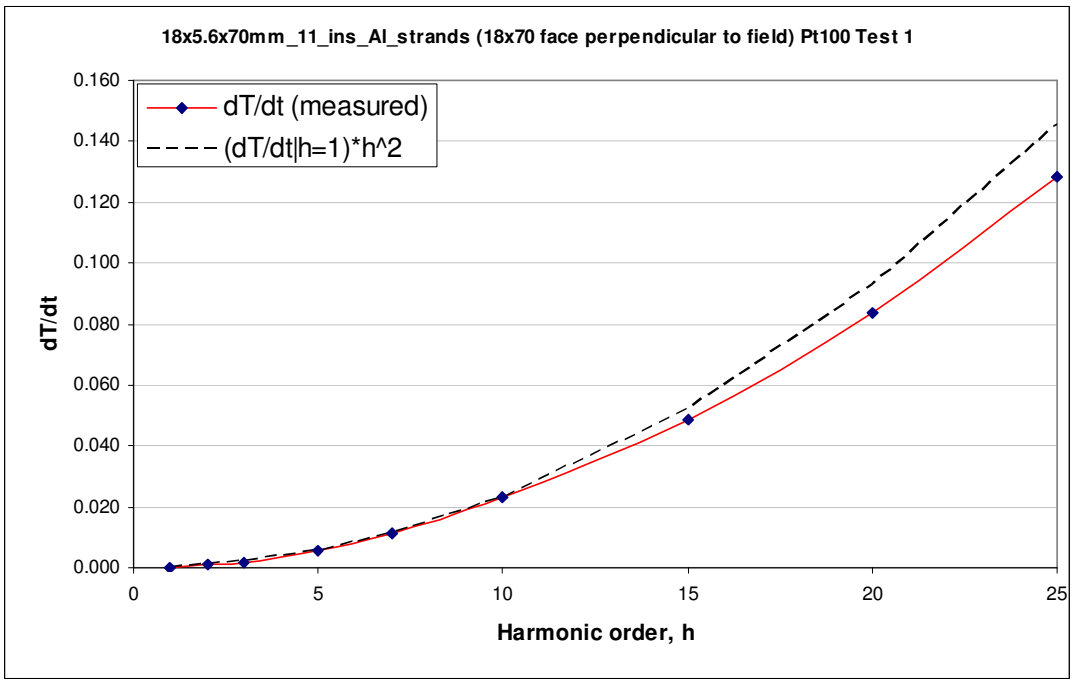

Figure 15 18x5.6 coil conductor temperature gradient. The dashed line shows the quadratic relationship based on the gradient at h=1

The fundamental gives a temperature gradient of 2.32e-4 K/s, which corresponds to a current of 34.7 A (i.e. a field density of 0.0188 T). Using equation (3), we obtain a loss value of 2700 x 900 x 2.32e-4 = 564 W/m^3.

Equation (5) gives a value of 677 W/ m^3. This is an error of only 17 %. It is likely that the end effect is less significant in this case, as the length to diameter of the individual strands exceeds 200, but we must confess that when the losses are as low as this, the derivation of the gradient from the very low temperature rise that occurs during our 40 s test period is likely to be subject to an error of at least ±20%. In 4 tests, the "best fit" gradient varied from 1.83e-4 to 3.68e-4 K/s. Our sensor thermally bonded to one of the stands on the face of the conductor, and although we remove the insulation from the strand at that point, the conductor as a whole is not such a perfect thermal conductor as the solid copper conductors tested earlier in this report.

The same observations are even more pertinent when the 5.6 mm face of the conductor faces the field, but nevertheless we produce the results for this case in Figure 16, where the current was 33.9 A, which creates a field of about 0.0183 T in the centre of our solenoid.

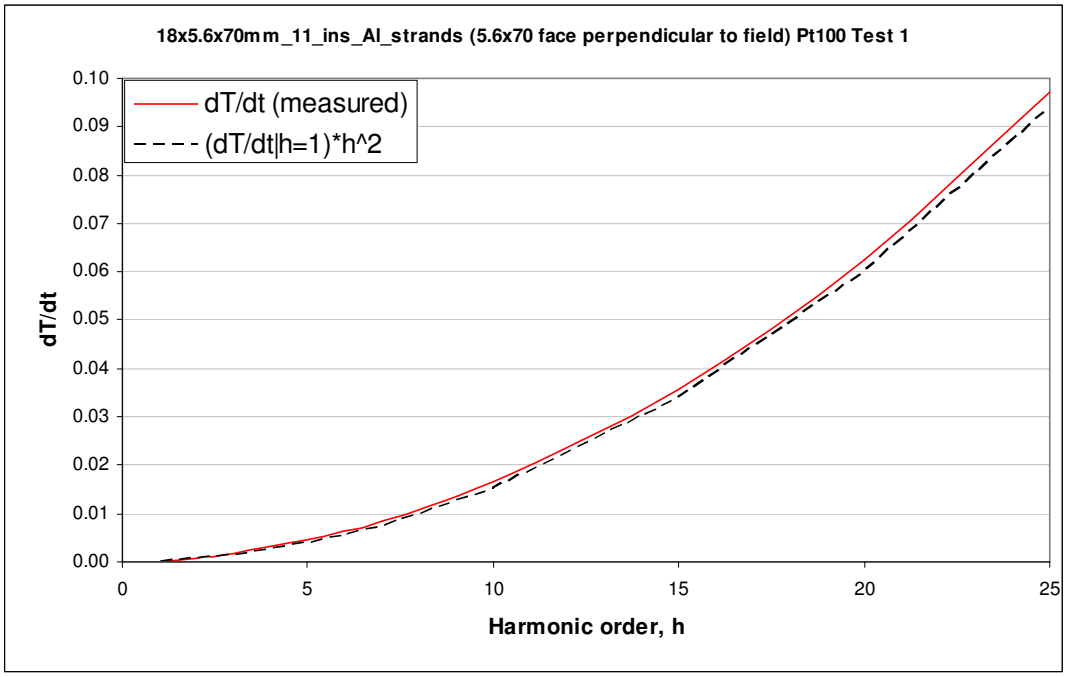

Figure 16 Temperature gradient as a function of harmonic order when the 5.6 mm dimension faces the field.

The losses at the fundamental, 50 Hz, are about 365 W/m^3 for the orientation shown in Figure 16.

There is clearly some error in these results at the low frequencies, although by the 3rd or 4th harmonic the losses rise to a high enough level for us to predict the gradient quite accurately. The dotted line in the figures, representing the hypothetical quadratic relation of losses with harmonic order is based on the measured gradient at the fundamental, however, and is likely to show some error. The main observations that can safely be made are that the losses develop quite close to quadratically (with respect to harmonic order) and that the (eddy current) losses in a stranded conductor are much less than they would be if the conductor were made of a solid section of the same dimension.

There is some evidence (as yet inconclusive due to the margin of error in our 50 Hz measurements) that the losses rise less steeply with increasing frequency when the dimension of the bundled conductor perpendicular to the magnetic field is greater than, say, 8 mm, even when the conductor is made up of individually insulated strands of about 3 mm diameter.

Figure 17 shows the temperature gradient of a bundled conductor (more or less circular) made up of 9 x 3.1 mm aluminium strands. The rise of losses with harmonic order is also less than quadratic.

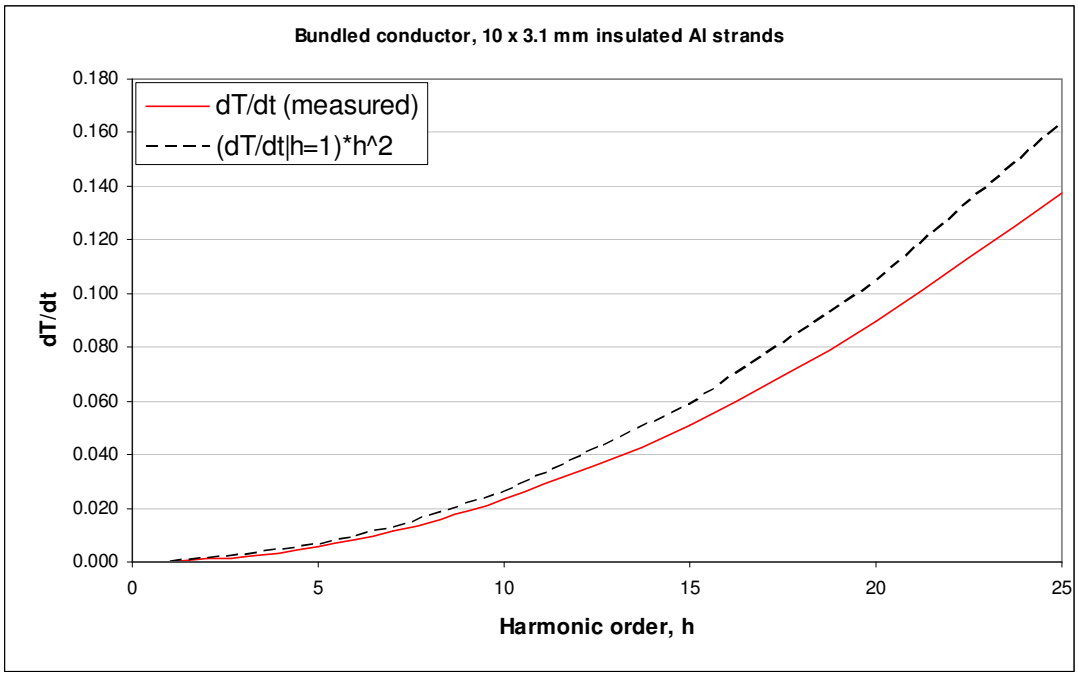

Figure 17 A bundled conductor consisting of 9 x 3.1 mm insulated Al strands

Part 2 Tests with new coil

Because of the low field strength and thermal interference of the coil used in the tests carried out in Part 1 of this report, we have set up a bigger coil, or rather, a stack of 3 9-layer coils with large 6.3 x 2.9 mm lacquered copper conductors, to run tests on more samples given to us by Nokian Capacitors (NC). The results show a significant improvement in quality. One or two other practical observations are also made about the insulated stranded conductors.

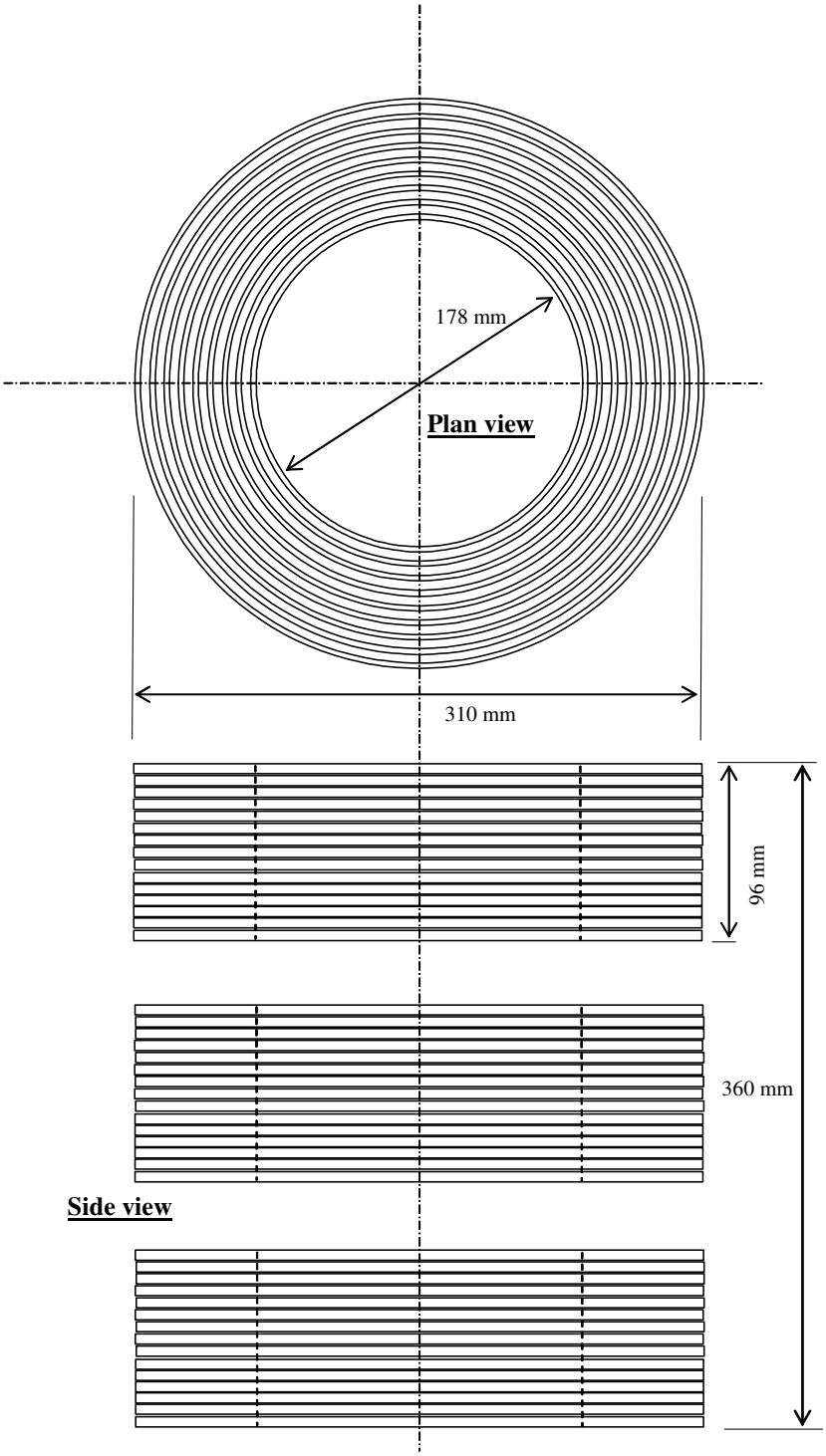

Figure 18 (New) test coils - each is 15 rows high by 9 deep. Conductor dimensions: 6.3 x 2.9 mm. Outer row of top coil has only 13 rows, and outer rows of bottom 2 coils have only 14 rows. The field density in the middle of the middle coil is 1.15 mT/A

Without any preamble here are the test results, which establish the relationship between eddy current losses and frequency.

Solid conductors

Figure 19 indicates that for this slightly thicker conductor, the correction factor may err on the conservative side, but the error is small.

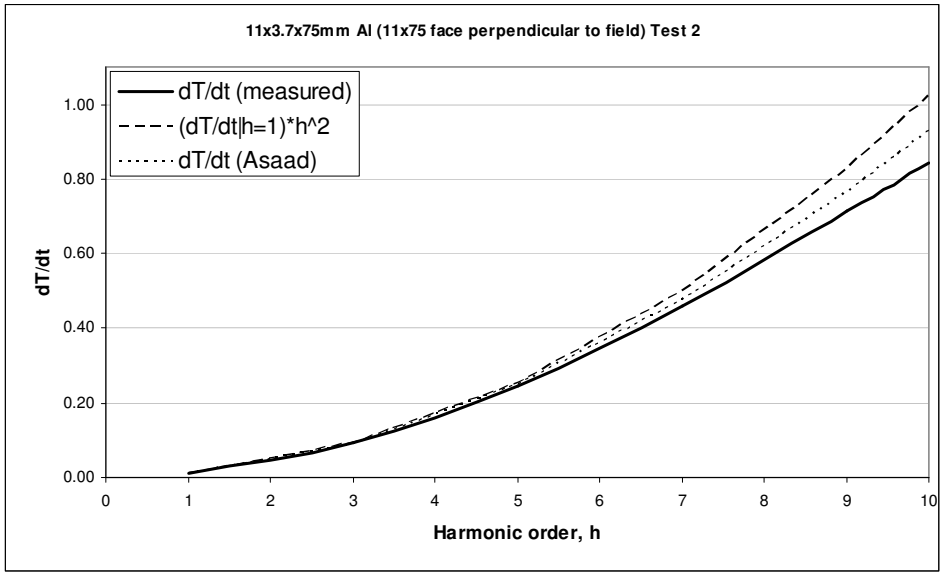

Figure 19 Temperature gradient, which is proportional to eddy current losses, vs. frequency, in an 11 mm aluminium conductor

The application of the correction factor to the losses at 50 Hz predicts losses at the higher harmonics that err on the conservative side when compared with the measured results. At 50 Hz, we seem to have slightly narrowed the error between losses calculated from the temperature rise (33.3 kW/m^3) and theoretical losses calculated from the field strength and geometry of the conductor (24.8 kW/m^3) to less than 23%, a significant improvement from Part 1, but it should be noted the theoretical value is very sensitive to the field density, for which we rely on measurements. A commercial meter that can only handle field strengths of less than 300 µT implies the coil has a field strength of about 1 mT/A, where as a home-made loop that could be used at test field strengths indicates the field is some 15 % higher, at 1.15 mT/A. The good news is that the field strength's relationship to current does not seem to be affected by the frequency. For more accurate loss calculations from temperature rise tests, we should lower the error in the field density.

Similar results are obtained with the other conductor sizes. Figure 20 shows results for a 14 mm conductor:

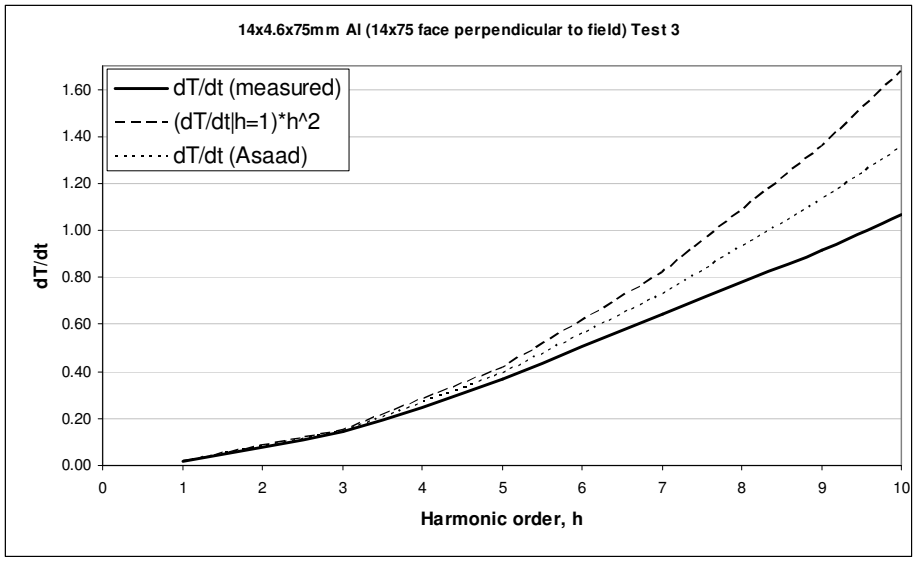

Figure 20 Temperature gradient vs. frequency in a 14 mm aluminium conductor

For the 14 mm conductor, the theoretical (40.4 kW/m^3) vs. temperature gradient derived losses (40.8 kW/m^3) show very little error. Contact resistance between sample and temperature sensor is likely to be the largest source of error, and it would seem that with a few improvements in the test setup, we should be able to quite accurately measure the real losses in absolute terms, and not just the relationship of losses and frequency.

Stranded conductors

Our attention now turns to stranded conductors, and this time round, the focus was to see what increase in eddy current losses is likely to be caused by high temperature chaffing of the conductors that may lacerate the insulation causing shorting of the strands.

The test results are as follows:

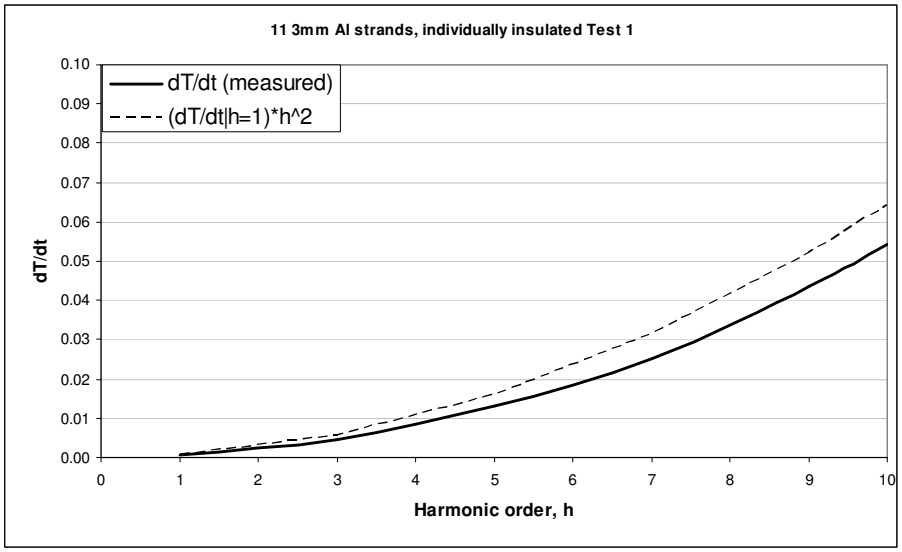

Figure 21 Temperature gradient of insulated stranded conductor vs. frequency

Although the temperature rise at 50 Hz is more reliable than in Part 1 of the report, there is still some margin of error due to the low temperature rise in these stranded conductors. Theoretical vs. measurement based losses are 2.4/1.56 kW/m^3, i.e., the error is about 35 %, as thermal contact resistance is an even bigger issue with these conductors (putting a flat based temperature sensor onto a round conductor strand).

The insulation was removed from the stranded sample, and then retested, Figure 22. The strands were not deliberately shorted, just pressed together, as if their insulation had been severely degraded in service. A slightly higher measurement based loss at 50 Hz occurred (1.61 kW/m^3), and the results with frequency show that the uninsulated sample has a loss profile with frequency that is closer to quadratic. Nevertheless, the losses are more than an order of magnitude less when compared to the solid conductors. We noted that the insulation was quite severely degraded when we heated a stranded conductor up to about 265 °C and then stressed the conductor by twisting and bending it.

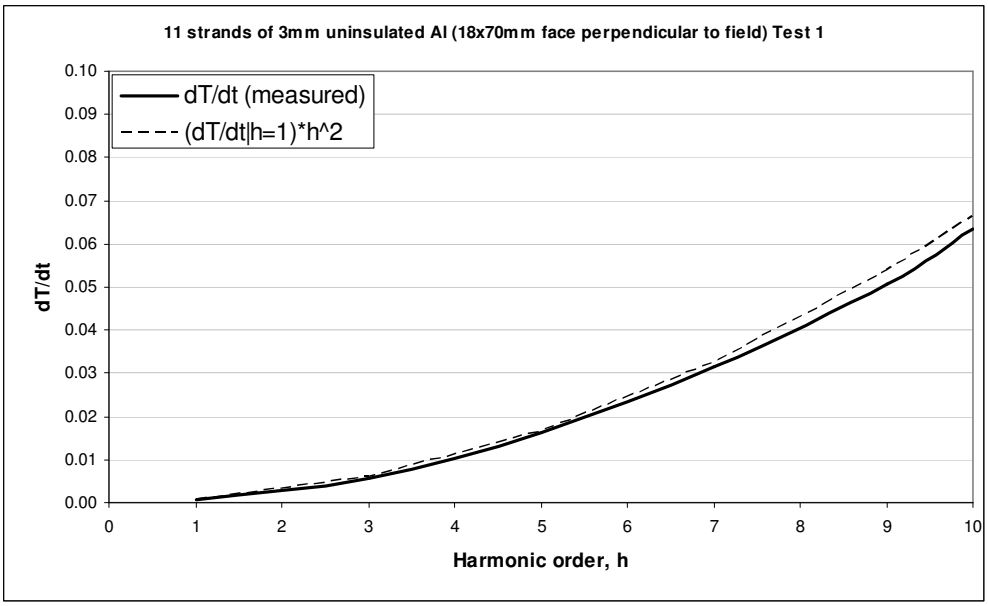

Figure 22 Temperature gradient of uninsulated stranded conductor vs. frequency

A more telling test, however, would be to assess the effect of the losses due to the current in the conductors when they are in service. The stranding means that the losses are more or less the same as dc losses, whereas going to solid conductors may result in uneven current distribution, due to skin and proximity tests. This will probably have a much larger bearing than the increase in eddy current losses, which may prove to be only marginal when compared to the I^2R losses in the conductors.

The final part of this section is concerned with the eddy current losses on the large aluminium members that support and carry current to the coil structure.

Larger structural members

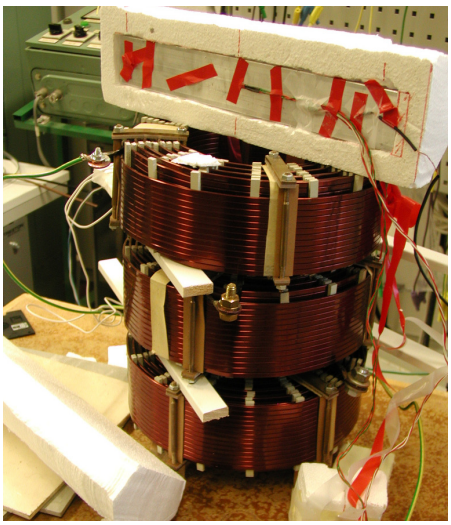

Figure 23 The test coils with the 60 x 10 x 400 mm aluminium sample. This test yielded no reliable measurements, as the required thermal insulation put the conductor outside the field concentration at the end of the coil. The picture nevertheless shows the placement of the Pt100 sensors, which gave measurable results when the insulated conductor was placed down the centre-line of the coils.

We were also given a 60x10x400 mm aluminium extrusion to test, shown in half of its insulation on top of the test coils in Figure 23. These members are used to support the coil windings. Unfortunately, because of the need to have some thermal separation between the coil and the sample, the only useful test we could make was placing the extrusion inside the coils along their centre-line. When mounted in line with the centre of the test coils, so that at least at the centre the 60 x 10 mm rectangular cross-section is subject to a uniform field, the 50 Hz losses calculated from a step temperature rise (17.7 kW/m^3) are about 14.5% lower should theoretically be achieved with a 10 mm section (20.7 kW/m^3) - this error is quite within the bounds of our experimental setup, however. The most reliable part of our testing is in the relationship of losses with frequency, which shows that field penetration at the centre of the 400 mm long member is significantly lower at frequencies above 100 Hz, see Figure 24.

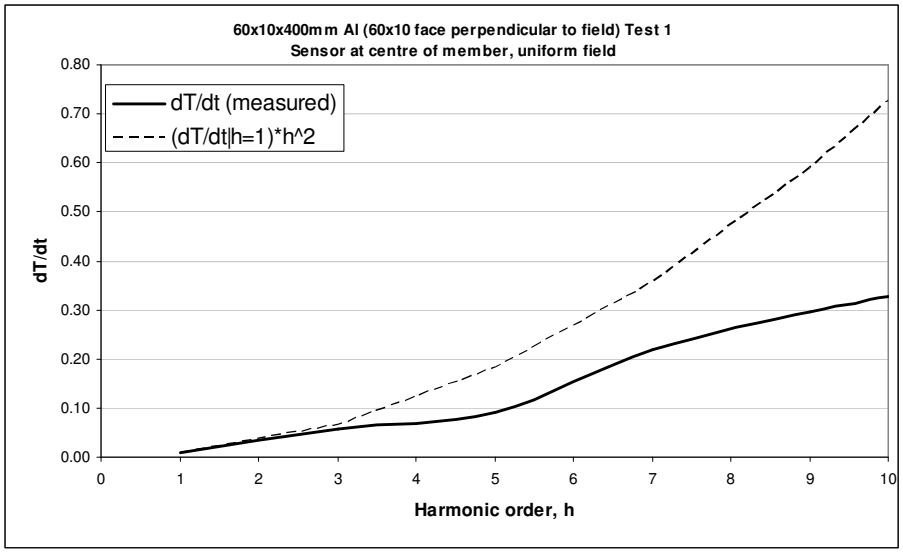

Figure 24 60 x 10 x 400 mm rectangular aluminium bar mounted along the centre-line of the coil. Temperature gradient vs. frequency for sensor mounted at centre of bar

A temperature sensor was also mounted at the end of the bar, in line with the top of the coil, where the flux density is much lower than in the centre of the coils or close to the end windings at the ends of the coils. The measurement-based losses were 10 kW/m^3. The same kind of pattern exists with as with the losses in the centre of the bar, i.e., it is far from a quadratic relationship with harmonic order, Figure 25.

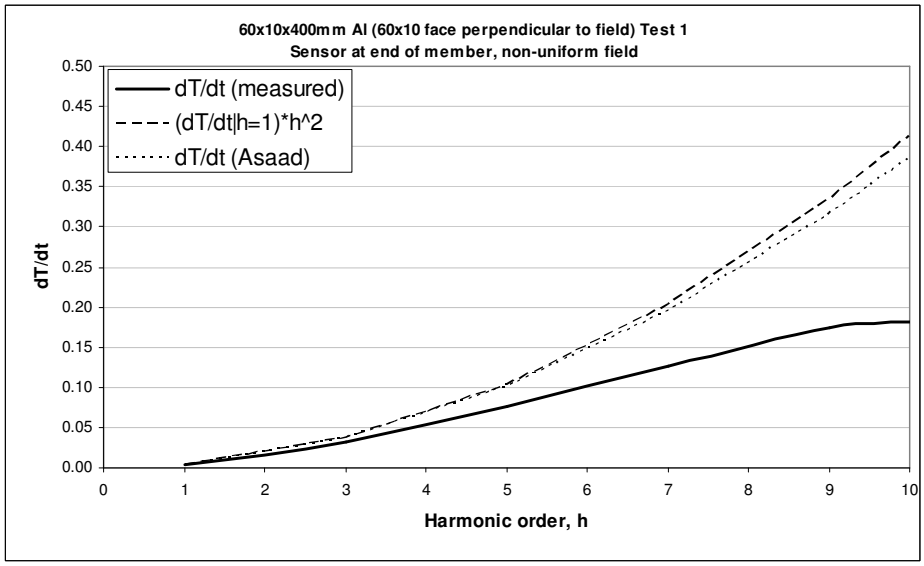

Figure 25 60 x 10 x 400 mm rectangular aluminium bar mounted along the centre-line of the coil. Temperature gradient vs. frequency for sensor mounted near end of bar.

Given that the 10 mm dimension of the structural members is always perpendicular to the coil, assuming radial symmetry, the eddy loss calculations should be based on this dimension using equation (4). The job will be to assess the field distribution and strength around actual coils, using

FEM simulations or perhaps field measurements. Equatione probably exist to cover the effect shown in Figs. 23 and 24, but if they don't...

It should be noted that these conductors have up to 400 A flowing through them, implying that the I^2R losses are (at room temperature) about 2.83e-8/(0.06x0.001) x 400^2 = 75.5 W/m = 1.26 MW/m^3, some 60 times greater than the eddy current losses...

Conclusions

The losses in solid rectangular conductors seem to develop with increasing harmonic order as predicted in (Elmoudi, 2005), and we would have to attribute the error in the absolute value of the losses calculated from the measured gradient to heat leakage and end effects in the experimental setup.

As far as the stranded conductors taken from air coils are concerned, it is clear that the induced eddy-current losses are much lower than they would be in a solid conductor of the same cross-sectional area. Excessive heating of the stranded conductors along with thermally induced mechanical wear in the strand insulation will slightly increase the eddy current losses and will make the relationship of those losses closer to the square of the harmonic order.

As a rough conclusion, while there is merit in developing our procedure to give more reliable absolute loss values, the ampacity of air coils is likely to be only marginally affected by eddy-current losses, and the most fruitful immediate area for research is probably in heat dissipation rather than in refining the loss calculations.

This notwithstanding, the experimental procedure that has been quite quickly developed using available power supplies and data logging equipment at TKK, has been quite effective, and warrants further work in terms of better thermal insulation of the sample from its samples, or in terms of further refinement of the analysis, to account for heat dissipation during the tests. If the industry is in the position to give us conductor samples, we are in the position to test them!

Appendix D

Construction and manufacturing method of air core reactor by NC

(19) Europäisches Patentamt
European Patent Office
Office européen des brevets

(11) EP 1 724 793 A2

(12) EUROPEAN PATENT APPLICATION

(43) Date of publication:
22.11.2006 Bulletin 2006/47

(51) Int Cl.:
H01F 41/06 *(2006.01)* ***H01F 27/32*** *(2006.01)*
H01F 37/00 *(2006.01)*

(21) Application number: **06113797.2**

(22) Date of filing: **11.05.2006**

(84) Designated Contracting States:
AT BE BG CH CY CZ DE DK EE ES FI FR GB GR HU IE IS IT LI LT LU LV MC NL PL PT RO SE SI SK TR
Designated Extension States:
AL BA HR MK YU

(30) Priority: **17.05.2005 FI 20055233**

(71) Applicant: **Nokian Capacitors Oy**
33330 Tampere (FI)

(72) Inventor: **Suonpää, Jorma**
33710, Tampere (FI)

(74) Representative: **Huhtanen, Ossi Jaakko**
Kolster Oy AB,
Iso Roobertinkatu 23,
P.O. Box 148
00121 Helsinki (FI)

(54) **Method and arrangement for reactor manufacturing, and a reactor**

(57) A reactor (1) is manufactured such that in a first step resin-dipped fibrous reinforcement material, such as roving thread (11), is wound to form a cylinder. On top of the obtained insulation layer there is wound an insulated conductor (5) to form a conductor layer (8). On the conductor layer (8) there is wound an intermediate layer (9) of resin-dipped fibrous reinforcement material. On the intermediate layer (9) there is wound a new insulated conductor layer (5). On top of the outermost conductor layer (5) there is wound an outer layer (7) of resin-dipped fibrous reinforcement material.

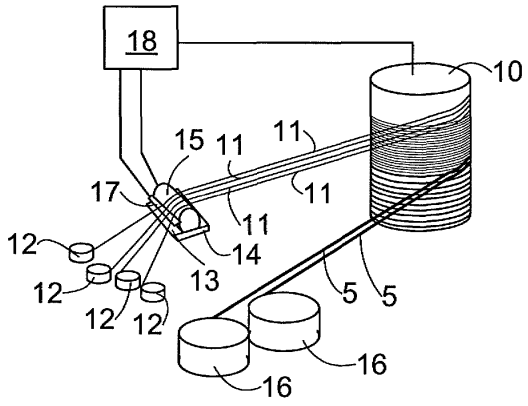

FIG. 3

EP 1 724 793 A2

Printed by Jouve, 75001 PARIS (FR)

Description

BACKGROUND OF THE INVENTION

[0001] The invention relates to a method for manufacturing a reactor, the method producing at least one coil having conductor layers and inside them an inner sheath of fibrous reinforcement material and resin, and outside an outer sheath of fibrous reinforcement material and resin.

[0002] The invention also relates to an arrangement for manufacturing a reactor, the arrangement comprising means for winding an insulated conductor to form a conductor layer so as to provide a coil.

[0003] The invention further relates to a reactor comprising at least one coil with conductor layers and inside them an inner sheath and outside an outer sheath.

[0004] Dry-insulated air-core reactors are used in a wide variety of applications. The reactors may be used, for instance, as damping choke coils in connection with compensating capacitor units, as filtering reactors to filter harmonics in electrical power networks, and as parallel reactors to compensate for capacitive reactive power of transmission lines. Further, the reactors may be employed in various filtration uses as current limiters. In addition, the reactors cover many other applications.

[0005] FI publication 70755 discloses a reactor whose coil consists of conductor bundles. Around the coil there is arranged permeable insulation material, which may be fibreglass fabric, for instance. Resin is impregnated on the insulation material. Corresponding reactors are also disclosed in publications EP 0084412 and FI 91570. To form coils from conductor bundles makes it difficult to dimension the coil accurately. For example, a slight change in capacity is difficult to implement in the reactor, because addition of conductor layers is performed one conductor bundle at a time. It is particularly difficult to get resin thoroughly impregnated around the reactor and between the conductors. Thus, it is relatively difficult to manufacture a reactor and it is a demanding task to make the reactor sufficiently rigid in its mechanical structure.

BRIEF DESCRIPTION OF THE INVENTION

[0006] The object of the present invention is to provide a novel solution for the manufacture of a reactor as well as a novel reactor.

[0007] The method of the invention is characterized by dipping fibrous reinforcement material in resin and winding the resin-dipped fibrous reinforcement material to form an inner sheath, winding a conductor layer of an insulated conductor or conductors outside the inner sheath, dipping fibrous reinforcement material in resin and winding the resin-dipped fibrous reinforcement material to form an intermediate layer on the conductor layer, winding a subsequent conductor layer of an insulated conductor or conductors outside the intermediate layer, whereby there will be provided at least two conductor layers and between each conductor layer there is formed an intermediate layer, and dipping fibrous reinforcement material in resin and winding the resin-dipped fibrous reinforcement material on top of the outermost conductor layer to form an outer sheath.

[0008] The arrangement of the invention is further characterized by comprising means for dipping fibrous reinforcement material in resin and applying the resin-dipped fibrous reinforcement material to form the coil's inner sheath, outer sheath and intermediate layers between the conductor layers.

[0009] Further still, the reactor of the invention is characterized in that the inner sheath and the outer sheath are obtained by winding the resin-dipped fibrous reinforcement material and that between the conductor layers there are intermediate layers which are obtained by winding the resin-dipped fibrous reinforcement material.

[0010] In the presented solution the reactor is produced such that in a first step resin-dipped fibrous reinforcement material, preferably thread, for instance roving thread, is wound to form a cylinder. On the obtained insulation layer there is wound an insulated conductor to form a conductor layer. On the conductor layer there is again wound an intermediate layer of resin-dipped fibrous reinforcement material, for instance roving thread. On the intermediate layer there is again wound a layer of insulated conductor. There are wound at least two layers of insulated conductors, but there may be even more conductor layers. Between each conductor layer there is wound an intermediate layer of resin-dipped fibrous reinforcement material, for instance roving thread. On top of the outermost conductor layer there is wound an outer layer of resin-dipped fibrous reinforcement material, for instance roving thread. In the above-described manner it is possible to apply resin evenly throughout the reactor. Resin insulation will be well applied also between the conductors, in particular the conductor layers. On the whole, the structure of the reactor becomes very solid. The implementation of the solution may also be relatively easily automated, which allows considerable savings in manufacturing costs. Moreover, the solution can be implemented at normal atmospheric pressure, i.e. without pressurization or partial vacuum, and despite that resin is very well introduced between the conductors.

BRIEF DESCRIPTION OF THE DRAWINGS

[0011] In the following the invention will be described in greater detail in the attached drawings, in which

Figure 1 is a schematic top view of a reactor;
Figure 2 is a schematic sectional side view of one coil in the reactor; and
Figure 3 is a schematic view of the solution for manufacturing the reactor.

DETAILED DESCRIPTION OF SOME EMBODIMENTS OF THE INVENTION

[0012] Figure 1 shows a reactor 1. The reactor 1 is a dry-insulated air-core reactor. The reactor 1 may be used, for instance, as a damping choke coil in connection with parallel compensating capacitor batteries or as a filtering reactor to filter harmonics from the electric power distribution network. Further, the reactor may be used, for instance, as a parallel reactive coil to compensate for capacitive reactive power in long, lightly loaded transmission lines. The reactor 1 may also be used as a current limiting reactor to limit short-circuit current, for instance, in connection with the electric power distribution network, or the reactor 1 may find its application in other suitable uses.

[0013] The reactor 1 comprises at least one cylindrical coil 2, but it may also comprise a plurality of nested, concentric cylindrical coils 2. In the case of Figure 1 the reactor 1 comprises three nested, concentric cylindrical coils 2. The coils 2 are separated from one another by means of supports 3 made of insulation material. Thus, between the coils 2 there is an air gap, whereby it is possible to ensure the cooling of the reactor 1. The coils 1 are connected with end bars 4 in a manner known per se. Typically the coils 2 are coupled in parallel.

[0014] Each coil 2 consists of conductors coated with insulation in accordance with Figure 2. The conductors 5 may be of aluminium or copper, for instance. The insulation covering the conductor may be made of polyethylene terephthalate (PET) membrane, paper, enamel, aramide paper, polytetrafluoroethylene (PTFE) or another suitable, relatively thin insulation material. The inner part of the coil 2 constitutes an inner sheath 6 and the outermost part of the coil 2 is an outer sheath 7. The conductors 5 form conductor layers 8. Between the conductor layers 8 there are intermediate layers 9.

[0015] The inner sheath is obtained by winding resin-dipped roving thread around a cylindrical form. Thereafter on the outside of the inner sheath there is wound a conductor 5 to form a conductor layer 8. On the conductor layer 8 there is wound an intermediate layer 9, which is also made of resin-dipped roving thread. Thereafter there is wound a subsequent conductor layer 8 and thereon a subsequent intermediate layer 9. On the second intermediate layer 9 there is wound a third conductor layer 8 and so on. Outside the fifth conductor layer, which in this case constitutes the outermost conductor layer, there is produced an outer sheath 7. The outer sheath 7 is also made of resin-dipped roving thread. Typically one coil comprises 1 to 20 conductor layers 8.

[0016] Figure 3 shows schematically an arrangement for manufacturing a reactor. The arrangement comprises a cylindrical form 10. The form 10 is rotated about its axis, whereby the roving threads 11 are wound around the form. The roving threads 11 are unwound from roving thread reels 12. The attached figures show only four roving thread reels 12, but advantageously the number of roving threads 11 simultaneously wound around the form 10 may be, for instance, 10 to 50 threads. The weight of the roving thread per unit of length, i.e. thread number is about 400 to 2,400 tex., for instance. By using 40 roving threads 11, for instance, it is possible to spread the roving threads over the form 10 as a strip that is several centimetres wide. Prior to winding onto the form 10 the roving threads 11 are dipped in resin 13. The resin may be epoxy resin or polyester resin, for instance.

[0017] The dipping of the roving threads may be carried out such, for instance, that the resin 13 is arranged in a container 14. On top of the container 14 there is arranged a cylinder 15, the lower part of which comes into contact with the resin 13 and as the cylinder 15 rotates it wets the roving threads 11 passing over it. The roving thread 11 dipped in resin 13 is wound around the form 10 in a plurality of layers. Thus is obtained an inner sheath 6. The thickness of the inner sheath may vary within the range of 1 to 10 mm, for instance.

[0018] After accomplishing the inner sheath 6 a first conductor layer 8 is wound thereon. The conductor layer 8 is made of an insulation-coated conductor 5 unwinding from a conductor reel 16. Figure 3 shows two conductors 5 to be wound simultaneously side by side in the axial direction. There may be 1 to 40 axially parallel conductors 5. The diameter of the conductor 5 may be 1 to 5 mm, for instance, when a round conductor 5 is used. If so desired, the conductor 5 may also be square or rectangular in shape. In Figure 3 the roving threads 11 and the conductor 5 are shown as wound simultaneously, but in practice their winding is not performed simultaneously, but the inner sheath 6 is prepared first, the roving threads 11 are cut and thereafter the conductor 5 is wound and so on.

[0019] After accomplishing the conductor layer 8 the conductor 5 is cut. Thereafter an intermediate layer 9 is wound on the conductor layer 8 with dipped 13 roving threads 11. On the intermediate layer 9 there is again wound a subsequent conductor layer 8, on which a new intermediate layer 9 and so on. The thickness of the intermediate layer 9 is about 0.1 to 0.2 mm, for instance. The thickness of the intermediate layer 9, i.e. the distance between the conductors 5 of two different conductor layers 8 is advantageously as small as possible. Thus, the intermediate layer 9 may be so thin that it need not be considered in dimensioning calculation of the reactor. On the other hand, there may also be thicker areas in the intermediate layer 9, which fill the holes resulting from cross sectional shapes of the conductors 5. Advantageously the amount of resin is such that substantially no air gaps exist between the conductor layers 8. The different conductor layers 8 are coupled electrically to one another in a desired manner, either in series or in parallel.

[0020] Outside the outermost conductor layer 8 there is wound an outer sheath 7 made of resin-dipped 13 roving threads 11. The thickness of the outer sheath 7 is about 1 to 10 mm. The intermediate layer 9 is provided with more resin 13 than the inner sheath 6 and the outer

sheath 7. This means that when the intermediate layer 9 is being produced the roving threads 11 are dipped wetter, i.e. more resin 13 is soaked in. When the intermediate layers 9 are provided with more resin 13 than the inner sheath 6 and the outer sheath 7, it is possible to ensure that resin will be applied between each conductor layer 8. This makes sure that the structure of the reactor is very rigid.

[0021] The amount of resin 13 may be controlled by means of a scraper 17, for instance. The scraper 17 is arranged in the vicinity of the cylinder 15. By adjusting the distance of the scraper from the cylinder with a control device 18 the amount of resin 13 to be applied to the roving threads 11 is controlled. When the scraper is further away from the cylinder 15 there is more resin on the cylinder to adhere to the roving threads 11. When the scraper 17 is arranged close to the cylinder 15 there is less resin on the cylinder 15 to adhere to the roving threads 11. The rotation speeds of the form 10 and the cylinder 15 also have an effect on the amount of resin. The rotation of the form 10 and the cylinder 15 are controlled with the control device 18. The cylinder 15 may also rotate freely driven by the roving threads 11.

[0022] For the sake of clarity Figure 3 does not show the arrangement's support structures or the like devices, such as rotating devices and, for instance, robotic arms by which the roving threads 11 and the conductors 5 are set into place when the winding starts. At the beginning of the winding the roving threads 11 and the conductors 5 may also be set into place manually. The resin 13 may be warmed prior to winding to lower the viscosity of resin.

[0023] After accomplishing the innermost coil 2 the supports 3 made of insulating material are arranged outside said coil and thereafter the inner sheath of the subsequent coil is wound on these supports 3 and on top of the inner sheath 6 a new conductor layer 8, whereafter an intermediate layer 9 and so on.

[0024] If so desired, it is also possible to produce the outer coils 2 on the form 10. In that case the reactor 1 is produced such that the readymade coils 2 are set in superposition and the supports 3 made of insulating material are arranged between them.

[0025] In addition to the roving threads 11, fibres in the axial direction of the coil 2 are also arranged in the inner sheath 6 and the outer sheath 7. This enhances the structural strength of the coil 2. When the coil is accomplished, the resin hardens. The hardening of resin may take place at room temperature, whereby the hardening typically takes about a couple of hours. If desired, the hardening may be accelerated by warming the resin in the coil. After the hardening the form 10 may be removed. If the form 10 is made of suitable material, it is also possible to leave it inside the innermost coil 2. Advantageously the conductor layers 8 are produced of one or more axially parallel conductors 5 by winding. Thus the mechanical solution of the arrangement is simple. Further, in connection with the reactor dimensioning it will be easy to change the reactor properties, when necessary, because it is possible to add just one wire turn, if necessary, and not a bundle of ten threads, for instance. One conductor layer 8 is produced by winding for instance 1 to 40 conductors simultaneously. It is further possible to arrange conductors into bundles of several conductors both in the axial and the radial directions, but in that case it will be slightly more difficult to get resin between each conductor to ensure the rigidity of the structure.

[0026] The diameter of the reactor 1 may vary from 30 cm to 4 m, and correspondingly the height of the reactor may vary from 30 cm to 4 m. Typically the weight of the reactor 1 then varies from 5 kg to 15,000 kg. The reactor 1 need not necessarily be an air-core reactor, but the presented solution may also be applied to the manufacture of an iron-core reactor. Most preferably the fibrous reinforcement material is a roving thread. Instead of the roving thread, i.e. untwisted or slightly twisted fibreglass bundle, it is possible to use any suitable fibreglass reinforcement for the manufacture of the reactor. Further, the most preferable roving thread to be used is the one that is fully untwisted, i.e. directly reeled. Thus, when an intermediate layer 9 is produced, for instance, the fibreglass bundle spreads evenly and neatly, and consequently the intermediate layer becomes relatively thin. Still further, the fibrous reinforcement material may be Kevlar or polyester, for instance. However, it is substantial that a wet blend of fibrous reinforcement material and resin is employed in the manufacturing.

[0027] In some cases features presented in this document may be used as such, irrespective of other features. On the other hand, features presented in this document may be combined, when necessary, to provide various combinations.

[0028] The drawings and the relating specification are only intended to illustrate the inventive idea. The details of the invention may vary within the scope of the claims.

Claims

1. A method for manufacturing a reactor, the method producing at least one coil (2) having conductor layers (8) and inside them an inner sheath (6) of fibrous reinforcement material and resin, and outside an outer sheath (7) of fibrous reinforcement material and resin, **characterized by**
   dipping fibrous reinforcement material in resin (13) and winding the resin-dipped (13) fibrous reinforcement material to form an inner sheath (6),
   winding a conductor layer (8) of an insulated conductor (5) or conductors (5) outside the inner sheath (6),
   dipping fibrous reinforcement material in resin (13) and winding the resin-dipped (13) fibrous reinforcement material to form an intermediate layer (9) on the conductor layer (8),
   winding a subsequent conductor layer (8) of an insulated conductor (5) or conductors (5) outside the

intermediate layer (9), whereby there will be provided at least two conductor layers (8) and between each conductor layer (8) there is formed an intermediate layer (9), and
dipping fibrous reinforcement material in resin (13) and winding the resin-dipped (13) fibrous reinforcement material on top of the outermost conductor layer (8) to form an outer sheath (7).

2. The method of claim 1, **characterized in that** the fibrous reinforcement material is fibreglass.

3. The method of claim 2, **characterized in that** the fibreglass is roving thread (11).

4. The method of claim 3, **characterized in that** the roving thread (11) is directly reeled roving thread.

5. The method of any one of the preceding claims, **characterized in that** the conductor layer (8) is produced by winding a single conductor (5) or only axially parallel conductors (5).

6. The method of any one of the preceding claims, **characterized by** arranging more resin in the intermediate layer (9) with respect to the length of the fibrous reinforcement material than in the inner sheath (6) and the outer sheath (7).

7. The method of any one of the preceding claims, **characterized by** arranging fibrous reinforcement material also in the axial direction in the inner sheath (6) and the outer sheath (7).

8. An arrangement for manufacturing a reactor, the arrangement comprising means for winding an insulated conductor (5) to form a conductor layer (8) so as to provide a coil (2), **characterized in that** the arrangement comprises means for dipping fibrous reinforcement material in resin (13) and for applying the resin-dipped (13) fibrous reinforcement material to form the coil's (2) inner sheath (6), outer sheath (7) and the intermediate layers (9) between the conductor layers (8).

9. The arrangement of claim 8, **characterized in that** the fibrous reinforcement material is fibreglass.

10. The arrangement of claim 9, **characterized in that** the fibreglass is roving thread (11).

11. The arrangement of claim 10, **characterized in that** the roving thread (11) is directly reeled roving thread.

12. The arrangement of any one of claims 8 to 11, **characterized in that** the conductor layer (8) is arranged for being produced of a single conductor (5) or only axially parallel conductors (5).

13. The arrangement of any one of claims 8 to 12, **characterized in that** the arrangement comprises a control means for controlling the amount of resin (13) to be applied in the fibrous reinforcement material such that the control device is arranged to apply more resin in the fibrous reinforcement material of the intermediate layer (9) with respect to its length than that of the inner sheath (6) and the outer sheath (7).

14. The arrangement of any one of claims 8 to 13, **characterized in that** the arrangement comprises means for arranging the fibrous reinforcement material in the axial direction in the inner sheath (6) and the outer sheath (7).

15. A reactor comprising at least one coil (2) with conductor layers (8) and inside them an inner sheath (6) and outside an outer sheath (7), **characterized in that** the inner sheath (6) and the outer sheath (7) are obtained by winding a resin-dipped (13) fibrous reinforcement material and that between the conductor layers (8) there are intermediate layers (9) which are obtained by winding the resin-dipped (13) fibrous reinforcement material.

16. The reactor of claim 15, **characterized in that** the fibrous reinforcement material is fibreglass.

17. The reactor of claim 16, **characterized in that** the fibreglass is roving thread (11).

18. The reactor of claim 17, **characterized in that** the roving thread (11) is directly reeled roving thread.

19. The reactor of any one of claims 15 to 18, **characterized in that** the conductor layer (8) is produced of single conductors (5) or simultaneously wound only axially parallel conductors (5).

20. The reactor of any one of claims 15 to 19, **characterized in that** the intermediate layers (9) comprise more resin in relation to the fibrous reinforcement material than the inner sheath (6) and the outer sheath (7).

21. The reactor of any one of claims 15 to 20, **characterized in that** the reactor (1) is an air-core reactor.

22. The reactor of any one of claims 15 to 21, **charac-**

terized
in that the inner sheath (6) and the outer sheath (7) comprise fibrous reinforcement material in the axial direction.

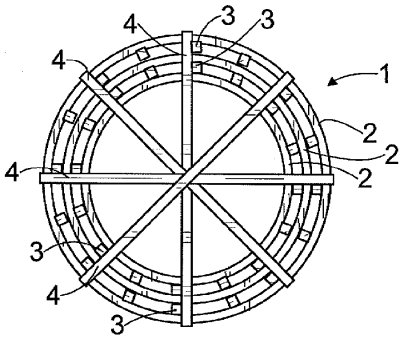

FIG. 1

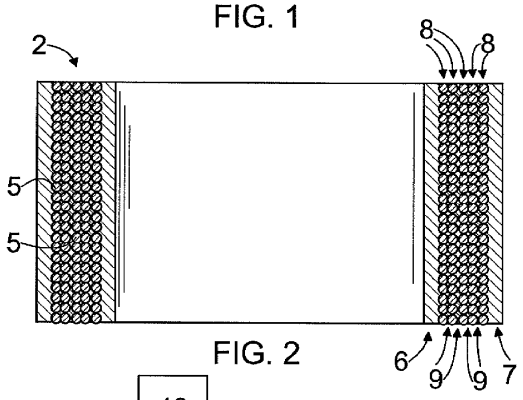

FIG. 2

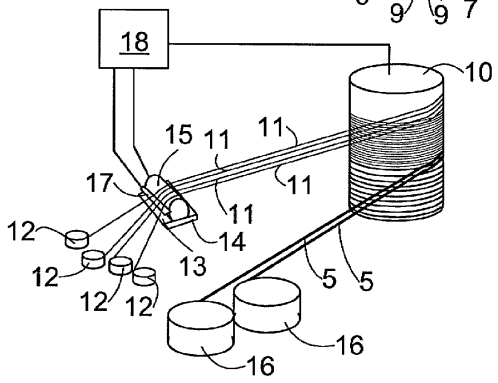

FIG. 3

REFERENCES CITED IN THE DESCRIPTION

This list of references cited by the applicant is for the reader's convenience only. It does not form part of the European patent document. Even though great care has been taken in compiling the references, errors or omissions cannot be excluded and the EPO disclaims all liability in this regard.

Patent documents cited in the description

- FI 70755 **[0005]**
- EP 0084412 A **[0005]**
- FI 91570 **[0005]**

ISBN 978-951-22-9343-8
ISBN 978-951-22-9344-5 (PDF)
ISSN 1795-2239
ISSN 1795-4584 (PDF)